

# **Oxidation of Transition Metal Complexes with 3,7-Diazabicyclo[3.3.1]nonane-Derived Ligands**

**INAUGURAL - DISSERTATION**  
**zur**  
**Erlangung der Doktorwürde**  
**der**  
**Naturwissenschaftlich-Mathematischen Gesamtfakultät**  
**der**  
**Ruprecht-Karls-Universität Heidelberg**

**vorgelegt von**  
**Máté Tarnai**  
**aus Budapest, Ungarn**

**2006**



**INAUGURAL - DISSERTATION**  
**zur**  
**Erlangung der Doktorwürde**  
**der**  
**Naturwissenschaftlich-Mathematischen Gesamtfakultät**  
**der**  
**Ruprecht-Karls-Universität Heidelberg**

**vorgelegt von**  
**Máté Tarnai**  
**aus Budapest, Ungarn**

**2006**

Tag der mündlichen Prüfung: 23. Juni 2006.



# **Oxidation of Transition Metal Complexes with 3,7-Diazabicyclo[3.3.1]nonane-Derived Ligands**

Gutachter: Prof. Dr. Peter Comba  
Prof. Dr. Gerald Linti



The work presented here was done between September 2002 and April 2006, under the supervision of Prof. Dr. Peter Comba at the Institute of Inorganic Chemistry, University of Heidelberg.

### *Acknowledgements*

It is my pleasure to thank *Prof. Dr. Peter Comba* to get acceptance in his research group, I thank for his continuous guidance, scientific advice and for the interesting research topic.

I am grateful to *Dr. Shigemasa Kuwata* for discussions about cobalt and vanadium chemistry and for his nice company to keep my Japanese in a good shape.

Without *Dr. Alexander Prikhod'ko* the magnetic measurements would not have been possible. I am grateful for his advice with regard to ion exchange chromatography, and for that he tolerated my neighbourhood in the lab.

I thank *Dr. Carlos López de Laorden* and *Dr. Jochen Bautz* for their ideas and comments about catalysis experiments.

I thank *Dr. Erik Schatz* for his plenty of synthetic ideas.

Without the help of the computational brigade, namely (*Dr.*) *Heidi Rohwer*, *Dr. Gopalan Rajaraman*, *Prof. Mihail Atanasov* and *Dr. Bodo Martin* I would have been completely lost in the Gaussian calculations.

Special thanks to *Dr. André Daubinet* for his help in the force field calculations.

Thanks to *Dr. Marion Kerscher* and *Maik Jakob* for their help in my everyday little troubles.

I am really grateful for my trainee, *Andrea Nies* who made great efforts in vanadium chemistry.

I express my gratitude to *Dr. Marion Kerscher*, *Dr. Gopalan Rajaraman* and (*Dr.*) *Heidi Rohwer* for proof-reading of the dissertation and for their scientific and grammatical comments.

Thanks also to other members of the group who made a great atmosphere in the lab:

*Christoph Busche*, *Dr. Arunashree Panda*, *Dr. Rosana Ferrari-Zijlstra*, *Dr. Xiangming Zhang*, *Prof. Kyaw Naing*, *Prof. Yang Kim*, *Dr. Karin Born*, *Nadine Brem*, *Laura Kleditsch*, *Martha Matuschek*, *Matthias Menzel*, *Alexander Bentz*, *Björn Seibold*, *Dr. Vera Müller*, *Thomas Schneider*, *Dr. Michael Merz*, *Dr. Kathrin Merz*

Extra thanks for:

- the *services of the University*: mass spectrometry of the Institutes and microanalysis service of Inorganic and Organic Chemistry for their contribution.

- *Dr. Hans Pritzkow*, *Prof. Dr. Hubert Wadepohl* for solving the crystal structures.

For *financial support* I express my gratitude to Universität Heidelberg (September 2002 – March 2003), to Graduiertenkolleg 850 (April 2003 – September 2003) and Deutscher Akademischer Austauschdienst (September 2003 – July 2006).





*Abbreviations:*

NMR	nuclear magnetic resonance
s	singlet
d	doublet
t	triplet
dd	doublet of doublets
J	coupling constant
Hz	hertz
ppm	parts pro million
IR	infrared (spectroscopy)
w	weak
m	medium
s	strong
vs	very strong
sh	shoulder
MS	mass spectroscopy
ESI	electrospray ionization
CI	chemical ionization
EI	electron impact
FAB	fast atom bombardment
MALDI	matrix assisted laser desorption ionization
UV-vis	ultraviolet-visible spectroscopy
$\epsilon$	molar absorption coefficient
DFT	density functional theory
GS	ground state
TS	transition state
SP	single point
hs	high spin
is	intermediate spin
ls	low spin
SCF	self consistent field
TZV	triple zeta valence (basis set)
TZVPP	tripel zeta valence plus polarization (basis set)
CV	cyclic voltammetry
EPR	electron paramagnetic resonance
SQUID	superconduction quantum interference device
h	hour
min	minute(s)
d	day(s)
TLC	thin layer chromatography
EtOH	ethanol
MeOH	methanol
DMF	dimethylformamide
DMSO	dimethylsulfoxide
THF	tetrahydrofurane
TEA	triethylamine
TEAHCl	triethylamine hydrochloride
RT	room temperature
eq	equivalent
TON	turnover number

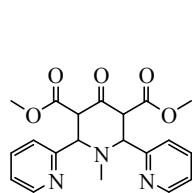


## Table of contents

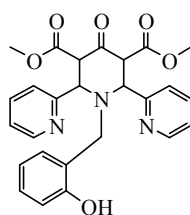
1. Abstract	1
2. Zusammenfassung	5
3. Introduction	9
4. Synthesis of bispidone ligands	
4.1. Introduction	13
4.2. Target ligands	15
4.3. Synthesis of mononucleating phenol-bispidone ligands	
4.3.1. Synthesis of N <sub>2</sub> py <sub>2</sub> PhOH	17
4.3.2. Synthesis of vanilbis	19
4.3.3. Synthesis of o-aminophenols through amidomethylation, synthesis of sulfobis	21
4.3.4. Synthesis of N <sub>2</sub> PhO <sub>2</sub> r	23
4.3.5. Synthesis of N <sub>2</sub> PhO <sub>2</sub> using benzyl as protection group	24
4.3.6. Synthesis of N <sub>2</sub> PhO <sub>2</sub> tBu	25
4.4. Synthesis of dinucleating phenol-bispidone ligands	
4.4.1. Synthesis of cresbis	26
4.4.2. Synthesis of tBuBis	28
5. Mono- and dinuclear copper(II) complexes with phenol-bispidone ligands as models for galactose oxidase and catechol oxidase	
5.1. Introduction	31
5.2. Copper(II) complexes with mononucleating phenol-bispidone ligands	34
5.3. Copper(II) complexes with dinucleating phenol-bispidone ligands	37
5.3.1. Copper complexes of cresbis	37
5.3.1.1. Synthesis of the complexes	37
5.3.1.2. EPR spectra	40
5.3.1.3. Force field calculations	43
5.3.1.4. SQUID measurements	44
5.3.1.5. Catecholase reaction	48
5.4. Copper(II) complex with sulfobis	49
6. Synthesis and oxidation of V(IV) and V(V) bispidone complexes	
6.1. Introduction	51
6.2. Vanadyl complexes	52
6.2.1. Synthesis of vanadyl complexes	52
6.2.2. Spectroscopy of the vanadyl complexes	52
6.2.3. Oxidation of the vanadyl complexes	55
6.3. Characterization of [V <sup>V</sup> =O(O <sub>2</sub> )(N <sub>2</sub> py <sub>3</sub> o)]ClO <sub>4</sub>	57
6.4. Oxidation of the oxo-peroxo-vanadium(V) to the oxo-superoxo vanadium(V) complex using chemical oxidants	59
6.5. Catalysis	62
6.5.1. Haloperoxidase test	62
6.5.2. Catalytic oxidation of olefins	65
6.5.2.1. Introduction	65
6.5.2.2. Oxidation of cyclooctene	66
6.5.2.3. Oxidation of cyclohexene	67

<i>7. Oxidative N-dealkylation in a cobalt-bispidone complex – mechanistic investigations</i>	
7.1. Introduction	69
7.2. Synthesis and spectroscopic characterization of the cobalt complexes	70
7.3. Oxidation of cobalt(II) complexes with H <sub>2</sub> O <sub>2</sub>	72
7.4. Intramolecular oxidative N-dealkylation in a cobalt-bispidone complex	75
7.4.1. Background	75
7.4.2. Dependence of the yield on the concentration of the oxidant	76
7.4.3. Structure of [Co <sup>II</sup> (N2py2a)(H <sub>2</sub> O) <sub>2</sub> ](ClO <sub>4</sub> ) <sub>2</sub>	78
7.4.4. What happens with the N7-methyl group after demethylation?	83
7.4.5. Oxidation of [Co <sup>II</sup> (N2py2)(OH <sub>2</sub> ) <sub>2</sub> ](ClO <sub>4</sub> ) <sub>2</sub> in methanol	84
7.4.6. Oxidation of [Co <sup>II</sup> (N2py2)(OH <sub>2</sub> ) <sub>2</sub> ](ClO <sub>4</sub> ) <sub>2</sub> in acetonitrile	86
7.4.7. Oxidative N-dealkylation in a cobalt(II)-bispidone complex with a benzyl substituent	88
7.4.8. Cobalt(III)-peroxide interactions	90
7.4.9. External substrates: [Co <sup>II</sup> (N2py2)(OH <sub>2</sub> ) <sub>2</sub> ] <sup>2+</sup> /H <sub>2</sub> O <sub>2</sub> system as catalyst?	95
7.4.10. Proposed mechanism of the oxidative N-dealkylation	96
7.4.11. DFT calculations for the proposed mechanistic pathway	101
<i>8. Other metal complexes of bispidone ligands</i>	
8.1. Other metal complexes of N2py2PhOH	115
8.1.1. Synthesis and characterization of the complexes	115
8.1.2. Oxidation of Fe <sup>II</sup> - and Mn <sup>II</sup> -N2py2PhOH complexes with H <sub>2</sub> O <sub>2</sub>	121
8.2 Manganese complexes of other bispidone ligands	123
8.2.1. Synthesis and oxidation of manganese(II) complexes with N <sub>4</sub> and N <sub>5</sub> bispidone ligands	123
8.2.2. Manganese(III) complexes of cresbis and tBuBis	128
<i>9. Experimental section</i>	
9.1. General	129
9.2. Syntheses	132
9.2.1. Synthesis of ligands and precursors	132
9.2.2. Synthesis of the copper(II) complexes	139
9.2.3. Synthesis of the vanadium complexes	143
9.2.4. Synthesis of the cobalt complexes	146
9.2.5. Synthesis of the manganese complexes	148
9.2.6. Synthesis of other complexes with N2py2PhOH	155
<i>10. References</i>	159
<i>Appendix</i>	169
A. Copper(II) and manganese(III) complexes of the bisphenolamine ligand	169
B. Additional DFT calculations for the proposed mechanistic pathway of the oxidative N-dealkylation in a cobalt-bispidone complex	170
C. Selected ESI-MS spectra	174
D. Crystal parameters	177

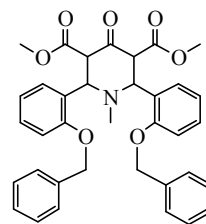
*Index of ligands and precursors:*



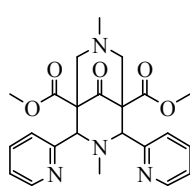
Npy2



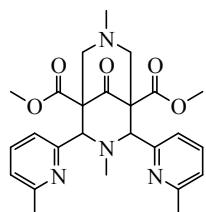
Npy2PhOH



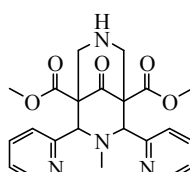
**Bzl-pip**



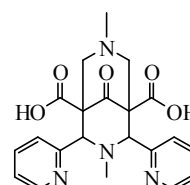
N2py2



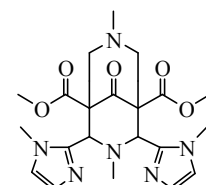
6MeN2py2



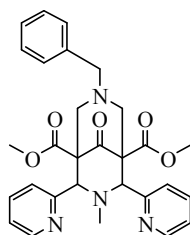
N2py2a



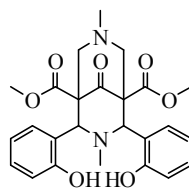
N2py2b



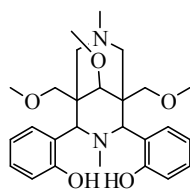
N2Im2



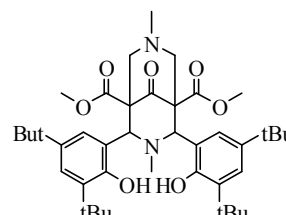
**N2py2Bz**



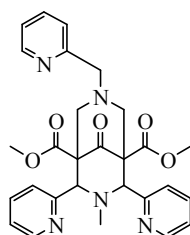
N2PhO2



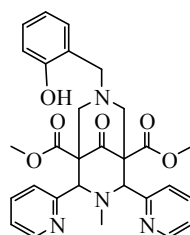
N2PhO2r



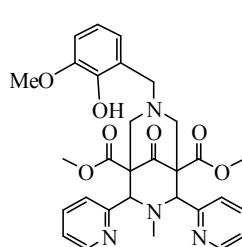
N2PhO2tBu



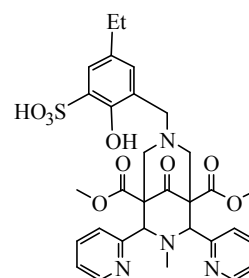
N2py3o



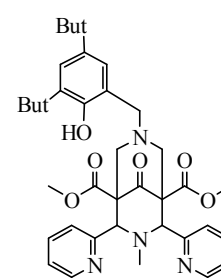
**N2py2PhOH**



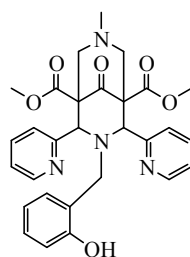
**vanilbis**



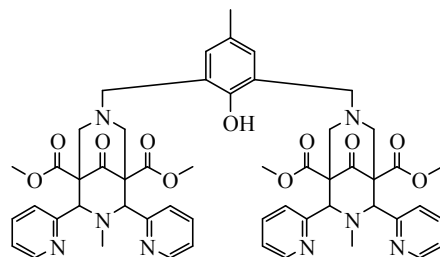
**sulfobis**



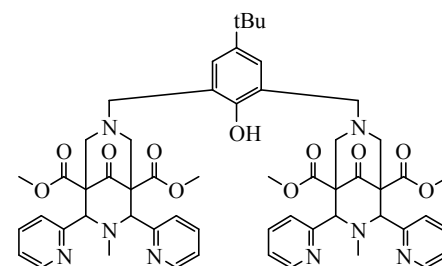
N2py2PhOhtBu



N2py2PhOH(u)



**cresbis**



**tBuBis**

New ligands and precursors are typed with bold characters



## 1. Abstract

A series of new 3,7-diazabicyclo[3.3.1]nonane (bispidone)-derived ligands with phenolic side chains were synthesized. The double Mannich condensation reaction to create the bicyclic bispidone was carried out successfully, though the isolation of the bispidones was not always straightforward. The preparation of the corresponding amine precursors was a very challenging task, which often led to more difficulties than the Mannich condensation itself. The preparation of the new bispidone ligands are described in Chapter 4.

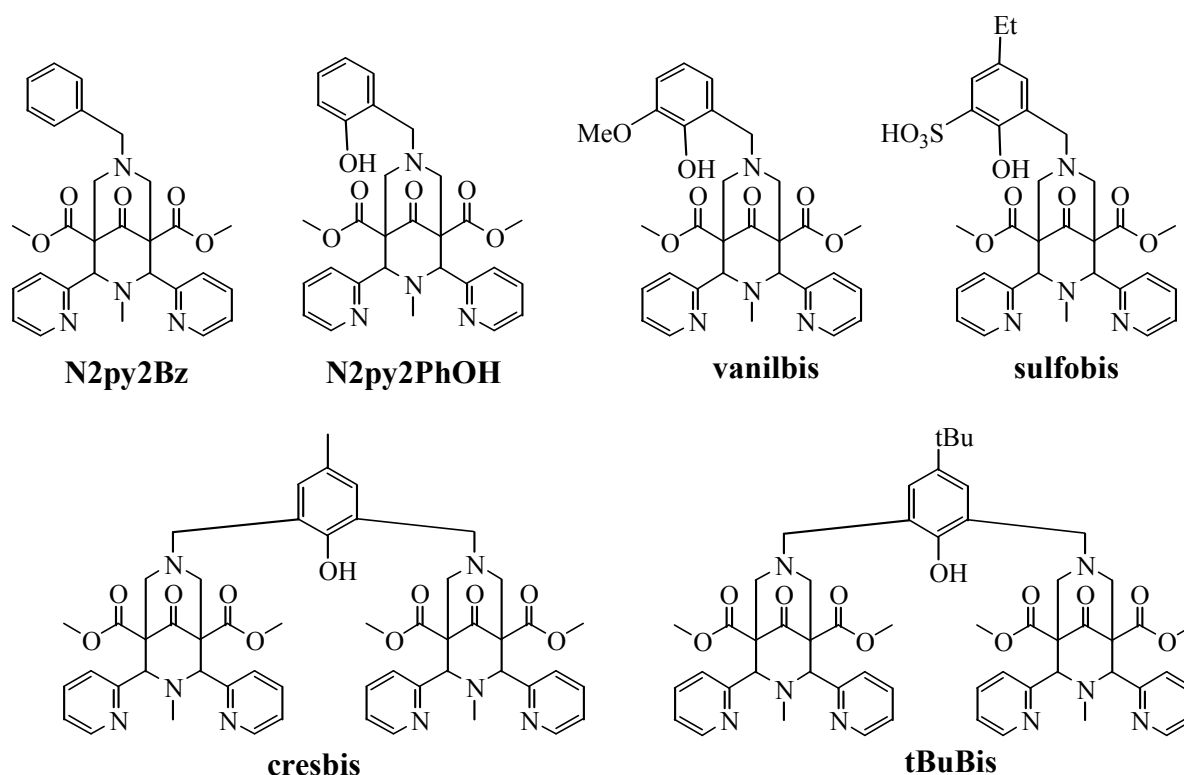


**Figure 1.1.** The prepared new 3,7-diazabicyclo[3.3.1]nonane derivatives

As structural models for the galactose oxidase enzyme, copper(II) complexes of the mononucleating phenol-bispidone ligands N2py2PhOH and vanilbis were prepared and structurally and spectroscopically investigated. These results are presented in Chapter 5. The crystal structure of the copper(II)-N2py2PhOH complex shows that the bispidone cavity is preorganized for copper(II) and that the incorporation of the phenolic moiety does not build up any strain in the ligand backbone (when compared to other known systems). The Cu(II)-N2py2PhOH complex disproportionates to a copper(I) salt and copper(II)-phenoxy radical.

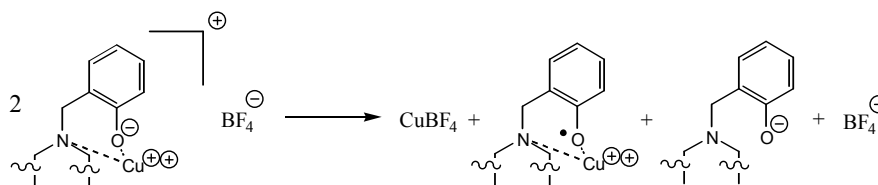


**Figure 1.2. Proposed disproportionation reaction for  $[\text{Cu}^{\text{II}}(\text{N}2\text{py}2\text{PhO})]\text{BF}_4$  in methanol**

Dicopper(II) complexes with the dinucleating bispidone ligands cresbis and tBuBis, were designed as structural models of catechol oxidase (Chapter 5). A combined spectroscopic, magnetometric and computational study revealed that by tuning the reaction conditions (applying an organic base or a basic alumina column in the synthesis), the distance between the copper(II) centers could be varied.

Vanadyl-complexes with N2py2 and N2py2PhOH were also prepared and their spectroscopic properties compared to the known  $[\text{V}^{\text{IV}}=\text{O}(\text{N}2\text{py}3\text{o})]^{2+}$  complex (Chapter 6). Oxidation of the latter complex was shown to produce V(V)-oxo-peroxo species in high yields in methanol. To solve the inconsistency of the O-O distance and O-O stretching frequency for the side-on bound peroxo unit in the so formed  $[\text{V}^{\text{V}}=\text{O}(\text{O}_2)(\text{N}2\text{py}3\text{o})]^+$  complex, a combined labeling and computational study was carried out. Further oxidation of this V(V)-oxo peroxo complex was possible using  $\text{Ce}^{4+}$ , as indicated by the EPR spectra.

A detailed spectrophotometric study was carried out to understand the nature of the reaction between the Co(II)-N2py2 complex with hydrogen peroxide (Chapter 7). The reaction products were both qualitatively and quantitatively analyzed using the hydrazine test reaction. Analogous reaction products were found when the complex of a structurally similar N2py2Bz ligand was used. Structural data obtained for complexes, which have been isolated from the reaction mixture, provided evidence on the dealkylation at the tertiary amine donor N7 in the ligand. (Figure 1.3)

Further details about the possible steps of the oxidative N-dealkylation were obtained from DFT calculations. From the results a mechanism was postulated. (Figure 1.4) Moreover, the catalytic activity of Co(II)-N2py2 /  $\text{H}_2\text{O}_2$  system in the oxidation of amines was investigated.



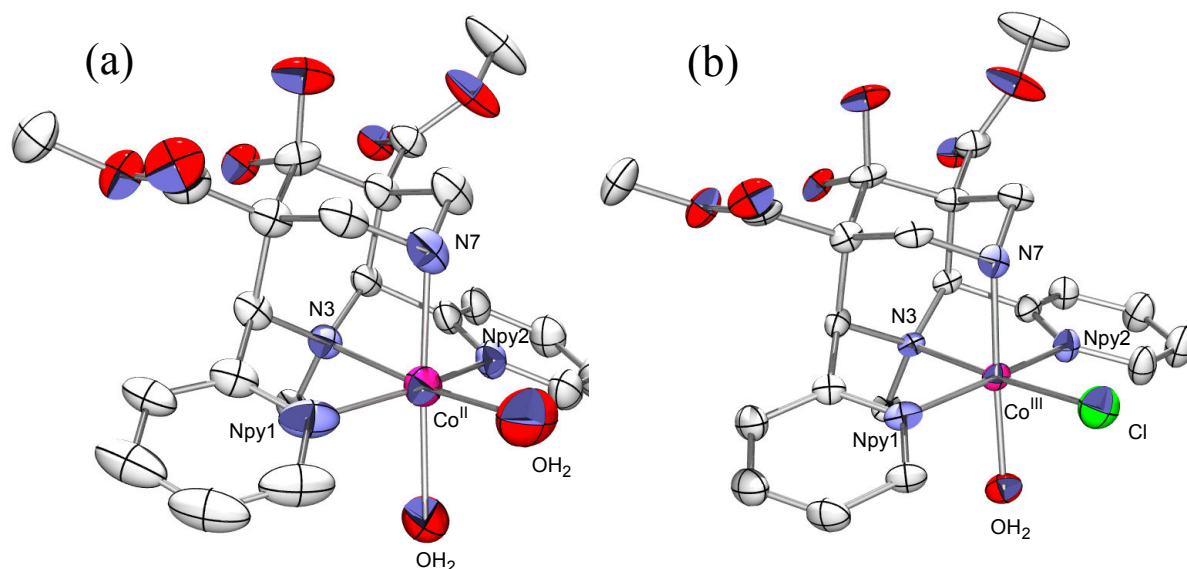


**Figure 1.3.** Crystal structures of  $[\text{Co}^{\text{II}}(\text{N}2\text{py}2\text{a})(\text{OH}_2)_2]^{2+}$  (a) and  $[\text{Co}^{\text{III}}(\text{N}2\text{py}2\text{a})(\text{OH}_2)\text{Cl}]^+$  (b)

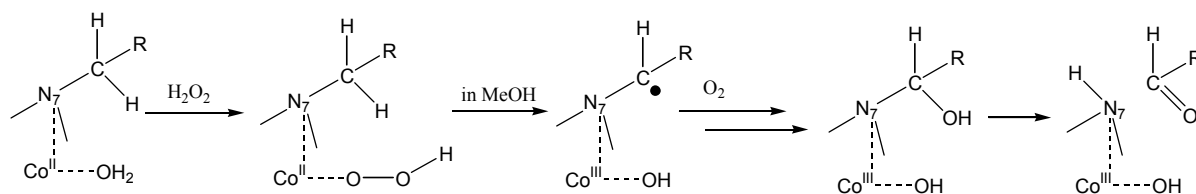


**Figure 1.4** Postulated mechanism for the intramolecular N-dealkylation

Manganese(II) complexes of known bispidone-type ligands with N4 or N5 donor set were prepared and their reaction with hydrogen peroxide was studied, in order to ascertain whether there is analogy with divalent iron complexes which show typical Fenton chemistry, with characterized high-valent iron species and have catalytic activity in olefin oxidation. These results are presented in Chapter 8. Interesting spectroscopic features of the manganese complexes with phenol-bispidone ligands are also reported in this chapter. The UV-vis spectra of the manganese(III)-N2py2PhOH complex demonstrate slow decomposition and possible pathways are discussed.



## 2. Zusammenfassung

Verschiedene neue, auf 3,7-Diazabicyclo[3.3.1]nonan (Bispidon) basierende Liganden, welche Phenolderivate als Seitenkette enthalten, wurden dargestellt. Die zweifache Mannich-Kondensationsreaktion, wodurch der Bizyklus aufgebaut wird, war erfolgreich, die Isolierung der gebildeten Bispidone jedoch nicht immer trivial. Die Darstellung der korrespondierenden Amin-Edukte war eine große Herausforderung und hat gelegentlich zu größeren Problemen geführt als die Mannich-Kondensation. Die Darstellung von neuen Bispidonliganden wird in Kapitel 4 beschrieben.

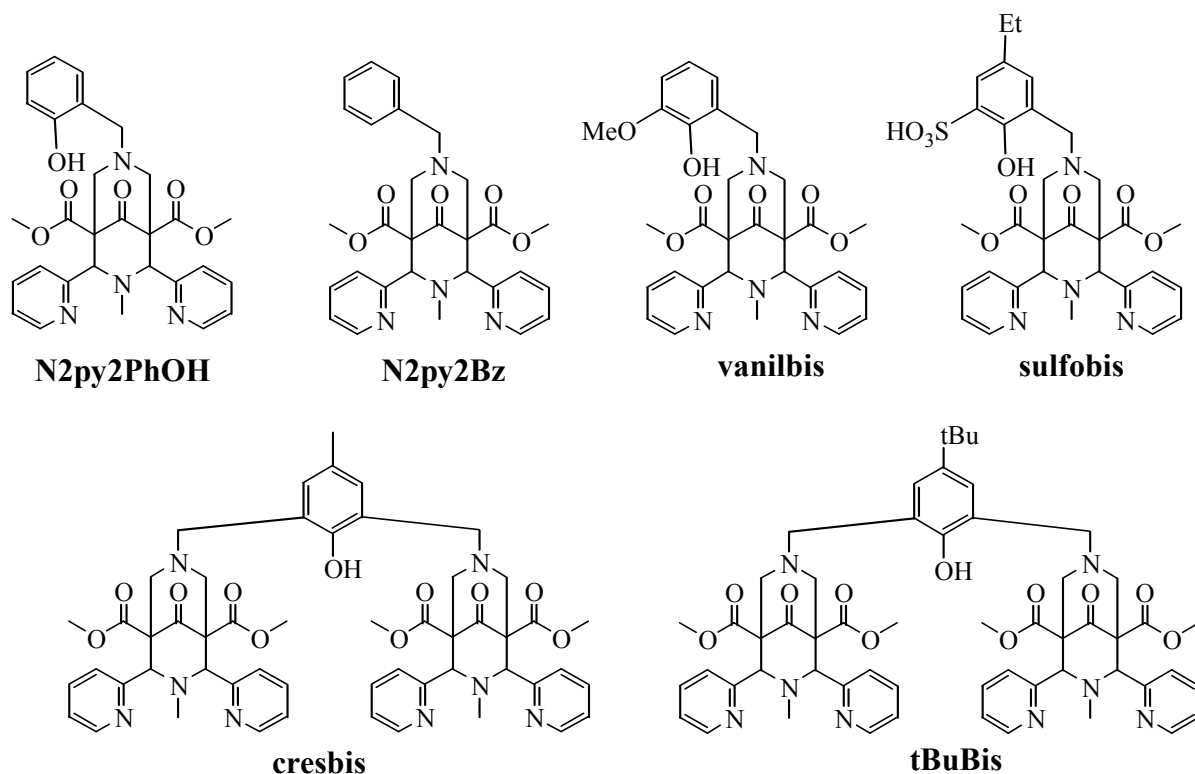
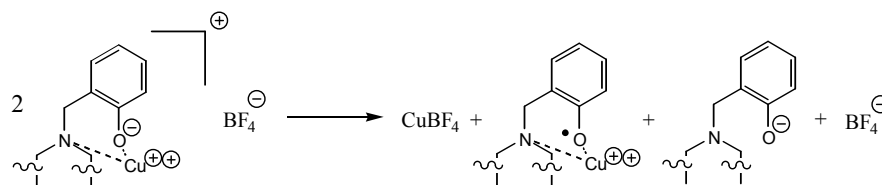


Abb. 2.1. Die dargestellten neuen 3,7-Diazabicyclo[3.3.1]nonan Derivaten

Als strukturelle Modelle des Galaktose Oxidase Enzyms wurden Monokupfer(II)-Komplexe mit Phenol-Bispidon Liganden (N2py2PhOH und vanilbis) dargestellt und strukturell und spektroskopisch untersucht (Kapitel 5). Die Kristallstruktur des Kupfer(II)-N2py2PhOH-Komplexes zeigt, dass das Ligandenloch für Kupfer(II) präorganisiert ist und dass im Vergleich zu bekannten Systemen der Einbau der Phenolgruppe keine weitere Spannung in das Ligandengerüst induziert. Der Kupfer(II)-N2py2PhOH-Komplex disproportioniert in Lösung zu Kupfer(I) und Kupfer(II)-Phenoxy Radikalen.



**Abb. 2.2. Vorgeschlagene Disproportionierung von  $[\text{Cu}^{\text{II}}(\text{N}2\text{py}2\text{PhO})]\text{BF}_4$  in Methanol**

Biskupfer(II)-Komplexe mit den Bispidonliganden *cresbis* and *tBuBis* wurden als strukturelle Modelle für Catechol Oxidase synthetisiert (Kapitel 6). Mittels spektroskopischer und magnetischer Messungen in Verbindung mit Kraftfeld Rechnungen wurde untersucht, inwiefern die Variation der Reaktionsbedingungen (Anwendung einer organischen Base oder einer basischen Säure) zur Änderung des Kupfer-Kupfer-Abstandes in den Komplexen führen kann.

Vanadyl-Komplexe mit  $\text{N}2\text{py}2$  und  $\text{N}2\text{py}2\text{PhOH}$  wurden dargestellt und ihre spektroskopischen Eigenschaften mit dem bekannten  $[\text{V}^{\text{IV}}=\text{O}(\text{N}2\text{py}3\text{o})]^{2+}$ -Komplex verglichen (Kapitel 7). Die Oxidation dieses Komplexes in Methanol führt zu einer V(V)-oxo-peroxo Spezies in hoher Ausbeute. Um die Widersprüchlichkeit in O-O Abstand und O-O Schwingungsfrequenz der side-on-Peroxo-Einheit im entstandenen  $[\text{V}^{\text{V}}=\text{O}(\text{O}_2)(\text{N}2\text{py}3\text{o})]^+$ -Komplex zu lösen, wurden DFT-Berechnungen und Studien mit isopenmarkiertem Wasserstoffperoxid durchgeführt. Die ESR-Spektren indizierten, dass die Weiteroxidation dieses V(V)-oxo peroxo Komplexes mit  $\text{Ce}^{4+}$  möglich war.

Eine detaillierte spektrophotometrische Untersuchung wurde durchgeführt, um die Art der Reaktion des  $\text{Co}(\text{II})\text{-N}2\text{py}2$ -Komplexes mit Wasserstoffperoxid zu klären (Kapitel 8). Die Produkte wurden mittels der Hydrazin-Testreaktion qualitativ und quantitativ analysiert. (Analoge Reaktionsprodukte wurden für den Komplex des strukturell ähnlichen  $\text{N}2\text{py}2\text{Bz}$ -Liganden gefunden). Die Röntgenstrukturen von aus der Reaktionsmischung isolierten Komplex-Kristallen lieferten Hinweise auf eine stattfindende Dealkylierung am N7-Donor des Liganden (Abb. 2.3). Weitere Einzelheiten über den Ablauf der oxidativen N-Dealkylierung wurden mittels DFT-Berechnungen erhalten. Anhand der Ergebnisse wurde ein Mechanismus postuliert (Abb. 2.4). Außerdem wurde die katalytische Aktivität des  $\text{Co}(\text{II})\text{N}2\text{py}2 / \text{H}_2\text{O}_2$ -Systems für die Oxidation von Aminen getestet.

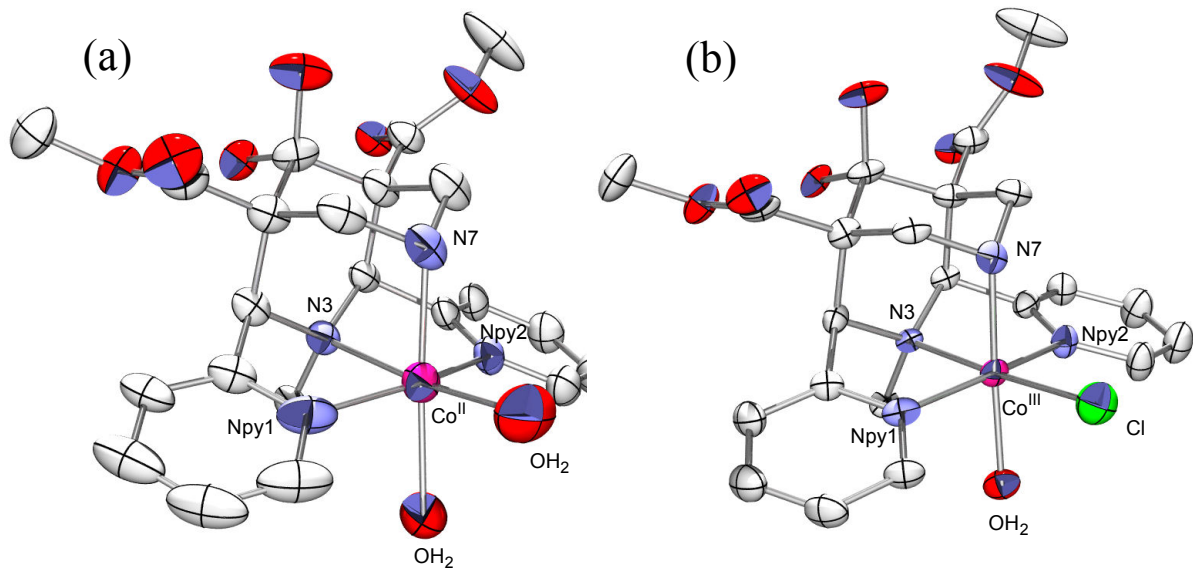


Abb. 2.3. Kristallstrukturen von  $[\text{Co}^{\text{II}}(\text{N}2\text{py}2\text{a})(\text{OH}_2)_2]^{2+}$  (a) und  $[\text{Co}^{\text{III}}(\text{N}2\text{py}2\text{a})(\text{OH}_2)\text{Cl}]^+$  (b)

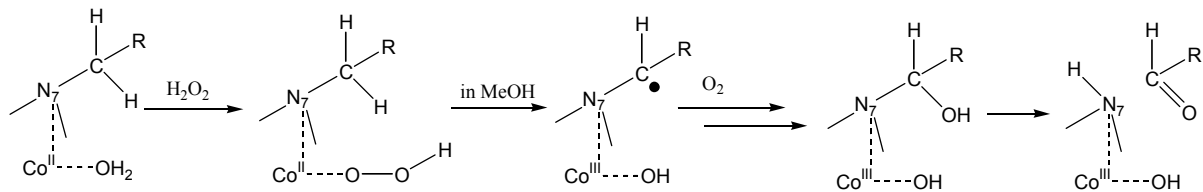


Abb. 2.4. Postulierter Reaktionsmechanismus für die intramolekulare N-Dealkylierung

Mangan(II)-Komplexe mit bekannten Bispidonliganden (mit N4- und N5-Donorsatz) wurden dargestellt und ihre Reaktion mit Wasserstoffperoxid wurde untersucht, um zu verstehen, ob eine Analogie zu divalenten Eisenkomplexen existiert, welche typische Fenton-Chemie zeigen und einige der gebildeten hochvalenten Eisenspezies katalytische Aktivität in der Oxidation von Olefinen zeigen. Diese Ergebnisse sind in Kapitel 8 präsentiert. Interessante spektroskopische Eigenschaften der Komplexe mit den Phenol-Bispidonliganden werden außerdem in diesem Kapitel behandelt. Für Untersuchungen zur Stabilität des Mangan(III)-N2py2PhOH-Komplexes wurden zeitabhängige UV-vis Spektren aufgenommen, die einen langsamen Zerfall der Mangan(III)-Spezies zeigen. Hierzu werden mögliche Reaktionspfade diskutiert.



### 3. Introduction

One of the main challenges in coordination chemistry is to find a correlation between structural and spectroscopic properties of metal complexes and their reactivities. During complexation the geometry around the metal ion is significantly changed. This change is strongly dependent on the arrangement and kind of ligand donors and has drastic effects on the properties. The spectroscopic changes can be explained by ligand field theory.<sup>1</sup>

The selectivity of a specific metal ion to a given ligand is a consequence of stabilization effects. Among these effects, preorganization<sup>2,3</sup> is of great importance. In a preorganized ligand the conformation of the metal-free form is the same as when the metal is coordinated to the ligand donors. In the optimal case, a preorganized ligand has a preference for a specific metal ion of ideal size. However, the elasticity of the coordination sphere (due to flat energy surfaces) can allow coordination of metal ions with a wide range of sizes. This effect has been observed in complexes of the highly rigid and preorganized bispidones (3,7-diazabicyclo[3.3.1]nonan-9-on derivatives,<sup>4,7</sup> Figure 3.1).

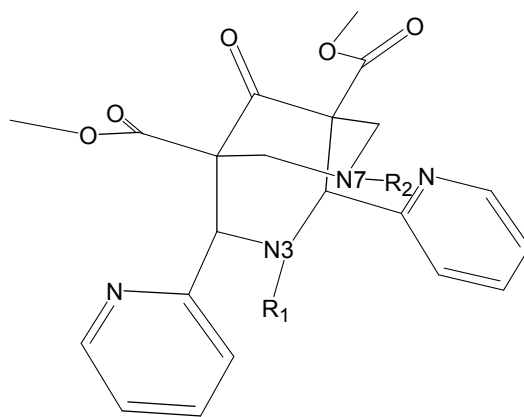


**Figure 3.1** The 3,7-diazabicyclo[3.3.1]nonan-9-on backbone

To achieve selectivity, electronic preferences also have to be met. Pearson's principle of hard and soft acceptors and donors (HSAB) categorizes the nature (ionic or covalent) and stability of metal-donor bonds.<sup>8</sup> Moreover, chelate effect,<sup>9</sup> macrocyclic effect<sup>10</sup> and solvent effects<sup>5</sup> must also be taken into account. Modification of the side chain groups in a bispidone, by selection of appropriate precursors in the synthesis, can change both the steric and the electronic properties of the corresponding metal complexes.

Oxidation of the central metal in complexes, leads often to significant modifications in structural and spectroscopic (magnetic, electronic) properties as well as in reactivities. Tuning of these properties is an efficient tool to develop new and active catalysts. For example, incorporation of electron donating groups in the side arms increases the electron density on the central metal ion, thereby stabilizing its oxidized form. This can be useful when designing complexes in which a metal center with a specific oxidation state is required.

Modeling the catalytic action of an enzyme requires consideration of both the electronic and structural features of its active site. The number and position of the donor groups taking part in metal ion coordination in the natural system has implications to the ligand design. Among others, flexibility of the coordination sphere and the availability of substrate binding sites (also steric demand) should be considered. The final goal is to tune the catalytic activity of the complexes to achieve activation of a specific reaction path by reducing the activation energy. This can be made possible by destabilization of the substrate in the substrate/catalyst complex, or by formation of a more stable transition state.<sup>3,11</sup>

The mononuclear copper enzyme galactose oxidase contains two tyrosine residues in the active site, one of which is oxidized to a tyrosyl radical in the catalytically active form of the enzyme and takes an active part in the oxidation of primary alcohols to aldehyde with the concomitant formation of H<sub>2</sub>O<sub>2</sub> from oxygen.<sup>12,13</sup> The stabilization of this radical species in model complexes has been achieved by tuning the electronic properties of the phenol ring. Incorporation of highly electron donating groups in ortho and para position could increase the electron density of the phenolic oxygen.<sup>14</sup> It was therefore of interest to investigate the copper(II) complexes of new bispidones with a phenolic side chain, to determine whether these can be stabilized in their phenoxy radical form.

The dicopper enzyme catechol oxidase catalyzes the conversion of *o*-catechols to *o*-quinones under aerobic conditions.<sup>15</sup> The catalytically active met-form of this enzyme has a side-on bound peroxide bridging the copper(II) centers.<sup>16</sup> As structural and functional mimics of catechol oxidase, numerous dicopper complexes have been reported.<sup>17-23</sup> It has been shown that cooperativity between the copper centers in binding the catechol substrate is a key aspect in the catalytic activity.<sup>16</sup> Strong reduction in the distance between the copper centers by using phenolate moiety as a bridging unit is a successful alternative.<sup>24</sup> From this, it was of interest to investigate whether the metal-metal separation in the dicopper complexes of newly designed,



dinucleating bispidone ligands with a bridging phenolate, shows some correlation in their ability to bind and oxidize catechol substrates.

Haloperoxidases are vanadium containing enzymes responsible for the halogenation of organic substrates in living organisms. The active site of this enzyme consists of a peroxo-vanadium(V) unit which binds a hydrogen peroxide co-oxidant and the substrate halogenide ion.<sup>25</sup> The question of whether the vanadium(V)-oxo-peroxo complexes of bispidone ligands act as active catalyst in the halogenation of organic substrates, arises.

Addition of hydrogen peroxide to the methanolic solution of the cobalt(II) complex with a tetradentate bispidone ligand has led not only to the oxidation of the central metal, but also to removal of an N-alkyl side chain.<sup>7</sup> Such intramolecular oxidative N-dealkylation is a major route in drug metabolism<sup>26,27</sup> and is often seen in oxidase and peroxidase enzymes such as horseradish peroxidase, cytochrome P450 and amine oxidase.<sup>28,29</sup> In low-molecular weight model complexes this reaction is also quite common, but more often seen in Cu-<sup>30</sup> and Fe-<sup>31</sup> containing systems. Relatively few examples with cobalt are known.<sup>32,33</sup> It was therefore of interest to study the oxidative N-dealkylation reaction in the above mentioned cobalt-bispidone complex in detail, in order to understand the reaction mechanism.

Iron complexes with bispidone-type ligands have been demonstrated to be efficient oxidation catalysts.<sup>34</sup> Their reaction with hydrogen peroxide was shown to produce catalytically active species,<sup>35</sup> which can lead to epoxidation or dihydroxylation of olefins. A lot of effort has been put into the development of low molecular weight, non-heme iron model complexes, which oxidize hydrocarbons in a Fenton-type reaction,<sup>36,37</sup> and relatively much is known about the efficiency of complexes with other transition metals.<sup>38-40</sup> Manganese(II) complexes of selected bispidone ligands were tested to ascertain whether their reaction with H<sub>2</sub>O<sub>2</sub> leads to some reactive intermediates.



## 4. Synthesis of bispidone ligands

### 4.1. Introduction

Bispidine-based compounds are found in nature as quinolizidine alkaloids and their most well known representative is sparteine. The first synthesis of bispidines was reported by Mannich and Mohs,<sup>41</sup> who condensed piperidine with formaldehyde and a primary amine.

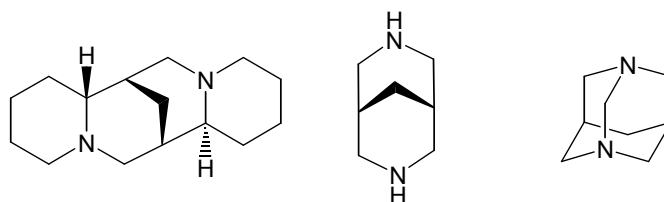


Figure 4.1. Structure of sparteine, bispidine and diazaadamantane

Generally, 3,7-diazabicyclo[3.3.1]nonane derivatives can be obtained via the following routes: (i) ring-cleavage reaction of diazaadamantane,<sup>42</sup> (ii) intramolecular cyclization of piperidines<sup>43</sup> and (iii) Mannich condensation.<sup>44</sup>

The most convenient method for the synthesis of 2,4-substituted bispidones is the last one, which actually comprises of two reactions: the first is the preparation of piperidone from 2 equivalents of aldehyde, 1 equivalent of primary amine and 1 equivalent of ketone with two activated acidic carbons in 1,3-position, using methanol or ethanol as solvent at 0°C and under strictly stoichiometric conditions;<sup>45,46</sup> the second reaction (preparation of bispidones) requires 1 equivalent of piperidone, 1.2 equivalents of the primary amine and 2.4 equivalents formaldehyde and it is carried out in refluxing methanol or ethanol in 2-3 hours.

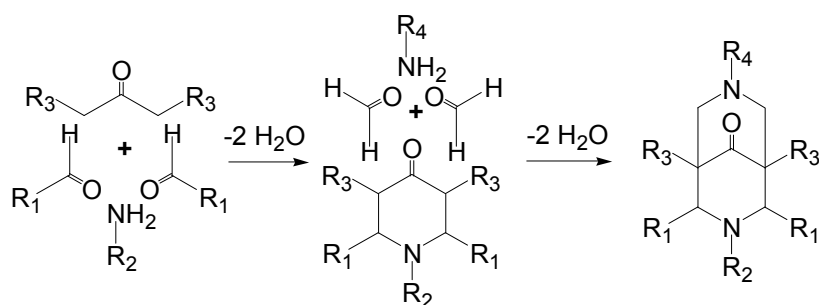
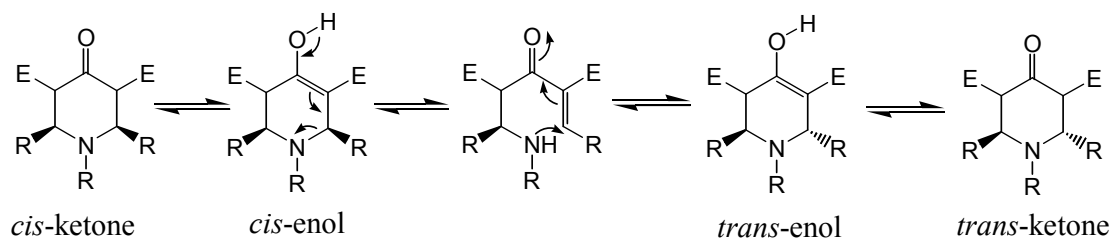


Figure 4.2. Two step synthesis of 3,7-diazabicyclo[3.3.1]nonanes

Both piperidones and bispidones were isolated as precipitates. When required, the solvent was reduced, completely removed, or treated with ultrasonic bath or flash chromatography on neutral alumina. By varying the substituents of the amine or aldehyde, different new bispidone ligands can be synthesized.

In alcoholic solution the piperidones always exist as an equilibrium mixture of the keto and enol forms.<sup>47</sup> The keto derivatives (cis/trans) initially tautomerize to the enol form which can then isomerize to the other (trans/cis) enol structure through ring opening. This enol form can tautomerize back to ketone. The ratio between the keto and enol structures depends on the degree of chelating H-bonds formed between the enolic proton and the keto oxygen, thus also on the nature of the solvent (polarity, protic or aprotic).



**Figure 4.3. Proposed mechanism of the piperidone isomerization**

Bispidones have three possible conformations: chair-chair, chair-boat and boat-boat (Figure 4.4). The interconversion between them is limited at room temperature, due to the rigidity of the bicyclic structure. From the point of view of coordination chemistry, the chair-chair conformation, in which the amino nitrogens face each other, is the most favorable conformer.

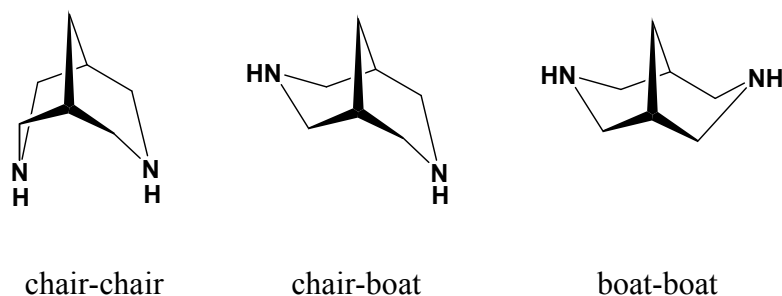


**Figure 4.4. Stable conformers of 3,7-diazabicyclo[3.3.1]nonanes**

The thermodynamically most stable conformer is usually the chair-chair one, which is also of importance for metal complexation. Sufficiently long reaction times under reflux lead to the exclusive formation of this conformer. Under such reaction conditions (reflux) not only conformational but also configurational changes occur in the structure of the bicycle. R1 groups (attached in 2,4 position) can be axial or equatorial, yielding endo/endo, endo/exo and exo/exo isomers. These structures are depicted in Figure 4.5 for the chair-chair conformer.

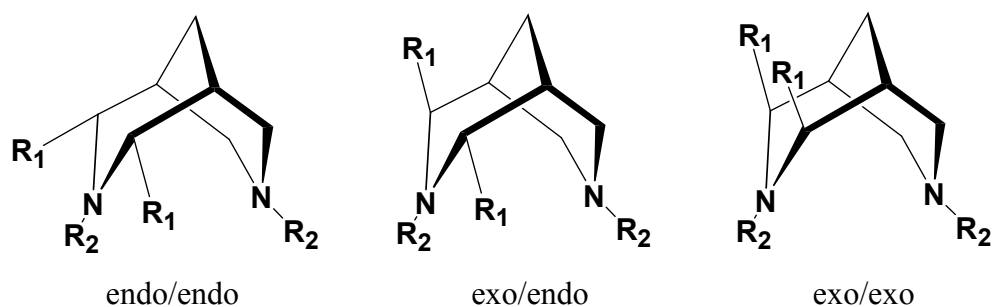


Figure 4.5. Configurational isomers of 2,4-substituted 3,7-diazabicyclo[3.3.1]nonanes

Among them the endo/endo configuration is the most suitable for metal complexation, having all donors in a favorable position. Since this isomer is the thermodynamically most stable one, adjusting the reaction conditions can lead exclusively to this desired highly preorganized structure.

#### 4.2. Target ligands

Bispidone ligands almost exclusively with a phenol moiety, were designed (Figure 4.6). One major group of these structures is based on the pentadentate N2py2PhOH ligand, which contains a phenol side chain at the N7 position. Incorporation of highly electron donating substituent(s) to the phenol moiety in ortho and para position, were expected to increase the electron density of the phenolic oxygen, which can be a crucial factor in the stabilization of phenoxy radicals formed by the oxidation of the phenol oxygen atom. Due to the increased electron density, a higher degree of charge-transfer interaction is expected for the metal-oxygen bond in their transition metal complexes. The extra stabilization can lead to a further increase in complex stability. The optimized synthesis of N2py2PhOH is described in this chapter together with the methoxy substituted vanilbis ligand. Attempts to prepare the bis-tBu derivative N2py2PhOHtBu are also presented.

The dinucleating ligands cresbis and tBuBis with a phenol linker were designed to mimic the active sites of dicopper enzymes, e.g. catecholases. The structure of these ligands shows high resemblance to the mononucleating ones, from where the N2py2-like bispidone cavity has been copied.

Bis-phenol ligands, with phenol groups attached in 2,4-positions to the bispidone backbone, were designed to use for the complexation with copper(II), in order to mimic the active site of galactose oxidase. Attempts to synthesize N2PhO2r, N2PhO2 and N2PhO2tBu are also reported and discussed in this chapter.

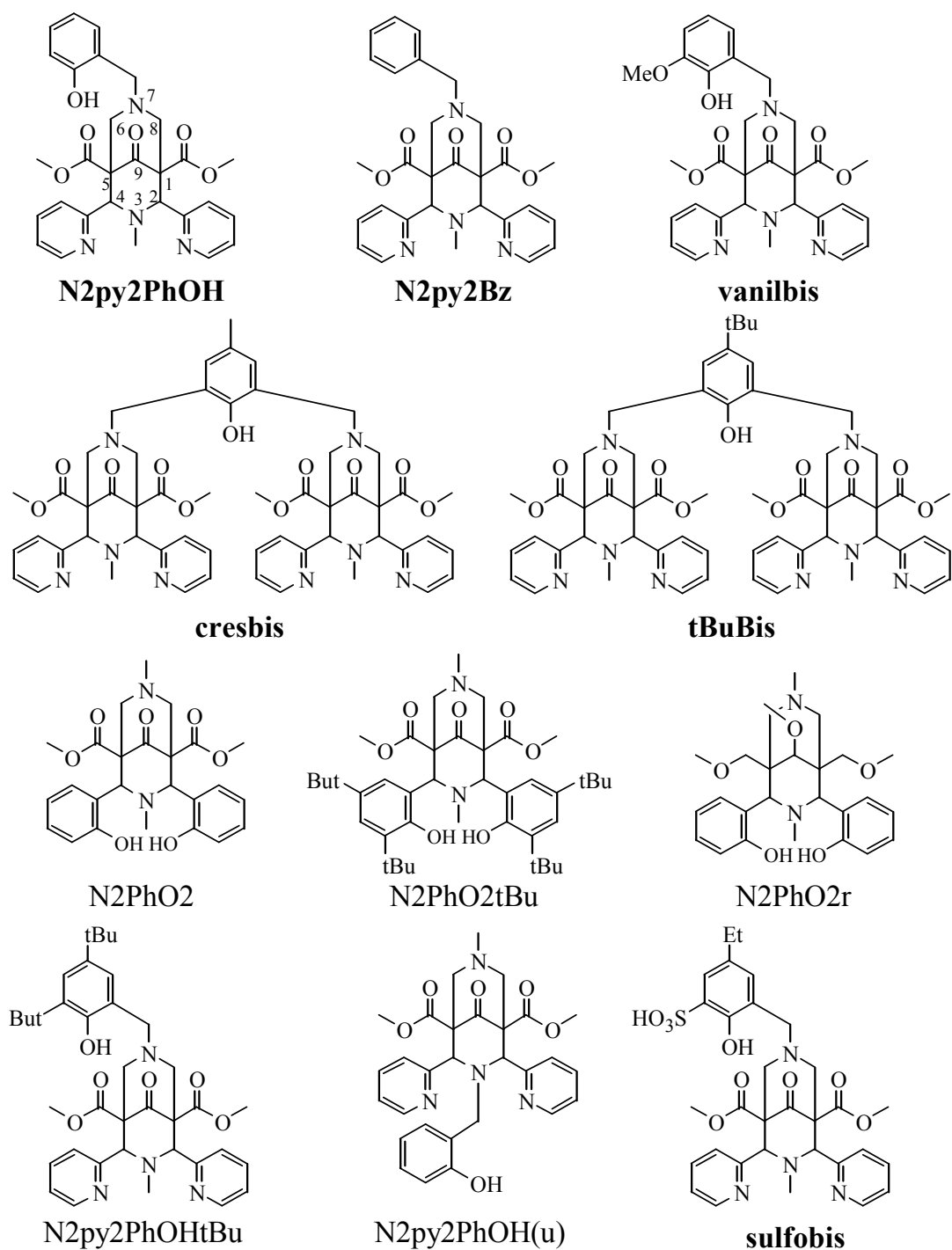
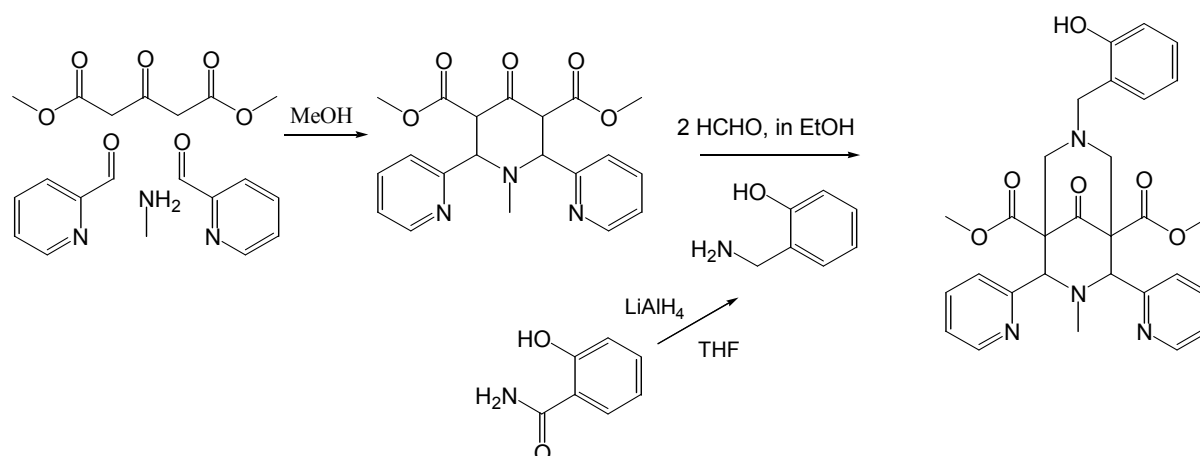


Figure 4.6. Structure of the ligands discussed in this chapter

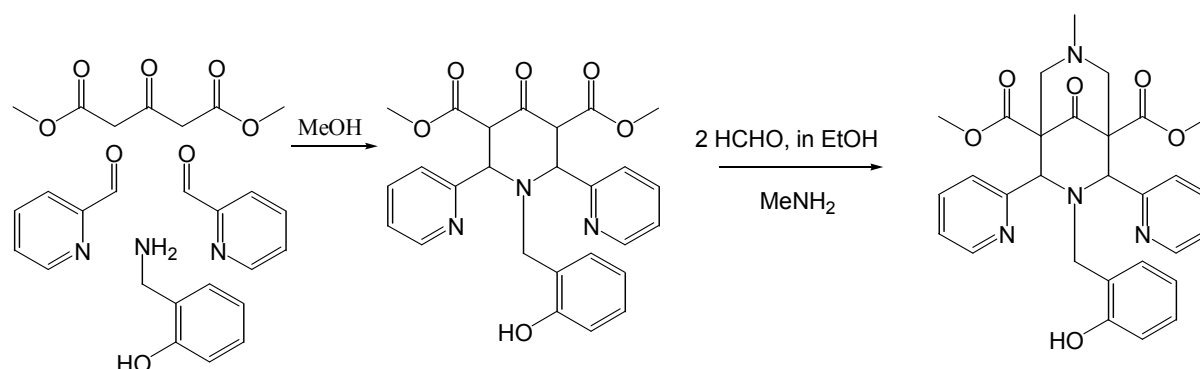
### 4.3. Synthesis of mononucleating phenol-bispidone ligands

#### 4.3.1. Synthesis of N2py2PhOH



Scheme 4.1. Synthetic route for the formation of N2py2PhOH

The amine precursor of N2py2PhOH was prepared by the reduction of salicylamide by LiAlH<sub>4</sub> in THF, optimizing a reported procedure.<sup>48</sup> The key step is the neutralization of phenolamine, since only the chargeless form will be extracted to the organic phase. The phenol-containing bispidone could be easily synthesized from this amine. Since o-hydroxy benzylamine itself is not soluble in ethanol, it was added to the reaction mixture as a solid. After addition, the amine is immediately dissolved, and the color of the solution becomes deeper, indicating that the Mannich condensation has taken place.



Scheme 4.2. Synthetic route for the formation of N2py2PhOH(u)

Attempts were made to synthesize the “unten”-analogue of N2py2PhOH, where the phenol moiety is attached to the N3, and N7 is methylated. The first step, the preparation of the NPy2PhOH piperidone, was relatively easy, but isolation of the product required an adjustment of the solvent system. Normally a recrystallization of the crude piperidone in a relatively small amount of dry ethanol is a successful method to get the pure product

precipitated in a reasonable time-scale. In our case the starting materials, picolylaldehyde and the phenolamine, may undergo a cyclization to form a benz-oxazoline derivative.<sup>49</sup> (Figure 4.7). This reaction requires presence of dry ethanol, which was normally used in our synthesis. This means however, that the addition of few drops of water may shift the equilibrium and the formation of the undesired side product can be avoided. Indeed, as an effect of the added water, the piperidone precipitated after some days.

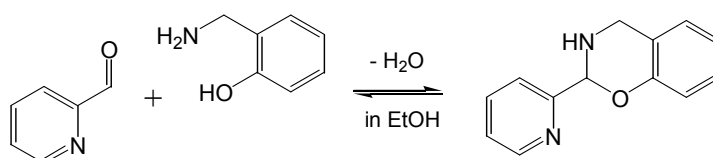


**Figure 4.7. Side reaction between the aldehyde and amine precursors during the preparation of the Npy2PhOH piperidone**

The second cyclization using the Npy2PhOH piperidone was unsuccessful. Here the phenol moiety is already attached to the piperidone, making it more sensitive to side reactions. The presence of formaldehyde and the basic methylamine give perfect conditions for hydroxymethylation. This kind of side reaction did not influence the formation of N2py2PhOH, probably because the added amine is a phenolamine, in which the phenolic group counterbalances the basicity of the amine unit.

#### *Crystal structure of N2py2PhOH*

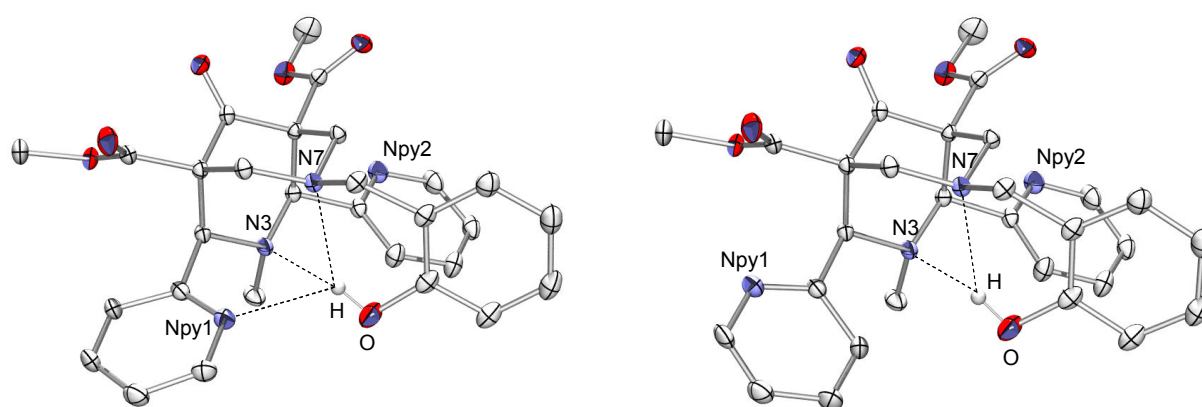


**Figure 4.8. The two conformers appearing in the disordered structure of N2py2PhOH ligand**

Crystals suitable for structure determination were obtained by recrystallization of the crude ligand from ethanol. One of the pyridine rings (Npy1) is disordered. The two conformations are



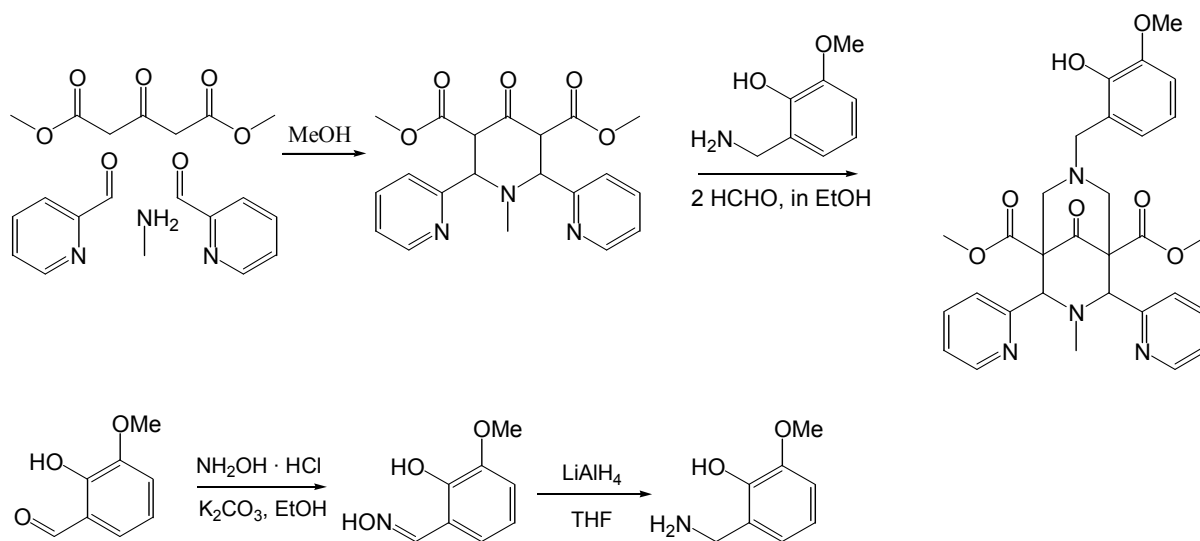
presented in Figure 4.8. The distance between the two amine nitrogens (2.901 Å) is the “standard” value for an unstrained bispidone cavity. Similar N3⋯N7 distances, measured in other bispidone ligands, demonstrate that the variation of the pendant groups does not significantly affect the geometry of the bicyclic cavity (2.899 Å in N2py2,<sup>50</sup> 2.867 Å in 6MeN2py2,<sup>50</sup> 2.933 Å in N2py4<sup>51</sup>). This indicates a high level of preorganization, with respect to the donors attached directly to the rigid bispidone backbone. The position of the phenol group is mainly determined by secondary interactions: the distance between the phenol hydrogen and the amine nitrogens falls into the typical interval for hydrogen bonds. ( $d(\text{N7}\cdots\text{HO}) = 2.153 \text{ \AA}$ ,  $d(\text{N3}\cdots\text{HO}) = 2.904 \text{ \AA}$ ). Further stabilization is achieved through the 6-membered ring formed by the N7-HO hydrogen bond. The two structural isomers differ in the position of one of the pyridine rings: in one structure the nitrogen donor faces the ligand cavity, while in the second structure it is rotated by approx. 180° away from the cavity. In the first geometry, a third H-bond is formed between the pyridine nitrogen and the phenol hydrogen ( $d(\text{Npy1}\cdots\text{HO}) = 2.356 \text{ \AA}$ ). This interaction is missing in the other isomer, which has a higher symmetry. Both pyridine nitrogens point away from the ligand cavity, and the positions of the two pyridines with respect to the bispidone cavity is similar, which is reflected in the torsion angles ( $\text{C1-C2-C}_A\text{-Npy1} = 66.53^\circ$ ;  $\text{C5-C4-C}_{A2}\text{-N2} = -74.21^\circ$  or  $\text{N3-C2-C}_A\text{-Npy1} = -166.91^\circ$ ;  $\text{N3-C4-C}_{A2}\text{-N2} = 160.97^\circ$ ). The rigidity of the bispidone backbone is highlighted by a constant N3⋯N7 distance (see above). The N3 and N7 amine donors, together with the donors of the side chains, make bispidone ligands highly preorganized.

DFT calculations were performed with the B3LYP functional at the 6-31G(d) level, and these show that both structures correspond to minima on the potential energy surface. The difference in their single point energies at triple zeta level (using the TZV basis set) is 8.20 kJ/mol, which is in accordance with a ~ 3:1 ratio between the two structures at room temperature. From this, the coexistence of the two forms (disorder of one pyridine ring) in the crystal structure can be explained. It is known that the rotation of the pyridine rings is hindered: the rotation barrier around the C2-aryl and C4-aryl axis was calculated to be 75 kJ/mol.<sup>52</sup> The disorder of the pyridine rings observed in the crystal structures (determined at 100 K) therefore corresponds to a real physical mixture of two kinetically stable isomers.

#### 4.3.2. Synthesis of vanilbis

The amine precursor for the *m*-methoxy-*o*-phenol-substituted bispidone (vanilbis) was synthesized from *o*-vanillin, which was first oximated<sup>53</sup> and the oxime then reduced with LiAlH<sub>4</sub> using a NaOH workup developed by Schaefer's group.<sup>54</sup> Surprisingly, the salt content

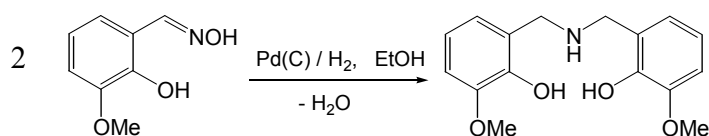
of the free phenolamine could not be removed by repeated washing with water, but this did not influence the following synthetic step and the cyclization with this precursor yielded the desired bispidone derivative.



**Scheme 4.3. Synthetic route for the formation of vanilbis**

For the reduction of o-vanillin aldoxime to form 2-methoxy-6-aminomethylphenol, several methods were tested. Reduction by zinc/acetic acid, based on the procedure of Michelsen, caused unexpected problems.<sup>55</sup> Normally the formed amine can be easily isolated from the reaction mixture, but in our case the reduced phenolamine was coordinated to zinc(II) ions, formed during the reaction from the elemental zinc reductant. This complexation is enhanced by the 6-membered chelate ring, and involves the phenol oxygen and the amine nitrogen of the phenolamine. In the reported procedure a workup using alkaline medium yields the free amine, but these conditions are also highly favorable for the coordination of the amine to zinc(II).

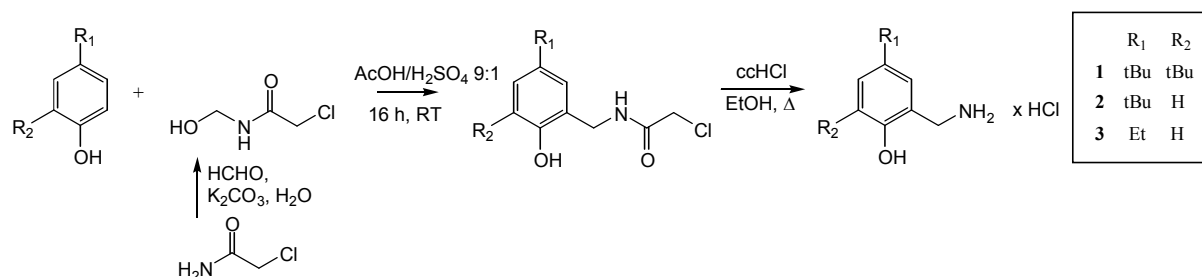
Catalytic hydrogenation of o-vanillin aldoxime with palladium/charcoal in ethanol gives no primary, but a secondary amine, which can be formally described as two primary amines condensed together (Scheme 4.4.). Such reduction pathways are known for different types of oximes (e.g.: salicylaldoxime, 2-furylaldoxime).<sup>56</sup>



**Scheme 4.4. Synthetic route for the formation of bis(2-hydroxy-3-methoxy-benzyl)amine**

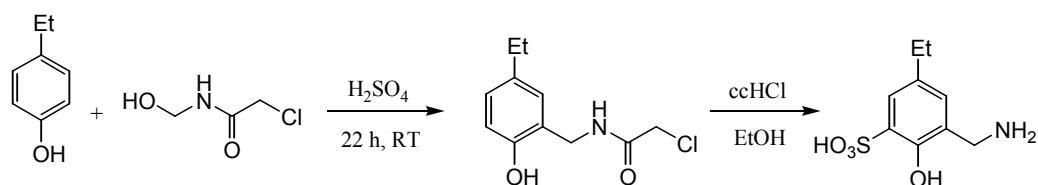
### 4.3.3. Synthesis of *o*-aminophenols through amidomethylation, synthesis of sulfobis

In order to incorporate a phenolic moiety at positions 3 or 7 on the bispidone, *o*-aminophenols have to be obtained as precursors for the Mannich condensations. Preparation of a series of such aminophenols was reported.<sup>57</sup> Optimized reaction conditions for phenols with substituents of different number, position and electronic nature are described. In all cases the amidomethylating agent *N*-hydroxymethyl-2-chloroacetamide was prepared by hydroxymethylation of 2-chloroacetamide with formaldehyde.<sup>58</sup> For monoamidomethylation a 9:1 acetic acid/sulphuric acid mixture was used. Under these conditions no 2,6-diamide is formed, only the monoamide. These amides were then hydrolyzed by hydrochloric acid in boiling ethanol. The precursor amino-hydrochlorides **1-3** were obtained in a pure form. Their analytical data and that of their intermediates (<sup>1</sup>H NMR, CI-MS, elemental analysis) are in accordance with the reported values.



**Scheme 4.5.** Synthetic route for the formation of substituted *o*-aminomethyl phenols via amidomethylation

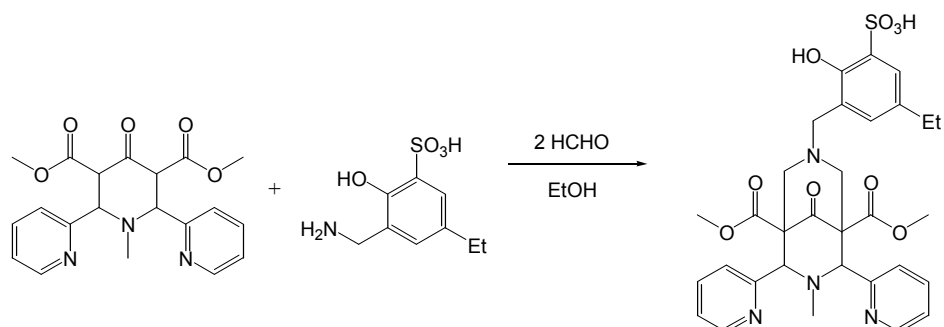
In the case of bis-aminomethyl precursors a different medium was reported to be efficient for the amidomethylation step.<sup>57</sup> When using pure sulphuric acid, phenols are amidomethylated at both (2 and 6) positions. Addition of ice gives a white precipitate (which is isolated as the diamide) and a black tar. Since the yields obtained were far below the reported values, more product was thought to be present in the tar. For this reason both the solid white diamide and the black tar were hydrolyzed with hydrochloric acid in boiling ethanol.



**Scheme 4.6.** Synthetic route for the formation of 6-sulfonato-2-(aminomethyl)-4-ethylphenol

In the first case, as expected, the diamino hydrochloride was formed. Surprisingly however, a monosulfonato-monoamino phenol was isolated from the black tar. From the <sup>1</sup>H-NMR, asymmetric substitution at 2 and 6 positions was deduced, giving two distinct singlet peaks

for the protons at positions 3 and 5. Elemental analysis ruled out the presence of any chloride in the sample.



**Scheme 4.7. Synthetic route for the formation of sulfobis**

The neutral sulfonated aminophenol was directly applied in the second Mannich-condensation to form the corresponding bispidone (Scheme 4.7.). The sulfonato-phenol-bispidone ligand sulfobis was isolated in the usual way (precipitation from the ethanolic solution), though with a relatively low yield. This probably is due to the presence of highly polar substituents, which increase the solubility in polar solvents. The ligand was characterized by ESI-MS and IR spectroscopies and elemental analysis. Unfortunately, no solvents suitable for  $^1\text{H-NMR}$  measurements were found. The fact that both positive and negative ESI-MS spectra gave the mole peaks at  $[\text{M}+1]^+$  and  $[\text{M}-1]^-$  position, indicates the presence of sulfonate, which can be easily deprotonated under the conditions of the MS-measurement. The two very intense bands at  $1240$  and  $1163\text{ cm}^{-1}$  in the IR spectrum lie in the typical range of sulfonates. Intense bands at  $1741$  and  $1439\text{ cm}^{-1}$ , assigned as  $\text{C}=\text{O}$  and  $\text{C}=\text{N}(\text{pyridine})$  stretching respectively, show the existence of the bispidone unit in the ligand.

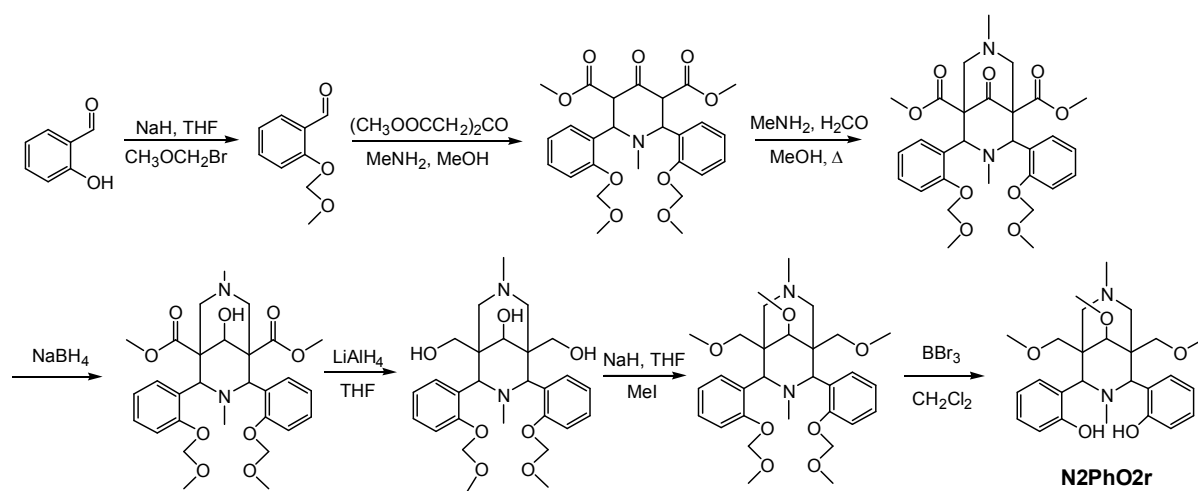
In case of the aminophenol-hydrochlorides **1-3**, the Mannich condensation reaction was not without difficulties. Since the bispidone formation occurs only if the amines are in free form, the hydrochloride salts first had to be neutralized. When stoichiometric amounts of aqueous  $\text{K}_2\text{CO}_3$  are added to the aqueous amine-hydrochlorides, the free amines **2** and **3** immediately precipitate, but their extraction fails.

Using the di-tert-butyl amine **1**, both the neutralization and the extraction were successful (the organic phase was purple), and the conversion to the free amine was above 90%. Using the typical conditions for bispidone synthesis to get  $\text{N}2\text{py}2\text{PhOHtBu}$ , the Mannich-condensation seemed to work and the ESI(+)-MS spectra indicated the presence of the desired bispidone in the reaction mixture ( $643.5\text{ }[\text{M}+\text{H}]^+$ ,  $\text{C}_{37}\text{H}_{46}\text{N}_4\text{O}_6 = \text{M}$ ). Other than the mole peak, a much more intensive peak, assignable to  $\text{N}2\text{py}2$  was also observed. From this spectrum it is not clear whether the  $\text{N}2\text{py}2$  signals originate from the bispidone formed, or simply as a fragment

in the MS-instrument. Although the formation of the desired N2py2PhOHTBu was confirmed, the ligand could not be isolated. This is probably due to the highly apolar and bulky tert-butyl groups, together with the polar phenolic unit.

In case of the mono tert-butyl and ethyl aminohydrochlorides **2** and **3**, the extraction with CHCl<sub>3</sub> was not successful and the direct use of their neutralized solutions did not lead to product formation, which was indicated by ESI-MS spectra recorded for the reaction mixtures after refluxing for 3 hours.

#### 4.3.4. Synthesis of N2PhO2r



**Scheme 4.8.** Synthetic route for the formation of N2PhO2r

Although the procedure for the preparation of this bis-phenol ligand has been reported,<sup>59</sup> to repeat this reaction led to several difficulties. In order to incorporate phenol groups in 2 and 4 positions, a phenol-aldehyde was used. The starting material, salicylaldehyde, had to be protected at the phenolic positions, since the presence of free OH-groups leads to several possibilities for unwanted side reactions (e.g. hydroxymethylation in the presence of formaldehyde). The methoxymethyl (MOM) group is a suitable choice, since it is highly resistant and was reported to be selectively removable.<sup>60</sup> Methylation could not be used, because removal of the methyl group might damage other parts of the bispidone structure. The first step gives MOM-protected salicylaldehyde, as reported, in almost quantitative yields. Using the protected aldehyde, the piperidone could be obtained in a usual manner, with relatively good yields, in consistence with the literature.

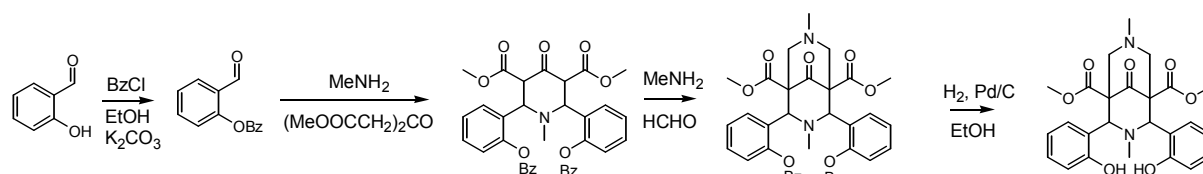
The second cyclization to get the MOM-protected bispidone, led to some unexpected problems: the Mannich reaction goes both forward and backward. Judging from <sup>1</sup>H NMR and MS spectra of the reaction mixture, both the MOM-bispidone and the retro-Mannich aldehyde

can be seen. As discussed at the beginning of this chapter, exhaustive heating is important to get more complete conversion and to obtain the bispidone in the desired conformation and configuration. It seems that longer heating enhances the retro reaction as well: the dense MOM-aldehyde is formed. From this dense oil it was extremely difficult to extract the MOM-bispidone as a white precipitate.

The protecting group cannot be directly removed at this stage, because of the sensitivity of the keto and ester groups, which need to be protected first. As expected, consecutive reduction with  $\text{NaBH}_4$  and  $\text{LiAlH}_4$ , reduced the keto and the ester units in relatively good yields. Direct application of  $\text{LiAlH}_4$  would have yielded a mixture of syn/anti isomers (depending on the position of the C9-bound OH group) and for this reason the reduction had to be carried out in two steps. The three alcoholic groups of the fully reduced bispidine were methylated, almost quantitatively, in consistence with literature. The final step, that is, isolation of the free bisphenol ligand after the removal of the MOM from the phenol groups was not successful. Although the reaction was carried out at  $-40^\circ\text{C}$ , as reported, and conversion was confirmed by TLC, it seems that the free ligand was decomposed during workup with base. Interestingly, a white precipitate could be isolated, but the MS did not indicate formation of the expected product. Attempts were made to check if the tetradentate ligand could be isolated in form of a metal complex, but addition of inorganic Cu(II) salt did not result in any deeper color (though Cu-phenolates are known to have a very intense charge-transfer band in the UV-vis spectrum around 450 nm), and treatment of this mixture on an SP-Sephadex C25 column showed no elutable components.

#### 4.3.5. Synthesis of N2PhO2 using benzyl as protection group

From the experience above, a new concept was developed, which uses a different protecting group, whose removal can be carried out under milder conditions. This step therefore does not influence the keto and ester moieties, such as was the case for the MOM group. For this reason, benzyl was chosen as protecting group. In this procedure, the further protection of the keto and ester units (reduction in two steps and methylation) could be omitted, which reduces the number of synthetic steps (Scheme 4.9).



Scheme 4.9. Synthetic route for the formation of N2PhO2

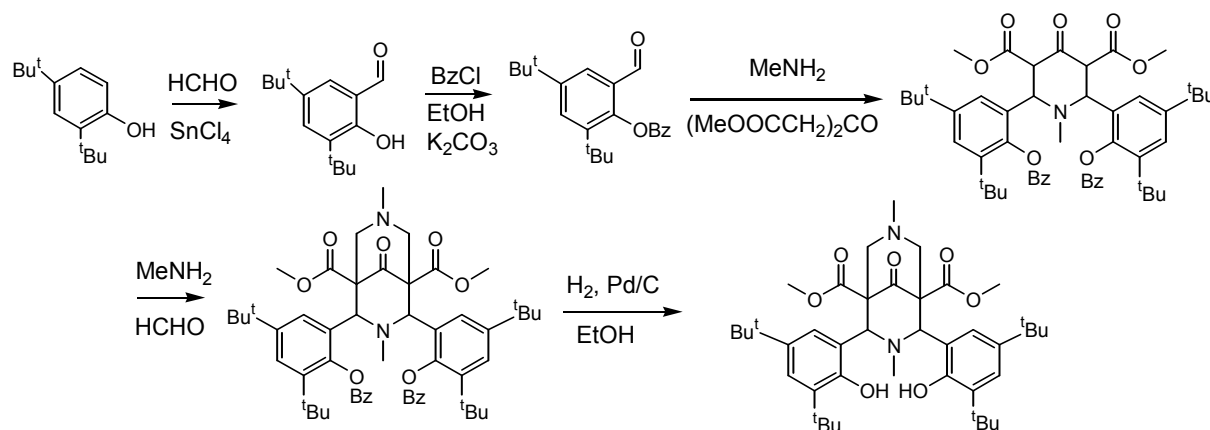
In the first step, salicylaldehyde was benzylated using a published procedure.<sup>61</sup> After workup, a mixture of benzylated salicylaldehyde and dibenzylether was obtained. Since dibenzylether is more volatile than the aldehyde, the two products could be separated under vacuum.

Using the benzylated aldehyde, a new piperidone derivative could be synthesized successfully, using the standard conditions.

Synthesis of the benzyl protected bispidone was carried out in a classical manner, namely adding 20% excess of formaldehyde and methylamine to the ethanolic slurry of the piperidone, followed by a 3 h reflux that gives a clear yellow/brownish solution. A quick solution mass-spectroscopic analysis revealed the formation of the product ( $649.29 [M+H]^+$ ), but the isolation lead to difficulties. Direct precipitation by addition of ethanol and methanol failed. Addition of solvents with different polarities (ether, hexane, THF, petrolether) did not precipitate the product, and a flash chromatography using basic alumina was also ineffective. Since the phenol groups are protected, this bispidone has only two efficient donors, i.e. the tertiary amine nitrogens. Therefore, isolation as a metal complex was not a useful alternative.

#### 4.3.6. Synthesis of *N2PhO2tBu*

As mentioned already, the main goal of the design of bis-phenol ligands was to mimic the structure and function of the mononuclear copper enzyme galactose oxidase, which is known to have two tyrosine phenolates in its active site. It is generally accepted and experimentally evidenced that during the enzymatic cycle the phenolic units are oxidized to phenoxy radicals.<sup>13</sup> Stabilization of such radical species requires a high electron density around the phenol oxygen. Several low-molecular-weight model complexes are known for this enzyme, which have efficient electron donating groups (e.g. tert-butyl) in ortho and para positions.<sup>14</sup> Inspired from previous studies, a bis-phenol bispidone with two tert-butyl groups on each phenolic unit was designed.



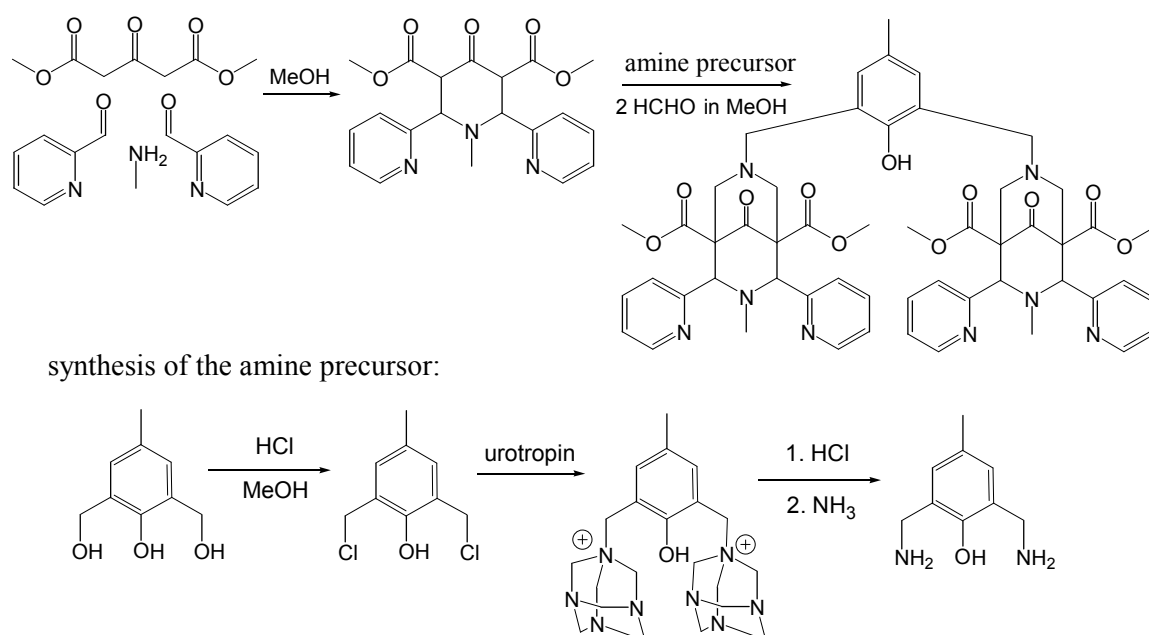
Scheme 4.10. Synthetic route for the formation of *N2PhO2tBu*

The synthetic strategy strongly resembles the previous one, but the substituted salicylaldehyde derivative had to be prepared first. The benzylated bis-tert-butyl salicylaldehyde was prepared according to reported procedures. In the first step a 2,4 di-tert-butylphenol was formylated with formaldehyde using  $\text{SnCl}_4$  catalyst,<sup>62</sup> followed by benzylation with benzyl chloride.<sup>63</sup> Both reactions worked well, with yields close to those reported. Using the obtained substituted and protected aldehyde, the first cyclization under classical Mannich conditions was carried out. The formation of the expected piperidone was confirmed by electrospray mass-spectrometry (ESI(+): 819.2  $[\text{M}+\text{H}]^+$ ), but none of the normally used approaches for isolation worked and no precipitate was formed from ethanolic or methanolic solutions. It is possible that, due to the presence of both the polar phenol group and the highly apolar bulky tert-butyl and benzyl groups the piperidone does not precipitate. Again, isolation in form of metal complexes was not possible due to the lack of a sufficient number of donors.

#### 4.4. Synthesis of dinucleating phenol-bispidone ligands

##### 4.4.1. Synthesis of cresbis

For the synthesis of the phenol-bridged bis-bispidone ligand cresbis not only a piperidone Npy2 and formaldehyde, but also a corresponding amine is required, as shown in Scheme 4.11. The amine precursor, 2,6-bis(aminomethyl)-4-methylphenol was synthesized according to a reported procedure, using 2,6-bis(hydroxymethyl)-4-methylphenol as starting material, which was bis-chlorinated using HCl gas in methanol. This intermediate was converted to a bis-urotropinium salt, which was hydrolyzed by concentrated HCl in ethanol and finally neutralized by aqueous ammonia.<sup>64</sup>

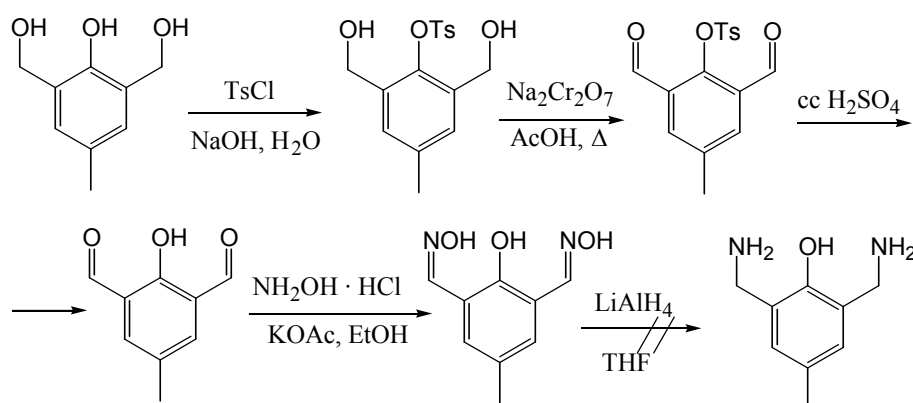


Scheme 4.11. Synthetic route for the formation of cresbis



To obtain yields close to the published values, the following points were shown to be crucial: During preparation of concentrated HCl solution in MeOH, cooling with a salt-ice mixture and vigorous stirring is required. Complete evaporation of the unreacted HCl and of the solvent had to be done at low temperature. During hydrolysis of the urotropinium salt with HCl it is not simple to judge if further heating leads to the formation of more formaldehyde (which is an indication that the hydrolysis is not complete). Heating for more than 5 hours does not improve the yield of the reaction. The amount of solvent at this hydrolysis step is relatively small, but heating till complete dryness should be avoided. The diamine-monohydrochloride salt final product precipitates as a jelly (as an effect of the added ammonia). This is still water soluble, and washing of the yellow product with water can redissolve some of it. However, a not thorough enough treatment with water can leave some  $\text{NH}_4\text{Cl}$  in the product.

Another synthetic route was also attempted for the preparation of the amine precursor.



**Scheme 4.12.** Synthesis route for the formation of 2,6-bis(aminomethyl)-4-methylphenol through a dioxime

The idea was to convert the alcoholic hydroxyl groups to aldehyde, then to oxime and finally to amines. The oxidation of aliphatic alcohol groups to aldehyde requires primarily the protection of the phenolic group via tosylation.<sup>65</sup> Oximation of the deprotected dialdehyde was performed according to a reported procedure,<sup>66</sup> using a large excess of hydroxylamine hydrochloride and potassium acetate in dry ethanol, and water for the precipitation of the oxime. Unfortunately, the reduction of the oxime with  $\text{LiAlH}_4$  was not successful and the product could not be isolated by extraction of the quenched aqueous THF phase with dichloromethane, even with careful control of the pH. It is likely that the pH-range in which the ligand exists as neutral species, is very narrow (both aliphatic amines and phenols have a  $\text{pK}_a$  value around 9). In case of a monoamino-monophenol it is easier to adjust the conditions,

since there is only one of each kind of substituent (see preparation of 2-aminomethylphenol in this Chapter), but the insertion of a second amine makes it more difficult to achieve a protonation/deprotonation of only one of two amines. Other reduction methods were also tested, but did not lead to the desired diamine. Catalytic reduction with Pd/C, for example, left the oxime intact, as was shown in the  $^1\text{H-NMR}$ .

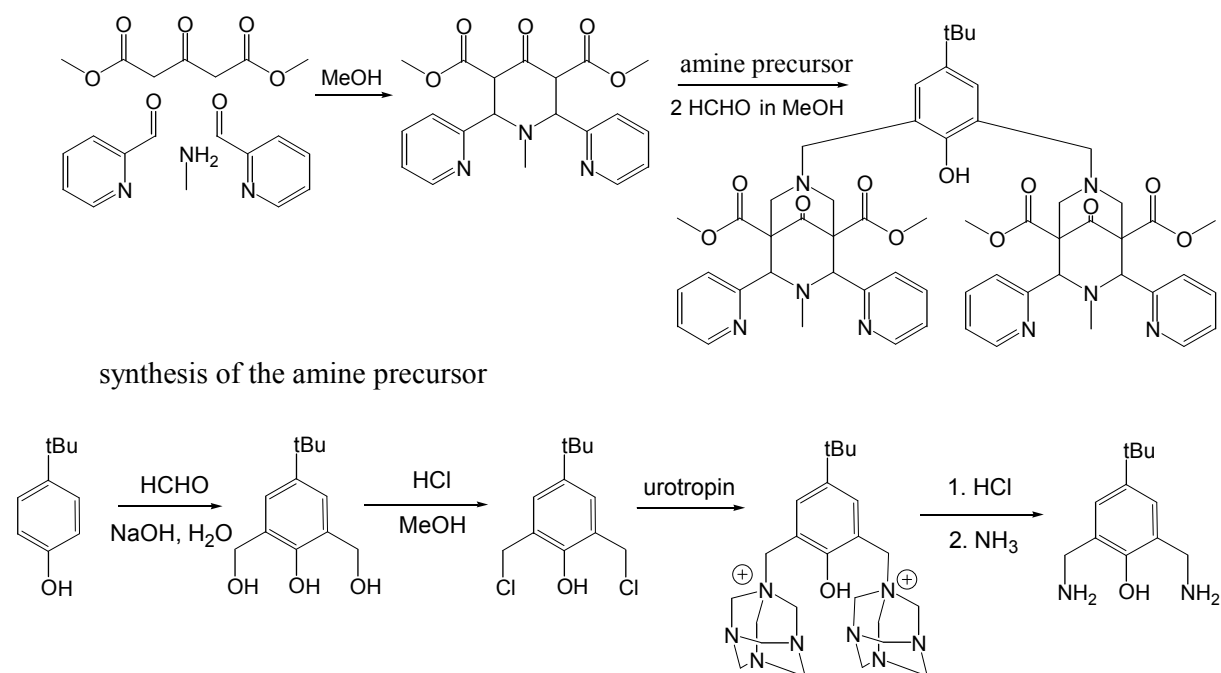
The diaminophenol precursor, prepared via the urotropinium-salt pathway, was used without further purification in the Mannich condensation reaction. Under the generally applied conditions for the conversion of piperidones to bispidones, the cresbis ligand was formed and isolated as a pale white precipitate after addition of water. Recrystallization of cresbis was unsuccessful, probably because of the low amount of the ligands obtained. The pale white color of the ligand is not the result of impurities, since flash chromatography on basic alumina does not retain any colored side products. The UV-vis spectrum shows an intense band at 420 nm. The existence of such a band may be related to the deprotonation of the phenol unit, or to a radical species. The sharp signals in the EPR spectra supported the latter possibility. In parallel with this, the significant broadening in the  $^1\text{H-NMR}$  spectra, together with the high noise level suggest the existence of paramagnetic species. Moreover, the elemental analysis fits perfectly when considering only the ligand with bound water molecules.

#### 4.4.2. Synthesis of *tBuBis*

The synthesis of the *tBuBis* ligand was carried out in analogy to that of cresbis. The analogous starting material, 2,6-bis(hydroxymethyl)-4-*tert*-butylphenol was prepared by bis-hydroxymethylation of 4-*tert*-butylphenol, using a known procedure and with alkaline solution of aqueous formaldehyde.<sup>67</sup> The formed triol was then treated in a similar way to that used in the synthesis of cresbis;<sup>64</sup> namely, substitution of alcoholic hydroxyl groups to chlorine with HCl gas in methanol, synthesis of a bis-urotropinium salt with hexamethylene-tetramine, which was then hydrolyzed with HCl/EtOH.

The yield is relatively low, but enough to perform the Mannich-condensation and get the *tBu*-phenol bridged bis-bispidone ligand, which was precipitated by the addition of water to the ethanolic solution of the crude product. Recrystallization was again not successful, probably because of the low amount obtained. Similar to cresbis, *tBuBis* appears as pale white solid, the color of which is not the result of impurities, since flash chromatography on basic alumina does not retain any colored side products. The UV-vis spectrum also shows an intensive band around 420 nm, which may be related to the deprotonation of the phenol group, or to a radical

species. The EPR and NMR spectra support the latter possibility, although the elemental analysis of tBuBis could not be fitted unambiguously.



**Scheme 4.13.** Synthetic route for the formation of tBuBis

One possibility, may be the coexistence of tBuBis and tBu-phenol in the sample. The ligand mass was unambiguously assigned in different MS-spectra (FAB, MALDI, ESI), but formation of the tBu-phenol from the diamine starting material is not feasible.

Another possible assignment could be a hydrated “large fragment”, Fragment<sub>1</sub>, which can be formally derived by the cleavage of the bond between N7 and the bridging methylene carbon (Figure 4.9). Although such a “species” is always seen in mass spectra, its formation and stabilization under normal conditions is not realistic. Furthermore, the original mole peak of the ligand cannot be explained by this structure.

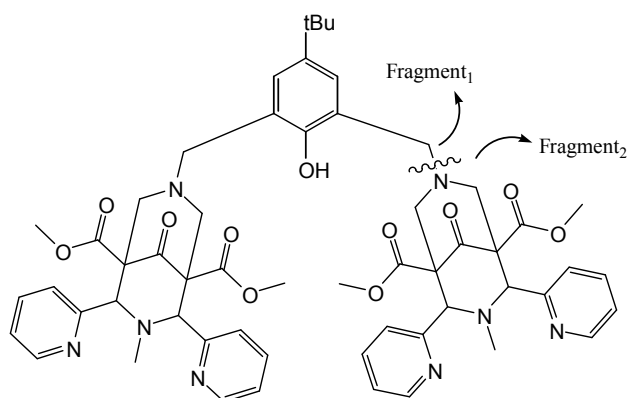


**Figure 4.9.** Structure of Fragment<sub>1</sub> and Fragment<sub>2</sub>, derived by homolytic cleavage of C-N7 bond in tBuBis

A third explanation would be a [2+2] cyclic dimer, which is hard to imagine from the synthetic point of view (substitution of the N3-methyl groups to the bridging phenol is not realistic, Figure 4.10). Moreover, the mole peak of such species was not seen in the mass spectra. The ratio between piperidone and the diamine was set to 1 : 2.4 and under these conditions a 2:2 structure is not to be expected.

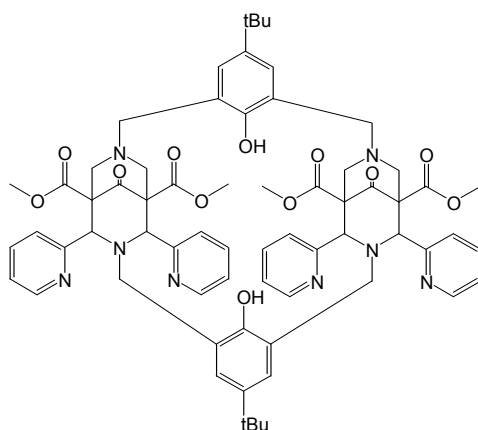


**Figure 4.10.** Structure of the hypothetical “[2+2] cyclic dimer”

The IR spectra of cresbis and tBuBis show almost identical pattern, with the only significant deviation found in the intensity of the C-H stretching bands, which is understandable, since in tBuBis there are more C-H bonds to vibrate (due to the presence of tert-butyl group, instead of a methyl group).

## 5. Mono- and dinuclear copper(II) complexes with phenol-bispidone ligands as models for galactose oxidase and catechol oxidase

### 5.1. Introduction

Galactose oxidase belongs to the few members of the mononuclear copper enzyme family and catalyzes the oxidation of primary alcohols to the corresponding aldehydes, with a concomitant reduction of  $O_2$  to  $H_2O_2$ .<sup>68,69</sup> The central copper is bound to two tyrosinates, two histidine imidazoles and a water co-ligand in a square-pyramidal geometry.<sup>12</sup> The oxidized (and catalytically active) form of the enzyme contains a copper(II) center, antiferromagnetically coupled to a tyrosyl radical, which is responsible for the hydrogen atom abstraction from the substrate molecule (Figure 5.1).

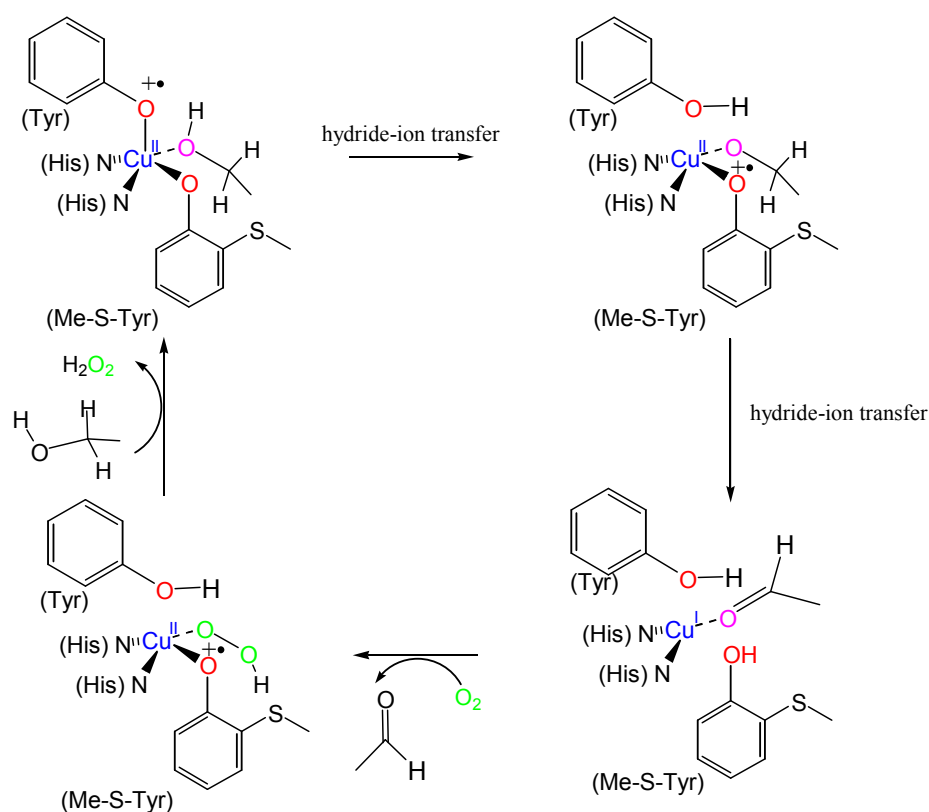


Figure 5.1. Proposed mechanism for the catalytic cycle of galactose oxidase<sup>13</sup>

The switch between the oxidized radical form and the reduced neutral phenol structure, and the concomitant change between the oxidation states of copper, are important elements in the catalytic cycle. In the first step, the phenoxyl radical initiates hydride-ion transfer from the primary alcohol by forming the primary aldehyde. At this stage the copper(II) center is reduced to the monovalent form. In the second step of the catalytic cycle, the product is

released and the central copper(I) is oxidized back to copper(II) by the reduction of elemental oxygen to hydrogen peroxide.<sup>13</sup>

As structural models for this enzyme, ligands containing pyridyl-alkylamines with one<sup>70,71</sup> or two<sup>14,72</sup> phenolate units have been the subject of numerous investigations. Copper(II) complexes of triazacyclononane derived ligands with different numbers of phenolic moieties attached to the macrocycle, were studied in detail.<sup>73,74</sup> Other types of ligand cores, such as salen<sup>75</sup> or tris-pyrazolyl borate with phenolate co-ligands<sup>76</sup> were also used as structural models for galactose oxidase. In general, the stability of the phenoxy radical complex species could be increased by attaching electron donating groups (<sup>t</sup>Bu) in the *o/p* position, thus increasing the electron density on the phenolic oxygen.

As for functional models, in most reported cases the first phase of the reaction, namely the interaction of the copper(II) phenoxy radical with primary alcohols, was studied in depth. Usually the catalytically active phenoxy radical species was electrochemically generated, and was directly treated with the substrate, without being isolated. Due to the efficiency of the oxidation (yields of the obtained aldehydes and hydrogen peroxide), the role of this copper(II) phenoxy radical species was assumed, but not experimentally supported.<sup>77</sup>

Catechol oxidases are ubiquitous plant enzymes which catalyze the oxidation of *ortho*-catechols to *ortho*-quinones in the presence of oxygen.<sup>15</sup> These enzymes belong to the type III copper proteins, characterized by a dinuclear copper active site. The crystal structure of catechol oxidase from sweet potatoes (*Ipomoea batatas*) has been reported in several forms. In the reduced deoxy Cu<sup>I</sup>...Cu<sup>I</sup> state three histidines are coordinated to each copper in a trigonal planar geometry, in the oxidized Cu<sup>II</sup>...Cu<sup>II</sup> met-form the coordination number around the copper centers increases by binding a hydroxide in a bridging mode which results in a distorted tetrahedral geometry at each of the two copper(II) centers.<sup>16</sup> The enzyme is EPR silent in the native met-form, due to a strong antiferromagnetic coupling between the OH-bridged copper(II) centers.<sup>78</sup>

Figure 5.2 shows one of the postulated mechanisms for the catalytic cycle of catechol oxidase. By removal of a loosely bound solvent molecule from the Cu<sub>A</sub> site in the dicopper(I) form of the enzyme, oxygen is coordinated in a bridging side-on ( $\mu$ - $\eta^2$ - $\eta^2$ ) mode to the oxidized form of catechol oxidase, forming a Cu(II)-peroxo complex. This is followed by the binding of *o*-catechol to copper(II) center. Monodentate coordination, following deprotonation of the catechol, has been proposed.<sup>16</sup> Two electrons from the substrate reduce the peroxo unit, which leads to cleavage of the O-O bond. One of the oxygens forms water by proton uptake and is

eliminated from the coordination sphere of the copper(II) centers. The removal of the oxidized substrate enables binding of another catechol, which can reduce the two copper(II) centers to the active dicopper(I) form, with the concomitant formation of o-quinone.

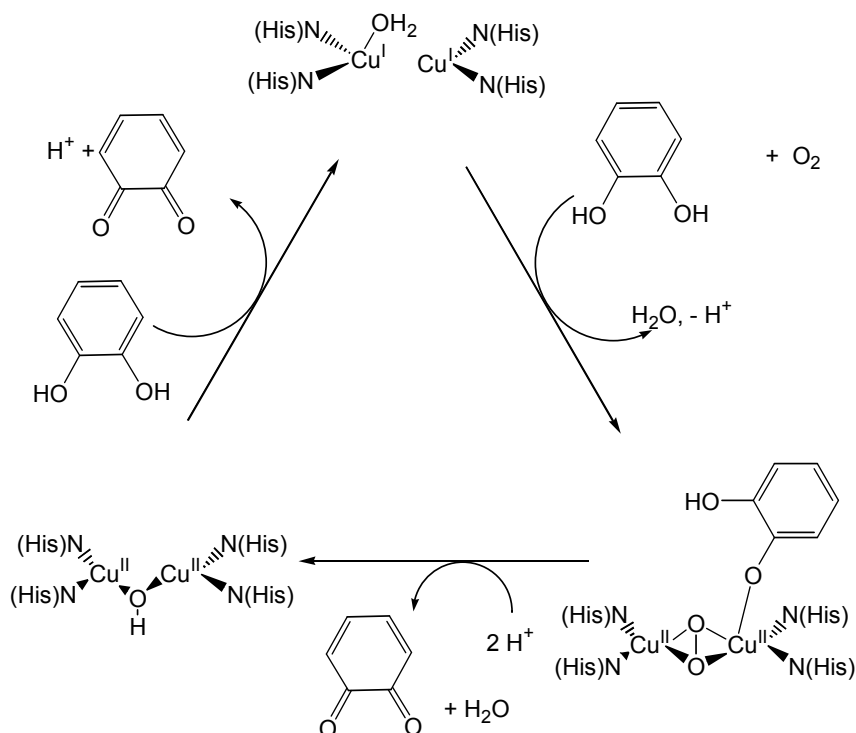


**Figure 5.2.** Postulated mechanism for the catalytic oxidation of o-catechol to o-quinone in catechol oxidase<sup>16</sup>

Another possible mechanism postulates bidentate coordination of o-catechol, bridging between the two copper centres.<sup>79</sup>

In this chapter the copper(II) complexes of mono- and dinucleating bispidone ligands, as structural models for galactose oxidase and catechol oxidase, are reported. The synthesis, characterization and some unusual properties of copper(II) complexes with the mononucleating ligands is presented.

The dinucleating ligands include a phenol bridge that connects the two rigid bispidone units. Several synthetic approaches were tested to bring the metal centers close to each other, in order to enable a bridging coordination mode by the phenolic oxygen. The degree of success will be discussed in the light of the EPR and magnetic measurements.

### 5.2. Copper(II) complexes with mononucleating phenol-bispidone ligands

Copper complexes of N2py2PhOH and vanilbis were prepared by mixing the methanolic solution of the ligands and of Cu(BF<sub>4</sub>)<sub>2</sub> in an equimolar ratio, yielding [Cu<sup>II</sup>(N2py2PhO)]BF<sub>4</sub> and [Cu<sup>II</sup>(vanilbisH<sub>1</sub>)]BF<sub>4</sub>, respectively. The methanolic solution of the complexes is dark brown, but they are green in the solid state. The microanalytical data showed that the phenolic group of the ligand is deprotonated (without the addition of base), and the formed HBF<sub>4</sub> is partially evaporated. UV-vis spectra of the complexes show intense charge-transfer bands at 450 and 473 nm, respectively. Such values, together with the absorption coefficients, are typical for Cu(II) complexes with coordinated phenolates.<sup>80</sup>

**Table 5.1. UV-vis and cyclic voltammetric data**

complex	CT $\lambda$ /nm ( $\epsilon$ )	d-d $\lambda$ /nm ( $\epsilon$ )	E <sub>1/2</sub> (mV) <sup>a</sup>
[Cu <sup>II</sup> (N2py2PhO)]BF <sub>4</sub>	450 (1220)	728 (200)	-1025
[Cu <sup>II</sup> (vanilbisH <sub>1</sub> )]BF <sub>4</sub>	473 (1040)	718 (220)	-1018

a: half-wave potentials are measured in MeCN against a Ag/0.01 M AgNO<sub>3</sub> electrode

During dissolution of [Cu<sup>II</sup>(N2py2PhO)]BF<sub>4</sub> in methanol, formation of a small amount of white crystalline solid was observed. This may be due to the partial disproportionation of copper(II) to yield an insoluble copper(I) salt and a copper(II) phenoxy-radical (Figure 5.2). An analogous phenomenon was observed by Shimazaki and co-workers, who found strong counter anion-dependence on the yield of the disproportionation reaction.<sup>81</sup>

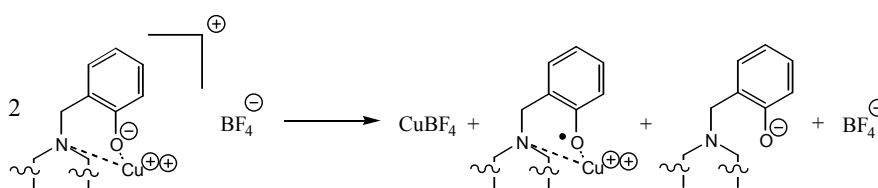


**Figure 5.2. Proposed disproportionation reaction for [Cu<sup>II</sup>(N2py2PhO)]BF<sub>4</sub> in methanol**

The large negative value of the Cu<sup>I</sup>/Cu<sup>II</sup> potential (see Table 6.1) in the cyclovoltammetric curve, explains the stabilization of the higher oxidation state, due to the charge transfer between the copper center and the phenolate oxygen, and gives a further support for the existence of a Cu-O bond.

The EPR spectrum of [Cu<sup>II</sup>(N2py2PhO)]BF<sub>4</sub> and the corresponding spin Hamiltonian parameters are shown in Figure 5.3.



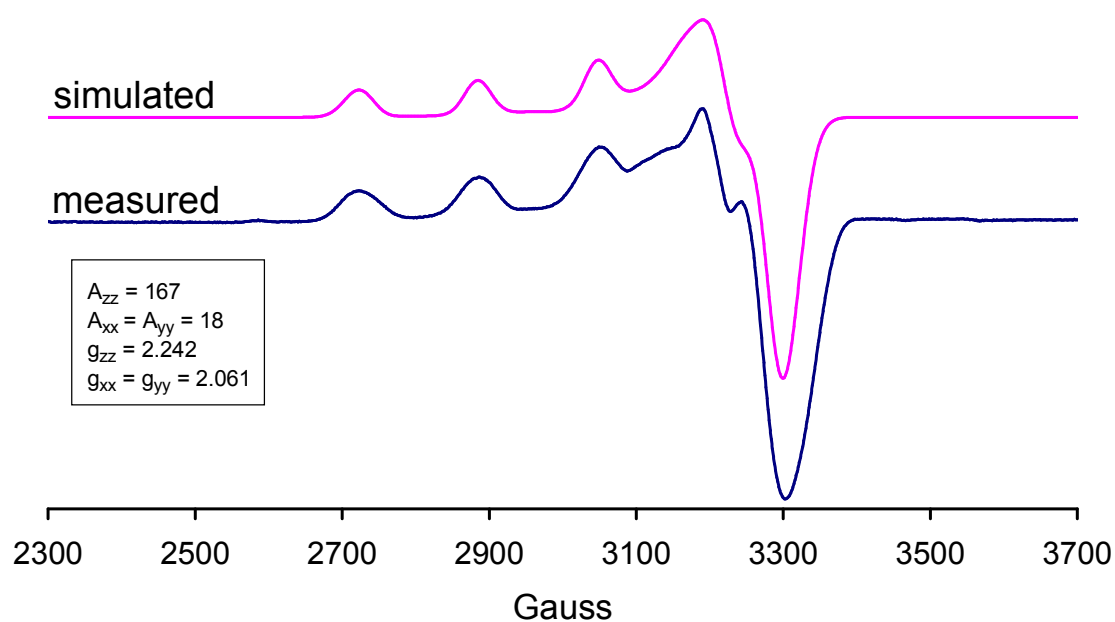


**Figure 5.3** Measured and simulated EPR spectra of  $[\text{Cu}^{\text{II}}(\text{N}2\text{py}2\text{PhO})]\text{BF}_4$ , recorded in DMF/water (2:1) at 125 K

Spectral parameters, determined by the simulation of the experimental spectrum using the program XSophe,<sup>82,83</sup> are in the range observed for other Cu(II) bispidone complexes.<sup>84,85</sup>

#### *Crystal structure of $[\text{Cu}^{\text{II}}(\text{N}2\text{py}2\text{PhO})]\text{BF}_4$*

Crystals suitable for structure determination were grown by ether diffusion into the methanolic solution of the complex. The cationic part of the complex is depicted in Figure 5.4. and selected bond lengths, bond angles and torsion angles are given in Table 5.2.

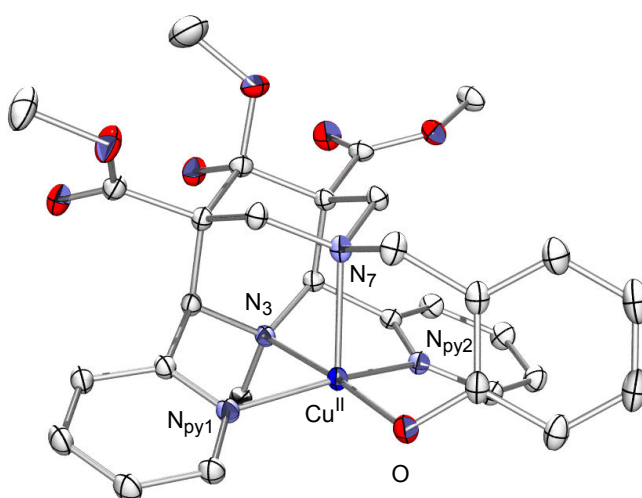


**Figure 5.4.** Crystal structure of  $[\text{Cu}^{\text{II}}(\text{N}2\text{py}2\text{PhO})]\text{BF}_4$

**Table 5.2. Selected bond lengths (Å) and bond angles (°)**

	[Cu <sup>II</sup> (N2py2PhO)]BF <sub>4</sub>	[Cu <sup>II</sup> (N2py2)(Cl)]Cl <sup>86</sup>
Bond distances		
Cu–N3	2.0335(12)	2.0423(25)
Cu–N7	2.2332(12)	2.2725(25)
Cu–Npy1	2.0326(12)	2.0204(25)
Cu–Npy2	1.9977(12)	2.0240(25)
Cu–O7	1.8972(11)	-
N3–N7	2.912	2.921
Npy1–Npy2	3.951	3.971
Bond angles		
Npy1–Cu–Npy2	157.29(5)	158.13(10)
N3–Cu–Npy1	81.62(5)	81.25(9)
N3–Cu–Npy2	81.17(5)	81.15(9)
Torsion angles		
C1–C2–C <sub>A</sub> –Npy1	-93.88	-90.7
C4–C5–C <sub>A</sub> –Npy2	87.82	86.4

The distance between the two aliphatic amino nitrogens N3 and N7 is 2.912 Å. This value is very close to that in the metal-free ligand (2.901 Å) (see in Chapter 4) which underlines again the high degree of preorganization of the ligand. This value of 2.921 Å is also almost the same as in related copper(II) complex of a tetradentate ligand, [Cu<sup>II</sup>(N2py2)(Cl)]Cl.<sup>6,86,87</sup> This implies that insertion of the phenolate as a fifth donor in [Cu(II)(N2py2PhO)]BF<sub>4</sub> does not cause further strain to the ligand backbone. The Cu–O7 distance (1.895 Å) is comparable to that of copper(II) complexes with monodentate O-donors.<sup>20,80,81</sup> Incorporation of the phenolic arm increases ligand denticity, and due to the extra charge-transfer interaction in comparison with the corresponding N2py2 complex, the complex stability is significantly increased. The only bond which shows a more pronounced deviation is the Cu–N7 bond, but the compression by 0.03 Å is a minor effect for this weak axial bond to the copper(II) center.

### 5.3. Copper(II) complexes with dinucleating phenol-bispidone ligands

#### 5.3.1. Copper complexes of *crebis*

##### 5.3.1.1. Synthesis of the complexes

In the literature it is suggested that variation of the reaction conditions (solvent, presence/absence of base) can lead to different coordination modes of a bridging phenolic oxygen.<sup>24</sup> This was demonstrated for the copper(II) complexes of 2,6-bis[(bis(2-pyridylmethyl)amino)methyl]-4-methylphenol (BPMP), which has a phenol unit bridging between two bis-picolyl amine arms<sup>24</sup> (Figure 5.5 and 5.6).

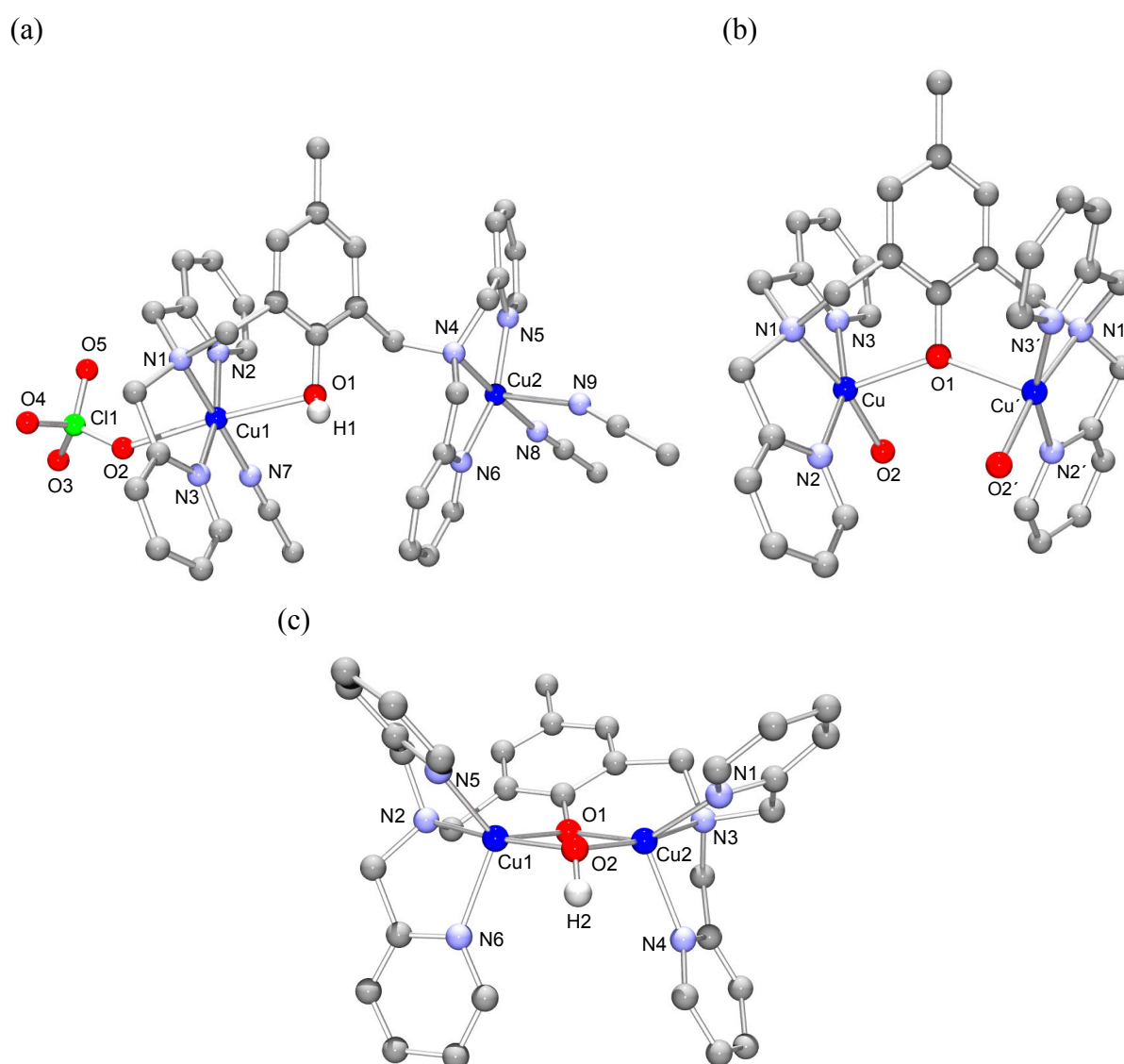
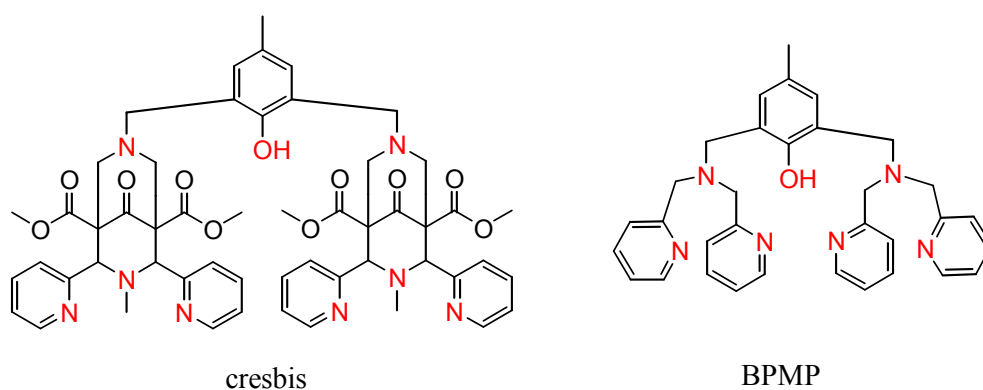


Figure 5.5. Crystal structures of dicopper-BPMP complexes<sup>24</sup> obtained (a) in MeCN without added base, (b) in acetone without added base, (c) in MeCN with triethylamine added

Cresbis shows a large resemblance to BPMP: the bridging unit is a cresol-diamine, and the side arm is a “rigidified” bis-picolyl amine, incorporated into the bispidone bicycle. The large difference between the two structures is the denticity: while in BPMP each side chain has 3 donors, the bispidone side chain incorporates 4 (two amines + two pyridines). (Figure 5.6)



**Figure 5.6. Structure of cresbis and BPMP ligand**

Mixing 2 eq of  $\text{Cu}(\text{ClO}_4)_2$  with the BPMP ligand in MeCN without addition of triethylamine yields a complex in which one of the copper centers binds only to the side chain donors of the ligand, while the other copper binds the phenolic oxygen as well. (Figure 5.5(a)) In other words, phenolate coordinates only to one copper(II). The distance between the metal centers is relatively large (6.94 Å), which hinders electronic communication between them.

When the reaction is carried out in acetone, without the addition of triethylamine, another structural motif is observed: the phenolate oxygen coordinates to both copper centers, but the fifth coordination site around the metal ions is occupied by a water molecule. (Figure 5.5(b)) The separation of the metals in this complex is 4.14 Å and larger than above. Performing the reaction in acetonitrile, but in the presence of 1 eq of triethylamine, the binding mode of the phenolic oxygen in the so formed complex turns out to be very different from the previous compounds (Figure 5.5(c)). The phenolate binds simultaneously to both copper centers and an additional hydroxide bridge also bridges the copper ions, forming a dicopper(II)- $\mu$ -phenolato- $\mu$ -hydroxo core, which is very similar to the structure proposed to take part in the catalytic action of catechol oxidase. The distance between the metal ions is significantly smaller (2.97 Å), and a moderate antiferromagnetic coupling between the copper(II) ions was measured.<sup>24</sup>

Inspired by this report, a series of dinuclear copper(II) complexes of cresbis was prepared.

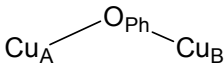
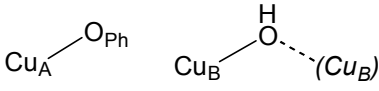
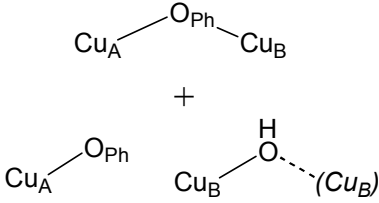
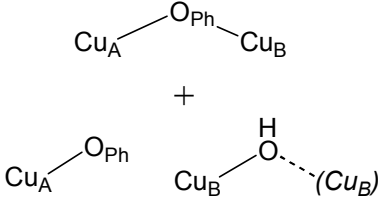
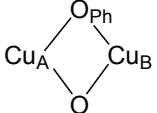
Complex **A** (see Table 5.3) was synthesized in a similar way to the  $[\text{Cu}^{\text{II}}(\text{N2py2PhO})]\text{BF}_4$  complex, by mixing stoichiometric amounts of  $\text{Cu}^{\text{II}}(\text{BF}_4)_2$  and the ligand in methanol. In analogy to the N2py2PhOH complex, the phenolic unit is deprotonated without addition of base. A part of the released  $\text{HBF}_4$  was removed during drying *in vacuo*. The UV-vis spectrum shows a broad shoulder centered at around 470 nm, in a pattern similar to the analogous  $\text{Cu}_2$ -BPMP complex.<sup>24</sup>

Complex **B** was obtained via the synthesis using a stoichiometric amount of triethylamine in acetonitrile, in accordance with the procedure of Torelli.<sup>24</sup> (Figure 5.5(b)). The ESI-MS indicates that the phenolic unit in this complex is indeed deprotonated (as was also the case when the complex was prepared without added base). In contrast to **A**, no shoulder could be found in the UV-vis spectrum of **B**.

**C** and **D** were synthesized from the above two complexes, passing them through neutral alumina column. The treatment did not influence the global constitution of the complex cations, as confirmed by ESI-MS, but the tetrafluoroborate anions were partially exchanged to hydroxide. This is indicated by elemental analysis and by the reduced intensities of the B-F stretching mode in their IR spectra. This strongly suggests that both **C** and **D** may be described as a mixture of **A** and **B**.

A further possibility to use base in the synthesis instead of using an organic base directly given to reaction mixture, is to treat **A** (which was obtained without addition of any external organic base) with basic alumina. In this complex **E**, the B-F stretching mode in the IR spectrum is completely missing, which indicates that the  $\text{BF}_4$  counter anions are exchanged to hydroxide. This is verified by the elemental analytical data. From the above analysis it is still not clear whether the formed hydroxide ions simply have exchanged the  $\text{BF}_4$  ions in **E**, or whether the binding mode around the copper centers is also changed by the basic medium of the column. It is probable that the strong donor hydroxide is coordinated to copper(II) during the treatment with the basic alumina column, and that the  $\text{BF}_4$  counter anions stay on the column simply because of charge neutrality. Despite numerous efforts, no crystals suitable for structure determinations were obtained for any of the above complexes. Additional information about the binding mode was obtained from EPR and magnetic measurements, which helped to deduce the degree of antiferromagnetic interaction between the copper(II) centers.

**Table 5.3. Properties of the different dicopper(II)-cresbis complexes**

<i>Complex</i>	<i>Reaction conditions</i>	<i>Postulated core structure</i>	<i>EPR</i>
<b>A</b>	Without added base in MeOH		Strong overlapping signals of 2 weakly interacting copper(II) centers
<b>B</b>	In presence of 1 eq triethylamine in MeCN		Weak and broad signals of dipolar coupled copper(II) centers
<b>C</b>	<b>A</b> passed through neutral alumina column		Moderately strong and broad signals of dipolar coupled copper(II) centers
<b>D</b>	<b>B</b> passed through neutral alumina column		Moderately strong and broad signals of dipolar coupled copper(II) centers
<b>E</b>	<b>A</b> passed through basic alumina column		silent

**5.3.1.2. EPR spectra**

The EPR spectrum of **A** shows intensive signals in a well resolved pattern, which indicate that the interaction between the metal centers is relatively weak (Figure 5.7(a)). As mentioned above, the deprotonation of the phenolic unit and its coordination to the copper(II) center is supported by analytical data. The question may arise, whether the phenolate binds only to one copper(II) center, as in one of the Cu<sub>2</sub>-BPMP complexes (Figure 5.5(a)) or forms a bridge between the two copper centers, similarly to another Cu<sub>2</sub>-BPMP complex (Figure 5.5(b)). Assuming the first scenario, the coordination sphere around the two metal ions should be markedly different: a charged phenolate oxygen binds to one copper (Cu<sub>A</sub>), while in case of the other metal center (Cu<sub>B</sub>), the fifth position may be occupied by a neutral solvent molecule (methanol or water, the latter can come from the crystal water content of the added Cu(BF<sub>4</sub>)<sub>2</sub> ·

6 H<sub>2</sub>O salt). Since a large difference in the ligand field of a charged phenolate and of a neutral O-donor solvent is expected, and this should also be seen in the EPR parameters. Therefore, formally a 1:1 “mixture” of two different spectra would be expected. In contrast, the EPR spectrum recorded for **A** cannot be interpreted as such a 1:1 mixture. From this, **A** is postulated to be a single bridged structure, as mentioned above as a second scenario. This single bridged Cu-O-Cu core motif was seen in the analogous Cu<sub>2</sub>-BPMP complex (Figure 6.5(b)). The EPR spectrum of this complex suggests a very weak interaction between the Cu centers.

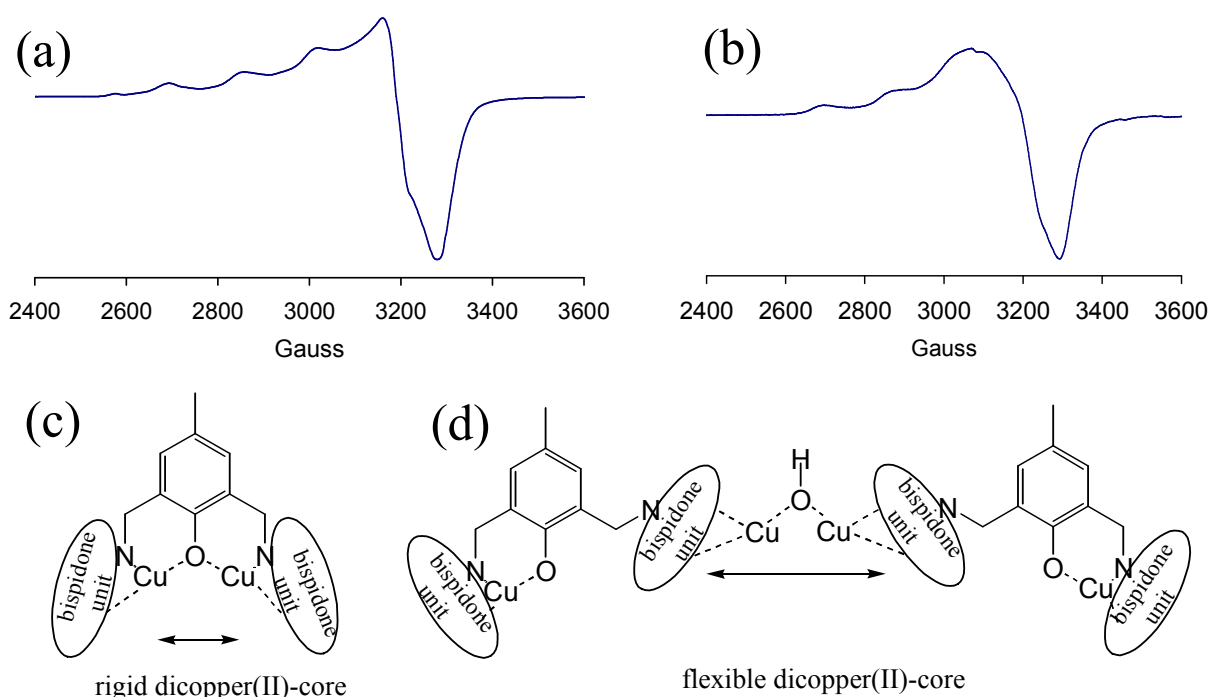


**Figure 5.7.** EPR spectra of **A** (a) and **B** (b) recorded in DMF/water 2:1 at 125 K, and postulated geometries for **A** (c) and **B** (d)

Signals in the EPR spectrum of **B** are much weaker than for **A**: 100 scans had to be accumulated to get the same signal intensity as was obtained for **A** from just a single scan (Figure 5.7(b)). The transitions are significantly broader, both in the parallel and in the perpendicular region. Apart from the broadening, this spectrum shows strong similarity to a spectrum typical for mononuclear Cu(II) complexes. It is therefore probable that only one copper (Cu<sub>A</sub>) gives signals in the spectrum, and that there is no intramolecular magnetic interaction between the two coppers, due to the large Cu<sub>A</sub>...Cu<sub>B</sub> separation. Moreover, the broadening is thought to be related to the other copper (Cu<sub>B</sub>), which could interact with a Cu<sub>B</sub> of another **B** molecule. Since only the four nitrogen donors of cresbis coordinate to Cu<sub>B</sub>, the fifth site can be occupied by a water molecule (this originates from the crystal water content

of the added  $\text{Cu}(\text{BF}_4)_2 \cdot 6 \text{H}_2\text{O}$  salt). The acidity of the copper(II)-bound water is larger than that of the uncoordinated one, therefore deprotonation of this water can be initiated in the presence of triethylamine, and this hydroxide can bind simultaneously to a  $\text{Cu}_\text{B}$  of another **B** molecule. Due to the steric hindrance of the bispidone units, bridging the copper centers of two independent molecules through a hydroxide ion requires a large separation between the metal centers. This means that the Cu-O-Cu angle also tends to be larger. It has been shown that the antiferromagnetic coupling between the copper ions is stronger when the Cu-O-Cu angle is larger.<sup>88</sup> As a result of the strong coupling, peaks assignable to  $\text{Cu}_\text{B}$  are not seen in the spectrum, and the transitions of  $\text{Cu}_\text{A}$  are significantly broadened.

In addition, both **C** and **D** (complexes treated with neutral alumina) gave EPR spectra with the pattern of **B**, but with signal intensities observed for **A**! This could mean that the degree of interaction between the copper ions lies between those of **A**- and **B**-type complexes. As mentioned above, in complexes **C** and **D** the tetrafluoroborate anions were partially exchanged to hydroxide ions. As a result, a mixture of **A** and **B** is formed, which explains the pattern of the EPR spectra of **C** and **D**.

Most surprisingly, **E** was completely EPR silent. Among Torelli's complexes, the one with bridging phenolate (Figure 5.6 (c)) also gave no signals in EPR. This was shown to be consistent with the observed double-bridged dicopper(II)- $\mu$ -phenolato- $\mu$ -hydroxo core in the crystal structure. Complex **E** has been prepared from **A** which is postulated to involve a  $\text{Cu}_\text{A}$ -O- $\text{Cu}_\text{B}$  core, with the phenolate bridge between the copper(II) centers. It has been suggested above that during the preparation of **E**, hydroxide ions of the basic alumina column coordinate to Cu(II) and the tetrafluoroborate ions therefore stay in the column due to charge neutrality. It is assumed that the hydroxide ion binds in a bridging mode. In the presence of a large excess of hydroxide ions, as found in the basic alumina column, the bridging hydroxide may be deprotonated and a  $\mu$ -phenolato- $\mu$ -oxo core may result. (Figure 5.8)

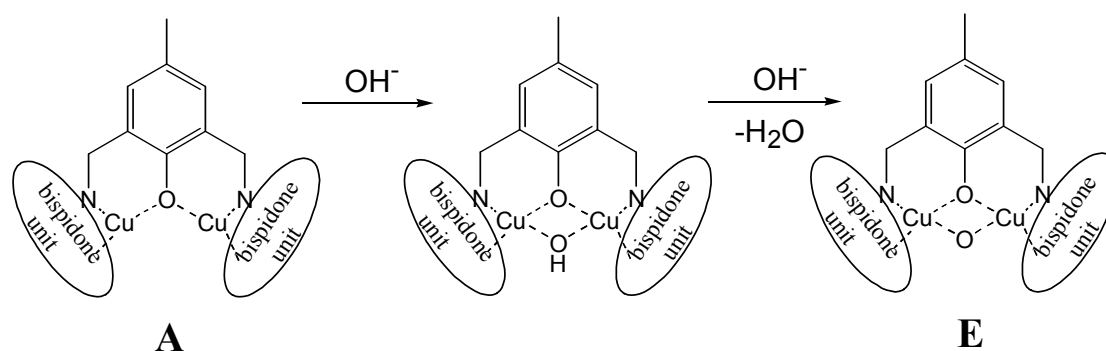


Figure 5.8. Proposed mechanism for the formation of **E** from **A**



### 5.3.1.3. Force field calculations

Molecular mechanics calculations for the assumed structures of **A** and **B** were performed using the MOMECC program<sup>89</sup> and force field.<sup>90</sup> The non-relevant 1,5 ester side chains and the 9-keto group were removed from the structures. As discussed previously, based on the EPR spectra and the spectroscopic and structural characterization of similar complexes,<sup>24</sup> a structure with bridging phenolate was expected for **A**, while coordination of the phenolic oxygen to only one copper center was postulated for **B** (see Fig. 5.9). For this calculation the effect of the bridging hydroxide which connects two independent molecules of **B**, was not taken into account, and ammonia was used as the fifth coordination site of Cu<sub>B</sub>. The main goal of this calculation was to compare the overall steric effects (the two bispidine units are relatively close to each other when with the bridging phenolate; in the other structure this effect is assumed to be negligible). Considering electrostatic effects, there are two electrostatically attractive copper-oxygen interactions in **A**, in which complex the phenolate bridges between the copper centers; while in **B** there is only one copper-oxygen interaction (note that the effect of the bridging hydroxide in **B** was not considered). However, it is generally accepted that molecular mechanics can be used to compute molecular properties which do not depend on electronic effects.

The MOMECC calculations indicate that there is only a 15 kJ/mol energy difference between the two structural isomers **A** and **B** (Figure 5.9), so that in terms of steric strain, the two species are similar. In other words, formation of both structures can be expected.

In the optimized structure of **B** the geometry within the bispidine backbone correlates with the crystal structure of [Cu<sup>II</sup>(N2py2PhO)]BF<sub>4</sub>, except for the Cu-N7 distance, which was calculated to be significantly shorter (calculated: 2.00 Å, measured: 2.23 Å). The Cu-O separation was calculated to be rather long (2.63 Å). The Cu-O bond lengths in **A** were calculated to be 2.43 Å, which is somewhat shorter than in the other structure, and may be a consequence of geometric constraints (repulsion between the two bispidone units).

The metal-metal separation in **A** was calculated to be 4.16 Å, a distance which allows for moderate interaction between the copper(II) centers. This is in agreement with the measured EPR spectrum, which shows overlapping spectra of two weakly interacting copper(II) centers, as a result of some degree of antiferromagnetic coupling. These results are similar to those obtained for the structurally analogous Cu<sub>2</sub>-BPMP complex (Figure 5.5(b)).<sup>24</sup>



Diamagnetic corrections were calculated by summing up the atomic diamagnetic susceptibility values (Pascal constants,  $\chi_i$ ), and considering the conversion between cgs and SI units.

$$\chi_{dia} = 10^{-6} \cdot \sum \chi_i (cgs) \quad (4)$$

From the above equations the molar paramagnetic susceptibility  $\chi_{para}$  can be expressed:

$$\chi_{para} = \frac{(\mu - \mu_C)M}{1000 \cdot m} - \chi_d \quad (5)$$

Where  $\mu$  = measured longitudinal magnetic moment (magnetization),  $\mu_C$  = correction for the capsule,  $m$  = weight of the sample,  $M$  = molecular weight of the sample,  $\chi_d$  = diamagnetic correction (Pascal constants).

Pierre Curie showed in 1895 that the molar paramagnetic susceptibility  $\chi_{para}$  is inversely proportional to the temperature<sup>91</sup>

$$\chi_{para} = \frac{N_A \cdot g^2 \cdot \mu_B^2}{3kT} \cdot S(S+1) \quad (6)$$

where  $\mu_B$  = Bohr magneton,  $N_A$  = Avogadro constant,  $k$  = Boltzmann constant,  $S$  = electrons spin,  $g$  = giromagnetic factor,  $T$  = absolute temperature.

This so called Curie law is valid only at low magnetic fields, and at not extremely low temperatures. Moreover, if there is a magnetic interaction between two magnetically active centers, the Curie law loses its validity. In such systems the coupling between the magnetic centers is also taken into account, and the molar paramagnetic susceptibility  $\chi_{para}$  is characterized by the Bleaney-Bowers equation:

$$\chi_{para} = \frac{N_A \cdot g^2 \cdot \mu_B^2}{kT[3 + \exp(-J/kT)]} \cdot S(S+1) \quad (7)$$

If  $J < 0$ , the coupling is antiferromagnetic, whereas a  $J > 0$  is an indication of a ferromagnetic interaction.  $J = 0$  is characteristic for non-interacting magnetic centers. In this case the Bleaney-Bowers equation reduces to the Curie law.

A  $\chi_{para}T$  vs.  $kT$  curve clearly shows the difference between the three systems (Figure 5.10):

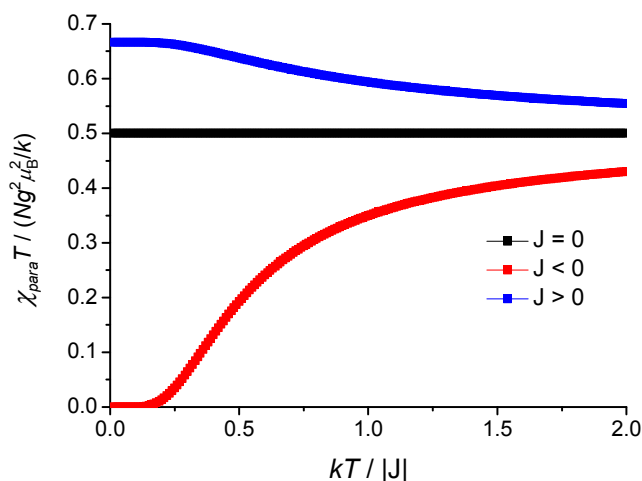


Figure 5.10.  $\chi_{para}T$  vs.  $kT$  curves for a dinuclear copper(II)-complex ( $S=1$ ), considering ferromagnetic ( $J>0$ ), antiferromagnetic ( $J<0$ ), or no ( $J=0$ ) interaction between the metal centers

As can be seen from this plot, in case of antiferromagnetic coupling the  $\chi_{para}T$  values are decreased with decreasing temperature and become 0 at very low temperatures. Ferromagnetic coupling is indicated when the decrease of temperature leads to higher  $\chi_{para}T$  values. For non-interacting magnetic centers  $\chi_{para}T$  is independent of the temperature.

As was described before, by the variation of reaction conditions, different types of dicopper complexes with the cresbis ligand could be isolated, which shows versatile patterns in their EPR spectra. This variation was postulated to originate from the different coordination modes around the copper(II) centers. To gain further insight into the copper-copper interactions, SQUID (superconducting quantum interference device) measurements were carried out. It was especially interesting to investigate the complexes which have overlapped, broadened EPR spectra (**B**), and those which were completely EPR silent (**E**).

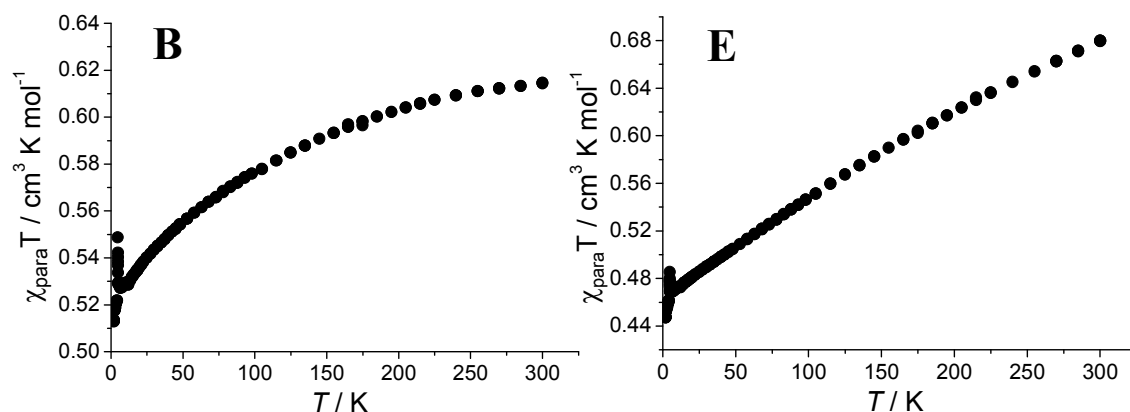


Figure 5.11.  $\chi_{para}T$  vs.  $T$  curve for **B** and **E**

The plots for **B** and **E** in Figure 5.11 show that the change in  $\chi_{para}T$  is relatively small. In both cases  $\chi_{para}T$  decrease with decreasing temperature, which is indicative of an antiferromagnetic coupling between the two copper centers. However, at very low temperatures the  $\chi_{para}T$  values do not converge to 0, which would be the case in an ideal system containing antiferromagnetically coupled magnetic centers. Comparing our two complexes, **E** shows a more significant change in  $\chi_{para}T$  values than **B**, which may reflect the degree of antiferromagnetic interaction. Also,  $\chi_{para}T$  values show saturation at room temperature in case of **B**, indicating to a moderate coupling, while for **E** the  $\chi_{para}T$  values increase further at temperatures larger than 300 K (the  $S=0$  excited state is not completely populated). This is indicative of a very strong antiferromagnetic coupling. These results parallel those of the EPR spectra of the complexes: the EPR silence of **E** indicated a more pronounced coupling (i.e. a shorter distance) between the copper(II) centers, than in **B**, where broad and weak signals were seen in the EPR spectrum. The reason for the difference in the magnetic properties of **B** and **E** lies in variation of the coordination mode of the dicopper cores, thus in the variation of the  $\text{Cu}\cdots\text{Cu}$  distances in the two complexes. (Figure 5.12)

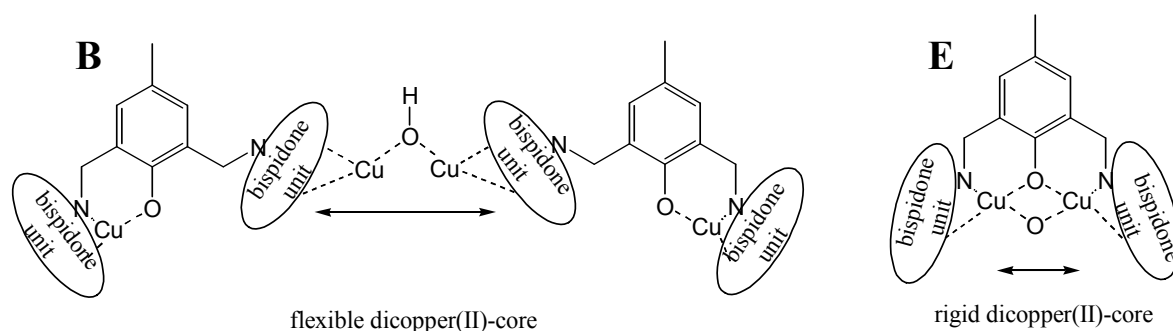


Figure 5.12. Effect of the rigidity/flexibility on the  $\text{Cu}\cdots\text{Cu}$  distance in **B** and **E**

In the case of **B**, the copper centers are bridged by a single hydroxide, which allows for larger variation in the Cu...Cu distance and also in Cu-O-Cu bond angles. The two sterically demanding bispidone units in **B** tend to be as far away as possible from each other. In case of **E** the two copper centers are intramolecularly bridged by the cresol unit, which connects the two rigid and bulky bispidone “side arms”. Due to geometric constraints the two chelate rings (involving N7, copper(II) and the cresol oxygen) keep the position of the copper(II) centers and the Cu-O-Cu angle fixed. Therefore, the Cu...Cu separation and the Cu-O-Cu angle are larger in **B** than in **E**, where steric repulsion of bispidones is counterbalanced by the geometric constraints of the intramolecular chelate rings. Due to this, the metal-metal separation in **E** is shorter than in **B**. This parallels the higher degree of antiferromagnetic interaction between the metal centers in **E**.

#### 5.3.1.5. Catecholase reaction

As shown from spectroscopic results and from magnetic measurements, there is an antiferromagnetic interaction between the copper centers in some dicopper(II) cresbis complexes. Existence of antiferromagnetic coupling in **B** and **E** suggests that the distance between the metal centers should not be too large, ensured by the suggested bridging coordination mode with a Cu-O-Cu motif. It has been postulated in this chapter that in the EPR silent species **E** a dicopper(II)- $\mu$ -phenolato- $\mu$ -hydroxo core may be present. This structural motif is also seen in the catalytically active met-form of the catechol oxidase enzyme. In order to understand whether the above mentioned dicopper(II)-cresbis complexes show not only structural resemblance to catechol oxidase, but can also mimic the enzymatic action, the reaction between the dicopper(II)-cresbis complexes with a bridging Cu-O-Cu motif (**B** and **E**) and a catechol derivative was studied. Addition of 2,4 di-tert-butyl catechol to **B** and **E** did not result in any change in the UV-vis spectra (theoretically an intense band at 400 nm should appear, corresponding to the oxidation of the substrate to the o-quinone).<sup>92,93</sup> One of the possible reasons for the inactivity of **B** and **E** is that even if the dicopper(II)- $\mu$ -phenolato- $\mu$ -hydroxo core is present in the catalyst, there should still be accessible free coordination sites around the copper(II) centers, where the catechol substrate can be bound. Considering that in such a double bridged structure each copper center is already six-coordinate (two amine nitrogens and two pyridine nitrogens from the bispidone core, and one phenolate and hydroxo oxygen from the double bridge), there is no space around the metal centers to bind the catechol substrate. Moreover, the bulky and rigid bispidone units cause a large steric hindrance, making it impossible for catechol to approach the copper centers.

#### 5.4. Cu(II) complex of sulfobis

Direct treatment of sulfobis with equimolar amount of  $\text{Cu}(\text{BF}_4)_2$  gives a red solution. Without the addition of any base, both the sulfonate and the phenolate groups are deprotonated, and a neutral complex is formed, which could not be purified by ion-exchange chromatography. The neutrality of the Cu-complex is further supported by the ESI-MS spectra, showing a peak assignable to the sodium adduct of the neutral complex species ( $700.4 [\text{Cu}^{\text{II}}(\text{sulfobisH}_1)]^+$ ,  $722.3 [\text{Cu}^{\text{II}}(\text{sulfobisH}_2) + \text{Na}]^+$ ). The various series of signals typical for copper(II) complexes in the EPR spectrum, indicate that at least 2 species exist in solution. Due to the broadening in the perpendicular region, x and y components of the spin Hamiltonians could not be accurately determined.

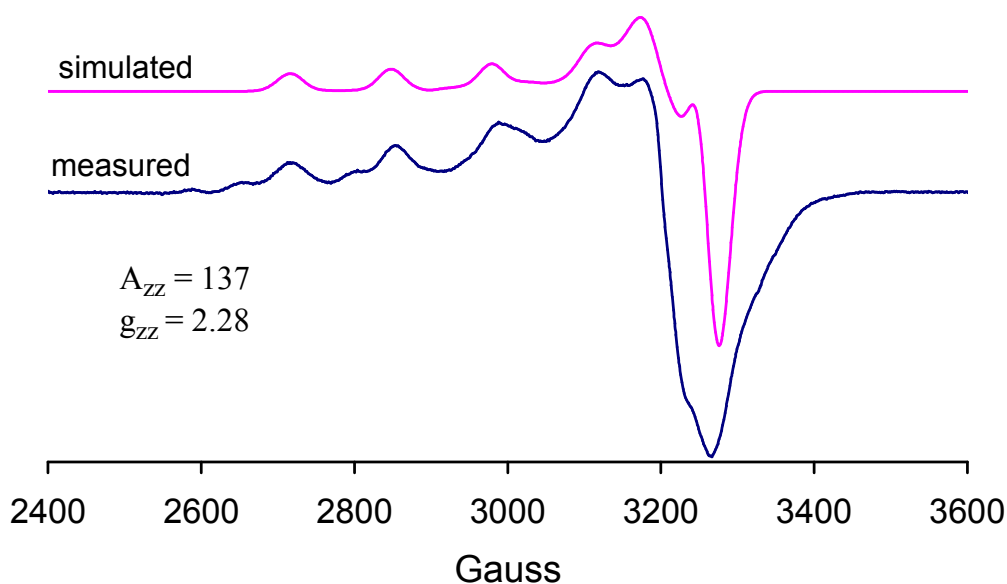
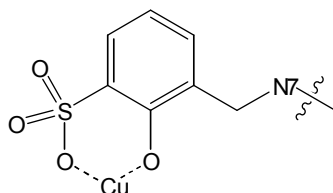


Figure 5.13. Measured and simulated EPR spectra of  $[\text{Cu}^{\text{II}}(\text{sulfobisH}_2)]$ , recorded in DMF/water (2:1)

The spin Hamiltonian parameters in the parallel region of the g-tensor, fitted for the main component found in  $[\text{Cu}^{\text{II}}(\text{sulfobisH}_2)]$ , are larger than the values obtained for the corresponding phenolate complex without the sulfonate unit (in  $[\text{Cu}^{\text{II}}(\text{N}2\text{py}2\text{PhO})]\text{BF}_4$   $g_{zz} = 2.242$ ). This indicates a lower level of delocalization of the unpaired electron on the ligand site, and a more ionic nature of the copper-oxygen bond, which may be the result of the participation of the sulfonate group in metal binding.

The presence of the sulfonato group with the phenolate moiety provides additional possibilities for metal coordination. In the neutral  $[\text{Cu}^{\text{II}}(\text{sulfobisH}_2)]$  complex both the phenolate and the sulfonate group are deprotonated, which is a strong indication for their participation in the binding to copper(II). Considering a coordination mode similar to one

observed in the crystal structure of  $[\text{Cu}^{\text{II}}(\text{N}2\text{py}2\text{PhO})]\text{BF}_4$  (Figure 5.4), involving amine and pyridine nitrogens and the phenolate oxygen, the oxygen of the additionally attached sulfonate group in sulfobis cannot be a sixth donor due to steric effects. Since sulfonate is a strong ligand, it is likely that it also binds to another copper(II): the closeness of the phenolic oxygen might allow a bidentate coordination with formation a 6-membered chelate ring.



**Figure 5.14. Proposed coordination of copper(II) to the sulfonated phenolic side chain in sulfobis**

Numerous efforts to crystallize this complex failed.



## 6. Synthesis and oxidation of V(IV) and V(V) bispidone complexes

### 6.1 Introduction

Vanadium plays an important role in biological systems. There is a considerable interest and activity in developing vanadium complexes as models for a variety of metalloenzymes, specifically for the mononuclear haloperoxidase enzymes, which catalyze the peroxide-dependent halogenation of organic substrates.<sup>94,95</sup> Vanadium(V) oxo-peroxo complexes have also been found to be catalytically active in the oxidation of organic substrates, e.g. epoxidation of alkenes, hydroxylation of alkanes and of aromatic compounds.<sup>96,97</sup> In addition, mononuclear vanadyl(IV) and oxo-peroxo vanadium(V) complexes are known to have insuline-mimetic properties.<sup>98,99</sup>

Tetra- and pentadentate bispidine-based ligands with tertiary amine, pyridine and phenolate donors, were used for the isolation and characterization of vanadium(IV) and vanadium(V) oxo and peroxo complexes. Metal sources of different oxidation states and different anions were applied. According to the HSAB concept, vanadium(IV) and (V) ions are relatively hard and weakly polarizable, and the interaction with the nitrogen donors of bispidine ligands are expected to be not especially favoured. However, a manifold of effects influencing complexation (preorganization, hole size) can drive the reaction in the direction of completion. The computed cavity size of the ligands with a well established molecular mechanics method<sup>100</sup> indicates that the vanadyl ion fits well into the ligand cavity. However, for the creation of stable complexes, there also needs to be a good fit with respect to the electronic properties. A possible explanation for the fact that the preparation of the complexes was not straightforward, is that the hard vanadyl-ion prefers binding to similarly hard, more electronegative donors (e.g. oxygen) and not so much to ligands with the softer nitrogen-donors, especially not to heteroaromatic donor groups. A hard-soft combination yields a moderately stable complex, which can be very sensitive to geometric constraints. Also, the preorganized bispidone ligands enforce a distorted octahedral geometry, and this deviation in structural parameters further lowers the complex stability. Binding the vanadyl ion to pentadentate ligands leads to formation of a saturated coordination sphere around the metal fragment (the sixth position is occupied by the vanadyl oxygen). In case of tetradentate ligands, one position remains free.

As mentioned above, according to HSAB theory, a moderate complex stability is expected, and this means that drastic reaction conditions (e.g. highly acidic medium, long refluxation time) should be avoided. Due to the hydrolysis of the ester groups, basic conditions should not

be considered. Several methods for the preparation of vanadyl complexes are reported in the literature.<sup>101,102</sup> Especially interesting is that a synthesis with bispidone-analogue ligands is also known.<sup>101</sup>

## 6.2. Vanadyl complexes

### 6.2.1. Synthesis of vanadyl complexes

The vanadyl complex with the pentadentate ligand N2py2PhOH was obtained from vanadyl sulphate as the vanadium source. Acetonitrile was used as the solvent and an equivalent amount of triethylamine was added to deprotonate the phenolic group. The complex was purified by means of ion exchange chromatography. Attempts with other vanadium(III) salts (chloride, acetylacetonate) did not lead to any complex formation. Interestingly, the method which was successful for the pentadentate ligands, did not succeed for the tetradentate N2py2 ligand, probably because of the lower ligand denticity and the consequently lower complex stability.

Treatment of N2py2 with the ethanolic solution of VO(OEt)<sub>3</sub> produced a deep green solution after refluxing overnight, from which a dark green solid precipitated after several days at 4°C. Characterization of the product confirmed the formation of the vanadyl-N2py2 complex.

The effect of the valence shell electron in the vanadyl ion (d<sup>1</sup>) is less pronounced than for late-transition metal ions (Cu<sup>2+</sup>, Zn<sup>2+</sup>), although their ionic radii are comparable. The single d-electron of vanadium can interact weakly with the lone pairs of the ligand in a “covalent” way.

### 6.2.2. Spectroscopy of the vanadyl complexes

The *IR spectra* for all complexes have no Bohlmann band (ca. 2600 cm<sup>-1</sup>), which typically appears for the free ligand (interaction between the lone pairs of the amine nitrogens), but is missing when a metal is coordinated. For [V<sup>IV</sup>=O(N2py2PhO)]Cl × TEAHCl × 2.5 H<sub>2</sub>O the *UV spectrum* shows only 1 d-d band at 571 nm. Coordination of the phenolate oxygen to the vanadium center is supported by the existence of a charge transfer band at 386 nm. The other d-d bands may be suppressed by the intense CT band, or they lie outside the recorded interval or part of the broad dd-band. In comparison, in the UV-vis spectrum of [V<sup>IV</sup>=O(N2py3o)](ClO<sub>4</sub>)<sub>2</sub>, all 3 d-d bands, expected for an octahedral d<sup>1</sup> system, could be assigned. While the xy → z<sup>2</sup> band appears as an intense shoulder at 363 nm, the xy → x<sup>2</sup>-y<sup>2</sup> and the xy → xz,yz transitions appear similarly as weak bands at 514 and 695 nm.<sup>7</sup>

*EPR spectra*

The EPR spectra of the three bispidine vanadyl compounds and of the vanadyl aqua ion are shown in Figure 7.1., the spin Hamiltonian parameters, obtained by spectra simulation,<sup>82,83</sup> are given in Table 7.1. The spectra are typical for vanadyl d<sup>1</sup> systems with a d<sub>xy</sub> ground state and a tetragonal geometry.<sup>103-105</sup>

**Table 6.1. EPR parameters of the vanadyl complexes**

	$A_{xx}/10^{-4}\text{cm}^{-1}$	$A_{yy}/10^{-4}\text{cm}^{-1}$	$A_{zz}/10^{-4}\text{cm}^{-1}$	$g_{xx}$	$g_{yy}$	$g_{zz}$
$[\text{V}^{\text{IV}}=\text{O}(\text{N}2\text{py}3\text{o})]^{2+}$ <sup>7</sup>	-51	-50	-153	1.988	1.977	1.950
$[\text{V}^{\text{IV}}=\text{O}(\text{N}2\text{py}2\text{PhO})]^+$	-54	-55	-158	1.979	1.972	1.947
$[\text{V}^{\text{IV}}=\text{O}(\text{N}2\text{py}2)]^{2+}$	-60	-60	-166	1.977	1.977	1.943
$\text{VOSO}_4$	-68	-68	-178	1.977	1.972	1.932

Both the A and g tensor parameters show a clear trend: the values (in particular the z-components) become smaller when N donors are replaced with O-donors (going from the N5 donor N2py3o ligand to N4O donor N2py2PhOH and to “O5” chromophore  $\text{VOSO}_4 \times 5 \text{H}_2\text{O}$ ). This trend parallels the type of chromophore and is consistent with the expected level of delocalization of the unpaired electron to the donor groups, with the softer N-donors leading to more covalent interactions than the harder O donors. Comparing the phenolate complex (of the ligand with N4O donor set) with the complex with the tetradentate N2py2 ligand, both the A and g tensor parameters are smaller in the latter case, which is probably due to the decreased symmetry around the metal center.

No intermediate species could be detected by EPR for the reaction between  $[\text{V}^{\text{IV}}=\text{O}(\text{N}2\text{py}3\text{o})]^{2+}$  and  $\text{H}_2\text{O}_2$ : the  $\text{V}^{\text{IV}}=\text{O}$  complex is directly oxidized to a vanadium(V) species. Not only the isotropic RT measurement, but also the low temperature series showed only the gradual decay of the vanadyl signals (and the simultaneous formation of the diamagnetic vanadium(V) species, which is shown by UV-vis spectroscopy).<sup>7</sup> This means that no vanadyl-peroxo intermediates could be trapped, although their existence can not be ruled out on the basis of this experiment.

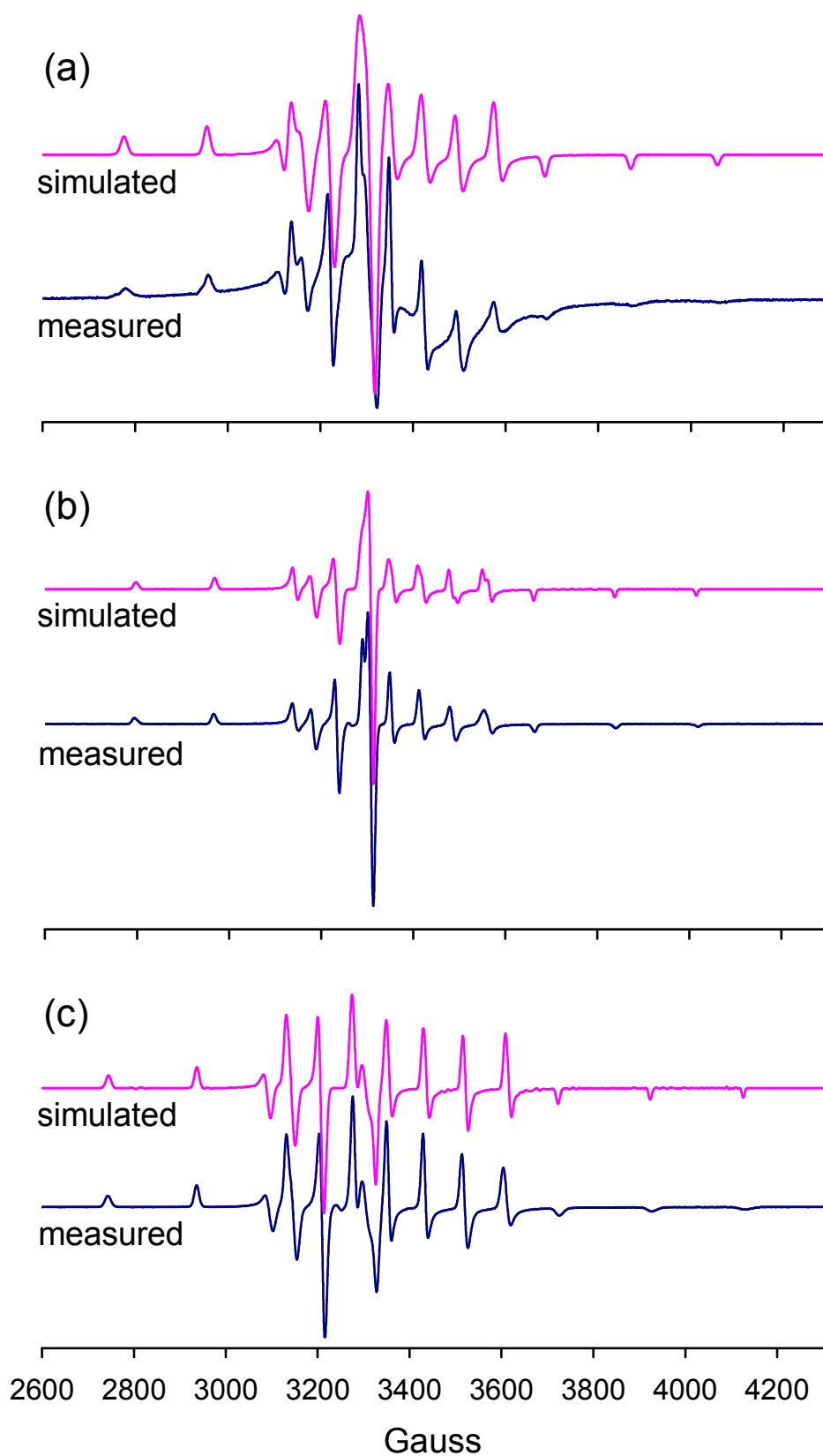


**Figure 6.1.** Measured and simulated EPR spectra of  $[V^{IV}=\text{O}(\text{N}2\text{py}2)](\text{ClO}_4)_2$ . (a),  $[V^{IV}=\text{O}(\text{N}2\text{py}2\text{PhO})]\text{Cl}$ . (b),  $\text{VOSO}_4$  (c). Spectra were recorded in  $\text{DMF}/\text{H}_2\text{O}$  2 : 1 at 125 K. For the spectral parameters see Table 6.1.

### 6.2.3. Oxidation of the vanadyl complexes

The oxidation of  $[\text{V}^{\text{IV}}=\text{O}(\text{N}2\text{py}3\text{o})]^{2+}$  with  $\text{H}_2\text{O}_2$  was performed by varying the oxidant concentration and the solvent, and the reactions were followed by UV-vis spectroscopy. By using a larger excess of hydrogen peroxide a higher conversion to the vanadium(V)-oxo peroxy complex is achieved in methanol (Figure 6.2). Quenching of the reaction after 2 hours, the product could be isolated in relatively good yields, by using ion-exchange chromatography. Interestingly, after 2 days reaction time, the initially orange product turns yellow, and the ESI-MS spectra show complete decomposition of the complex: the charge-transfer band of the  $[\text{V}^{\text{V}}=\text{O}(\text{O}_2)(\text{N}2\text{py}3\text{o})]^+$  complex at 450 nm is suppressed by evolution of bands below 400 nm.

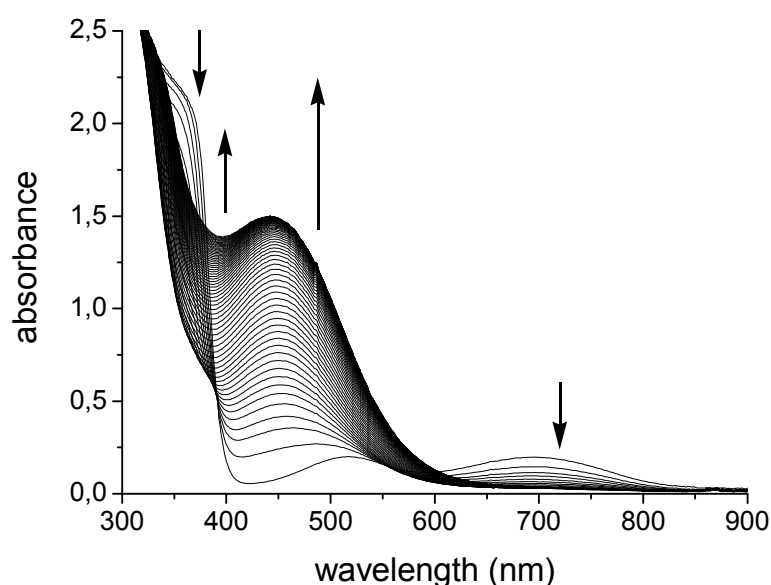


**Figure 6.2.** Time-dependent UV-vis spectra (recorded in 5 minutes intervals) for the reaction between 11 mM  $[\text{V}^{\text{IV}}=\text{O}(\text{N}2\text{py}3\text{o})](\text{ClO}_4)_2$  and 30 eq  $\text{H}_2\text{O}_2$  in methanol at 25°C.

Formation of the  $[\text{V}^{\text{V}}=\text{O}(\text{O}_2)(\text{N}2\text{py}3\text{o})]^+$  complex in acetonitrile is retarded, and similarly to methanol, the product has a maximum abundance after 2 hours, in comparison with the decomposition products (Figure 6.3).

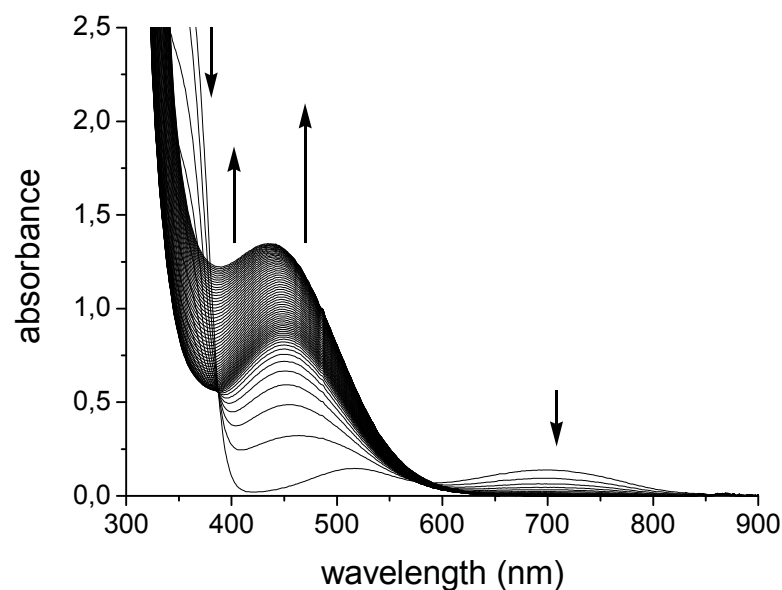


**Figure 6.3.** Time-dependent UV-vis spectra (recorded in 5 minutes intervals) for the reaction between 11 mM  $[V^{IV}=O(N2py3o)](ClO_4)_2$  and 300 eq  $H_2O_2$  in acetonitrile at 25°C.

Interestingly, aprotic solvents (e.g. DMF) enhance the formation of side products, and the rate of decomposition is significantly higher than observed for reactions carried out in protic solvents (Figure 7.4). After 1 h reaction time the product complex  $[V^V=O(O_2)(N2py3o)]^+$  has maximum abundance in comparison with decomposition products, but the absolute “yield” is significantly smaller than in methanol. Large absorption increments below 500 nm after 1 h reaction time indicate complete decomposition of the vanadium(V)-oxo peroxy complex: indeed, ESI-MS spectra showed no peaks assignable to  $[V^V=O(O_2)(N2py3o)]^+$ .

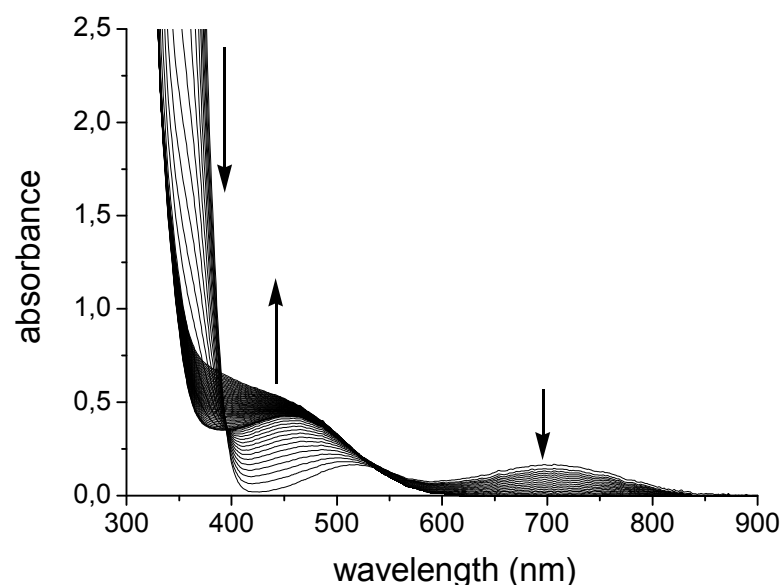


**Figure 7.4.** Time-dependent UV-vis spectra (recorded in 5 minutes intervals) for the reaction between 11 mM  $[V^{IV}=O(N2py3o)](ClO_4)_2$  and 300 eq  $H_2O_2$  in DMF at 25°C.

It is generally accepted that the reaction between vanadyl complexes and hydrogen peroxide produces hydroxyl radicals.<sup>106</sup> The yield of vanadium(V)-oxo-peroxo complex formation follows the trend of the hydroxyl radical quenching ability of the solvent: the best results were obtained in methanol. Attempts to use a buffer to determine the effect of pH all failed since the applied buffer components were shown to bind to vanadium. Thus even if the metal was oxidized, the buffer component occupied the position of peroxide.

The oxidation of  $[\text{V}^{\text{IV}}=\text{O}(\text{N}2\text{py}2\text{PhO})]^+$  was significantly slower than for  $[\text{V}^{\text{IV}}=\text{O}(\text{N}2\text{py}3\text{o})]^{2+}$ . The CT-band of the phenolate (386 nm) shifted slowly to another intense band (450 nm), which was assigned to a vanadium-peroxo charge transfer. The reason for the lower oxidation rate lies in the difference of the coordinative bonds, which need to be cleaved first, before the peroxide binds to vanadium. Breaking a bond between a soft pyridine nitrogen and hard vanadium requires significantly less energy than cleaving a vanadium – phenolate bond, which is a typical hard-hard interaction with a charge-transfer character.

### 6.3. Characterization of $[\text{V}^{\text{V}}=\text{O}(\text{O}_2)(\text{N}2\text{py}3\text{o})]\text{ClO}_4$

Three vibrations were found in the low energy part of the IR spectrum, at 890, 932 and 962  $\text{cm}^{-1}$ , respectively. Considering literature values, the band at 962  $\text{cm}^{-1}$  may be attributed to the V=O stretching vibration. The other two are tentatively assigned to the O-O modes. To confirm the latter assumption, a labeling study was also performed, using  $\text{H}_2^{18}\text{O}_2$  as oxidant. In the IR spectrum of the  $[\text{V}^{\text{V}}=\text{O}(^{18}\text{O}_2)(\text{N}2\text{py}3\text{o})]^+$  complex, the bands at 932 and 890  $\text{cm}^{-1}$  are shifted to 887 and 850  $\text{cm}^{-1}$ , respectively (Figure 7.5). The experimentally determined isotope shifts correlate well with the theoretically expected value. Similar isotope shifts are observed in the nitrate salts of the complex.

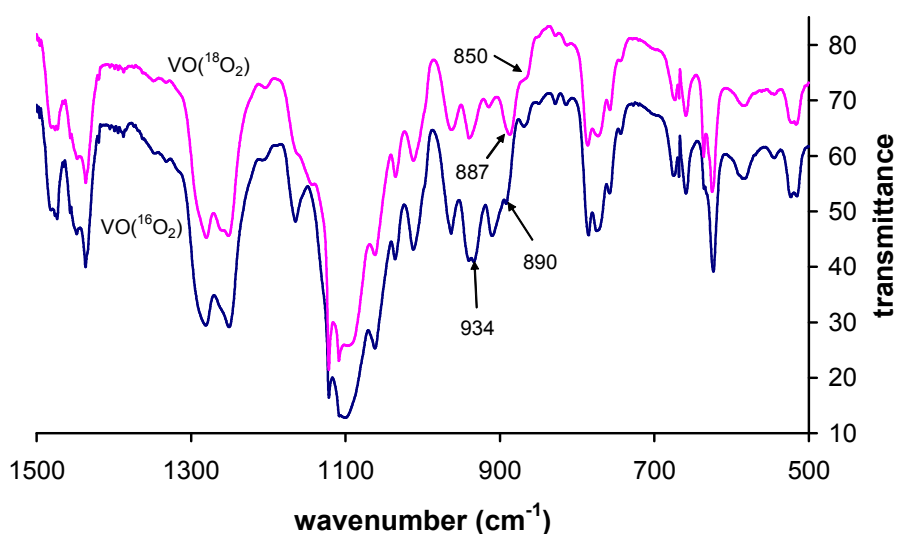


Figure 7.5. IR spectra of  $[\text{VO}(^{16}\text{O}_2)(\text{N}2\text{py}3\text{o})]\text{ClO}_4$  and  $[\text{VO}(^{18}\text{O}_2)(\text{N}2\text{py}3\text{o})]\text{ClO}_4$ . Bands shifted due to isotope effect are denoted

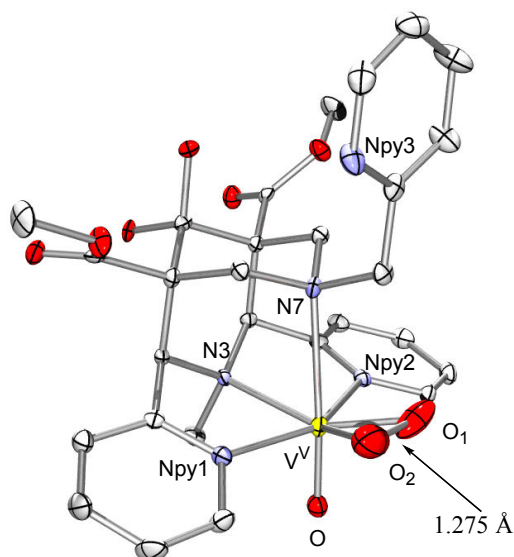


Figure 7.6. Crystal structure of  $[V^V=O(O_2)(N_2py_3o)]ClO_4$ <sup>7</sup>

The obtained crystallographic data seem to be inconsistent with the expected relationship between O-O stretching frequency and the O-O bond length, which show a linear correlation: compounds with an O-O bond length in the range of 1.4-1.5 Å and a  $\nu_{OO}$  between 800 and 930  $cm^{-1}$  are categorized as peroxides, whereas compounds with an O-O bond length of 1.2-1.3 Å and  $\nu_{OO}$  between 1050 and 1200  $cm^{-1}$  belong to the superoxide category.<sup>107</sup> In the crystal structure of  $[V^V=O(O_2)(N_2py_3o)]ClO_4$ , the O-O bond length is 1.275 Å (Figure 7.6), which falls clearly into the range of superoxides. This result suggests that the O-O stretching frequencies should appear at ca. 1250  $cm^{-1}$ . In contrast with this, the above discussed labeling studies show that the O-O stretching mode of the side-on bound peroxide appears at much lower frequencies, typical for a peroxide, not for a superoxide. Although the crystal structure was determined at low temperature, it could not be completely ruled out that the unusually short O-O bond length is simply a consequence of an artefact from vibrational effects. To get additional support for the unusually short O-O distance in the vanadium-bound peroxide, several attempts were made to crystallize  $[V^V=O(O_2)(N_2py_3o)]^+$ , in both the perchlorate and nitrate form, but all without success. Theoretically there are two possibilities to describe our complex: as the vanadium(V)-oxo-peroxo or as the vanadium(IV)-oxo-superoxo form. Due to the above described discrepancies, further spectroscopic and computational studies were done to get more insight to the electronic structure. From the ESI-MS spectra, the cationic peak at 616.4 can be assigned both as  $[V^{IV}=O(O_2^-)(N_2py_3o)]^+$  or as  $[V^V=O(O_2^{2-})(N_2py_3o)]^+$ , since both have the same overall charge. The UV-spectrum clearly shows the complete lack of d-d bands, which supports the existence of the  $d^0$  vanadium(V)-peroxo structure, and even the observed CT-transition correlates well with values reported for



side-on bound peroxides. Moreover, the complex is completely EPR-silent: this can be assigned to a diamagnetic structure or to a paramagnetic one with antiferromagnetic coupling. For this complex a  $^1\text{H-NMR}$  could be recorded, supporting again the diamagnetic structure.

To get further support for the correct assignment of the side-on bound peroxy / superoxy unit, DFT calculations were performed, using the B3LYP functional and the 6-31G(d) basis set. The overall multiplicity of the cationic part of the complex is strongly dependent on the oxidation state of the vanadium center and that of the side-on bound entity. In case of the diamagnetic vanadium(V)-oxo-peroxy complex the multiplicity is 1, both the  $d^0$  vanadium(V) and the peroxide have no free electrons. Considering a  $d^1$  vanadium(IV) center with a superoxide (with a single unpaired electron), the overall multiplicity is 3, assuming a ferromagnetic interaction between the two free electrons. When the spins of vanadium(IV) and superoxide cancel each other due to an antiferromagnetic interaction, formally a singlet state is generated, similar to the V(V)-oxo-peroxy case. Geometry optimizations have been performed for both spin states ( $S=0$  and  $S=1$ ), using the crystal structural data as a starting structure. Interestingly, both calculations led to the same optimized structure. The obtained O-O bond length for the optimized structure was 1.415 Å, which is significantly larger than determined crystallographically, and typical for a peroxide, not for a superoxide. The calculated O-O stretching frequency ( $1005\text{ cm}^{-1}$ ) lies in the range for peroxides. Interestingly, the Mulliken spin densities for the optimized structure of the  $S=1$  state showed no spin on both the central vanadium and the peroxy/superoxy unit. Instead, spin densities close to 1 are observed for two carbon atoms. These results are consistent with a vanadium(V)-oxo-peroxy species.

#### **6.4. Oxidation of oxo-peroxy vanadium(V) to oxo-superoxy vanadium(V) complex using chemical oxidants**

In the literature, only one case is reported for an oxidation of a vanadium(V)-oxo-peroxy complex, and the very unstable V(V)-oxo superoxy species was isolated as the product of an electrochemical oxidation.<sup>108</sup> The use of chemical oxidants is not without precedent but there are several drawbacks for such reactions: exclusively inorganic (not ligand-bound)  $\text{V}^{\text{V}}$ -oxo-peroxy species as starting materials were investigated, the reactions were merely kinetically analyzed and the existence of  $\text{V}^{\text{V}}$ -oxo-superoxy species was only mechanistically proposed.<sup>109,110</sup> For this reason it is still a challenge to oxidize  $\text{V}^{\text{V}}$ -oxo-peroxy complexes with chemical oxidants.

*Oxidation with Co<sup>3+</sup>*

Co<sup>3+</sup> was reported to oxidize inorganic oxo-peroxo vanadium(V).<sup>109</sup> Co<sup>3+</sup> as a free ion is stable only in strongly acidic conditions, in which the [V<sup>V</sup>=O(O<sub>2</sub>)(N<sub>2</sub>py<sub>3</sub>o)]<sup>+</sup> complex is no longer stable (at very acidic pH, the ligand donors are protonated). Indeed, the addition of this oxidant leads to partial decomposition of the complex. The UV-vis spectra show no conversion of [V<sup>V</sup>=O(O<sub>2</sub>)(N<sub>2</sub>py<sub>3</sub>o)]<sup>+</sup> to [V<sup>IV</sup>=O(N<sub>2</sub>py<sub>3</sub>o)]<sup>2+</sup> and no VO<sup>2+</sup> complex species could be assigned in the mass spectrum. Attempts were made to use a combination of VO<sub>3</sub><sup>+</sup> and VO<sup>2+</sup> (which was proposed to accelerate further the oxidation of the peroxovanadium(V) species),<sup>109</sup> but again, no decay of the VO<sub>3</sub><sup>+</sup> band was detected by using UV-vis spectroscopy. Interestingly, a new band appeared at 470 nm, which can be related to the exchange between VO<sub>3</sub><sup>+</sup> and Co<sup>3+</sup> or to the decomposition of the VO<sub>3</sub><sup>+</sup>-complex to ligand and free VO<sub>3</sub><sup>+</sup>-ion. At higher pH cobalt(III) can only be stabilized only by complexation, and inert complexes are not suitable as oxidants.

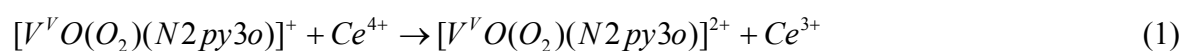
*Oxidation with KO<sub>2</sub>*

The orange methanolic solution of [V<sup>V</sup>=O(O<sub>2</sub>)(N<sub>2</sub>py<sub>3</sub>o)]<sup>+</sup> turns light violet after the addition of 20 eq KO<sub>2</sub> at -40°C. The superoxide radical peak was not seen in the EPR (although this was the only paramagnetic material in the sample), so it was not possible to differentiate between a free or a vanadium-bound superoxide. Since signals assignable for paramagnetic VO<sup>2+</sup>-species were also not seen, the possibility of a reaction pathway involving peroxide-superoxide exchange followed by a disproportionation to the vanadyl-complex and to oxygen can be excluded (for details, see below in this section).

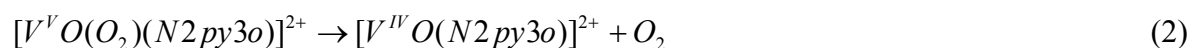
*Oxidation with Ce<sup>4+</sup>*

Preliminary qualitative test reactions have shown that addition of 1 eq of Ce<sup>4+</sup> to the orange acetonitrile solution of [V<sup>V</sup>=O(O<sub>2</sub>)(N<sub>2</sub>py<sub>3</sub>o)]<sup>+</sup> causes a color change to pale yellow at -40°C. Addition of H<sub>2</sub>O<sub>2</sub> to this mixture returns the orange color, which may indicate the regeneration of the original [V<sup>V</sup>=O(O<sub>2</sub>)(N<sub>2</sub>py<sub>3</sub>o)]<sup>+</sup> complex. The pale yellow color may be attributed to Ce<sup>3+</sup> or to a V<sup>V</sup>-oxo-superoxo species, which is assumed to absorb at this wavelength range. In order to clarify what species are formed after the addition of Ce<sup>4+</sup>, an EPR spectroscopic study was carried out. Performing the reaction again at -40°C, the probe was frozen after 5 min at 110 K, and measured. (Figure 6.7). The strong signals of paramagnetic Ce<sup>3+</sup> appear (typical set of peaks for a d<sup>1</sup> system without a nuclear spin), but no peaks assignable for vanadium species could be observed (the metal remains pentavalent). This indicates a rapid reduction of Ce<sup>4+</sup>. When the probe was defrosted and re-frozen, a new set of peaks appeared, typical for a VO<sup>2+</sup>-species. Keeping the sample for longer at -40°C, the

$\text{VO}^{2+}$  peak set becomes more intense, but there is no change in the intensity of the  $\text{Ce}^{3+}$  signals. This means that the formation of the  $\text{VO}^{2+}$ -species does not result from a reaction with the oxidant  $\text{Ce}^{4+}$ . Putting these observations together, we assume that in the first step  $\text{Ce}^{4+}$  oxidizes the  $\text{V}^{\text{V}}$ -oxo peroxy complex to the superoxy form, which, although EPR active, cannot be seen due to the presence of other paramagnetic component ( $\text{Ce}^{3+}$ ), which gives significantly more intensive signals than the  $\text{V}^{\text{V}}$ -bound superoxide.



This step is followed by an intramolecular disproportionation: the  $\text{V}^{\text{V}}$  oxo-superoxy complex is transformed to  $\text{VO}^{2+}$ -complex and to molecular oxygen.



The lifetime of the superoxy complex below  $-80^\circ\text{C}$  is relatively long, and the slow conversion of this species to  $\text{VO}^{2+}$  and  $\text{O}_2$  was only observed at  $-40^\circ\text{C}$ .

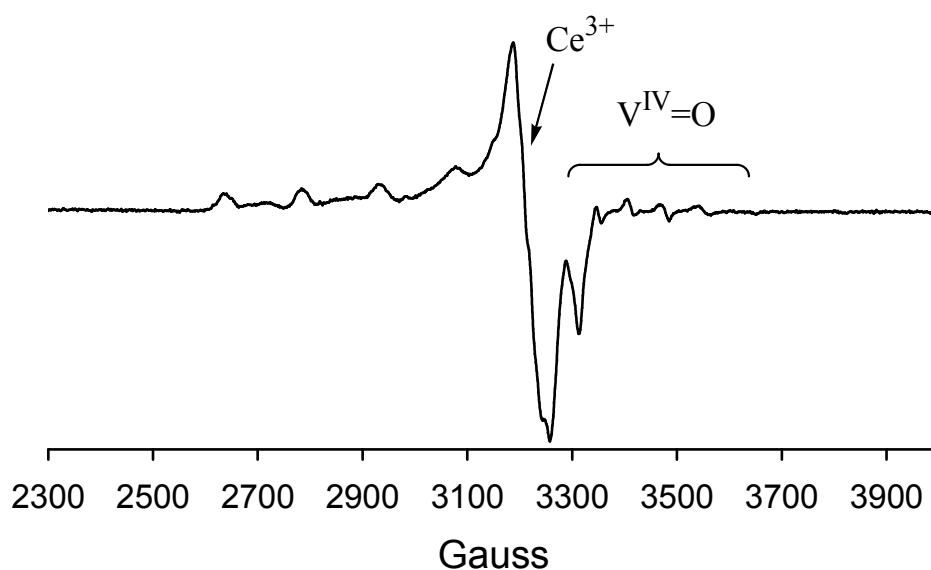
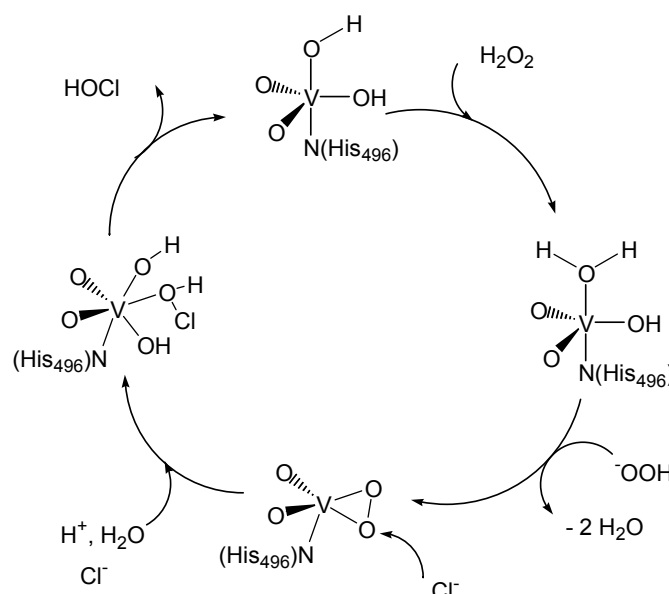


Figure 6.7.  $[\text{V}^{\text{V}}=\text{O}(\text{O}_2)(\text{N}2\text{py}3\text{o})]^+ + 1 \text{ eq } \text{Ce}^{4+}$  after refrosting for 10 min, in MeCN:DMF 1:2

## 6.5. Catalysis

### 6.5.1. Haloperoxidase test

Haloperoxidases are vanadium enzymes responsible for the oxidation of halides to the corresponding hypohalous acids or to other two-electron oxidized halogenating intermediates. In presence of nucleophilic substrates, halogenated compounds are formed *in vivo*.<sup>94</sup> These halogenation reactions occur probably as a part of the host defence system, to prevent the biocidal effects of hypohalous acids. In the absence of organic substrates, the  $X^+$  form of the halide oxidizes hydrogen peroxide to elemental oxygen. The active site of haloperoxidases isolated from *Curvularia inaequalis* consists of a trigonal bipyramidal monovanadium site, coordinated to 3 non-protein oxo groups in the equatorial plane, and to one histidine and a hydroxy group at the axial positions.<sup>25,111</sup> The oxidized peroxy form of the enzyme contains a metal-coordinated peroxy unit, an oxygen and a histidine in the basal plane and an oxo-oxygen in axial position.



**Figure 6.8. Proposed catalytic cycle of haloperoxidases**<sup>39</sup>

When a hydrogen peroxide approaches the active site, the axial OH-unit is protonated and the hydroperoxide is generated (Figure 6.8). The weakly bound axial water dissociates, and a side-on bound peroxy intermediate is formed, with the concomitant removal of another water molecule. Attack of a halide ion on the peroxide and uptake of a proton leads to the formation of HOCl and the native site is regenerated. It can be seen that the catalytically active intermediate is the peroxy-vanadium structure that reacts directly with the halide ion in presence of acid.

Bromination of the organic dye Phenol Red was carried out under conditions reported by Pecoraro and coworkers:<sup>112</sup> 0.5 mM  $[V^V=O(O_2)(N_2py_3o)]^+$ , 15.0 mM  $Bu_4NBr$ , 5.0 mM  $H_2O_2$ , 5.0 mM triflic acid and 1.25 mM Phenol Red in acetonitrile at 0°C. 20  $\mu$ L aliquots were injected into 910  $\mu$ L phosphate buffer (pH = 7.1) and the absorbance at 590 nm (absorption maximum of the tetrabrominated dye) was recorded.

The reaction requires the fully protonated form of the dye (under highly acidic condition), since the o/p bromination of a phenol is much faster than that of a phenolate (change in the inductive effect). The tetrabromination of Phenol Red gives Bromophenol Blue (Figure 7.10), which can be selectively measured by UV-vis spectroscopy at 590 nm. At this wavelength the absorption of the unreacted Phenol Red is negligible. The acid needs to contain a non-coordinating anion, which does not influence the vanadium center. In this test triflic acid was used. The  $pK$  values of the phenolic groups vary largely from the solvent and under strictly non-aqueous conditions the added acid protonates the two phenol moieties completely. The presence of traces of water in the aqueous  $H_2O_2$  solution does not influence the reaction.<sup>112</sup>

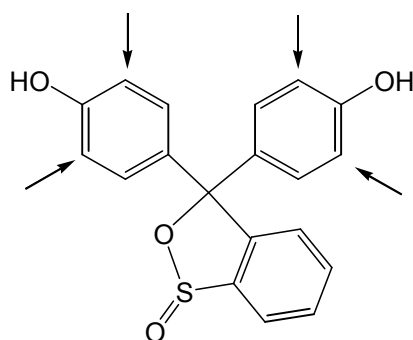


**Figure 6.9. Phenol Red, and its four bromination sites. The tetrabrominated dye is Bromophenol Blue**

In the first step the product Bromophenol Blue was calibrated by UV-vis, and the degree of dilution after the reaction was determined, in order to match the suitable absorbance interval. To the acetonitrile solution of Phenol Red and  $[V^V=O(O_2)(N_2py_3o)]^+$ ,  $H_2O_2$  was added, and the mixture was cooled to 0°C. This was followed by the addition of a large excess of tetrabutylammonium-bromide, ensuring a constant ionic strength in the solution ( $\mu = 15$  mM). The reaction was initiated by the injection of the acid. Aliquots, taken from the reaction mixture after given reaction times, were injected to a phosphate buffer (pH = 7.1). At this pH, the product Bromophenol Blue is in its single deprotonated form, with a characteristic absorption maximum at 590 nm. Moreover, the presence of water, and the neutral pH of the buffer completely quench the bromination of the dye.

The generally accepted mechanism for the bromination of organic substrates with a vanadium(V)-oxo-peroxo complex<sup>112</sup> in presence of hydrogen peroxide, contains the following steps:

In the first step, the catalyst oxidizes the halide ion to the +1 form, with a concomitant consumption of acid, and production of a dioxo-vanadium(V) species.



The halogen in oxidation state of +1 performs an electrophilic attack on the organic substrate:



The active catalyst is then regenerated by the reaction of the dioxo-vanadium(V) species with hydrogen peroxide:



The presence of large excess of acid is necessary, since oxidation of 1 eq halide consumes 1 eq acid.

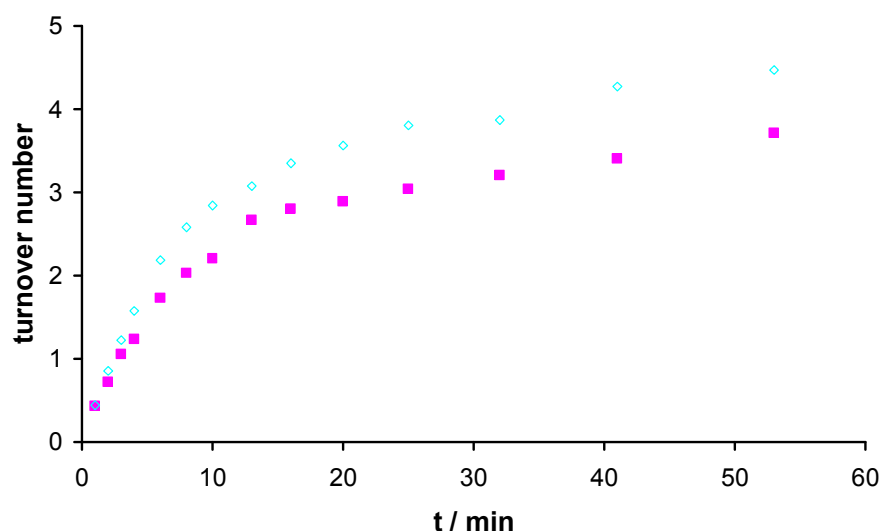


**Figure 6.10. Turnover numbers for the formation of Bromophenol Blue as a function of time. In presence (■), in the absence (◇) of  $[\text{V}^{\text{V}}=\text{O}(\text{O}_2)(\text{N}2\text{py}3\text{o})]^+$  complex**

The blind test was carried out in a similar way to the “original” reaction, but without adding  $[\text{V}^{\text{V}}=\text{O}(\text{O}_2)(\text{N}2\text{py}3\text{o})]^+$ . The observed turnover numbers in presence of the vanadium complex were around 10% smaller than that of the blank system (Figure 6.10).

One possible reason for the inactivity of  $[\text{V}^{\text{V}}=\text{O}(\text{O}_2)(\text{N}2\text{py}3\text{o})]^+$  in the bromination reaction can be that vanadium in this complex is bound to a ligand with N5 donor set. In most of the reported examples ligands containing some oxygen donors were utilized (carboxylate and phenolate coordination); such a chromophore is seen also at the active site of haloperoxidases.<sup>39</sup>

Another possible reason for the inactivity of  $[V^V=O(O_2)(N_2py_3o)]^+$ , is that the coordination sphere of vanadium in the complex is already saturated. In the mechanism of the bromide oxidation, expansion of the coordination sphere in the  $V^V$ -oxo-peroxo complex is proposed.<sup>25,39,113</sup> Such a mechanism is not feasible in our case, since some of already existing coordinative bonds must first be cleaved. Breaking a  $V^V$ -peroxo bond is difficult due to the energetically favoured hard-hard interaction, while cleaving just one V-N bond would destabilize the other metal-ligand bonds. The four N-donor atoms of the rigid and preorganized  $N_2py_3o$  ligand coordinate simulatenously to vanadium and a stepwise formation of the vanadium-complex with lower ligand denticity is not probable.

### 6.5.2. Catalytic oxidation of olefins

#### 6.5.2.1 Introduction

Oxidation of olefins using cheap and easily accessible hydrogen peroxide in presence of relatively non-toxic metal salts or complexes has received increasing attention in recent years.<sup>114</sup> Catalytic systems which are highly efficient and selective are good candidates for the large scale production in the industry. Although homogeneous catalysts have a serious drawback when compared to heterogenous systems, namely the difficulty of their recirculation, more information can be gained about their method of action at a molecular level, and thus systematically even more active catalysts can be designed. Among the homogeneous catalysts, much work has been done with porphyrin complexes<sup>115</sup> as functional models for heme iron enzymes, the most well known representative of which is Cytochrome P450.<sup>28</sup> Other classes of complexes, using salen-<sup>116</sup> and triazacyclononane-based ligands,<sup>117</sup> represent another productive area in catalytic olefin oxidation. Complexes of pyridine-based ligands were also extensively investigated and numerous examples were shown to be efficient catalysts in the oxidization of olefins. Among them, different Fe(II) complexes developed by Que and coworkers were investigated from the perspective of biomimetic non-heme catalysts.<sup>118,119</sup> Complexes of other metals as iron were scarcely studied as non-heme catalysts, a dimanganese(III) system investigated by the Unilever group<sup>120</sup> and a cyclam-based manganese(IV) complex developed by Busch and co-workers<sup>40</sup> belong to the few examples. One reported vanadium-based appeared some decades ago, using a vanadium(V)-oxo-peroxo complex with simple co-ligands such as  $\alpha$ -substituted pyridines or pyridine-N-oxides.<sup>97</sup> The development of this field was strongly hindered by the problem of solubility and for this reason, not many achievements have been made, although vanadium compounds (mostly purely inorganic) have been widely used as oxidation catalysts in the industry, almost

exclusively as heterogeneous catalysts. The design of efficient, low-molecular weight vanadium-complexes has remained a challenge up to now.

The catalytic activity of  $[\text{V}^{\text{IV}}=\text{O}(\text{N}2\text{py}3\text{o})]^{2+}$  and  $[\text{V}^{\text{V}}=\text{O}(\text{O}_2)(\text{N}2\text{py}3\text{o})]^+$  in the oxidation of cyclohexene and cyclooctene have been tested, and the results are presented below.

### 6.5.2.2. Oxidation of cyclooctene

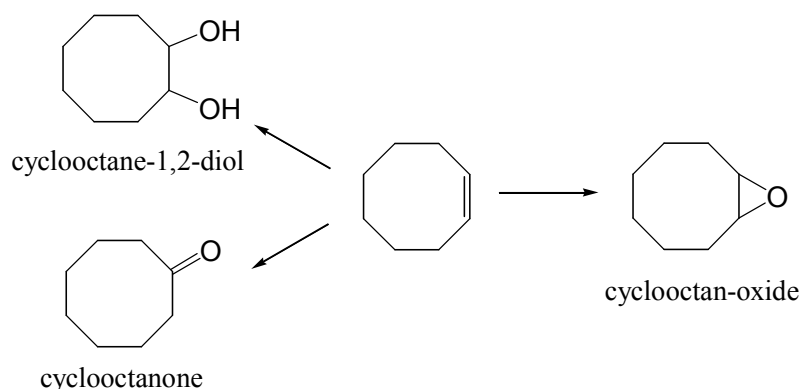


**Figure 6.11. Possible oxidation products of cyclooctene**

The oxidation of cyclooctene was demonstrated to be efficiently catalyzed by some Fe(II) bispidine complexes, in presence of  $\text{H}_2\text{O}_2$  in acetonitrile.<sup>34</sup> The catalytic oxidation of cyclooctene was carried out according to a reported procedure.<sup>34</sup>

**Table 6.1. Turnover numbers of the different oxidation products**

Catalyst system	Conditions	ketone	epoxide	diol
$[\text{V}^{\text{IV}}=\text{O}(\text{N}2\text{py}3\text{o})]^{2+}$	10 $\text{H}_2\text{O}_2$ , 20°C, 30+5 min	0.11	0.31	-
$[\text{V}^{\text{IV}}=\text{O}(\text{N}2\text{py}3\text{o})]^{2+}$	200 $\text{H}_2\text{O}_2$ , 40°C, 16 h	0.30/20	21.3/20	0.48/20
$[\text{V}^{\text{V}}=\text{O}(\text{O}_2)(\text{N}2\text{py}3\text{o})]^+$	no $\text{H}_2\text{O}_2$ , 20°C, 30+5 min	-	0.34	-
$[\text{V}^{\text{V}}=\text{O}(\text{O}_2)(\text{N}2\text{py}3\text{o})]^+$	no $\text{H}_2\text{O}_2$ , 40°C, 16 h	-	0.28	-
$[\text{V}^{\text{V}}=\text{O}(\text{O}_2)(\text{N}2\text{py}3\text{o})]^+$	10 $\text{H}_2\text{O}_2$ , 20°C, 30+5 min	0.15	0.26	-
$[\text{V}^{\text{V}}=\text{O}(\text{O}_2)(\text{N}2\text{py}3\text{o})]^+$	200 $\text{H}_2\text{O}_2$ , 40°C, 16 h	0.30/20	11.7/20	0.74/20

The  $[\text{V}^{\text{IV}}=\text{O}(\text{N}2\text{py}3\text{o})]^{2+}/\text{H}_2\text{O}_2$  system was slightly active, when using 10 eq of hydrogen peroxide: the TON for the products are significantly below 1. The turnover number for cyclooctanone was 0.11, while for cyclooctane-oxide it was determined to be 0.31. Formation of alcohol products was not detected. When longer reaction times are applied, higher temperature and higher  $\text{H}_2\text{O}_2$  concentrations (200 eq  $\text{H}_2\text{O}_2$ , 16 h, 40°C), the amount of the



epoxide is significantly larger, even when considering a correction for the turnover numbers due to the different  $\text{H}_2\text{O}_2$  concentrations. Surprisingly, much less ketone and diol is produced, than the epoxide.

With  $[\text{V}^{\text{V}}=\text{O}(\text{O}_2)(\text{N}2\text{py}3\text{o})]^+$  alone as catalyst (without the addition of hydrogen peroxide), only a slight activity was found: the only formed product was the epoxide, with turnover number of 0.34 (20°C, 30+5 min) and 0.28 (40°C, 16 h).

The combination of  $[\text{V}^{\text{V}}=\text{O}(\text{O}_2)(\text{N}2\text{py}3\text{o})]^+$  and  $\text{H}_2\text{O}_2$  as catalyst, led to production of small amounts of ketone and epoxide, comparable to the values measured for the  $[\text{V}^{\text{IV}}=\text{O}(\text{N}2\text{py}3\text{o})]^{2+}/\text{H}_2\text{O}_2$  system, under normal conditions (20°C, 10 eq  $\text{H}_2\text{O}_2$ ). Similarly to the  $[\text{V}^{\text{IV}}=\text{O}(\text{N}2\text{py}3\text{o})]^{2+}/\text{H}_2\text{O}_2$  case, when more drastic reaction conditions were used, an almost selective formation of epoxide was observed.

### 6.5.2.3. Oxidation of cyclohexene

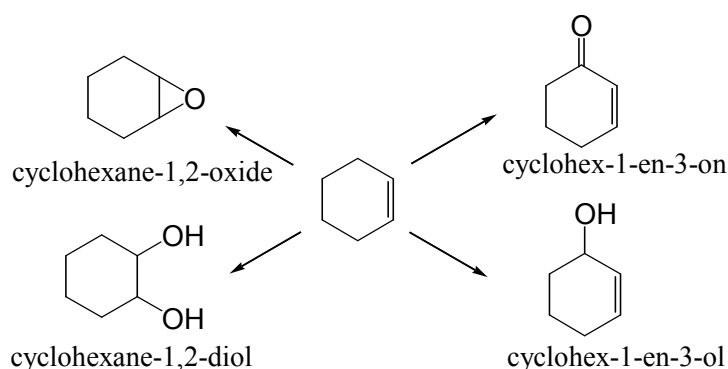


Figure 7.13. Possible oxidation products of cyclohexene

The  $\text{V}^{\text{V}}$ -oxo-peroxo complex was inactive as catalyst, both in presence and in the absence of  $\text{H}_2\text{O}_2$ . None of the possible oxidation products were detected on the chromatograms. Applying 0.7 mM  $[\text{V}^{\text{IV}}=\text{O}(\text{N}2\text{py}3\text{o})]^{2+}$ , 7 mM  $\text{H}_2\text{O}_2$  and 1000 eq substrate at 20°C, only slight activity is observed. The turnover numbers for the formation of cyclohexene-1-ol are under 0.1, while for cyclohexene-1-one they are under 0.3, and these values are even lower than expected for a simple stoichiometric reaction. No formation of non-allylic oxidation products (diol, epoxide) was detected.

Under the conditions of 0.7 mM  $[\text{V}^{\text{IV}}=\text{O}(\text{N}2\text{py}3\text{o})]^{2+}$  and 140 mM  $\text{H}_2\text{O}_2$  at 40°C for 16 h, a stoichiometric conversion to the epoxide (TON=1.00), and a low amount of the cyclohexane-1,2-diol (TON=0.46) was obtained. Among the allylic products, only a small amount of cyclohexene-1-ol (TON=0.42) was detected, but the high turnover with respect to cyclohexene-1-one (TON=40.7), suggests that the autoxidation pathway (involvement of air

oxygen) was operative. Furthermore, large amounts of side-product (probably cyclohexene-hydroperoxide) were also formed, which supports the above stated mechanism.<sup>121,122</sup>

**Table 6.2. Turnover numbers of the different oxidation products**

Catalyst system	Conditions	enone	epoxide	enol	diol
$[\text{V}^{\text{V}}=\text{O}(\text{O}_2)(\text{N}2\text{py}3\text{o})]^+$	no $\text{H}_2\text{O}_2$ , 20°C, 30+5 min	-	-	-	-
$[\text{V}^{\text{V}}=\text{O}(\text{O}_2)(\text{N}2\text{py}3\text{o})]^+$	10 $\text{H}_2\text{O}_2$ , 20°C, 30+5 min	-	-	-	-
$[\text{V}^{\text{IV}}=\text{O}(\text{N}2\text{py}3\text{o})]^{2+}$	10 $\text{H}_2\text{O}_2$ , 20°C, 30+5 min	< 0.3	-	< 0.1	-
$[\text{V}^{\text{IV}}=\text{O}(\text{N}2\text{py}3\text{o})]^{2+}$	200 $\text{H}_2\text{O}_2$ , 40°C, 16 h	40.7	1.00	0.42	0.46
-	200 $\text{H}_2\text{O}_2$ , 40°C, 16 h	< 0.7	-	-	-

It is not without precedence that the oxidation of cyclohexene leads almost exclusively to the formation of allylic products (cyclohex-1-en-3-ol [enol] and cyclohex-1-en-3-one [enon]), as such a product distribution was reported when using  $\text{V}_2\text{O}_5$  as catalyst in presence of  $\text{H}_2\text{O}_2$ .<sup>123</sup>

A control reaction under the same conditions, with the exception of the addition of the vanadyl complex, gave exclusively the enon product, in a very small concentration (TON < 0.7). Since the ketone was the only product, we can assume that autoxidation was operative. The presence of the catalyst simply increases the amount of the ketone, without influencing the formation of non-allylic products. It was suggested that the oxidation of cyclohexene under air can follow an autoxidation pathway leading to the allylic products.<sup>124</sup>

It is generally accepted that the reaction between vanadyl-ions and  $\text{H}_2\text{O}_2$  produces hydroxyl radicals.<sup>106</sup> The activity of  $[\text{V}^{\text{IV}}=\text{O}(\text{N}2\text{py}3\text{o})]^{2+}$  may be attributed to the action of the formed hydroxyl radicals. The fact that the amount of the ketone was significantly larger than that of the alcohol, suggests a cooperative action of hydroxyl radicals and hydrogen peroxide: after hydroxylation the peroxide initiates further oxidation of the alcohol to ketone.

The reason for the very low activity may be the result of the saturated coordination sphere around vanadium, because there is no space for binding the substrate. It was proposed that when a vacant site on the vanadium site is present, the olefin is able to coordinate, leading to the formation of epoxides.<sup>39</sup> This may explain why we see only allylic oxidation products (ketone + alcohol), but no epoxide.

When comparing the results with that of the cyclooctene case, we can conclude that cyclooctene was almost selectively oxidized to epoxide, only traces of ketone and diol was found; whereas in case of the cyclohexene oxidation, the main product was the ketone. The large difference is that cyclohex-1-en-3-on is an allylic product, resulting from autoxidation. Such a reaction pathway is never seen for cyclooctene.

## 7. Oxidative N-dealkylation in a cobalt-bispidone complex – mechanistic investigations

### 7.1. Introduction

Oxidative N-dealkylation is a major pathway in drug metabolism,<sup>26,27</sup> and this may involve various peroxidase or oxidase enzymes, such as lipogenase, horseradish peroxidase, bleomycin, methemoglobin, cytochrome C, cytochrome P450 and amine oxidases.<sup>28,29</sup> An AlkB protein can repair damaged DNA sequences through an N-dealkylation reaction, which makes this enzyme a promising candidate for practical application in biotechnology.<sup>125</sup> The two major reaction pathways, dehydrogenation (metal-based one electron transfer) and H-atom abstraction (C-based radical mechanism) have been proposed and studied in detail.<sup>126</sup> A number of low molecular weight model complexes, primarily with iron and copper, have been shown to mimic these processes with either dioxygen or peroxide as oxidant. (Figure 7.1).

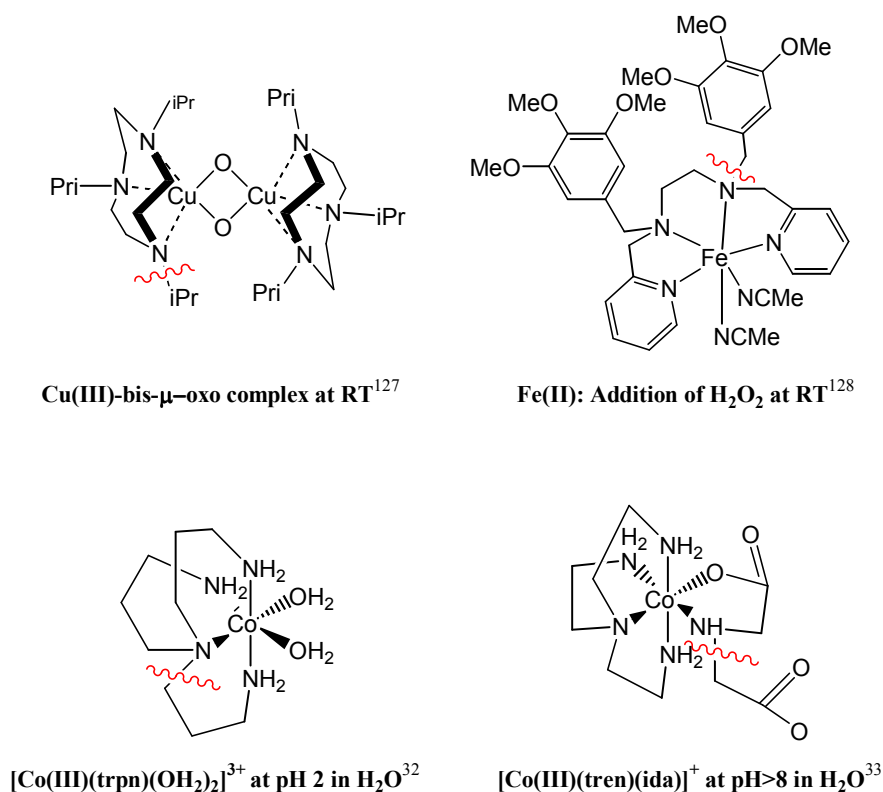


**Figure 7.1. Examples for low-molecular weight model complexes which undergo intramolecular oxidative N-dealkylation**

Among the investigated model systems, copper(III)-bis- $\mu$ -oxo complexes represent a large category. These complexes are stable at  $-80^\circ\text{C}$ , but at room temperature they are converted to Cu(II)-hydroxo complexes with the concomitant cleavage of an N-alkyl group, most often a

benzyl group.<sup>30,127,129-132</sup> ( $\mu$ -1,1-hydroperoxo)dicopper(II) complexes demonstrate similar behaviour; they can be stabilized at  $-80^{\circ}\text{C}$ , but at room temperature an N-alkyl side chain is removed.<sup>133,134</sup> There are considerably less examples for iron complexes. A diiron-tetracarboxylate complex developed by Lippard and coworkers reacts with oxygen at room temperature, leading to the loss of an N-benzyl side chain.<sup>31,135</sup> The effect of the addition of hydrogen peroxide is nicely demonstrated in a mononuclear iron(II) complex, which is up to now the sole example for the intramolecular N-dealkylation in a transition metal complex, initiated by  $\text{H}_2\text{O}_2$ .<sup>129</sup> There are only few examples with cobalt-based systems involved in intramolecular oxidative N-dealkylation.<sup>32,33</sup> In both cases the dealkylation takes place in aqueous solutions of cobalt(III) complexes, in acidic<sup>32</sup> or in basic<sup>33</sup> medium. In general the cobalt/dioxygen (hydrogen peroxide) chemistry is dominated by the formation of  $\mu$ -peroxo- and  $\mu$ -superoxo dicobalt(III) complexes and their hydrolysis to mononuclear cobalt(III) products;  $\mu$ -peroxo-dicobalt(II) and mononuclear cobalt(II) as well as cobalt(III) hydroperoxo complexes have also been reported, but only rarely have they been studied in detail.<sup>136</sup>

It has been reported that the reaction between the Co(II)-N2py2 complex with hydrogen peroxide leads not only to oxidation of cobalt(II) to cobalt(III), but also to elimination of the N7-bound methyl group.<sup>7</sup> In this chapter a detailed spectroscopic, kinetic and computational study is presented, to gain a better insight into the reaction mechanism. Moreover, spectroscopic characterization and oxidation of cobalt(II) complexes with novel bispidone ligands are also reported.

## 7.2. Synthesis and spectroscopic characterization of the cobalt complexes

$[\text{Co}^{\text{II}}(\text{N}2\text{py}2\text{PhO})(\text{OH}_2)]\text{ClO}_4$  was prepared in the presence of 1 equivalent of triethylamine. This complex was isolated as a precipitate after the addition of water. Deprotonation of the phenolic group was confirmed by elemental analysis (loss of one perchlorate changes the elemental composition significantly) and mass spectroscopy ( $588.6 [\text{Co}^{\text{II}}(\text{N}2\text{py}2\text{PhO})]^+$ ). The d-d bands, typical for octahedral cobalt(II) complexes, appear as shoulders in the UV-vis spectrum, since these are strongly overlapped by a more intense band (480 nm ( $\epsilon = 147$ ), 519 nm ( $\epsilon = 118$ ), 553 nm ( $\epsilon = 121$ )). The charge transfer transition also has absorption maximum in this wavelength range.

$[\text{Co}^{\text{II}}(\text{N}2\text{py}2\text{Bz})(\text{OH}_2)_2](\text{ClO}_4)_2$  was prepared as the  $[\text{Co}^{\text{II}}(\text{N}2\text{py}2)(\text{OH}_2)_2](\text{ClO}_4)_2$  complex,<sup>7</sup> by mixing equimolar amount of  $\text{Co}(\text{ClO}_4)_2$  and the ligand in methanol at room temperature.

*UV-spectra*

Three bands are expected for octahedral Co(II) complexes ( $d^7$  configuration). The lowest energy transition  ${}^4T_{1g}(F) \rightarrow {}^4T_{2g}(F)$  falls into the NIR region. The  ${}^4T_{1g}(F) \rightarrow {}^4A_{2g}(F)$  transition is in the range of 530-550 nm for all complexes. The expected transition of  ${}^4T_{1g}(F) \rightarrow {}^4T_{1g}(P)$  appears as two separate peaks, since the  ${}^4T_{1g}(P)$  term is splitted to two terms,  ${}^4E_g(P)$  and  ${}^4A_{2g}(P)$ , due to the distortion of the octahedral geometry around the central cobalt ion.

**Table 7.1 Absorption maxima (nm) with extinction coefficients in paranthesis, for the cobalt(II) complexes and for their oxidized forms (obtained after treatment with 170 eq  $H_2O_2$ )**

	N2py2Bz	N2py2PhOH	N2py2 <sup>7</sup>
Co(II)	463(18.9)	480(147)	425(13.8)
	517(19.1)	519(118)	486(19.0)
	551(14.4)	553(121)	533(16.6)
Co(III)	499(79)	544(1050)	508(124)

The extinction coefficients of the N2py2 and of the N2py2Bz complexes are in a similar range, which can be explained by the close analogy in structure of the two ligands. Both are tetradentate and differ only in the side chain attached to N7. The methyl and benzyl moieties have almost no electronic influence on the coordination around cobalt(II).

The most intense bands among the Co(II) complexes were found in the phenolate complex, where again 3 bands were observed. It seems that the Co-O charge transfer band is strongly overlapped with the 3 d-d bands, so the clear absorption maxima can not be determined.

*Redox potentials*

Among the complexes  $[Co^{II}(N2py2PhO)(OH_2)]ClO_4$  shows the lowest redox potential, which is due to the charge transfer character of the coordinating deprotonated phenolate unit. Comparing the redox potentials, it seems that the effect of the single negatively charged phenolate moiety on the stabilization of cobalt(III) in the complex (75 mV), is around the same as in the chloro complexes of the pentadentate ligands N2py3o (92 mV) and N2py3u (136 mV), in which one chloride is coordinated.<sup>7</sup>

**Table 7.2 Redox potentials (mV) of the Co-complexes in acetonitrile vs. Ag/AgNO<sub>3</sub> (0.01 M)**

Complex	$E_{1/2}$
$[Co^{II}(N2py2Bz)(OH_2)_2](ClO_4)_2$	471 <sup>a</sup>
$[Co^{II}(N2py2PhO)(OH_2)]ClO_4$	75
$[Co^{II}(N2py2)(OH_2)_2](ClO_4)_2$ <sup>7</sup>	653

a: only cathodic wave

### 7.3. Oxidation of cobalt(II) complexes with H<sub>2</sub>O<sub>2</sub>

The oxidation of the cobalt(II) complexes was followed by UV-vis spectroscopy (Figure 8.2). In the case of N2py2PhOH, a considerably lower complex concentration had to be used due to the large  $\epsilon$  values. The expected conversion of the divalent form to cobalt(III) took place and the three weak bands of cobalt(II) were converted to a single more intense peak, typical of cobalt(III). The peaks of the cobalt(III) products are given in Table 7.1, the pseudo first order rate constants are summarized in Table 7.3.

**Table 7.3. Pseudo first order rate constants on the oxidation of 11 mM cobalt(II) complexes with 170 eq 30% H<sub>2</sub>O<sub>2</sub> in MeOH at 25°C**

Complex	$k$ ( $10^{-3} \text{ s}^{-1}$ )
$[\text{Co}^{\text{II}}(\text{N}2\text{py}2\text{Bz})(\text{OH}_2)_2](\text{ClO}_4)_2$	0.875
$[\text{Co}^{\text{II}}(\text{N}2\text{py}2\text{PhO})(\text{OH}_2)]\text{ClO}_4^{\text{a}}$	7.00
$[\text{Co}^{\text{II}}(\text{N}2\text{py}2)(\text{OH}_2)_2](\text{ClO}_4)_2^7$	1.86

a: 2.0 mM complex with 40 eq H<sub>2</sub>O<sub>2</sub>

The pseudo-first order rate constants for the oxidation of cobalt(II) complexes of the two tetradentate ligands (N2py2 and N2py2Bz), were shown to be the smallest among the investigated bispidone systems. Indeed, in the above two complexes cobalt(II) was stabilized to the largest extent, which is indicated by their redoxpotentials (see above). The cobalt(II) complex with the pentadentate N2py2PhOH ligand was oxidized faster by H<sub>2</sub>O<sub>2</sub> than the tetradentate ones, which can be related to its lower redoxpotential: the measured half-wave potentials for N2py2PhOH complexes were lower than for N2py2 and N2py2Bz, i.e. the trivalent form of the cobalt complexes with pentadentate ligands is more stabilized.

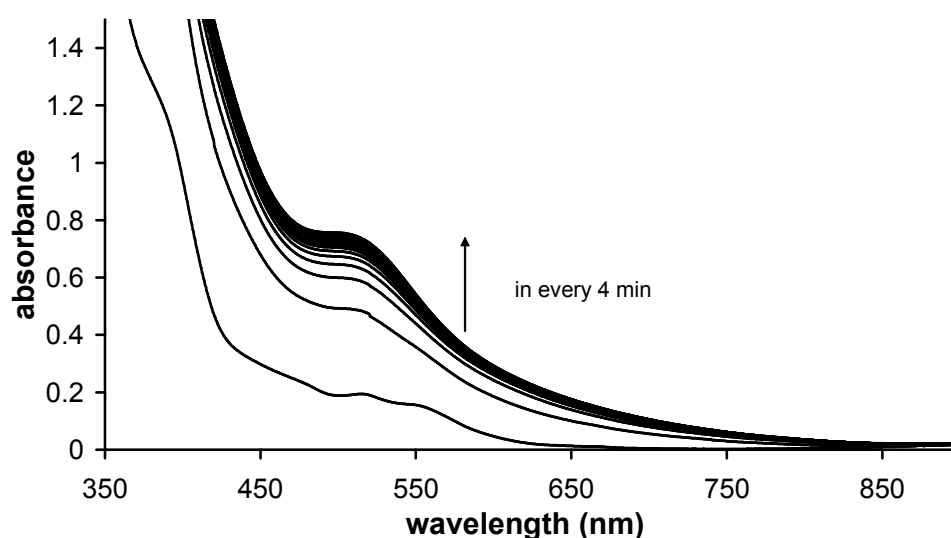


**Figure 7.2. Time-dependent UV-vis spectra for the oxidation of 11 mM  $[\text{Co}^{\text{II}}(\text{N}2\text{py}2\text{Bz})(\text{OH}_2)_2](\text{ClO}_4)_2 + 170 \text{ eq H}_2\text{O}_2$  in methanol. Spectra were recorded in 4 minute intervals**

As was shown above, cobalt(II) bispidone complexes could be successfully oxidized with hydrogen peroxide. The isolation of the oxidation products (complexes with trivalent cobalt) was possible, using ion exchange chromatography. (Dowex 50) The strongly binding chloride ions of the eluent (1 M HCl) occupied the free position(s) around the metal.

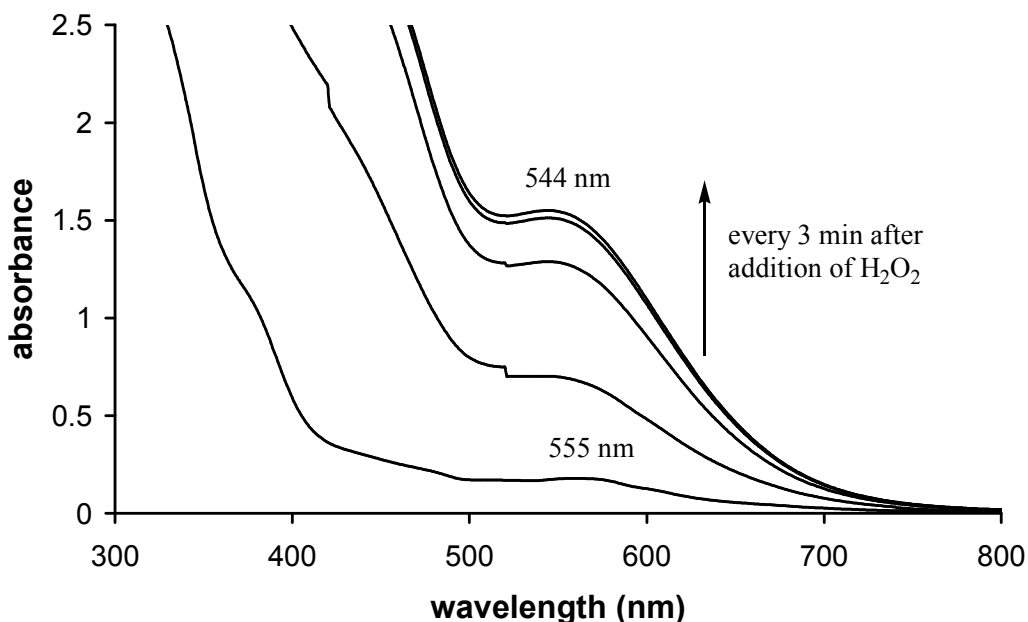


**Figure 7.3.** Time-dependent UV-vis spectra for the oxidation of  $[\text{Co}^{\text{II}}(\text{N}2\text{py}2\text{PhO})(\text{OH}_2)]\text{ClO}_4$  with 40 eq  $\text{H}_2\text{O}_2$  in methanol at  $25^\circ\text{C}$ . Spectra were recorded in 3 minute intervals

After oxidation with  $\text{H}_2\text{O}_2$ , the deprotonated phenolate in the  $\text{Co}(\text{N}2\text{Py}2\text{PhO})$  complex remains coordinated to the oxidized cobalt center, which is indicated by the strong charge-transfer band (544nm ( $\epsilon=1050$ )). This absorption coefficient is significantly larger than in any other known bispidone complexes that have only N-donor sites ( $\epsilon$  values are in the range of 120-290).<sup>7</sup> During purification using a Dowex column the acidic medium of the eluent 1 M HCl protonates the phenol moiety (this was proven by elemental analysis, which fits with the protonated ligand and 3 chloride ions in the structure). The protonated phenolic side chain most probably remains coordinated to cobalt(III), and the decreased value of the absorption coefficient for the charge-transfer band (from 1050 to 860) may be a consequence of the protonation (loss of the charge in the phenolate). The removal of the phenol from the coordination sphere and the binding of two chlorides in a *cis* fashion, would lead to significantly smaller  $\epsilon$  values: in a *cis*-dichloro cobalt(III) complex of a tetraazamacrocycle, the band at 525 nm is moderately strong ( $\epsilon = 101$ ).<sup>137</sup> In addition, the blue *cis*-dichloro cobalt(III) complex with the demethylated  $\text{N}2\text{py}2$  ligand shows relatively weak bands in the UV-vis spectrum (372 nm ( $\epsilon = 324$ ) and 561 nm ( $\epsilon = 99$ )). From these it seems likely that the protonated phenolate in  $[\text{Co}^{\text{III}}(\text{N}2\text{py}2\text{PhOH})\text{Cl}]\text{Cl}_2$  remains coordinated. Since no reference

UV-vis data for *cis*-chloro-phenol Co(III) complexes are available, a direct comparison with known values was not possible. A crystal structure would have provided a direct evidence for the coordination mode, but despite numerous efforts, no crystals suitable for structure determination could be grown. The  $^1\text{H}$  NMR spectrum showed that only the phenolic protons give sharp peaks, the others are significantly broadened (Figure 8.4).

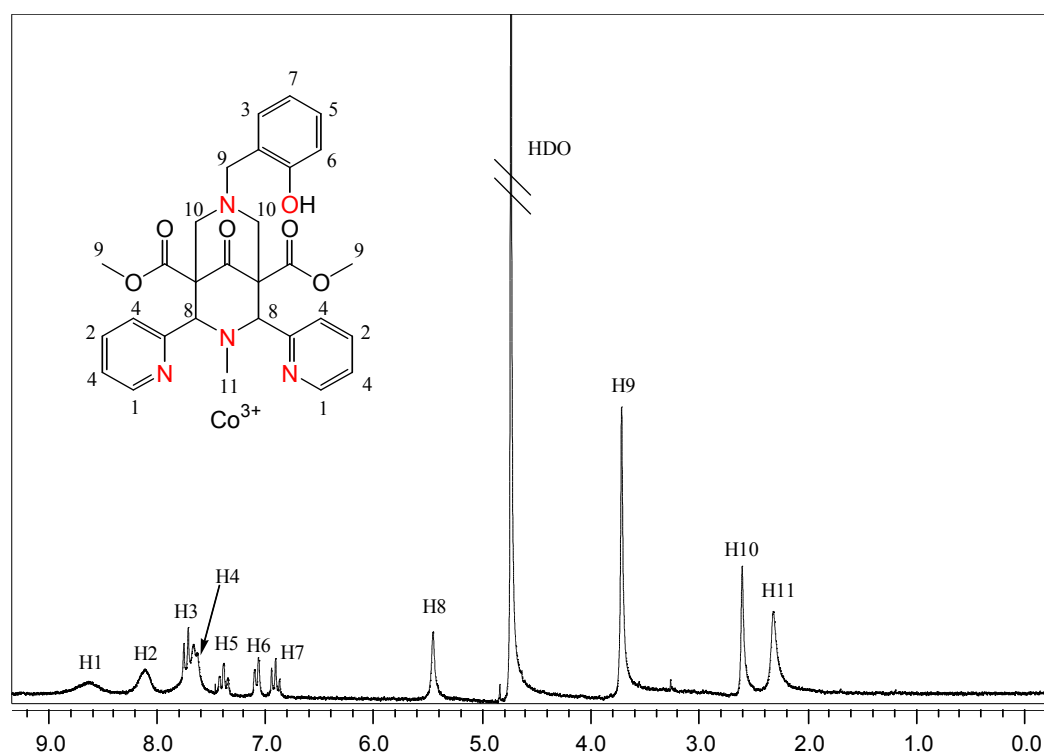


Figure 7.4.  $^1\text{H}$  NMR spectrum of  $[\text{Co}^{\text{III}}(\text{N}_2\text{Py}_2\text{PhOH})\text{Cl}]\text{Cl}_2$  in  $\text{D}_2\text{O}$



#### 7.4. Intramolecular oxidative N-dealkylation in a cobalt-bispidone complex

##### 7.4.1. Background

The diaqua cobalt(II) complex of N2py2 is highly inert, and Co(II) was demonstrated to fit perfectly to the ligand cavity without causing significant strain in the ligand backbone. In strong contrast to other cobalt(II) complexes, it cannot be oxidized with air. Addition of a stronger oxidant, hydrogen peroxide, to a methanolic solution of  $[\text{Co}^{\text{II}}(\text{N}2\text{py}2)(\text{OH}_2)_2](\text{ClO}_4)_2$  leads not only to the oxidation of the central metal, but also to the removal of the N7-bound methyl group (Figure 7.5).

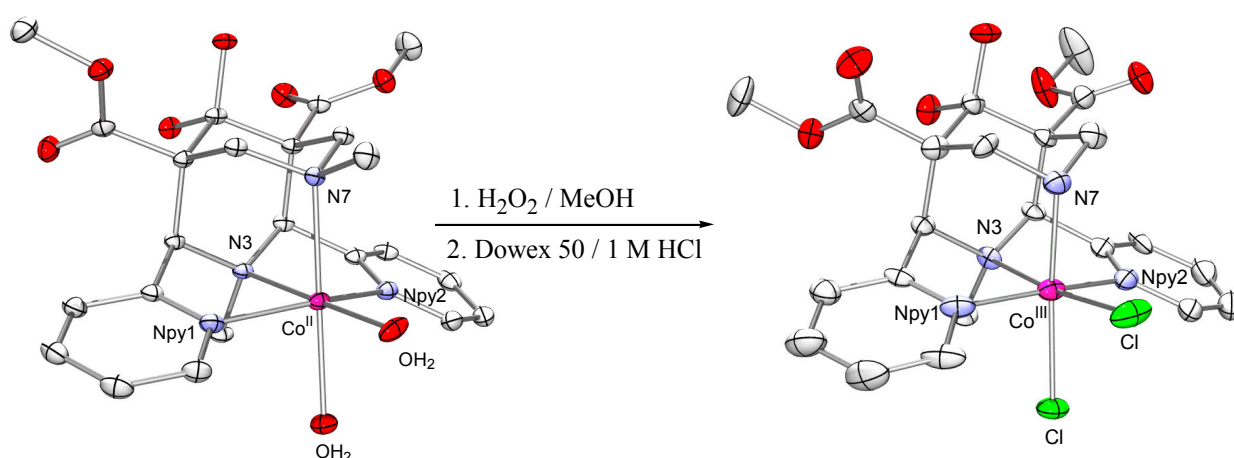


Figure 7.5. Oxidation of  $[\text{Co}^{\text{II}}(\text{N}2\text{py}2)(\text{OH}_2)_2](\text{ClO}_4)_2$  leads to a dealkylated Co(III)-complex

For complexes with penta- or hexadentate ligands this phenomenon was not detected. The redox potential of  $[\text{Co}^{\text{II}}(\text{N}2\text{py}2)(\text{OH}_2)_2](\text{ClO}_4)_2$  is unusually high, which indicates that its oxidation has a significant activation barrier. It was proposed that for this reason, the oxidant can induce some additional processes with similar barriers.<sup>7</sup> The oxidation of the Co(II) complexes of pentadentate ligands is faster, and the possibility of a side reaction is thus significantly smaller. Indeed, for those complexes, no demethylation was observed. The preference of the removal of the N7-bound methyl group over the N3-bound methyl group may be related to the difference in binding strength of the free coordination sites *trans* to N3 and *trans* to N7. Coordination of hydroperoxide in a monodentate fashion is preferred in equatorial position, since such a bond is shorter (and therefore more stable) than the axial ones.<sup>7,138</sup>

The aim of this work was to investigate this intramolecular N-dealkylation reaction in detail, to identify intermediate species and to elucidate the reaction mechanism.

#### 7.4.2. Dependence of the yield on the concentration of the oxidant

The oxidation of  $[\text{Co}^{\text{II}}(\text{N}2\text{py}2)(\text{OH}_2)_2](\text{ClO}_4)_2$  (6.7 mM methanolic solution), using different amounts of hydrogen peroxide was followed by UV-vis spectroscopy (Figures 7.6 and 7.7).

It was found that up to a limit of 20 eq of  $\text{H}_2\text{O}_2$  the conversion of cobalt(II) to cobalt(III) is strongly dependent on the amount of added oxidant. A further increase of the  $\text{H}_2\text{O}_2$  concentration leads to almost no change in the absorbance limit, i.e. in the yield of cobalt(III) complex..

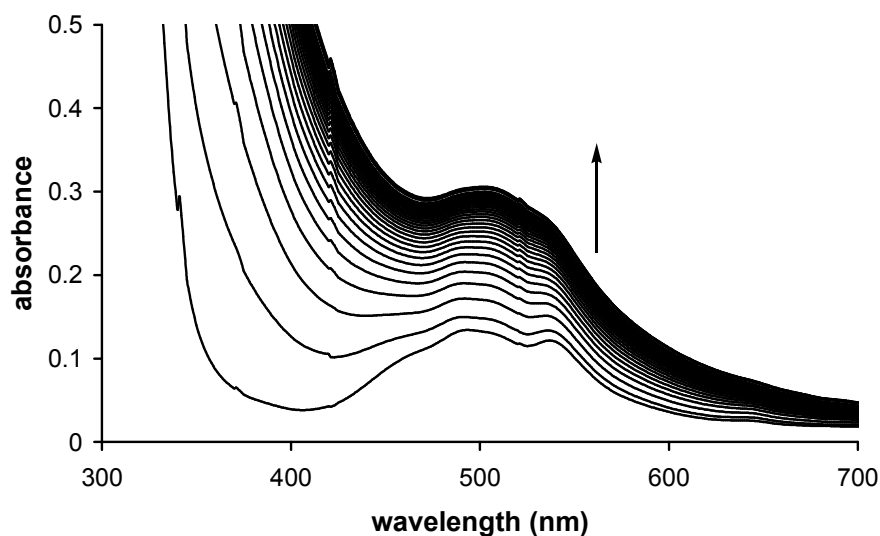


Figure 7.6. Time-dependent UV-vis spectra of the oxidation of 6.7 mM  $[\text{Co}^{\text{II}}(\text{N}2\text{py}2)(\text{OH}_2)_2](\text{ClO}_4)_2$  with 10 eq  $\text{H}_2\text{O}_2$  in methanol. Spectra were recorded in 5 minute intervals

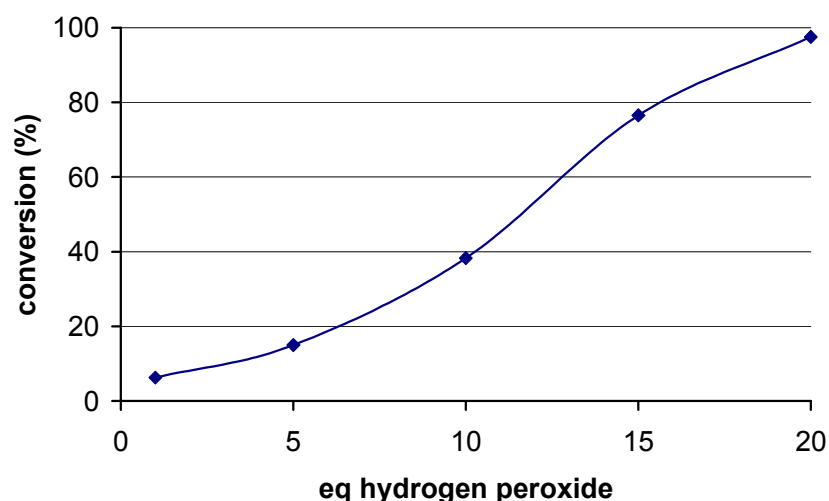


Figure 7.7. Conversion of Co(II) to Co(III) in 6.7 mM methanolic solution of  $[\text{Co}^{\text{II}}(\text{N}2\text{py}2)(\text{OH}_2)_2](\text{ClO}_4)_2$  as a function of the added hydrogen peroxide

To gain further insight into the reaction mechanism, ESI-MS spectra have been recorded for the reaction mixtures with different amounts of hydrogen peroxide.

**Table 7.4** Peaks and their assignment of the ESI-MS spectra recorded after 1 day reaction time for the reaction between 6.7 mM  $[\text{Co}^{\text{II}}(\text{N}2\text{py}2)(\text{OH}_2)_2](\text{ClO}_4)_2$  with 12 eq  $\text{H}_2\text{O}_2$  in methanol. Species with the original (not demethylated) N2py2 ligand are black, species with the demethylated N2py2a ligand are red

mass		assignment	intensity
241.9	M/2	$[\text{Co}^{\text{II}}(\text{N}2\text{py}2\text{a})]^{2+}$	30%
248.7	M/2	$[\text{Co}^{\text{II}}(\text{N}2\text{py}2)]^{2+}$	30%
257.9	M/2	$[\text{Co}^{\text{II}}(\text{N}2\text{py}2)(\text{OH}_2)]^{2+}$	30%
		$[\text{Co}^{\text{II}}(\text{N}2\text{py}2\text{a})(\text{MeOH})]^{2+}$	
264.8	M/2	$[\text{Co}^{\text{II}}(\text{N}2\text{py}2)(\text{MeOH})]^{2+}$	30%
		$[\text{Co}^{\text{II}}(\text{N}2\text{py}2\text{a})(\text{EtOH})]^{2+}$	
482.1	M	$[\text{Co}^{\text{II}}(\text{N}2\text{py}2\text{aH}_1)]^+$	10%
496.3	M	$[\text{Co}^{\text{II}}(\text{N}2\text{py}2\text{H}_1)]^+$	3%
500.2	M	$[\text{Co}^{\text{II}}(\text{N}2\text{py}2\text{a})(\text{OH})]^+$	3%
514.3	M	$[\text{Co}^{\text{III}}(\text{N}2\text{py}2\text{aH}_1)(\text{O}_2)]^+$	30%
		$[\text{Co}^{\text{II}}(\text{N}2\text{py}2)(\text{OH})]^+$	
516.3	M	$[\text{Co}^{\text{II}}(\text{OOH})(\text{N}2\text{py}2\text{a})]^+$	30%
532.3	M	$[\text{Co}^{\text{III}}(\text{N}2\text{py}2\text{aH}_1)(\text{O}_2)(\text{OH}_2)]^+$	10%
		$[\text{Co}^{\text{II}}(\text{N}2\text{py}2)(\text{OH})(\text{OH}_2)]^+$	
534.4	M	$[\text{Co}^{\text{II}}(\text{OOH})(\text{N}2\text{py}2\text{a})(\text{OH}_2)]^+$	10%
546.3	M	$[\text{Co}^{\text{III}}(\text{N}2\text{py}2\text{aH}_1)(\text{O}_2)(\text{MeOH})]^+$	30%
		$[\text{Co}^{\text{II}}(\text{N}2\text{py}2)(\text{OH})(\text{MeOH})]^+$	
548.3	M	$[\text{Co}^{\text{II}}(\text{OOH})(\text{N}2\text{py}2\text{a})(\text{MeOH})]^+$	30%
596.4	M	$[\text{Co}^{\text{II}}(\text{N}2\text{py}2)(\text{ClO}_4)]^+$	5%
614.2	M	$[\text{Co}^{\text{II}}(\text{N}2\text{py}2)(\text{ClO}_4)(\text{OH}_2)]^+$	10%
628.3	M	$[\text{Co}^{\text{II}}(\text{N}2\text{py}2)(\text{ClO}_4)(\text{MeOH})]^+$	15%
642.2	M	$[\text{Co}^{\text{II}}(\text{N}2\text{py}2)(\text{ClO}_4)(\text{EtOH})]^+$	20%

Based on Figure 7.7, a 50% conversion ratio was expected with 12 eq  $\text{H}_2\text{O}_2$  and, indeed, an approximately 1 : 1 mixture of cobalt(II) and cobalt(III) species were found by ESI-MS (Table 7.4). The two oxidation states could also be separated on a Sephadex ion exchange column (the pink band of cobalt(II) complexes is eluted first, followed by the brown cobalt(III) complexes, owing to its higher charge). Among the signals, there were some which can be assigned to species that contain no N7-bound methyl group. Spectra of the same sample were measured after several days. Only cobalt(II) complexes were then observed. It is likely that the cobalt(III) compounds were reduced back to the divalent form, although this occurred in the presence of  $\text{H}_2\text{O}_2$ .

With 18 eq of  $\text{H}_2\text{O}_2$  an almost complete oxidation of cobalt(II) can be expected from the data in Figure 7.7. Indeed, in the ESI-MS spectrum the intensity of the original peaks for the cobalt(II) complex (e.g.  $[\text{Co}^{\text{II}}(\text{N}2\text{py}2)(\text{ClO}_4)]^+$  596.4, or  $[\text{Co}^{\text{II}}(\text{N}2\text{Py}2\text{H}_1)]^+$  496.2) are significantly smaller compared to those with 12 eq  $\text{H}_2\text{O}_2$ . However, some new peaks appear,

which can all be assigned to cobalt(III) species ( $[\text{Co}^{\text{III}}(\text{N}2\text{py}2)(\text{O}_2)]^+$  529.3,  $[\text{Co}^{\text{III}}(\text{N}2\text{py}2)(\text{MeOH})(\text{O}_2)]^+$  and  $[\text{Co}^{\text{III}}(\text{N}2\text{py}2\text{a})(\text{EtOH})(\text{O}_2)]^+$  561.3). This assignment was confirmed by labelling studies, using  $\text{H}_2^{18}\text{O}_2$  as oxidant. These signals are shifted to 4 mass units higher values, which confirms the presence of coordinated peroxide (Table 7.5). The assignment of some peaks was ambiguous: these can be assigned to species with the original (N2py2) or the demethylated ligand (N2py2a). However, the demethylation can be proven, by with a spectrum of the identical sample after several days, when only cobalt(II) species are present.

**Table 7.5. Major peaks in the ESI-MS spectrum and their assignment, recorded after 1 day reaction time for the reaction between 6.7 mM  $[\text{Co}^{\text{II}}(\text{N}2\text{py}2)(\text{OH}_2)_2](\text{ClO}_4)_2$  with labelled and unlabelled  $\text{H}_2\text{O}_2$  in methanol. Species with the original (not demethylated) N2py2 ligand are black, species with the demethylated N2py2a ligand are red**

18 eq $\text{H}_2\text{O}_2$ ; peaks with larger intensity			
mass	intensity	assignment	
528.3	27%	$[\text{Co}^{\text{III}}(\text{N}2\text{py}2\text{H}_1)(\text{O}_2)]^+$	peroxo complex, no demethylation
546.4	25%	$[\text{Co}^{\text{III}}(\text{N}2\text{py}2\text{aH}_1)(\text{MeOH})(\text{O}_2)]^+$	demethylated peroxo complex
561.3	21%	$[\text{Co}^{\text{III}}(\text{N}2\text{py}2)(\text{MeOH})(\text{O}_2)]^+$	peroxo complex, no demethylation
12 eq $\text{H}_2^{18}\text{O}_2$ ; peaks with larger intensity			
532.3	15%	$[\text{Co}^{\text{III}}(\text{N}2\text{py}2\text{H}_1)(^{18}\text{O}_2)]^+$	peroxo complex, no demethylation
551.3	10%	$[\text{Co}^{\text{III}}(\text{N}2\text{py}2\text{a})(\text{MeOH})(^{18}\text{O}_2)]^+$	demethylated peroxo complex
565.3	7%	$[\text{Co}^{\text{III}}(\text{N}2\text{py}2)(\text{MeOH})(^{18}\text{O}_2)]^+$	peroxo complex, no demethylation
18 eq $\text{H}_2^{18}\text{O}_2$ ; peaks with larger intensity			
523.3	11%	$[\text{Co}^{\text{III}}(\text{N}2\text{py}2\text{H}_1)(^{18}\text{O}_2)]^+$	peroxo complex, no demethylation
537.4	10%	$[\text{Co}^{\text{III}}(\text{N}2\text{py}2\text{a})(\text{OH}_2)(^{18}\text{O}_2)]^+$	demethylated peroxo complex
551.3	44%	$[\text{Co}^{\text{III}}(\text{N}2\text{py}2\text{a})(\text{MeOH})(^{18}\text{O}_2)]^+$	demethylated peroxo complex
565.3	24%	$[\text{Co}^{\text{III}}(\text{N}2\text{py}2)(\text{MeOH})(^{18}\text{O}_2)]^+$	peroxo complex, no demethylation

#### 8.4.3. Structure of $[\text{Co}^{\text{II}}(\text{N}2\text{py}2\text{a})(\text{H}_2\text{O})_2](\text{ClO}_4)_2$

Our aim was to isolate the oxidized cobalt(III) complex *in situ* from the reaction mixture of the methanolic solution of  $[\text{Co}^{\text{II}}(\text{N}2\text{py}2)(\text{H}_2\text{O})_2](\text{ClO}_4)_2$  to which 30%  $\text{H}_2\text{O}_2$  was added. Despite our expectation, ether diffusion produced pink crystals. Under the same conditions, but with shorter crystallization time, a Co(III)-N2py2a complex with water and ethoxy co-ligands was isolated.<sup>7</sup>

The structures  $[\text{Co}^{\text{II}}(\text{N}2\text{py}2\text{a})(\text{H}_2\text{O})_2](\text{ClO}_4)_2$  and of its precursor complex  $[\text{Co}^{\text{II}}(\text{N}2\text{py}2)(\text{H}_2\text{O})_2](\text{ClO}_4)_2$  differ by the N7-substituent, H or  $\text{CH}_3$ ; the oxidation state of cobalt, the two water co-ligands and the counter anion in the two structures are practically identical. The valency of cobalt in  $[\text{Co}^{\text{II}}(\text{N}2\text{py}2\text{a})(\text{H}_2\text{O})_2](\text{ClO}_4)_2$  is derived from the stoichiometry and from the data of elemental analysis. In addition, the three d-d bands (456, 496 and 534 nm) in the UV-spectrum of the crystals are typical for high-spin octahedral cobalt(II)-complexes.

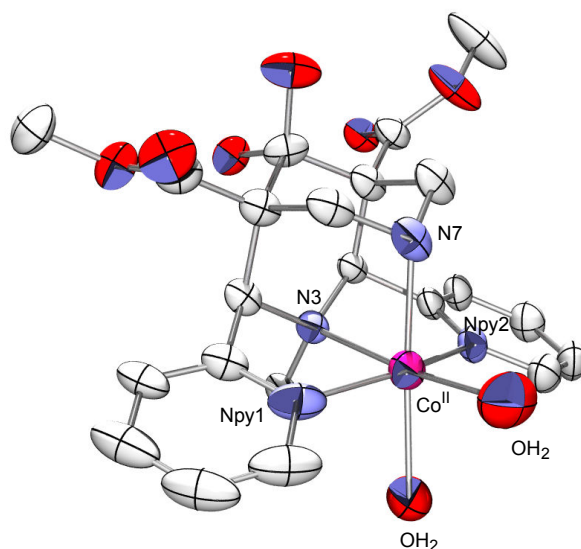


Figure 7.8. Crystal structure of  $[\text{Co}^{\text{II}}(\text{N}2\text{Py}2\text{a})(\text{H}_2\text{O})_2](\text{ClO}_4)_2$

Table 7.6 Selected bond lengths and angles (X-ray), together with computed values (DFT: [B3LYP/6-31G(d)] ) of  $[\text{Co}^{\text{II}}(\text{N}2\text{Py}2\text{a})(\text{H}_2\text{O})_2](\text{ClO}_4)_2$

	$[\text{Co}^{\text{II}}(\text{N}2\text{py}2\text{a})(\text{H}_2\text{O})_2](\text{ClO}_4)_2$		$[\text{Co}^{\text{II}}(\text{N}2\text{py}2)(\text{H}_2\text{O})_2](\text{ClO}_4)_2$ <sup>6</sup>	
	X-ray	DFT	X-ray	DFT
Co-N7	2.151(6)	2.183	2.2183(18)	2.215
Co-N3	2.115(4)	2.136	2.1592(18)	2.129
Co-Npy1	2.096(7)	2.119	2.120(2)	2.114
Co-Npy2	2.089(5)	2.120	2.087(2)	2.115
Co-O <sub>1</sub> (eq)	2.064(6)	2.105	2.0428(18)	2.098
Co-O <sub>2</sub> (ax)	2.136(6)	2.328	2.1991(18)	2.377
N3-N7	2.831	2.953	2.908	3.003
Npy1-Npy2	4.084	4.148	4.090	4.141
N3-Co-N7	83.56(19)	86.27	83.30(6)	87.43
N3-Co-Npy1	79.1(2)	79.67	77.62(7)	79.85
N3-Co-Npy2	79.62(18)	79.59	78.38(7)	79.77
Npy1-Co-Npy2	156.7(2)	156.18	153.13(7)	156.51

The crystals of this complex were grown from the reaction mixture of  $[\text{Co}^{\text{II}}(\text{N}2\text{py}2)(\text{H}_2\text{O})_2](\text{ClO}_4)_2$  with  $\text{H}_2\text{O}_2$ . Formally there is no change in the oxidation state of the metal, despite the addition of the hydrogen peroxide oxidant. During the reaction the central cobalt(II) is oxidized to cobalt(III), as was proved by UV-vis and mass spectroscopy (see above). Reduction of cobalt(III) to cobalt(II) with  $\text{H}_2\text{O}_2$  needs also to be considered. The intensity of the peaks assigned as cobalt(III)-peroxo compounds in the ESI-MS spectrum, increases with increasing reaction time (see Table 7.5). This indicates that the peroxide is coordinated to the cobalt center, and that it might also act as a reducing agent. For complexes where the coordinated peroxide was substituted with the stronger ligand, such a reduction was not observed (on a Dowex ion-exchange column the peroxide is protonated by the eluent 1 M HCl and can be washed out easily as the neutral hydrogen peroxide). For the re-reduction of the cobalt(III) center, the presence of coordinated peroxide therefore is necessary. The demethylation reaction, on the other hand, is irreversible.

The Co-N distances in the demethylated complex are significantly shorter than in the methylated form (decrease of 0.05-0.08 Å), and the size of the bispidone cavity (N3-N7 distance) is also smaller (2.83 Å instead of 2.90 Å). The cavity compression is probably due to the differences at the N7 substituent. Secondary amines are stronger amines as the tertiary amines ( $pK_a$  of trimethylamine: 9.81,  $pK_a$  of dimethylamine 10.73).<sup>139</sup> A similar effect was reported for manganese(II) complexes with different constitutions at the “cap”. The keto form reduces the basicity of the tertiary amines, which results in longer M-N7 distances.<sup>6</sup> This is in analogy to our system, where a secondary amine with stronger basicity enforces a shorter Co-N7 and N3-N7 distance in the demethylated  $[\text{Co}^{\text{II}}(\text{N}2\text{py}2\text{a})(\text{H}_2\text{O})_2]^{2+}$ , when compared to the precursor  $[\text{Co}^{\text{II}}(\text{N}2\text{py}2)(\text{H}_2\text{O})_2]^{2+}$ , with an N7 methyl group. The most pronounced effect is the shortening of the axial bonds (Co-N7 and Co-O<sub>2</sub><sup>ax</sup>). Interestingly, the bond angles around the cobalt center are more or less the same as in  $[\text{Co}^{\text{II}}(\text{N}2\text{py}2)(\text{H}_2\text{O})_2](\text{ClO}_4)_2$ .

Structures of  $[\text{Co}^{\text{II}}(\text{N}2\text{py}2)(\text{H}_2\text{O})_2]^{2+}$  and  $[\text{Co}^{\text{II}}(\text{N}2\text{py}2\text{a})(\text{H}_2\text{O})_2]^{2+}$  were optimized by DFT calculations at the 6-31G(d) level, using the crystal structures as starting geometries. Selected bond lengths and bond angles are also presented in Table 7.6. Similarly to the crystal structures, the Co-N7 distance is shorter in the optimized N2py2a complex than in the complex with the non-demethylated ligand. However, the compression of the Co-N7 bond distance is not that significant (0.03 Å) than it was found in crystal structures (0.07 Å). Similarly the Co-O<sub>2</sub><sup>ax</sup> bond was calculated to be shorter by 0.05 Å for the N2py2a complex (in the crystal structures the difference of the two bond lengths was 0.06 Å). Interestingly the axial bonds (both Co-N7, and Co-O<sub>2</sub><sup>ax</sup>) are calculated to be longer than it was measured for

the crystals. Especially remarkable is the elongation of the Co-O<sub>2</sub><sup>ax</sup> bonds, which are almost 0.2 Å longer in the structures calculated by DFT.

As discussed above, the compression of the Co-N7 bond by demethylation at N7 may be the consequence of the change in basicity of the N7 amino nitrogen, but it may also be attributed to changes in the geometry of the rigid bispidone cavity. Geometry optimization of the metal-free ligands N2py2 and N2py2a were performed (at 6-31G(d) level) and the calculated N3...N7 bite distances were compared to the values determined for the corresponding complexes. This data set together with X-ray data are presented in Table 7.7.

**Table 7.7. Measured (X-ray) and calculated [B3LYP/6-31G(d)] N3-N7 bite distances for the free ligands and their cobalt(II)-complexes.**

	d(N3...N7) in ligands		d(N3...N7) in cobalt(II) complexes	
	X-ray	DFT	X-ray	DFT
N2py2	2.901 Å	3.000 Å	2.908 Å	3.003 Å
N2py2a	-	2.971 Å	2.831 Å	2.953 Å

It emerges that the calculated bite distances are overestimated by around 0.1 Å by DFT. As discussed above, the demethylation results in a decrease of by 0.07 Å in the bite distance of the cobalt(II) complexes. This trend is well reproduced by DFT calculations. As in the crystal structures, incorporation of cobalt(II) into the cavity of the N2py2 ligand has almost no effect on the bite distance. Both the observed and calculated difference in the N3...N7 distances between the metal-free and coordinated ligand are less than 0.01 Å. Therefore, practically no change in ligand geometry is necessary to form the cobalt(II) complex. That is, no strain is built up in N2py2. This supports the high degree of stabilization of the Co(II)-N2py2 complex. The calculated bite distance in the N2py2a ligand is around 0.03 Å shorter than in N2py2, but 0.02 Å longer than in the Co(II)-N2py2a complex. This indicates that the demethylation itself already causes some compression in the ligand cavity, and that complexation of cobalt(II) with N2py2a leads to a further reduction in the N3...N7 distance. From this, it seems as though both steric and electronic effects play role in the cavity compression. However, these very small differences are at the limit of significance, both for observed and computed distances, i.e. the steric effects are unimportant.

Since atomic charges may be related to some electronic effects, Mulliken atomic charges for central cobalt(II) and the N-donor atoms in the optimized structures of Co(II)-N2py2 and Co(II)-N2py2a complexes were compared.

**Table 7.8. Calculated Mulliken atomic charges for  $[\text{Co}^{\text{II}}(\text{N}2\text{py}2)(\text{OH}_2)_2]^{2+}$  and  $[\text{Co}^{\text{II}}(\text{N}2\text{py}2\text{a})(\text{OH}_2)_2]^{2+}$** 

	Co	Npy1	Npy2	N3	N7
$[\text{Co}^{\text{II}}(\text{N}2\text{py}2)(\text{OH}_2)_2]^{2+}$	0.9837	-0.6068	-0.6074	-0.5791	-0.5236
$[\text{Co}^{\text{II}}(\text{N}2\text{py}2\text{a})(\text{OH}_2)_2]^{2+}$	0.9875	-0.6094	-0.6101	-0.5779	-0.6817

The changes in the atomic charge are almost negligible in case of the pyridine nitrogens and also for N3 and the central cobalt. The only significant but small difference is seen for N7. The more electronegative N7-methyl carbon in N2py2 is replaced by a less electronegative hydrogen atom. Due to the increase of electron density on N7 in  $[\text{Co}^{\text{II}}(\text{N}2\text{py}2\text{a})(\text{OH}_2)_2]^{2+}$  complex, the polarization of the Co-N7 bond is more pronounced and can explain the further decrease of the Co-N7 distance when N7 is demethylated.

Another possible reason for the Co-N7 bond compression is the decrease in steric repulsion between the N7-methyl group and the water coordinated to cobalt in the equatorial position. Strain energies of  $[\text{Co}^{\text{II}}(\text{N}2\text{py}2)(\text{OH}_2)_2]^{2+}$  and the demethylated complex were calculated by molecular mechanics, using the MOMECC program<sup>89</sup> and force field.<sup>90</sup> Single point energies were calculated for the crystal structural data. Since the two complexes differ by a methyl group, the overall strain energies cannot be directly compared. For this reason, two additional structures were generated, in which the N7-methyl group in  $[\text{Co}^{\text{II}}(\text{N}2\text{py}2)(\text{OH}_2)_2]^{2+}$  was replaced by a hydrogen atom (“Co(II)N2py2-Me”), and the N7-H in  $[\text{Co}^{\text{II}}(\text{N}2\text{py}2\text{a})(\text{OH}_2)_2]^{2+}$  was replaced by a methyl group (“Co(II)N2py2a+Me”), keeping the geometries otherwise intact. The energies for these two pairs of “isomers” can be directly compared. These obtained results are shown in Table 7.9.

**Table 7.9. Strain energies calculated by MOMECC force field**

	E (kJ/mol)	
$[\text{Co}^{\text{II}}(\text{N}2\text{py}2)(\text{OH}_2)_2]^{2+}$	121.09	$\Delta E =$
Co(II)N2py2a+Me	113.95	7.14
$[\text{Co}^{\text{II}}(\text{N}2\text{py}2\text{a})(\text{OH}_2)_2]^{2+}$	112.95	$\Delta E =$
Co(II)N2py2-Me	135.68	-22.75

From these data, the energy differences between the two  $[\text{Co}^{\text{II}}(\text{N}2\text{py}2\text{a})(\text{OH}_2)_2]^{2+}$  and the two  $[\text{Co}^{\text{II}}(\text{N}2\text{py}2)(\text{OH}_2)_2]^{2+}$  isomers can be compared. The strain energy difference in the demethylated  $[\text{Co}^{\text{II}}(\text{N}2\text{py}2\text{a})(\text{OH}_2)_2]^{2+}$  isomers are larger by around 15.5 kJ/mol, which implies that the steric repulsion induced by the N7-methyl group is only a minor effect. The larger steric energy in “Co(II)N2py2-Me” was confirmed by a more detailed analysis of the



strain energy components: the nonbonded interaction in this “isomer” was 15 kJ/mol higher in energy than in  $[\text{Co}^{\text{II}}(\text{N}2\text{py}2)(\text{OH}_2)_2]^{2+}$ . It emerges that when demethylation at N7 takes place, the “original” geometry of the ligand is no longer favourable (“Co(II)N2py2-Me”) and through bond compression an energetically more stable  $[\text{Co}^{\text{II}}(\text{N}2\text{py}2\text{a})(\text{OH}_2)_2]^{2+}$  structure is formed.

The intramolecular N-dealkylation reaction has a stabilizing effect: when the cobalt(II) center is oxidized to cobalt(III), a very inert complex is formed, which enforces a close to octahedral geometry around the metal center, with short metal-donor distances. To achieve these ideal bond lengths, a significant compression of the cavity, i.e. a shortening of the Co-N bonds, is required. As discussed above, an effect of the demethylation at N7 is that the basicity of this amine is increased, which reduces the Co-N7 distance. Since the Co(III)-N7 distance is significantly shorter than the corresponding bond length in the initial cobalt(II) complex, a change of the basicity, via demethylation can further stabilize the trivalent form.

From the shorter cobalt(III)-donor bonds it can be expected that further shortening of these bonds through oxidation from cobalt(II) to cobalt(III) requires less energy than in case of the  $[\text{Co}^{\text{II}}(\text{N}2\text{py}2)(\text{OH}_2)_2](\text{ClO}_4)_2$ : indeed, the redox potential of  $[\text{Co}^{\text{II}}(\text{N}2\text{py}2\text{a})(\text{OH}_2)_2](\text{ClO}_4)_2$  shows an anodic wave at 27 mV (around 400 mV lower potential than for  $[\text{Co}^{\text{II}}(\text{N}2\text{py}2)(\text{OH}_2)_2](\text{ClO}_4)_2$ ), implying an easier oxidation of the demethylated Co-complex. The ease of oxidation is not only thermodynamically favored: oxidation of  $[\text{Co}^{\text{II}}(\text{N}2\text{py}2\text{a})(\text{OH}_2)_2](\text{ClO}_4)_2$  with 170 eq  $\text{H}_2\text{O}_2$  takes place with an around 2-times larger rate (pseudo-first order rate constant  $3.44 \times 10^{-3} \text{ s}^{-1}$ ) than for the cobalt complex with the N7-methyl group ( $1.86 \times 10^{-3} \text{ s}^{-1}$ ).

#### **8.4.4. What happens to the N7-methyl group after demethylation?**

For a large number of reported examples (mostly iron and copper complexes) of intramolecular oxidative N-dealkylation, it has been proposed and experimentally shown that the tertiary amine (which is involved in the oxidation) is converted to a secondary amine and an aldehyde. In many cases it is difficult to prove directly the formation of the aldehyde, especially if it is very volatile.

The question arises, whether our reaction is also an oxidative dealkylation, i.e. the removed alkyl group is oxidized to aldehyde. The identification of ketones and aldehydes, and their

quantitative determination by the formation of coloured (and in aqueous ethanol insoluble) hydrazone compounds, has been known for decades.<sup>140</sup>

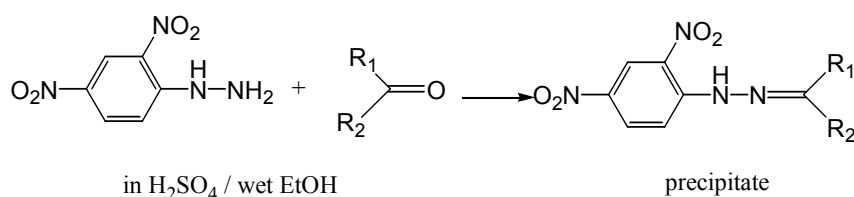


**Figure 7.9. Derivatization of keto compounds with 2,4-dinitrophenylhydrazine (hydrazine test)**

To the acidified aqueous ethanolic solution of dinitrophenylhydrazine, was added the solution containing [Co<sup>II</sup>(N2py2)(OH<sub>2</sub>)<sub>2</sub>](ClO<sub>4</sub>)<sub>2</sub> complex oxidized with H<sub>2</sub>O<sub>2</sub>, which led to immediate precipitation of a hydrazone. This indicates that a compound with a keto group was present in the methanolic [Co<sup>II</sup>(N2py2)(OH<sub>2</sub>)<sub>2</sub>]<sup>2+</sup>/H<sub>2</sub>O<sub>2</sub> system. ESI(-)-MS spectrum shows an intense peak at 209.2, which corresponds to [M-H]<sup>-</sup> of the hydrazone formed between dinitrophenylhydrazone and formaldehyde.

The yield of the demethylation relative to the amount of the [Co<sup>II</sup>(N2py2)(OH<sub>2</sub>)<sub>2</sub>](ClO<sub>4</sub>)<sub>2</sub> present was 28%. For other model complexes, similar values have been obtained.<sup>135</sup>

For the formation of formaldehyde, the coexistence of [Co<sup>II</sup>(N2py2)(OH<sub>2</sub>)<sub>2</sub>](ClO<sub>4</sub>)<sub>2</sub> and H<sub>2</sub>O<sub>2</sub> is necessary, no aldehyde was detected when only [Co<sup>II</sup>(N2py2)(OH<sub>2</sub>)<sub>2</sub>](ClO<sub>4</sub>)<sub>2</sub> or only the oxidant was added to methanol. Also when the [Co<sup>II</sup>(N2py2a)(OH<sub>2</sub>)<sub>2</sub>](ClO<sub>4</sub>)<sub>2</sub> was used in the reaction, no hydrazone was produced. This suggests that the N7-bound methyl group is responsible for the formation of formaldehyde and that the aldehyde is not the oxidation product of solvent methanol.

#### 7.4.5. Oxidation of [Co<sup>II</sup>(N2py2)(OH<sub>2</sub>)<sub>2</sub>](ClO<sub>4</sub>)<sub>2</sub> in methanol

All reactions described in Sections 8.4.3 and 8.4.4 were performed in methanol, by the addition of variable amounts of hydrogen peroxide and under aerobic conditions. Under these conditions the N7-bound methyl group was removed and oxidized to formaldehyde. It is also important to know whether oxygen from the air plays a role in the demethylation at N7 and/or in the oxidation of cobalt(II) in [Co<sup>II</sup>(N2py2)(OH<sub>2</sub>)<sub>2</sub>](ClO<sub>4</sub>)<sub>2</sub>.

When the oxidation of [Co<sup>II</sup>(N2py2)(OH<sub>2</sub>)<sub>2</sub>](ClO<sub>4</sub>)<sub>2</sub> in methanol was performed under argon, the hydrazone test was negative, no formaldehyde formation was observed. In parallel, the ESI-MS spectra show only species with the precursor N2py2 and not of the N7-demethylated ligand. (e.g.: [Co<sup>III</sup>(N2py2)OH]<sup>2+</sup> 257.52, [Co<sup>II</sup>(N2py2)MeOH]<sup>2+</sup> 264.56, [Co<sup>III</sup>(N2py2)(O<sub>2</sub>)]<sup>+</sup> 529.09, [Co<sup>II</sup>(N2py2)(OH<sub>2</sub>)<sub>2</sub>(OH)]<sup>+</sup> 550.06, [Co<sup>III</sup>(N2py2)(O<sub>2</sub>)(MeOH)]<sup>+</sup> 561.02). This

indicates that not only the oxidant  $\text{H}_2\text{O}_2$ , but also the presence of oxygen, is an important condition for the N7-demethylation.

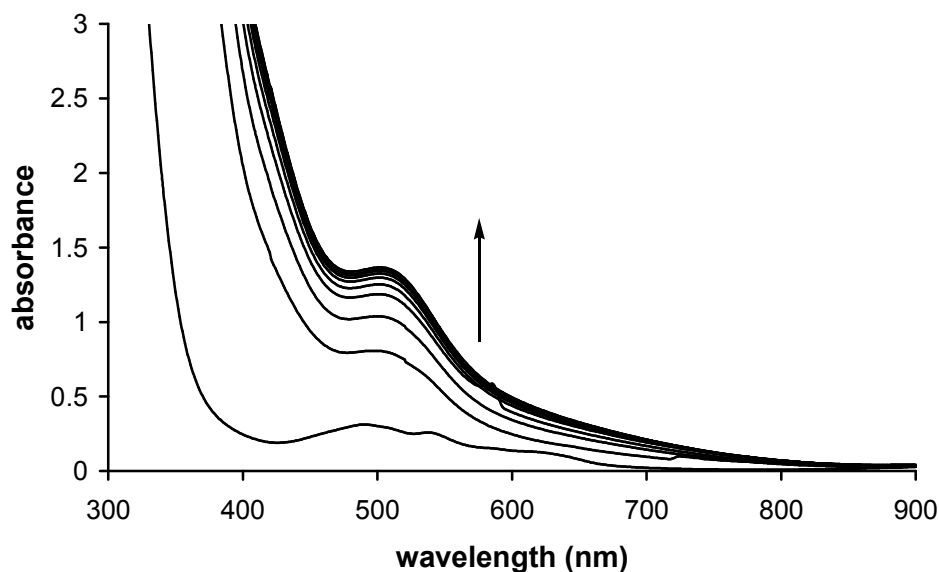


Figure 7.10. Time-dependent UV-vis spectra for the oxidation of 11 mM  $[\text{Co}^{\text{II}}(\text{N}2\text{py}2)(\text{OH}_2)_2](\text{ClO}_4)_2$  with 170 eq  $\text{H}_2\text{O}_2$  in methanol, under anaerobic conditions. Spectra were recorded in 5 minute intervals

The rate constant for the oxidation of  $[\text{Co}^{\text{II}}(\text{N}2\text{py}2)(\text{OH}_2)_2](\text{ClO}_4)_2$  under Ar was determined under the same conditions as used in the kinetic study of the other complexes (11 mM complex with 170 eq  $\text{H}_2\text{O}_2$ ).<sup>7</sup> The reaction is clearly first order, which can be seen by the linearity of the half-logarithmic plot. The determined rate constant ( $2.12 \times 10^{-3} \text{ s}^{-1}$ ) (Figure 8.11) is very similar to when the same system was measured in air ( $1.86 \times 10^{-3} \text{ s}^{-1}$ ). Therefore it appears that the rate of oxidation of the cobalt(II)-center in  $[\text{Co}^{\text{II}}(\text{N}2\text{py}2)(\text{OH}_2)_2](\text{ClO}_4)_2$  is independent of the presence of oxygen.

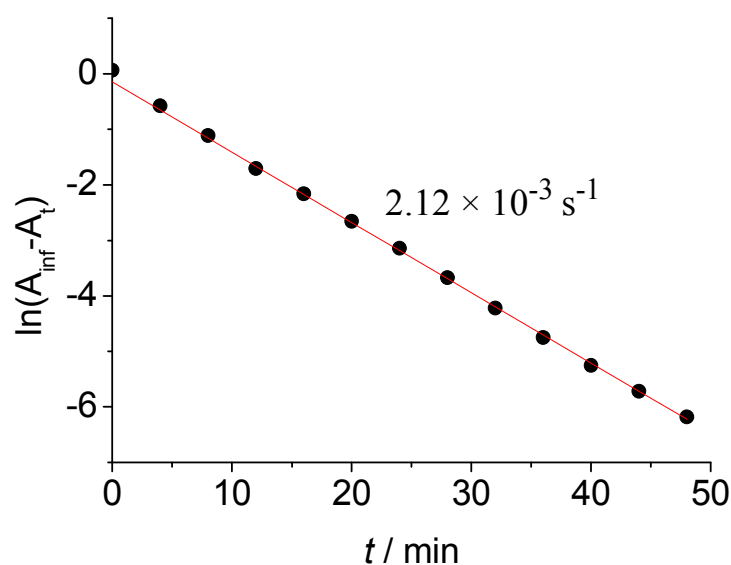


Figure 8.11. Half-logarithmic plot for the oxidation of 11 mM  $[\text{Co}^{\text{II}}(\text{N}2\text{py}2)(\text{OH}_2)_2](\text{ClO}_4)_2$  with 170 eq  $\text{H}_2\text{O}_2$  in methanol, under anaerobic conditions.

When the oxidation of  $[\text{Co}^{\text{II}}(\text{N}2\text{py}2)(\text{OH}_2)_2](\text{ClO}_4)_2$  was performed at  $-40^\circ\text{C}$ , there is no observable reaction (the time-dependent UV-spectra show no change). This is in strong contrast to the  $\text{Fe}(\text{II})/\text{H}_2\text{O}_2$ -chemistry, where some intermediate species can be trapped and further investigated at this temperature (iron(III)-hydroperoxo species).<sup>141</sup> It seems that in the cobalt-bispidone systems, the oxidation has a relatively high energy barrier, so that at low temperature no reaction takes place. A sufficient increase in temperature to make oxidation of the cobalt(II)-center possible allows a large number of reactions to take place, either simultaneously or in a consecutive manner. So when the metal center is oxidized, a large variety of different species are formed (see Table 7.4 and 7.5).

#### 8.4.6. Oxidation of $[\text{Co}^{\text{II}}(\text{N}2\text{py}2)(\text{OH}_2)_2](\text{ClO}_4)_2$ in acetonitrile

Oxidation reactions were also carried out in acetonitrile. Oxidation of 6.78 mM of  $[\text{Co}^{\text{II}}(\text{N}2\text{py}2)(\text{OH}_2)_2](\text{ClO}_4)_2$  in acetonitrile, in presence of 20 eq  $\text{H}_2\text{O}_2$ , led to the formation of a new species with maximum intensity after 30 min reaction time: the color of the solution changes from pink to intense yellow (shoulder at 646 nm ( $\epsilon = 17$ ) in the UV-vis spectrum). After 1 day the solution turns deep brown, the shoulder in the spectrum almost completely disappears, a new intense band is formed at 455 nm ( $\epsilon = 180$ ), and a shoulder around 600 nm. The reaction was followed also by ESI-MS. A new set of peaks at 257.01, 286.56 and 614.05 were detected for the deep yellow intermediate which were assigned as  $[\text{Co}^{\text{III}}(\text{N}2\text{py}2)(\text{OH})]^{2+}$ ,  $[\text{Co}^{\text{II}}(\text{N}2\text{py}2)(\text{HOOH})(\text{MeCN})]^{2+}$  and  $[\text{Co}^{\text{II}}(\text{N}2\text{py}2)(\text{OOH})(\text{MeCN})_2]^+$ , respectively. In the spectrum recorded after a reaction time of 1 day, the above species are not seen, instead, new peaks appeared at 549.11, 567.07 and 588.12, assigned to  $[\text{Co}^{\text{III}}(\text{N}2\text{py}2)(\text{OH}_2)(\text{OH})_2]^+$ ,  $[\text{Co}^{\text{III}}(\text{N}2\text{py}2)(\text{OH}_2)_2(\text{OH})_2]^+$  and  $[\text{Co}^{\text{III}}(\text{N}2\text{py}2)(\text{OH}_2)(\text{MeCN})(\text{O}_2)]^+$ , respectively. Interestingly, in acetonitrile no species with the N7-demethylated ligand were found, which is in agreement with the fact that the hydrazine test was negative. No formaldehyde is formed.

The oxidation reaction in acetonitrile was also performed under conditions of the kinetic studies (11 mM complex + 170 eq  $\text{H}_2\text{O}_2$ ) (Figure 7.12). Here also, an intermediate species was observed, with maximum intensity after 30 min reaction time. The shoulder at 646 nm is significantly broader. The original 3 d-d bands of  $[\text{Co}^{\text{II}}(\text{N}2\text{py}2)(\text{OH}_2)_2](\text{ClO}_4)_2$  disappear and a more intense new peak evolves at 511 nm ( $\epsilon = 105$ ), corresponding to a Co(III) species. After 30 min reaction time the shoulder at 646 nm gradually disappears, and gives rise to some new bands. An isobestic point at 665 nm is observable for spectra recorded after 30 min reaction time. The absorption intensities below 432 nm reach a maximum value at 96 min reaction time, and then this starts to decrease. In parallel, the intensities between 432 and 665 nm

continuously grow and after 1 day a clear peak at 445 nm ( $\epsilon = 200$ ) and a strong shoulder at 575 nm ( $\epsilon = 109$ ) appears.

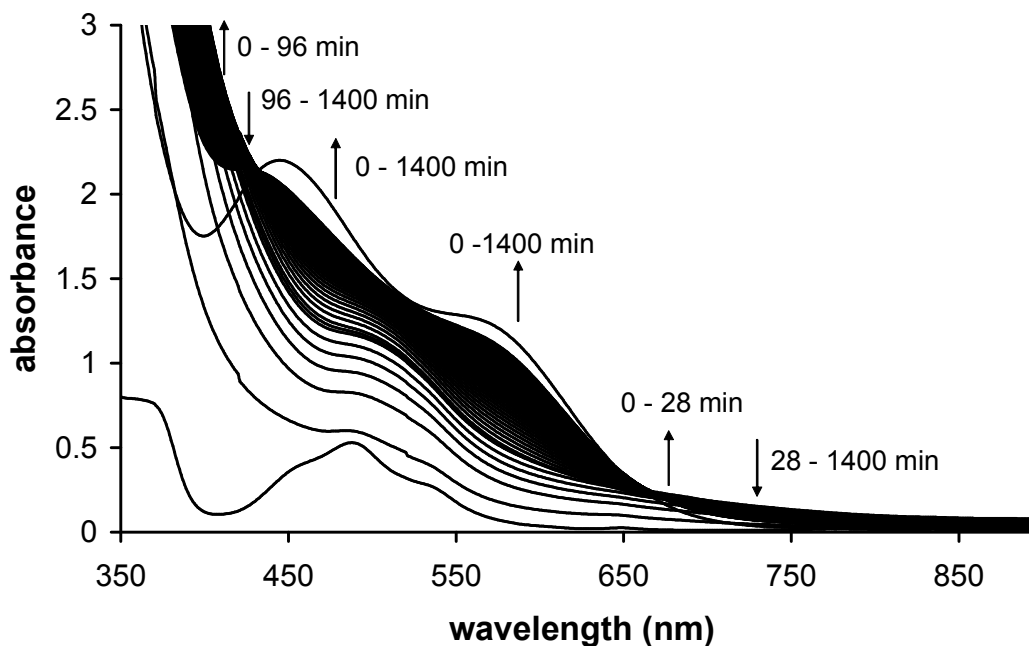


**Figure 7.12.** Time-dependent UV-vis spectra for the oxidation of 11 mM  $[\text{Co}^{\text{II}}(\text{N}2\text{py}2)(\text{OH}_2)_2](\text{ClO}_4)_2$  with 170 eq  $\text{H}_2\text{O}_2$  in acetonitrile. Spectra were recorded in 4 minute intervals

Surprisingly, the second and the third process (28 to 96 min and after 96 min, respectively) follow pseudo-first order kinetics, and the rate constants were determined to be  $1.70 \times 10^{-4} \text{ s}^{-1}$  and  $1.40 \times 10^{-4} \text{ s}^{-1}$ , respectively. Although the first reaction seems to involve oxidation (considering that the 3 weak d-d bands of cobalt(II) change to a more intense single band), it does not follow pseudo-first order kinetics, so we cannot compare the oxidation rate constants in methanol and acetonitrile.

A possible reason for the oxidation without intramolecular N-demethylation is that this acetonitrile is coordinated to the axial site trans to N7. The strong ligand field of the coordinated solvent may affect the ligand exchange processes. Coordination of hydroperoxide by substitution of the strong acetonitrile donor is not favoured, which explains why the oxidation of the cobalt(II) center of  $[\text{Co}^{\text{II}}(\text{N}2\text{py}2)(\text{OH}_2)_2](\text{ClO}_4)_2$  in acetonitrile is slower than in methanol. Moreover, the easily exchangeable hydroperoxide has no time to attack the N7-bound methyl group. The cobalt(III)-bound water or hydroxide in the oxidized species is easily exchanged by the strong acetonitrile donor. The ligand field of the coordinated solvent can stabilize the low-spin cobalt(III) species. From this it is not surprising that the re-reduction of the central cobalt to the divalent form was not observed in acetonitrile.

#### 7.4.7. Oxidative N-dealkylation in a cobalt(II)-bispidone complex with benzyl substituent

In order to test whether the N-dealkylation at N7 in a cobalt(II)-bispidone complex leads to the cleavage of substituents other than methyl, oxidation of  $[\text{Co}^{\text{II}}(\text{N2py2Bz})(\text{OH}_2)_2](\text{ClO}_4)_2$  with  $\text{H}_2\text{O}_2$  was investigated in detail. The N2py2Bz ligand differs from N2Py2 only in the N7-bound substituent. It can be obtained in good yields, using benzylamine instead of methylamine for the the second Mannich condensation step, to afford the bicyclic bispidone. For comparative purposes, oxidation of  $[\text{Co}^{\text{II}}(\text{N2py2Bz})(\text{OH}_2)_2](\text{ClO}_4)_2$  with  $\text{H}_2\text{O}_2$  was carried out under the same conditions as with  $[\text{Co}^{\text{II}}(\text{N2py2})(\text{OH}_2)_2](\text{ClO}_4)_2$ , namely:

1. aerobic oxidation in methanol
2. anaerobic oxidation in methanol
3. aerobic oxidation in acetonitrile

1. When the reaction between  $[\text{Co}^{\text{II}}(\text{N2py2Bz})(\text{OH}_2)_2](\text{ClO}_4)_2$  and  $\text{H}_2\text{O}_2$  was carried out in methanol under aerobic conditions, the hydrazine test was positive. The precipitated hydrazone was assigned to the benzaldehyde-derivative. The fact that no hydrazone from formaldehyde was detected, supports the conclusion that methanol oxidation may be ruled out. From this it is also clear that no dealkylation takes place at the N3 position, which is consistent with the results obtained for  $[\text{Co}^{\text{II}}(\text{N2py2})(\text{OH}_2)_2](\text{ClO}_4)_2$ .

2. In analogy with the  $[\text{Co}^{\text{II}}(\text{N2py2})(\text{OH}_2)_2](\text{ClO}_4)_2$  case, the  $[\text{Co}^{\text{II}}(\text{N2py2Bz})(\text{OH}_2)_2](\text{ClO}_4)_2$  complex was also incapable of producing aldehyde in the oxidation in methanolic solution under argon: no hydrazone was produced in the hydrazone test. Also, the ESI-MS spectrum shows that only species with the original ligand were present after oxidation (e.g.  $[\text{Co}^{\text{II}}(\text{N2py2Bz})(\text{OH})]^+$  591.3,  $[\text{Co}^{\text{III}}(\text{N2py2Bz})(\text{O}_2)]^+$  605.3,  $[\text{Co}^{\text{III}}(\text{N2py2Bz})(\text{O}_2)(\text{OH}_2)]^+$  623.3).

3. In strong contrast to  $[\text{Co}^{\text{II}}(\text{N2py2})(\text{OH}_2)_2](\text{ClO}_4)_2$  complex,  $[\text{Co}^{\text{II}}(\text{N2py2Bz})(\text{OH}_2)_2](\text{ClO}_4)_2$  showed no intermediate formation in the UV-spectra during the oxidation with  $\text{H}_2\text{O}_2$  in acetonitrile: only a single process could be followed, while the 3 d-d bands of Co(II) are converted to 2 more intense shoulders at 550 and 650 nm (Figure 7.13). The pseudo-first order rate constant of the oxidation of 6.78 mM complex in presence of 10 eq  $\text{H}_2\text{O}_2$  in MeCN was measured to be  $9.1 \times 10^{-5} \text{ s}^{-1}$  (Figure 7.14). Mass spectra show again that in this process no debenzylation takes place, with  $[\text{Co}^{\text{III}}(\text{N2py2Bz})(\text{O}_2)]^+$  605.3,  $[\text{Co}^{\text{III}}(\text{N2py2Bz})(\text{O}_2)(\text{OH}_2)]^+$  623.3 as the major peaks.

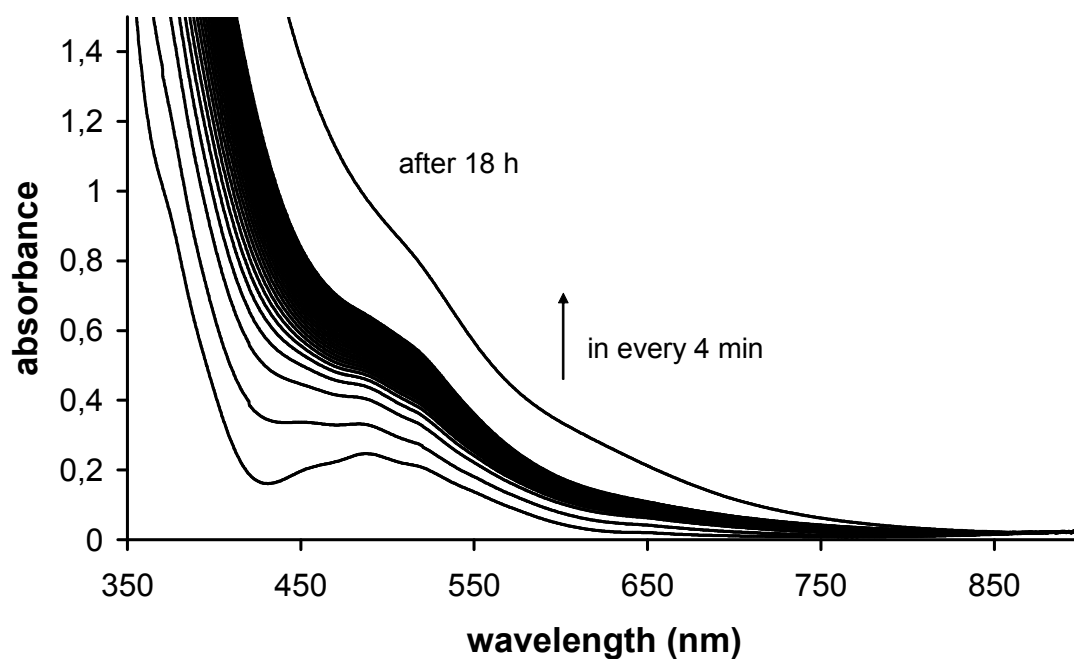


Figure 7.13. Time-dependent UV-vis spectra for the oxidation of 6.78 mM  $[\text{Co}^{\text{II}}(\text{N}2\text{py}2\text{Bz})(\text{OH}_2)_2](\text{ClO}_4)_2$  with 10 eq  $\text{H}_2\text{O}_2$  in acetonitrile. Spectra were recorded in 4 minute intervals

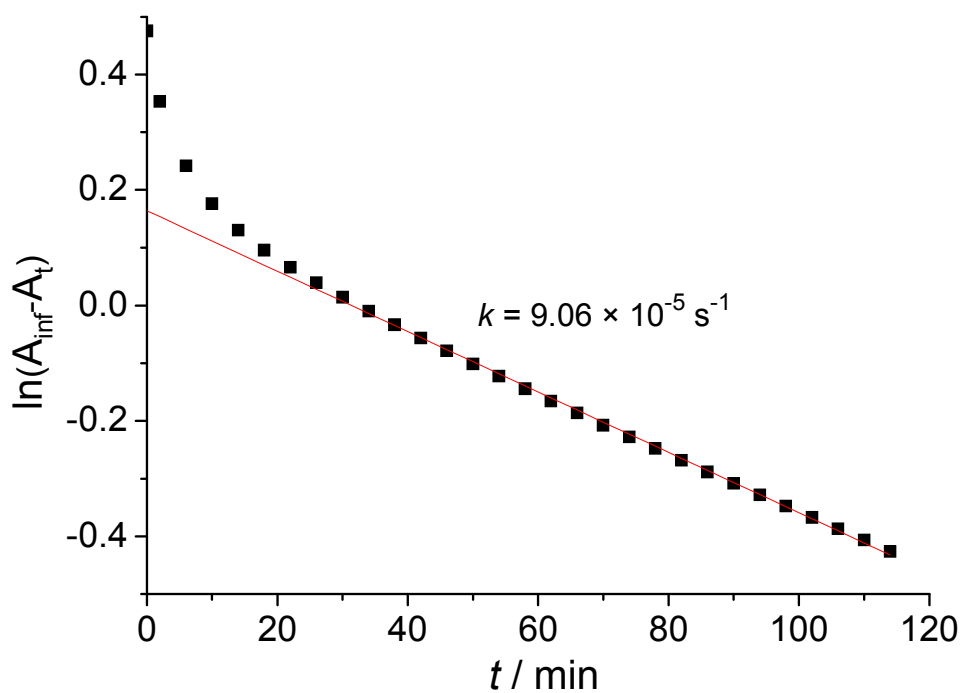


Figure 7.14. Half-logarithmic plot for the oxidation of 6.78 mM  $[\text{Co}^{\text{II}}(\text{N}2\text{py}2\text{Bz})(\text{OH}_2)_2](\text{ClO}_4)_2$  with 10 eq  $\text{H}_2\text{O}_2$  in acetonitrile.

#### 7.4.8. Cobalt(III)-peroxide interactions

The reaction between the  $[\text{Co}^{\text{III}}(\text{N}2\text{py}2\text{b})(\text{CO}_3)]\text{PF}_6$  complex<sup>7</sup> (Figure 7.15) and hydrogen peroxide was investigated in order to understand whether there is an interaction between the cobalt(III) center and peroxide. In contrast to N2py2, the N2py2b ligand has hydrolyzed ester groups, and the N7-amine is a tertiary amine with a methyl group attached to it. The question of whether the addition of  $\text{H}_2\text{O}_2$  leads to the cleavage of this methyl group, arises.

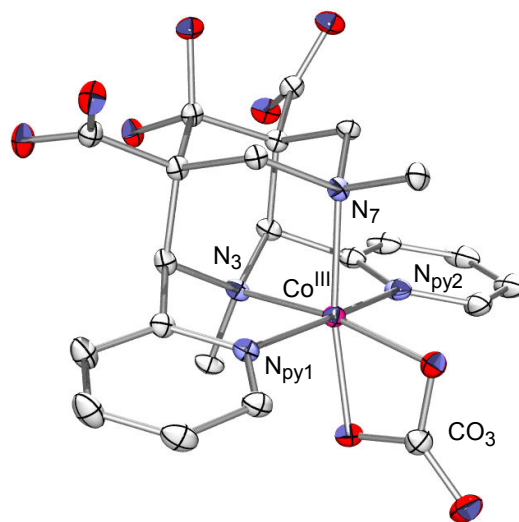


Figure 7.15. Crystal structure of  $[\text{Co}^{\text{III}}(\text{N}2\text{py}2\text{b})(\text{CO}_3)]\text{PF}_6$ <sup>7</sup>

In the first step, the coordinated carbonate ligand was removed by the addition of 2 eq of  $\text{HClO}_4$  to the methanolic solution of the complex, followed by gentle heating (to eliminate carbon dioxide formed from carbonate) and the addition of 10 eq of  $\text{H}_2\text{O}_2$ . ESI spectra show that the removal of the carbonate from the coordination sphere of cobalt(III) was successful: the cationic part of the complex  $[\text{Co}^{\text{III}}(\text{N}2\text{py}2\text{b})(\text{CO}_3)]^+$  at 530.0 was not seen. Interestingly, peaks with coordinated peroxide were also not detected. One probable reason is that in this case the pH of the solution remains unchanged, while in the  $[\text{Co}^{\text{II}}(\text{N}2\text{py}2)(\text{OH}_2)_2]^{2+}/\text{H}_2\text{O}_2$  system the reaction between cobalt(II) and  $\text{H}_2\text{O}_2$  produces hydroxide ions, which can enhance deprotonation of the oxidant and its subsequent coordination to the cobalt center. This may also explain the other unusual result, namely that no peaks were seen that could be assigned to species which have gone through N-dealkylation. Typical peaks in the spectrum were  $[\text{Co}^{\text{III}}(\text{N}2\text{py}2\text{b})\text{H}_2]^+$  466.4, and  $[\text{Co}^{\text{III}}(\text{N}2\text{py}2\text{bH}_1)(\text{ClO}_4)]^+$  566.4. (the N2py2b ligand contains two carboxyl groups that can be further deprotonated)

The fact that no removal of the N-alkyl side chain takes place in a Co(III) complex after addition of hydrogen peroxide, suggests that only cooperation between the divalent cobalt



complex and hydrogen peroxide leads to oxidative N-dealkylation: the active species is formed between the cobalt(II)-bispidone complex and the oxidant  $\text{H}_2\text{O}_2$ .

Attempts were also made to isolate *cobalt(III)-peroxo complexes of the demethylated N2py2a ligand*. As described before, the  $[\text{Co}^{\text{III}}(\text{N}2\text{py}2\text{a})(\text{Cl})_2]\text{ClO}_4$  complex was prepared by the oxidation of  $[\text{Co}^{\text{II}}(\text{N}2\text{py}2)(\text{OH}_2)_2](\text{ClO}_4)_2$  with hydrogen peroxide in methanol, and was purified by ion exchange chromatography.<sup>7</sup> As an effect of the eluent 1 M HCl, the free coordination sites around the cobalt center are occupied by chloride ions.<sup>7</sup> Removal of these chlorides in the isolated solid  $[\text{Co}^{\text{III}}(\text{N}2\text{py}2\text{a})(\text{Cl})_2]\text{ClO}_4$  complex is necessary to achieve coordination of peroxide.  $[\text{Co}^{\text{III}}(\text{N}2\text{py}2\text{a})(\text{Cl})_2]\text{ClO}_4$  was treated with 2 eq of  $\text{AgClO}_4$  in water. After stirring overnight in the dark the resulting  $\text{AgCl}$  was filtered off. With the remaining dark pink filtrate two experiments were performed:

#### *Experiment 1*

Addition of 40 eq  $\text{H}_2\text{O}_2$  to the aqueous solution, obtained after treatment of  $[\text{Co}^{\text{III}}(\text{N}2\text{py}2\text{a})(\text{Cl})_2]\text{ClO}_4$  with 2 eq  $\text{AgClO}_4$ , induces gradual changes in the UV-vis spectra after several hours. The build-up of weak shoulders to the original band at 520 nm could be followed (the weak shoulders appear at 440 nm and 587 nm, determined from difference spectra). A continuous absorbance increase below 400 nm was found (Figure 7.16 and 7.17), which suppressed the original band at 357 nm ( $\epsilon = 160$ ). The ESI-spectrum recorded after a 2 day reaction time shows the existence of  $[\text{Co}^{\text{III}}(\text{N}2\text{py}2\text{a})(\text{O}_2)]^+$  (515.08). Therefore, binding of peroxide to cobalt(III) was evidenced. The fact that a peak for  $[\text{Co}^{\text{III}}(\text{N}2\text{py}2\text{a})(\text{Cl})]^+$  (518.05) was also seen in the ESI-MS spectrum, indicates that the removal of the chloride was not complete.

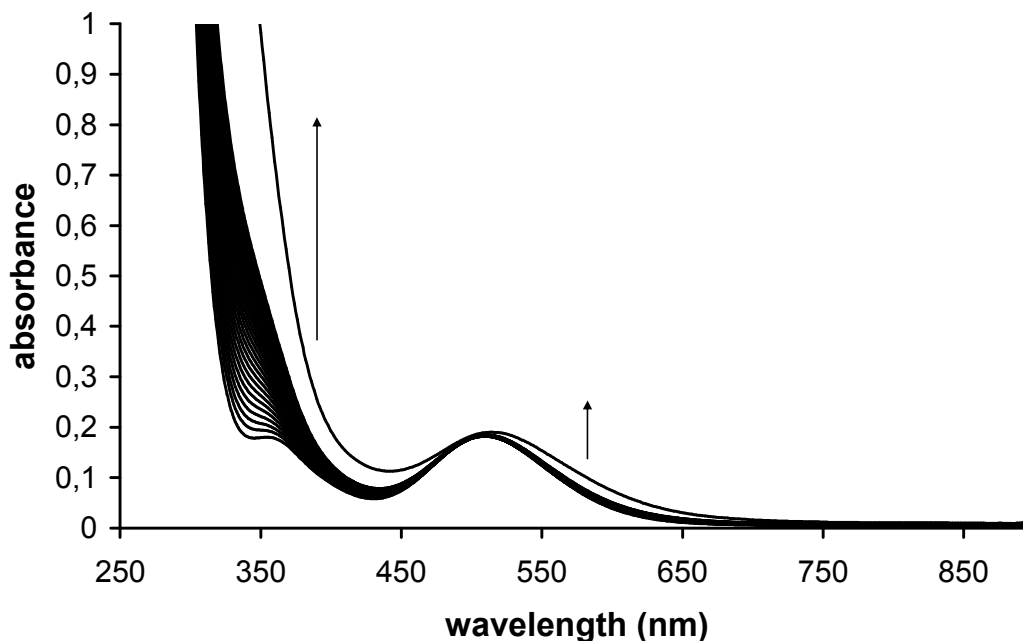


Figure 7.16. Time-dependent UV-vis spectra for the reaction between 1.1 mM  $[\text{Co}^{\text{III}}(\text{N}2\text{py}2\text{a})(\text{Cl})_2]\text{ClO}_4$ , treated with 2 eq  $\text{AgClO}_4$  in water, and 40 eq  $\text{H}_2\text{O}_2$ . Spectra were recorded in 5 minutes intervals.

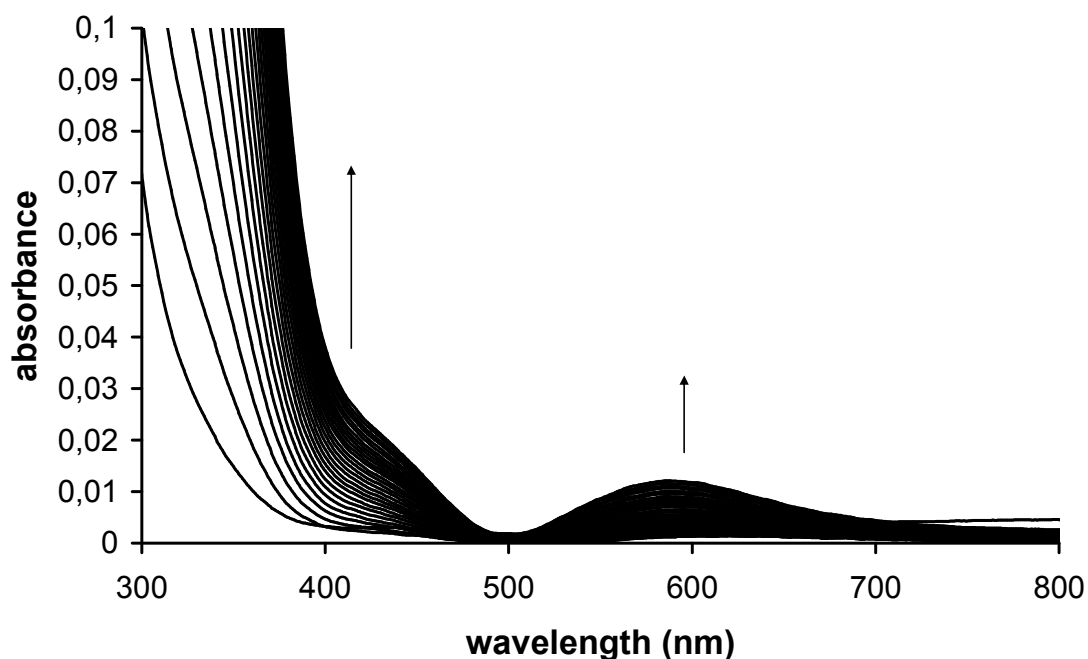


Figure 7.17. Difference UV-vis spectra for the reaction between 1.1 mM  $[\text{Co}^{\text{III}}(\text{N}2\text{py}2\text{a})(\text{Cl})_2]\text{ClO}_4$ , treated with 2 eq  $\text{AgClO}_4$  in water, and 40 eq  $\text{H}_2\text{O}_2$ . Spectra were recorded in 5 minutes intervals.

### Experiment 2

The aqueous solution, obtained after treatment of  $[\text{Co}^{\text{III}}(\text{N}2\text{py}2\text{a})(\text{Cl})_2]\text{ClO}_4$  with 2 eq  $\text{AgClO}_4$ , was completely evaporated, the remaining solid was redissolved in methanol and an excess of  $\text{H}_2\text{O}_2$  was added. Finally, the mixture was subjected to ether diffusion. After 2 days violet

needles were grown. The crystal structure together with selected bond lengths and angles are presented in Figure 7.18 and Table 7.7.

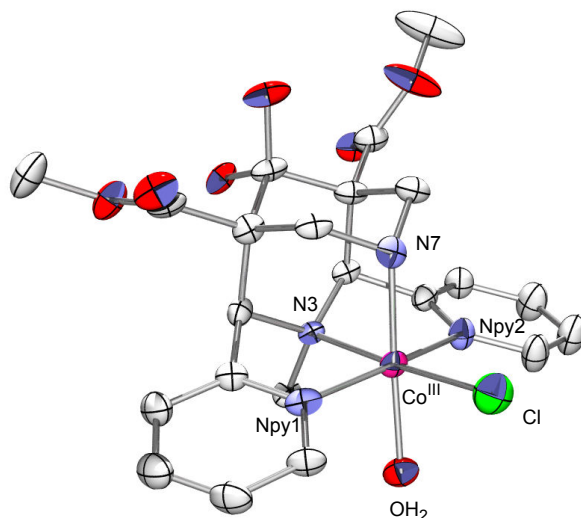


Figure 7.18. Crystal structure of  $[\text{Co}^{\text{III}}(\text{N}2\text{py}2\text{a})(\text{Cl})(\text{OH}_2)](\text{ClO}_4)_2$

Table 7.7. Selected bond lengths and angles of  $[\text{Co}^{\text{III}}(\text{N}2\text{py}2\text{a})(\text{Cl})(\text{OH}_2)](\text{ClO}_4)_2$

	$[\text{Co}^{\text{III}}(\text{N}2\text{py}2\text{a})(\text{Cl})(\text{OH}_2)](\text{ClO}_4)_2$	$[\text{Co}^{\text{III}}(\text{N}2\text{py}2\text{a})(\text{Cl})_2]\text{ClO}_4$ <sup>7</sup>
Co-N7	1.979(4)	2.018(7)
Co-N3	1.956(4)	1.965(6)
Co-Npy1	1.945(4)	1.957(7)
Co-Npy2	1.925(4)	1.918(7)
Co-O(ax)	1.961(4)	-
Co-Cl(eq)	2.2169(17)	2.2536(23)
N3-N7	2.715	2.75
Npy1-Npy2	3.846	3.84
N3-Co-N7	87.55(17)	87.50(26)
N3-Co-Npy1	84.27(17)	83.46(26)
N3-Co-Npy2	84.59(17)	83.81(26)
Npy1-Co-Npy2	164.26(17)	165.14(28)
C1-C2-C <sub>A</sub> -Npy1	84.28	86.8
C5-C4-C <sub>A</sub> -Npy2	-81.69	-80.6

The bond lengths and angles are in good agreement with the values of the parent dichloro complex,  $[\text{Co}^{\text{III}}(\text{N}2\text{py}2\text{a})(\text{Cl})_2]\text{ClO}_4$ . As can be seen in the structure, only one of the two coordinated chlorides was removed by the treatment of the dichloro complex with  $\text{AgClO}_4$ , namely the more labile axially coordinated chloride. It is well known that the preorganized and rigid structure of the bispidone backbone enforces metal coordination in such a way, that shorter M-N3 and longer M-N7 bonds are found. In other words, an elongated axis is created

in the axial direction. Metal complexes of tetradentate bispidones have two free ligation sites to coordinate co-ligands. Since M-N3 bonds are shorter than M-N7 bonds, binding of a co-ligand *trans* to N3 (in the equatorial position) results in shorter, thus also stronger bonds, than coordination *trans* to N7 (in axial position). Therefore, breaking a bond between the metal and the axial co-ligand requires less energy, than bond cleavage in the equatorial plane (*trans* to N3).

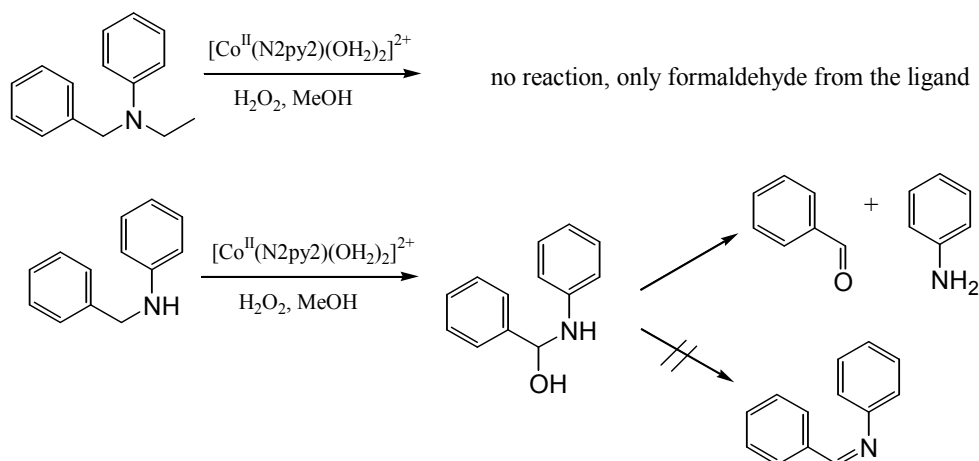
The Co-N7 distance in  $[\text{Co}^{\text{III}}(\text{N}2\text{py}2\text{a})(\text{Cl})(\text{OH}_2)](\text{ClO}_4)_2$  is around 0.04 Å shorter than in the dichloro complex. This may be due to the lack of charge-transfer coming from the axially bound water molecule. Neutral water, in comparison with chloride, can transfer much less electron density to the cobalt(III) center and the trans-effect is therefore less pronounced. The Co-N7 distance for N2py2a complexes is shorter than for a complex where the ligand contains an N7-methyl group (N2py2b).<sup>7</sup> This trend is also observed for the cobalt(II) complexes (see above).

From the crystal structure it seems that when only one of the two chloride co-ligands is removed, the added hydrogen peroxide does not bind in a monodentate mode to occupy the one and only free coordination site around cobalt(III) center. Since hydrogen peroxide was added as a 30% aqueous solution to the mixture, a significant amount of water is present in the solution. Under these conditions the coordination of water may be favoured over peroxide. However, the addition of some base may induce deprotonation of  $\text{H}_2\text{O}_2$  and thus its binding to cobalt(III). Coordination of peroxide to the cobalt(III) center might also be possible in a bidentate mode. Analogous 7-coordinate side-on peroxo iron(III) bispidine complexes were calculated to be stable species.<sup>141</sup>

In aqueous solution both a cobalt(III)-peroxo and a monochloro cobalt(III) species was evidenced by ESI-MS spectroscopy. In the crystallization experiment, not only the violet needles could be seen, but also a fine, deep purple precipitate, which did not form crystals. It is probable that in this compound both chlorides were removed, which would explain the ESI-MS results measured for the aqueous solution. As was seen in the time-dependent UV-spectra, the exchange of water to peroxide is kinetically controlled. Since a relatively small amount of  $\text{H}_2\text{O}_2$  was used for crystallization, it cannot be excluded that within the time frame of the crystal formation the exchange to peroxide (or hydroperoxide) was not complete.

### 7.4.9. External substrates: $[\text{Co}^{\text{II}}(\text{N}2\text{py}2)(\text{OH}_2)_2]^{2+} / \text{H}_2\text{O}_2$ system as catalyst?

Several enzymes in nature can accelerate the dealkylation of amines.<sup>28,29</sup> Conversion of tertiary to secondary amines, by formation of aldehyde from the cleaved N-alkyl side chain is considered to be one possible pathway in metabolism.<sup>26,27</sup> To mimic the function of such enzymes, a large number of transition-metal complexes have been investigated. Among others, Fe(III)-porphyrins,<sup>142-144</sup> Ru(III)-EDTA,<sup>145</sup> Cu(III)-bis- $\mu$ -oxo<sup>146</sup> and Cu(II)-phenanthroline complexes<sup>147</sup> were shown to be efficient functional models. Tertiary amines can be oxidized also by aqueous bromine,<sup>139</sup> hexacyanoferrate(III)<sup>148</sup> and neutral permanganate.<sup>149</sup> Photochemical oxidation with heterocyclic N-oxides can also convert tertiary amines to a secondary amine and an aldehyde.<sup>150</sup> The only reported cobalt-containing catalyst is a salen-based cobalt(II) complex which can oxidize a series of N-butyl anilines under aerobic conditions.<sup>151</sup>



**Scheme 7.1.** Summary on the reactions of  $[\text{Co}^{\text{II}}(\text{N}2\text{py}2)(\text{OH}_2)_2]^{2+}$  with external substrates

As described before, by the reaction with hydrogen peroxide under aerobic conditions in methanol, the  $[\text{Co}^{\text{II}}(\text{N}2\text{py}2)(\text{OH}_2)_2](\text{ClO}_4)_2$  complex loses the methyl group attached to N7 in an intramolecular oxidative N-dealkylation. The question arises, whether intermolecular, as well as intramolecular oxidation can take place. That is, can the  $[\text{Co}^{\text{II}}(\text{N}2\text{py}2)(\text{OH}_2)_2](\text{ClO}_4)_2$  complex act as catalyst and oxidize external substrates?

The tertiary amine N-benzyl-N-ethyl-aniline remains intact after treatment with  $[\text{Co}^{\text{II}}(\text{N}2\text{py}2)(\text{OH}_2)_2]^{2+}/\text{H}_2\text{O}_2$  in MeOH. No aldehyde (benzaldehyde or acetaldehyde) from the substrate was detected with the hydrazine test, only formaldehyde formation was observed. This is formed exclusively from the  $[\text{Co}^{\text{II}}(\text{N}2\text{py}2)(\text{OH}_2)_2](\text{ClO}_4)_2$  complex by removal of the N7-bound methyl group. In strong contrast, addition of the secondary amine N-benzyl-aniline to equimolar amount of  $[\text{Co}^{\text{II}}(\text{N}2\text{py}2)(\text{OH}_2)_2](\text{ClO}_4)_2$  in presence of excess  $\text{H}_2\text{O}_2$  in MeOH produces not only formaldehyde from the ligand, but also benzaldehyde, which can be

isolated in form of hydrazone. A combined gravimetric and  $^1\text{H}$  NMR spectroscopic analysis allowed to determine the yield of dealkylation and the yield of N-debenzylation of the external substrate was determined to be 37.8%. The yield of formaldehyde production was 19.8%, which is somewhat lower than when the ligand is oxidized in the absence of an external amine substrate. Control experiments using only  $\text{H}_2\text{O}_2$  or only the cobalt(II) complex gave negative hydrazine tests for both substrates, so the oxidant was shown to be  $[\text{Co}^{\text{II}}(\text{N}2\text{py}2)(\text{OH}_2)_2]^{2+}/\text{H}_2\text{O}_2$ .

It is well known that, within the series of amines the tertiary amines are the most difficult to oxidize and primary amines the easiest.<sup>139</sup> Using a methanolic solution of the  $[\text{Co}^{\text{II}}(\text{N}2\text{py}2)(\text{OH}_2)_2]^{2+}/\text{H}_2\text{O}_2$  system, the conversion of the tertiary amine (N-benzyl-N-ethyl aniline) was not observed, but the secondary amine N-benzylaniline was oxidized to the corresponding aldehyde. We assume that the oxidation occurs via an  $\alpha$ -hydroxyl amine intermediate, which can be stabilized in two different ways. By bond rearrangements this species can be transformed to a primary amine and an aldehyde (“retro Schiff-base reaction”), the second possibility is the completion of the Schiff base reaction, leading to an imine. Due to the fact that no peak, assignable for such an imine, was seen in the ESI-MS spectrum, it can be concluded that the stabilization of the hydroxylamine intermediate follows exclusively via the retro Schiff-base reaction pathway.

#### 7.4.10. Proposed mechanism of the oxidative N-dealkylation

From the experimental evidence described above, the following points should be highlighted: As oxidant, only hydrogen peroxide could oxidize the cobalt(II) center in the complexes with tetradentate N2py2 and N2py2Bz ligands. These lose the N7-bound alkyl rest during the oxidation. The alkyl rest is transformed to the corresponding aldehyde, which could be qualitatively and quantitatively proven by the hydrazine test reaction. Dealkylation was seen when using methanol as solvent, but not in acetonitrile. No reaction takes place, when a Co(III) complex is mixed with hydrogen peroxide. The presence of oxygen from air was another important factor, in the removal of the N7-bound methyl or benzyl group; no reaction took place under anaerobic conditions.

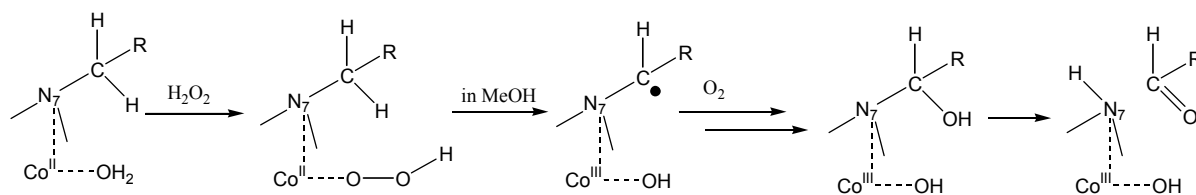


**Figure 8.19. Simplified overview of the proposed mechanism for the intramolecular N-dealkylation**

In our proposed mechanism the first step is the formation of a cobalt(II) hydroperoxo species:  $\text{H}_2\text{O}_2$  can coordinate to the cobalt(II) center by exchanging the equatorial water co-ligand. As discussed earlier in this chapter, equatorial (*trans* to N3) binding is preferred over the axial one (*trans* to N7) owing to the differences in the bond lengths and thus also in bond strengths. From this, monodentate binding of hydroperoxide is stabilized at *trans* to N3 position. The coordinated hydroperoxide can rotate freely, but for steric reasons can only approach the methyl group at N7. A reaction involving the N3-bound methyl group can be ruled out.

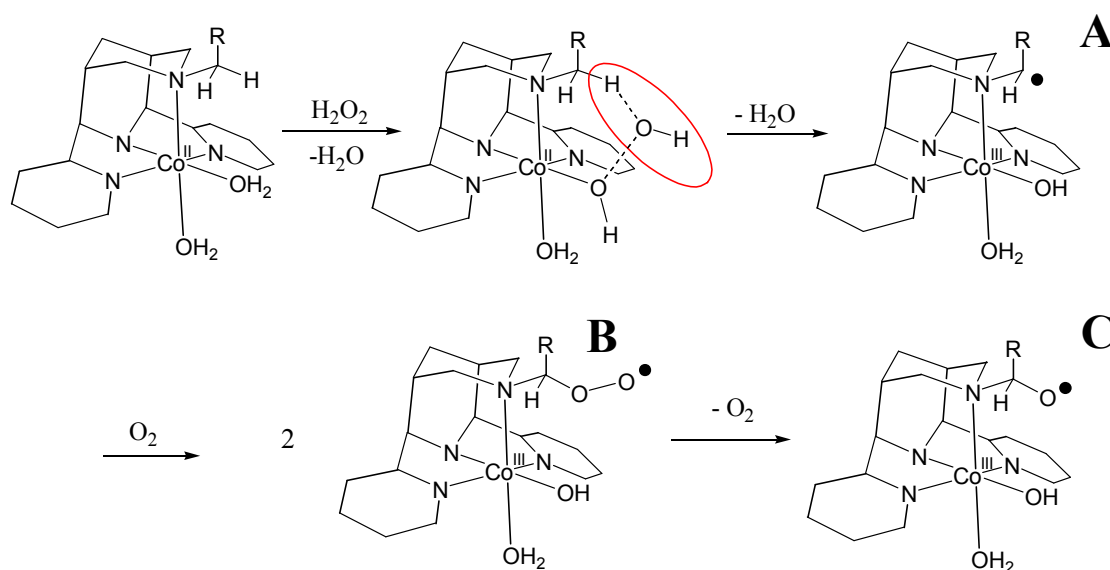
Bispidone ligands with higher denticity have also been investigated before and theoretically only one of them, namely the pentadentate N2py3u, would be suitable for the N-dealkylation reaction. It contains an additional picolyl group attached to N3, which occupies the *trans* to N7 position, but the equatorial *trans* to N3 position is free, so a labile water molecule can be replaced by a hydroperoxide, as proposed for the tetradentate cobalt(II) complexes. This cobalt(II)-N2py3u complex has an N7-bound methyl group (in analogy with N2py2), so it has the same features which are proposed to play a key role in the first step of dealkylation. Surprisingly, with the N2py3u complex, no dealkylation takes place. The reason for this is probably the lower redoxpotential (300 mV) in comparison with the N2py2 complex, which stabilizes cobalt(III) relative to cobalt(II). The oxidation occurs more “smoothly”, (with lower activation energy) which does not reach the barrier of the N-dealkylation.<sup>7</sup>

This cobalt(II) hydroperoxo species was seen only in acetonitrile, and from mass spectroscopic evidence it can be claimed that the solvent molecule can be bound to this species, which leads to further stabilization, probably due to ligand field effects.

The second step takes place only in methanol and involves homolytic cleavage of two bonds: the O-O bond of the coordinated hydroperoxide and one C-H bond of the N7-bound methyl (or methylene) group, leading to a carbon-based radical species. The central cobalt(II) is oxidized by the bound peroxide to get a cobalt(III)-hydroxide. A very similar step is described for dopamine- $\beta$ -monooxygenase enzyme, where a copper(II)-hydroperoxo species attacks a C-H bond of an N $\beta$ -methylene unit, and produces a carbon-centered radical by hydrogen atom abstraction and formation of a copper(III)-oxo species.<sup>29</sup>

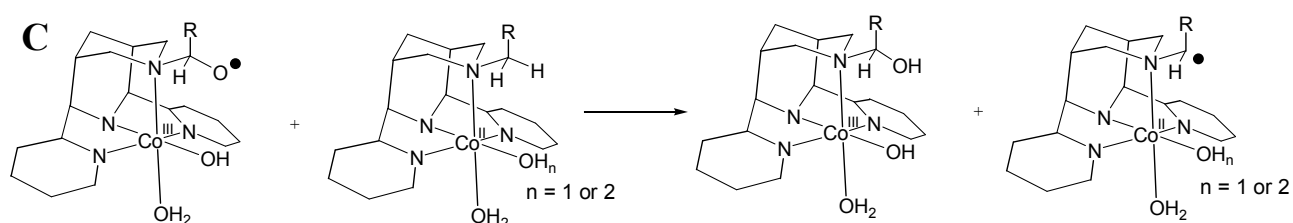
In the next step the carbon-based radical species gets hydroxylated, a reaction in which the role of oxygen seems to be important, since anaerobic tests did not show oxidation of the ligand, only of the metal. The necessity for oxygen in the reaction strongly suggests that the mechanism follows a radical pathway.

The mechanism of aerobic oxidation of hydrocarbons has been widely investigated and several reaction pathways have been proposed.<sup>152</sup>



**Scheme 7.2. Proposed detailed mechanism for the intramolecular oxidative N-dealkylation (charges omitted)**

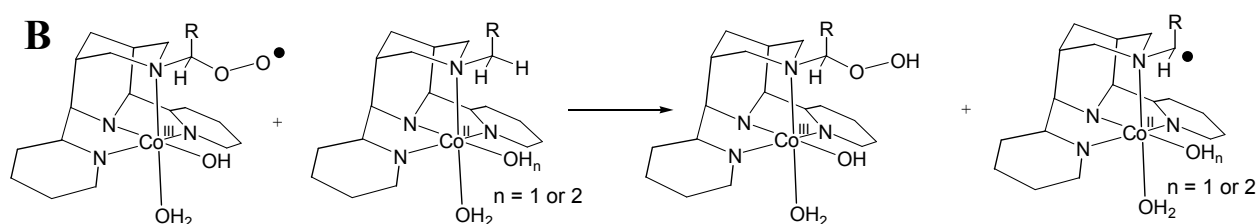
Radical based oxidations with oxygen involve the formation of peroxy and oxo radicals which can be stabilized by further hydrogen atom transfer. On the basis of these mechanisms, we assume that the cobalt(III)-hydroxo species with the carbon based radical (species **A** in Scheme 7.2) reacts with oxygen and forms a peroxy radical species (denoted as **B** in Scheme 7.2). This reaction may also be thermodynamically favored: the structurally analogous radical derived from trimethylamine by hydrogen atom abstraction, was shown to react with molecular oxygen in an exothermic reaction, which was explained by the high bond cleavage enthalpy of the C-O bond in the resulting peroxy radical species.<sup>153</sup> Two molecules of the peroxy radical species (after forming a tetroxide) can eliminate oxygen<sup>154</sup> to produce an alkoxy radical cobalt(III)-hydroxo species (denoted as **C** in Scheme 7.2). Both intermediate radical species can initiate hydrogen atom abstraction (Scheme 8.3 and 8.4)



**Scheme 7.3. Hydrogen atom abstraction by the alkoxy radical species (charges omitted)**



The alkoxy radical species can abstract a hydrogen atom from species where the N7-methyl group is intact, for example from a cobalt(II)-N2py2-diaqua or from a cobalt(II)-N2py2-aqua/hydroxo species, depending on the pH of the solution. As a result, an  $\alpha$ -hydroxylated cobalt(III) complex species is formed, together with a carbon based radical containing cobalt(II) species. The latter can react directly with oxygen to form a peroxy radical, and the cobalt(II) center can be oxidized with hydrogen peroxide, yielding a cobalt(III)-hydroxo species and a hydroxyl radical. OH-radicals are easily quenched in methanol, so these can play no further role in the mechanism.

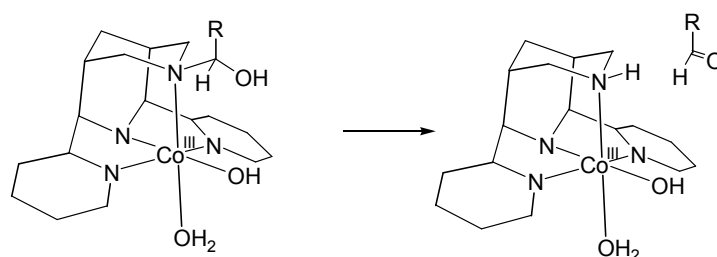


**Scheme 7.4. Hydrogen atom abstraction by the peroxy radical species (charges omitted)**

Similar hydrogen atom abstraction can be initiated by the peroxy radical species **B**, forming an  $\alpha$ -hydroperoxyl amine.

The peroxy and oxo radical species **B** and **C** can also react with the external amine substrates, and abstract a hydrogen atom from their  $\alpha$ -methylene groups in a fashion presented in Scheme 7.3 and 7.4. The resulting carbon based radical amine species, which is formally analogous to species **A**, can react further with oxygen to form a peroxy (**B**) and oxo (**C**) radical species and follow the reaction pathways described in Schemes 7.2-7.4.

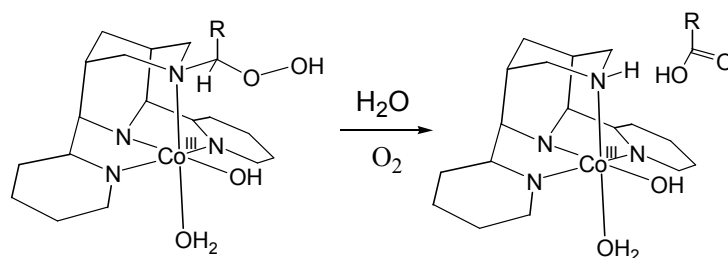
The peroxy and oxo radicals can be dimerized to tetroxide and peroxides respectively. These reactions are dead-ends from the point of the autoxidation.



**Scheme 7.5. Retro Schiff-base reaction of  $\alpha$ -hydroxylamine species (charges omitted)**

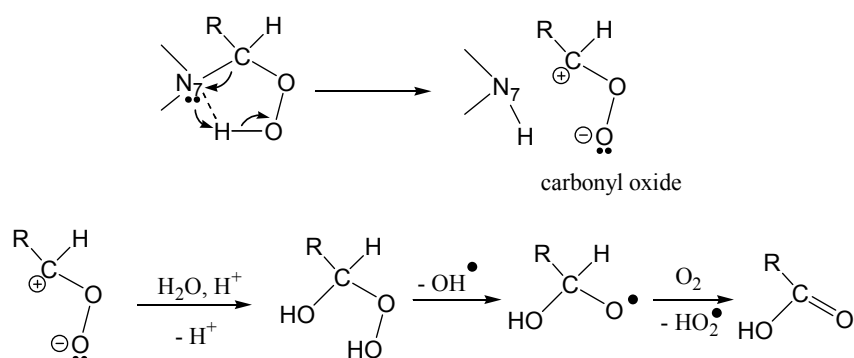
The last step is the conversion of the  $\alpha$ -hydroxylamine to the corresponding secondary amine and aldehyde through a “retro Schiff-base reaction”. There is no possibility to stabilize this  $\alpha$ -hydroxylamine in the form of a Schiff-base imine since there is no hydrogen atom to abstract from the tertiary amine at N7.

The  $\alpha$ -hydroperoxylamine species can also decompose:



**Scheme 7.6. Decomposition of  $\alpha$ -hydroperoxylamine species (charges omitted)**

The hydrogen atom of the hydroperoxyl unit in the  $\alpha$ -hydroperoxylamine species can approach the tertiary N7 nitrogen (see Scheme 7.7). Through a 5-membered ring transition state a rearrangement may take place, which yields a secondary amine and a carbonyl oxide. This carbonyl oxide is a typical intermediate in ozonolysis reactions and it shows a high reactivity toward water. It has recently been demonstrated in a computational study, that among the various pathways, the hydration of a carbonyl oxide is the energetically most favourable reaction.<sup>155</sup> The resulting hydroxyalkyl-hydroperoxide is decomposed via cleavage of the peroxy bond to form OH radicals. The co-produced hydroxyalkoxy radical subsequently reacts with oxygen to form carboxylic acid and a hydroperoxy radical. It has been shown that the possible alternative route for the decomposition of hydroxyalkyl-hydroperoxide, that is the formation of aldehyde and hydrogen peroxide, has a higher activation barrier.<sup>156</sup>



**Scheme 7.7. Proposed mechanistic pathway for the decomposition of  $\alpha$ -hydroperoxylamine species**

This reaction route may explain why the absolute yield of the aldehyde formation is far from stoichiometric. If both the hydroxo and hydroperoxo routes are feasible, the sum of the resulting aldehyde and the carboxylic acid should give 100%.

From the fact that the N-dealkylation occurs only in methanol, the involvement of hydroxyl-radicals in the mechanism can be excluded.

**7.5.10. DFT calculations for the proposed mechanistic pathway**

To gain further support for the proposed mechanism of the intramolecular oxidative N-dealkylation, DFT calculations have been carried out. The three-parameter hybrid exchange and correlation functional, B3LYP,<sup>157,158</sup> has been shown to provide accurate geometries for transition-metal containing systems,<sup>159</sup> and was therefore used throughout.

**7.5.10.1. Conversion of cobalt(II)-hydroperoxo / cobalt(II)-hydrogen peroxide species to cobalt(III) carbon based radical species**

The reaction step is the conversion of the cobalt(II)-hydroperoxo species to a cobalt(III) species with a carbon-based radical. This step can occur from either a cobalt(II)-hydroperoxo or a cobalt(II)-hydrogen peroxide species since both have been observed in the ESI-MS spectra (Figure 7.20).

The first pathway starts from a cobalt(II)-hydroperoxo species, which is presumed to be high-spin. As product, a high-spin cobalt(III)-oxo species is postulated to form, followed by a spin transition from high-spin to low-spin, since octahedral cobalt(III) complexes are generally more stable in the low spin form. However, the presence of a radical in this species makes the assumption somewhat ambiguous. For this reason structures were calculated for both spin states.

The second pathway differs only in a presence of one extra proton and starts from a cobalt(II)-hydrogen peroxide species instead of the hydroperoxo analogue. This reaction may be chemically more relevant, producing a “more believable” cobalt(III)-hydroxo species.

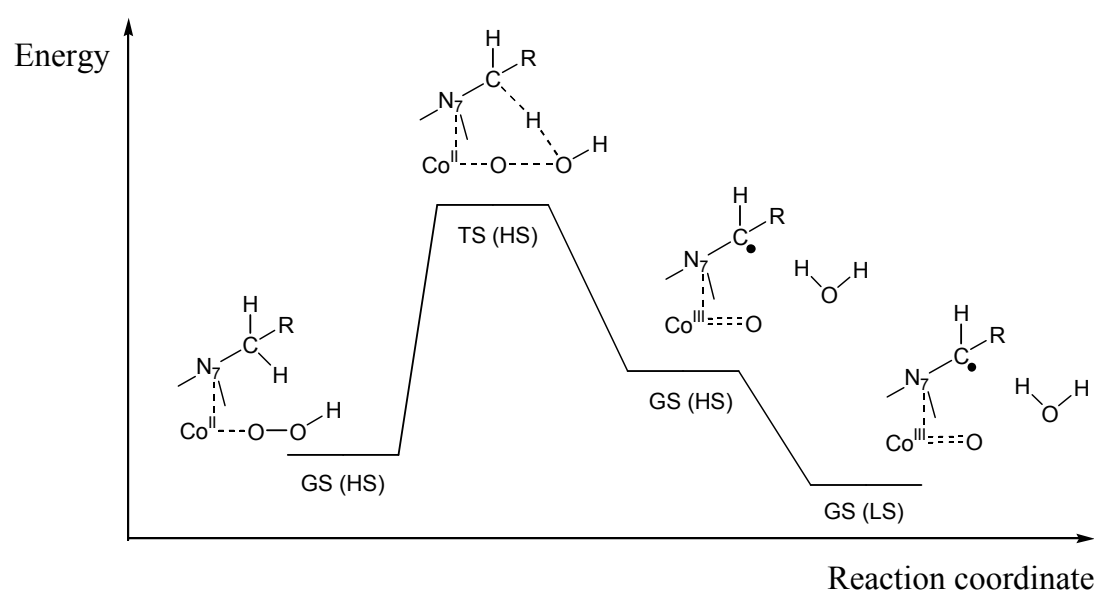


**Figure 7.20 (a)** Schematic energy profile for the conversion of cobalt(II) hydroperoxide to cobalt(III) radical species, GS = ground state, TS = transition state

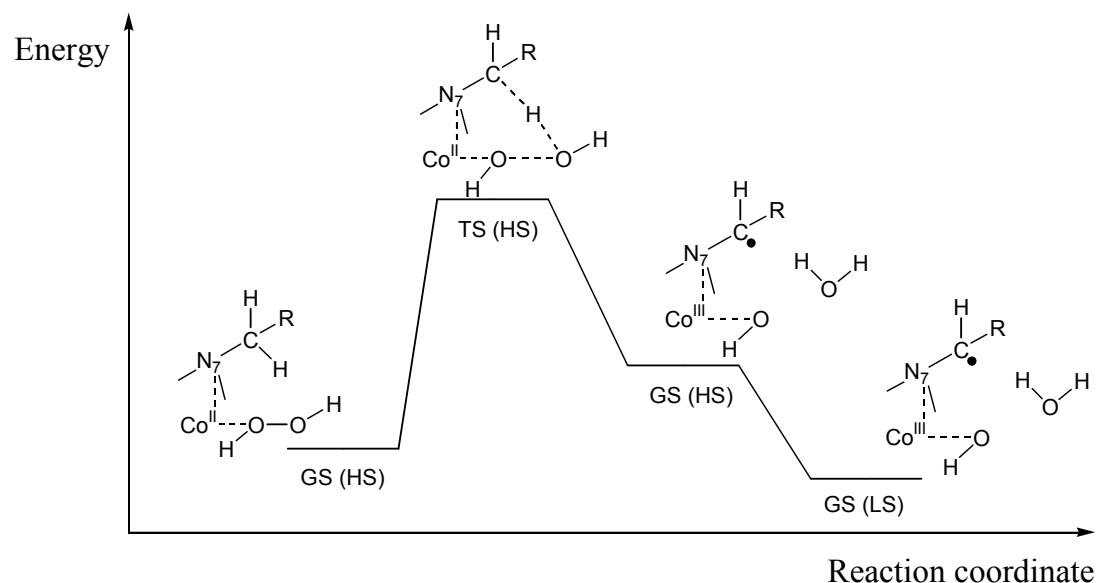


**Figure 7.20 (b)** Schematic energy profile for the conversion of cobalt(II) hydrogen peroxide to cobalt(III) radical species, GS = ground state, TS = transition state

*The cobalt(II) hydroperoxo/hydrogen peroxide species*

To optimize the cobalt(II)-hydroperoxo species, crystal structures of the diaqua cobalt(II) complex with N2py2 were taken as starting structure, when the equatorial water co-ligand is replaced with hydroperoxide.

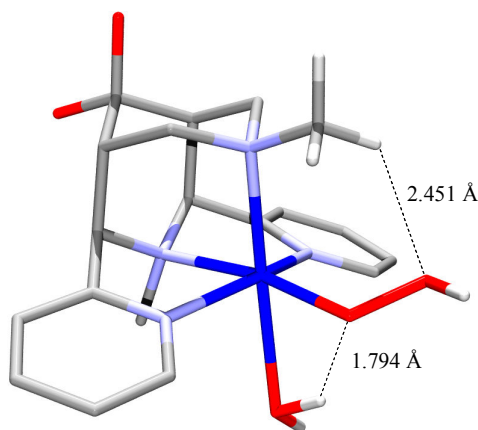


**Figure 7.21.** Optimized structure of high-spin cobalt(II)-hydroperoxo species using 6-31G(d) basis set

When using the isomer with the longer Npy1-Npy2 separation (entry 31)<sup>6</sup> as initial guess, a geometry optimization at 6-31G(d) level could be successfully performed (Figure 7.21). Note that optimization with the other crystal structure could be done only with the STO-3G basis set. The above mentioned hydrogen bonds are also observable in this structure, however, the bond distances are significantly longer: 2.451 Å for the chelate bond and 1.794 Å for the water-hydroperoxide interaction. Here the role of hydrogen bonds seems to be not

overestimated, indeed, the axial water remains more or less in the Co-N7 defined axis. The fact that all the calculated frequencies of this structure are positive, shows that the optimized structure corresponds to an energy minimum on the potential surface. A single point energy at TZVPP<sup>160</sup> (Co) / TZV<sup>161</sup> (other atoms) level could also be determined. From this energy and that of cobalt(II)-diaqua complex (see in Section 7.4.3) the reaction energy of the formal exchange between equatorial water and hydroperoxide could be calculated to +27.3 kJ/mol (the co-reactant H<sub>2</sub>O<sub>2</sub> and the product oxonium ion were separately minimized).

Although from our experimental evidence the cobalt(II) bispidone complexes are thought to be high-spin, for comparative purpose attempts were made to calculate the corresponding low-spin state of cobalt(II)-hydroperoxo species, but despite our efforts, none of these calculations converged.

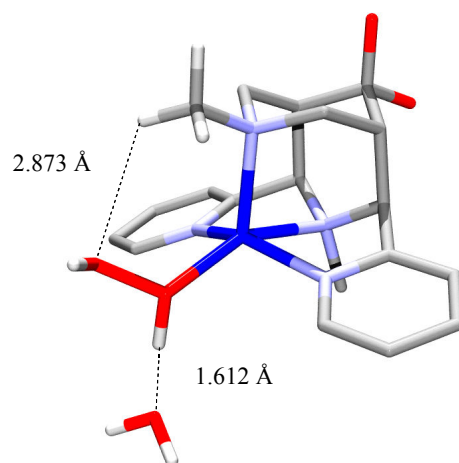


**Figure 7.22.** Optimized structure of high spin cobalt(II)-hydrogenperoxide species using 6-31G(d) basis set

Considering the second mechanistic pathway, in the first step a hydrogen peroxide is postulated to substitute the *trans* to N3 bound water molecule. Calculations of complexes were made for both spin states, using both initial guess geometries (see above for details). From the four possibilities only one of them (high-spin with the guess structure of “entry 31”<sup>6</sup>) converged (Figure 7.22). In contrast to the cobalt(II) hydroperoxo species, the axial water molecule is removed from the coordination sphere of the central cobalt(II) ion and becomes H-bonded to the coordinated hydrogen peroxide. Such a phenomenon is not unusual in DFT calculations involving copper(II) complexes, where weak axial bonds are often cleaved.<sup>162</sup> As a result, the cobalt(II) center is 5-coordinate, and for geometric reasons the initially equatorial Co-O bond of hydrogen peroxide moves below the plane determined by the N3, Npy1 and Npy2 nitrogen atoms. Due to this, the non-coordinating oxygen of H<sub>2</sub>O<sub>2</sub> is situated even further from the hydrogen atoms of the N7-methyl group ( $d(\text{O}\cdots\text{H}) = 2.873 \text{ \AA}$ ).

This distance, though longer than the corresponding distances in any of the calculated Co(II)-hydroperoxo structures, is still suitable for the C-H activation step. This optimized structure corresponds to a real minimum, all frequencies are positive. The single point energy at TZVPP(Co) / TZV(other atoms) level could also be determined and the value shows that the reaction between the cobalt(II)-diaqua complex and hydrogen peroxide to get cobalt(II)-hydrogen peroxide and water is exothermic (-18.1 kJ/mol).

*Calculation of the transition state: QST3 calculations*

As a first attempt for the determination of the transition state of the cobalt(II)-hydroperoxo reaction pathway a QST3 calculation was performed. QST3 is a geometry-based approach, using guessed structures of the reactant and the product, to find the transition state. For the reactant, the optimized Co(II)-hydroperoxo species was used as starting point. For the product cobalt(III)-oxo radical species, a guess was made. Considering that a single reaction step with bond-breaking and -making should not change the overall multiplicity of the system, the cobalt(III)-oxo species has to be high spin (like the reactant). The extent of the cavity compression in the bispidone ligand part could not be judged, since crystal structures for cobalt(III) bispidones are only available for the much more favored low spin state (octahedral low spin cobalt(III) complexes are known to be very stable and inert). The Co-N distances in a high spin cobalt(III)-complex species should be longer than in the low-spin analogues, but due to the change in the ion size, they should be smaller than in a hs cobalt(II) species. As initial guess, an optimized Co(II) structure was taken for this Co(III)-oxo radical species. The converged TS structure is shown in Figure 7.23.

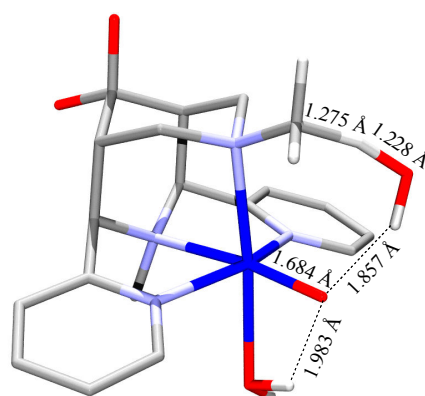


**Figure 7.23.** QST3-optimized hs transition state structure, using 6-31G(d) basis set (TS2)

The structure shows a build-up of a 7-membered ring instead of the expected 6-membered ring. The O-O bond of the hydroperoxide is not simply elongated but already cleaved, and the hydrogen of the OOH moiety forms a H-bond with the equatorial oxygen ( $d(\text{O}\cdots\text{H}) = 1.857$

Å). Judging from the distances ( $d(\text{C}\cdots\text{H}) = 1.275 \text{ \AA}$   $d(\text{O}\cdots\text{H}) = 1.228 \text{ \AA}$ ) the activated hydrogen of the N7-methyl group is formally shared both by the methyl carbon and the oxygen. In parallel with this, the Mulliken spin densities of these two atoms are nearly the same, close to -0.5, which corresponds to the delocalization of the spin on the two atoms. The single negative frequency is related to a stretching mode where the hydrogen is oscillating between the N7-methyl carbon and the oxygen along the axis determined by the three atoms. The distance between central Co and the equatorial oxygen (1.684 Å) is typical for a double-bonded oxygen, with a formal oxidation state of -2. Considering this and the overall charge, the transition state can be best described as a cobalt(III)-oxo species. The Mulliken charge on the central cobalt is 50% more than in any of the optimized cobalt(II) species (Co(II)-OOH or Co(II)-H<sub>2</sub>O<sub>2</sub>), which supports the trivalent state of cobalt in this species. The Mulliken charges on each carbon are the same (close to 0) which means that, in agreement with the expectations, the N7-bound methyl carbon is also chargeless. The oxygens of the original hydroperoxide (the equatorial “oxo” and the other one close to the activated C-H bond) possess almost the same Mulliken charge, so these are most probably in the same oxidation state. Since the equatorial oxygen is thought to be an oxo-oxygen, the other one is formally part of a water molecule, which activates the C-H bond. Considering structural features, this one is not the expected transition state, since the cobalt(III)-oxo unit and the formed water molecule strongly resembles the product. It is very probable that this reaction is, in fact, a two-step process, and that this transition state corresponds to the TS of the second step of the reaction (TS2). The single point energy at TZVPP/TZV level shows that our transition state has 136 kJ/mol activation barrier with respect to the cobalt(II)-hydroperoxo species. The transition state calculation for the other reaction pathway (starting with the cobalt(II)-hydrogen peroxide species) was not successful with QST3.

*Calculation of the transition state: TS transition state search*

The initial structure for a TS transition state search was based on the optimized geometry of the cobalt(II)-hydroperoxo species, and bonds that were expected to take part in the concerted mechanism were elongated. Starting structures, generated by concerted elongation of a C-H bond (of the N7-methyl group) and the O-O bond of the hydroperoxide, were optimized to a transition state very similar to that obtained by QST3. One completely different transition state was obtained.

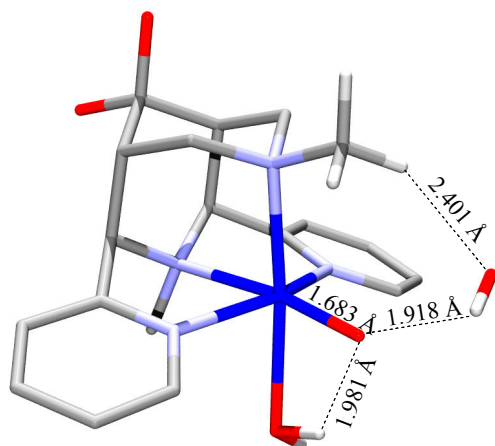


Figure 7.24. Transition-state structure with a *hs* electronic configuration (6-31G(d) basis set)

In this structure the O-O bond is cleaved but the initially elongated C-H bond returns to an unstrained distance. Moreover, a cleavage product of the O-O bond, a hydroxyl radical is formed (the spin density on its oxygen is close to -1), and it is hydrogen bonded to the oxo oxygen. The one negative frequency, calculated for this structure indicates that it is a transition state. The formation of this transition state from the cobalt(II)-hydroperoxy species has an activation barrier of 97 kJ/mol. Since no elongated C-H bond is observed in this structure, it is postulated to be the first transition state (TS1) on the reaction pathway, which is directly formed from the cobalt(II)-hydroperoxy species.

#### *Optimization for the product Co(III) C-based radical species*

Since the QST3 transition state calculation gave a structure very close to the product state, it served as a starting structure for a high spin cobalt(III)-oxo radical species. The optimized structure is depicted in Figure 7.25.

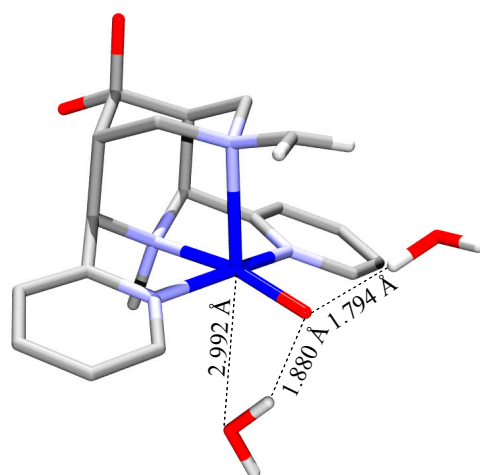
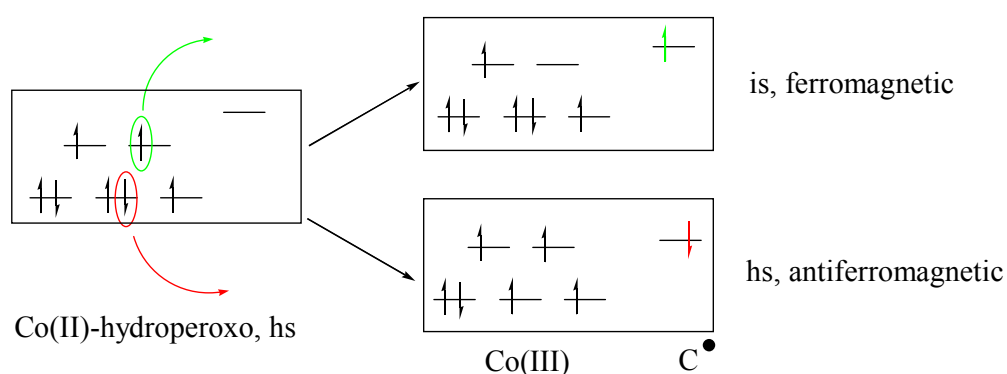


Figure 7.25. Structure of cobalt(III)-oxo radical species obtain after normal geometry optimization ( $S=3/2$ )



The Mulliken spin densities of the optimized structure show that two unpaired electrons are localized on the central cobalt(III) and one on the radical carbon. This corresponds to an intermediate spin cobalt(III) species with the metal center ferromagnetically coupled to the radical. Although such an electron configuration is unusual, formation of this species cannot be excluded on the basis of the symmetry rules. As it was already seen in other optimized structures, the axial water is removed from the coordination sphere of the cobalt center. This structure corresponds to a true minimum (all calculated frequencies were positive). Single point energy at TZVPP/TZV level could be calculated and showed that the formation of this species from the high-spin cobalt(II)-hydroperoxo species is endothermic (+172 kJ/mol).

Considering the formation of the radical species, theoretically there are two different routes, depending upon whether the free electron of the carbon radical is in a spin-up or a spin-down state.



**Figure 7.26. Two possible electron configurations of cobalt(III)-oxo C-radical species ( $S=3/2$ )**

Since the “normal” optimization led exclusively to the is cobalt(III)-oxo radical species, calculation of the other isomer required a treatment of the starting structure, which gave an initial guess with orbital coefficients corresponding to the hs state, without changing geometric parameters. The initial guess was generated by using the high ligand field theory option of the Jaguar 5.0 program.<sup>163</sup> Geometry optimization of this initial guess does not change the distribution of the spins, so the convergence leads to the desired hs cobalt(III)-oxo species with a spin-down electron on the radical carbon.

As expected, the spin distribution of the optimized structure remained the same as it was in the initial guess. Similar to the is electronic isomer, the hydrogen of the axial water forms a hydrogen bond with the equatorial oxo oxygen. The central cobalt is six-coordinate, though the axial Co-O bond is elongated. Comparing the energetics of the two isomers, the hs species is more stable than the is one (89 kJ/mol). Consequently, the formation of hs cobalt(III)-oxo radical species from cobalt(II)-hydroperoxo species is endothermic (+106 kJ/mol).

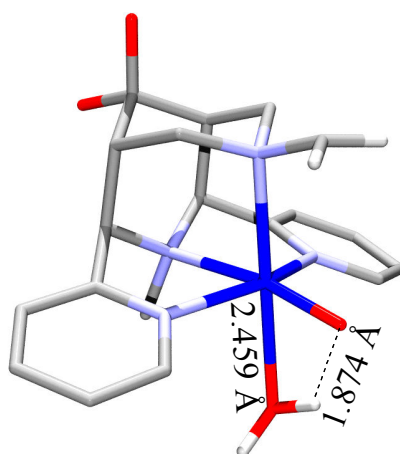


**Figure 7.27. Optimized structure of hs cobalt(III)-oxo radical species (S=3/2)**

Optimization of the cobalt(III)-oxo radical in the  $1s$  state was also carried out, in order to investigate whether the formed hs species are further stabilized by a change in spin state. As an initial guess, the crystal structure of  $[\text{Co}^{\text{III}}(\text{N}2\text{py}2\text{b})(\text{CO}_3)]^+$  was taken, replacing the co-ligand with water and an oxo oxygen, and setting the Co-O bond distances to values typical for such bonds. Since the direct optimization did not converge, preoptimization of the orbitals was necessary in Jaguar. Finally the geometry was optimized using the orbital coefficients obtained from the preoptimization.

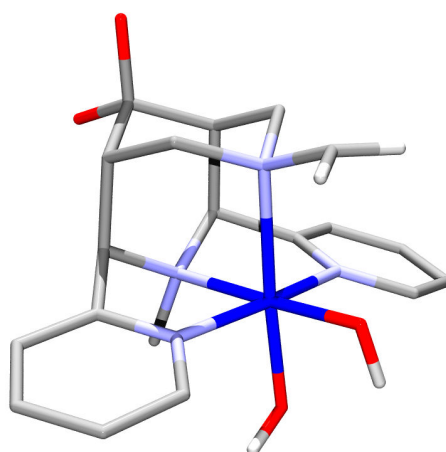


**Figure 7.28. Optimized structure of  $1s$  cobalt(III) radical species**

The Co-N distances fall within the range typical for  $1s$  cobalt(III)-complexes. (e.g.: Co-Npy1 1.933 Å, Co-Npy2 1.939 Å). Interestingly a proton from the axial water co-ligand was transferred to the oxo oxygen, resulting in a cobalt(III)-dihydroxo species. Considering the energetics, this species is more stable than the S=3/2 species: formation of  $1s$  cobalt(III)-dihydroxo species from hs cobalt(III)-oxo and  $1s$  cobalt(III)-oxo species is exothermic (reaction energies were calculated to be -64 and -153 kJ/mol, respectively).

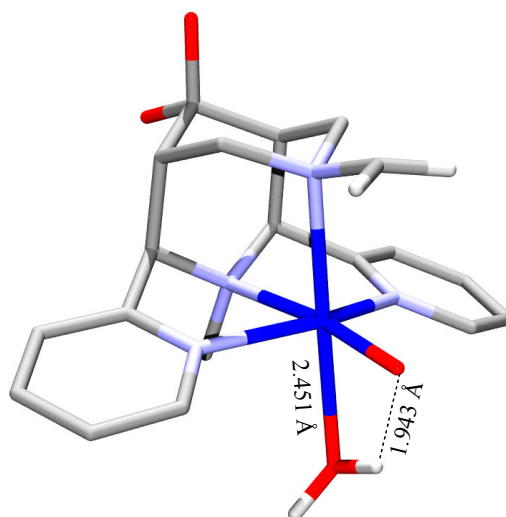


**Figure 7.29.** Optimized structure of hs cobalt(III)-oxo radical species (S=5/2)

The optimized geometry for the hs cobalt(III)-species with ferromagnetically coupled C-radical largely resembles to the other hs isomer. Direct formation of this species from cobalt(II)-hydroperoxo species is not allowed on the basis of symmetry rules. The energy for this reaction is 0.071 kJ/mol higher than for the formation of the S=3/2 hs isomer (the electron on the C-radical in spin-down state). This means that the hs cobalt(III) species has a S=3/2 ground state (as expected for antiferromagnetic coupling), and the coupling constant between the cobalt(III)-center and the carbon radical is negative ( $J = -5.96 \text{ cm}^{-1}$ ). This value indicates a relatively weak coupling, a possible reason being that the free electron is localized on the radical carbon.

#### 8.5.10.2. Conversion of Co(II)-hydroperoxo /H<sub>2</sub>O<sub>2</sub> species to Fenton products

In the previous subchapter different optimized transition state structures were presented. One of them (TS2) contained a cobalt(III)-species with an equatorial oxo unit, to which a hydroxyl radical is hydrogen bound (Figure 7.24). This hydroxyl radical can initiate C-H activation at the N7-methyl group, as presented in the QST3-optimized transition state structure TS1 (Figure 7.23), but the hydroxyl radical can also be removed from the cobalt(III)-oxo species (the N7-methyl unit remains intact). This latter reaction route corresponds to Fenton chemistry, yielding oxidized metal and hydroxyl radical.<sup>164</sup> Inspired by this, cobalt(III)-oxo and hydroxo species, considering both hs and ls states, were investigated in detail.

The optimized structures for the above species are presented in Figure 7.30.

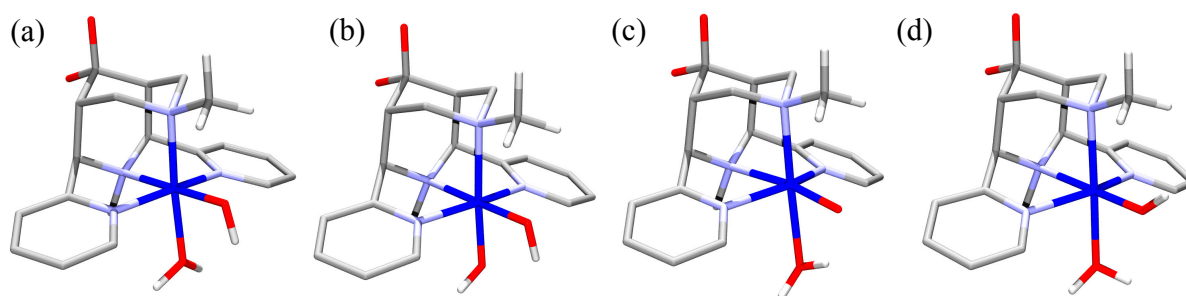


**Figure 7.30.** Optimized structure of (a) ls cobalt(III)-hydroxo species, (b) ls cobalt(III)-dihydroxo species, (c) hs cobalt(III)-oxo species, (d) hs cobalt(III)-hydroxo species

Similarly to the radical analogue, the ls cobalt(III)-oxo-aqua species is isomerized to the dihydroxo form. All structures correspond to true minima on the potential energy surface, indicated by their exclusively positive frequencies. Single point energies for these species and for hydroxyl radical were determined by using TZVPP (Co) / TZV (other atoms) basis set. Formation of a hs cobalt(III)-oxo species and a hydroxyl radical from cobalt(II)-hydroperoxo species is endothermic (+123 kJ/mol). In comparison, when the cobalt(II)-hydroperoxo species reacts to a hs cobalt(III)-oxo radical species and water, the reaction is somewhat less endothermic (+106 kJ/mol), thus thermodynamically more favourable. These reaction energies are relatively high. It is important to mention that the calculations were made in the gas phase, where the stabilization of species by solvation is not possible. It has been shown that hydration of a hydroxyl radical with 2 water molecules leads to around 100 kJ/mol stabilization.<sup>165</sup> Comparing the energies obtained for gas phase calculation, it emerges that TS1 structure which contains a hydroxyl radical H-bonded to a cobalt(III)-oxo unit, is 27 kJ/mol more stable than the separately optimized cobalt(III)-oxo species and a hydroxyl radical. A proper treatment of solvent effects is expected to stabilize the Fenton products (especially the hydroxyl radical). This must also be reflected in their overall energies, their formation from TS1 should be exothermic (without considering solvent effects was endothermic, +27 kJ/mol).

From TS1 there is a possibility of C-H activation by OH radical that can lead to TS2. This step is energetically demanding, the energy difference between the two transition states is +39 kJ/mol. This energy difference is larger than for the reaction producing the Fenton products (cobalt(III)-oxo species and hydroxyl radical) from TS1. This implies that a pure kinetic control would give exclusively the Fenton products. Due to the fact that experimentally a mixture of dealkylated and non-dealkylated species are observed as products of the reaction between cobalt(II) and H<sub>2</sub>O<sub>2</sub>, the role of both kinetic and thermodynamic control seems to be important.

In strong contrast to the cobalt(III)-hydroxo radical species, their analogues with intact N7-methyl group were optimized in both spin states as 6-coordinate cobalt-complexes. Formation of the hs cobalt(III)-hydroxo species from the cobalt(II)-hydrogen peroxide is highly endothermic (+119 kJ/mol), similarly to the analogous reaction step of the cobalt(II)-hydroperoxide route. Again, solvation of the released hydroxyl radical can lead to significantly smaller reaction energies. Conversion of the hs species to its ls form is an energetically favourable reaction (-28 kJ/mol). For comparison, 5-coordinate structures were also calculated, generating the starting structures from the 6-coordinate ones by removal of the axial water molecule.

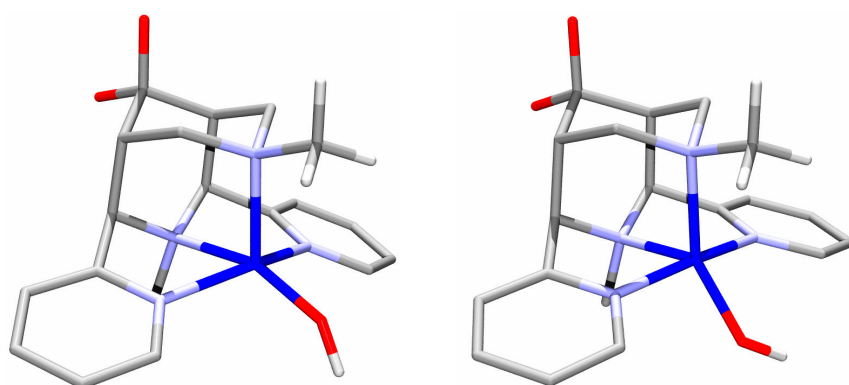


**Figure 7.31. Optimized structures of the 5-coordinate species: a.) hs cobalt(III)-hydroxo species; b.) ls cobalt(III)-hydroxo species**

Both the ls and hs cobalt(III)-hydroxo species are less stable in their 5-coordinate form, being 68 kJ/mol and 73 kJ/mol higher in energy than the corresponding 6-coordinate structures. This implies that in the cobalt(II)-hydrogen peroxide reaction pathway the formation of Fenton-products with 5-coordinate cobalt is thermodynamically less favoured. Although the cobalt(II)-hydrogen peroxide species was calculated to be 5-coordinate, the obtained results suggest that the re-coordination of the axial water is expected.

An overview of the energetics of each reaction step involving the optimized species is depicted in Figure 7.32.

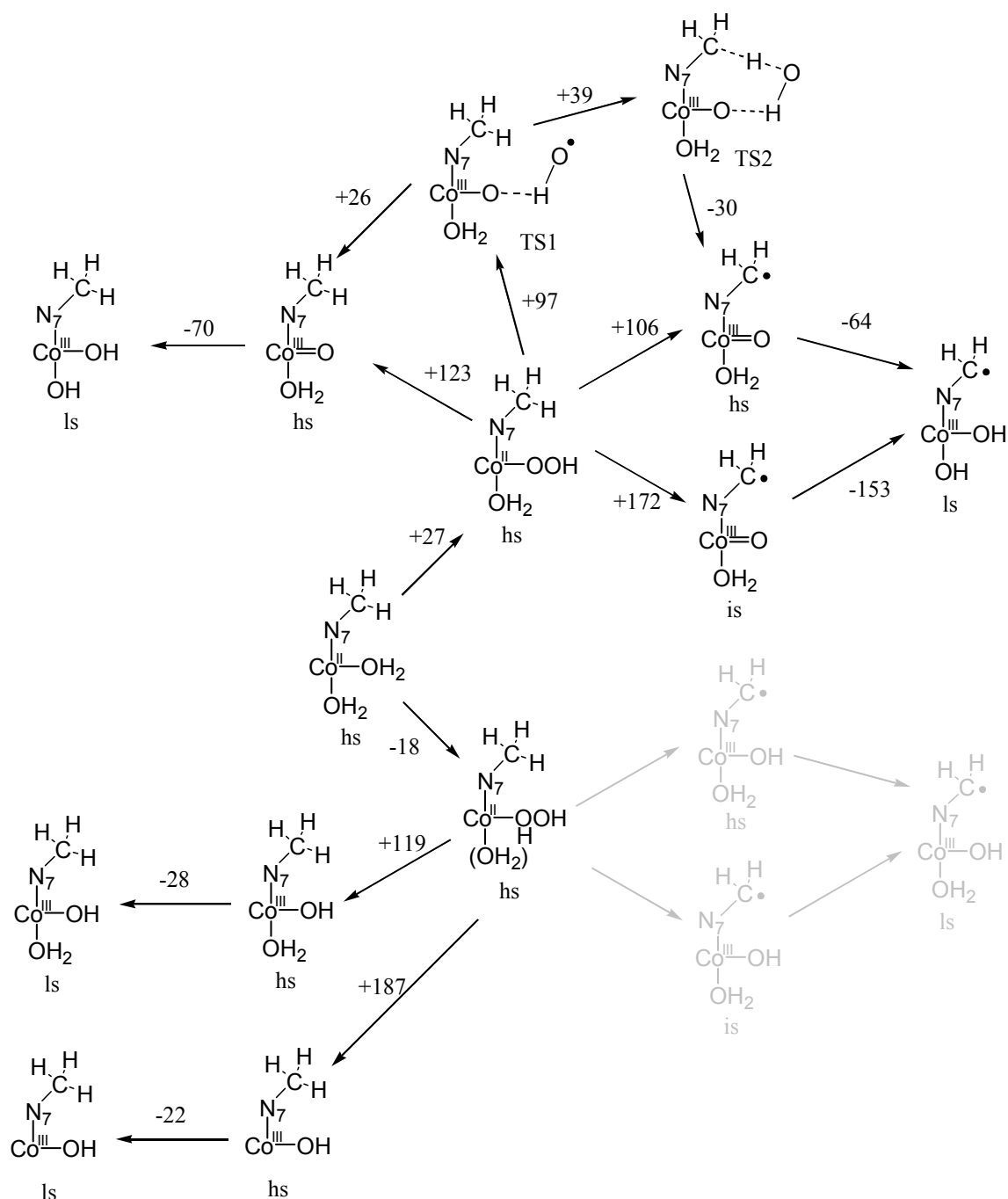


**Figure 7.32.** Overview on the optimized species and the energetics of the possible reaction routes. The grey species could not be successfully optimized

From the detailed discussion in this chapter, the following points should be highlighted:

1. Binding of hydroperoxide by the replacement of an equatorial water molecule is less favourable than substitution to hydrogen peroxide. Removal of the axial water molecule from the coordination sphere of cobalt(II) in the latter species leads to further stabilization, since the 6-coordinate hydrogen peroxide species is energetically less favourable than the optimized 5-coordinate structure.

2. The TS1 structure is already a “second generation” transition state, since not only the O-O bond is elongated but the hydrogen atom of the formed hydroxyl radical is H-bonded to the equatorial oxo oxygen: this H $\cdots$ O distance is shorter than the separation between the two oxygens.
3. If the reaction starting from the Co(II)-hydroperoxo species is thermodynamically controlled, it should follow the radical pathway leading to cobalt(III)-oxo radical species and water (Fenton route: +123 kJ/mol, cobalt(III)-radical reaction: +106 kJ/mol). However, if the reaction is kinetically controlled, the Fenton pathway is preferred: this required formation only of TS1, while the other route goes through a more energy demanding TS2 transition state.
4. A H-bonded hydroxyl radical seems to be stabilized (the O $\cdots$ H distances in TS1 and TS2 are very close), so if the hydroxyl radical is not removed from the environment of the bispidone complex, it “survives”. With a simple rotation of the Co-O $\cdots$ H-O torsion angle in TS1, the oxygen of the hydroxyl radical can approach the hydrogen of N7-methyl group and activate the C-H bond leading to TS2.
5. Conversion from a hs to a ls cobalt(III) species is an energetically favourable process, in both the Fenton- and the cobalt(III)-radical pathways.





## 8. Other metal-complexes of bispidone ligands

### 8.1. Other metal complexes of N2py2PhOH

#### 8.1.1. Synthesis and characterization of the complexes

Complexation of the N2py2PhOH ligand with other metal ions (mostly with transition metal ions: Ni<sup>II</sup>, Zn<sup>II</sup>, Cd<sup>II</sup>, Fe<sup>II</sup>, Pb<sup>II</sup>, Mn<sup>II</sup>, Mn<sup>III</sup>) was studied, and the isolated complexes were fully characterized and investigated by spectroscopic methods. All complexes were obtained from a methanolic solution with stoichiometric mixtures of the ligand and the corresponding metal salts.

The light blue [Ni<sup>II</sup>(N2py2PhO)]ClO<sub>4</sub> was prepared by the addition of 1 equivalent triethylamine base. The analytical data (elemental analysis, mass spectra) show that the phenolate unit is deprotonated in the complex. The very weak d-d band at 568 nm is typical for octahedral high-spin nickel(II) bispidone complexes.<sup>51</sup> The other two d-d bands are too weak or lie outside the recorded wavelength interval.

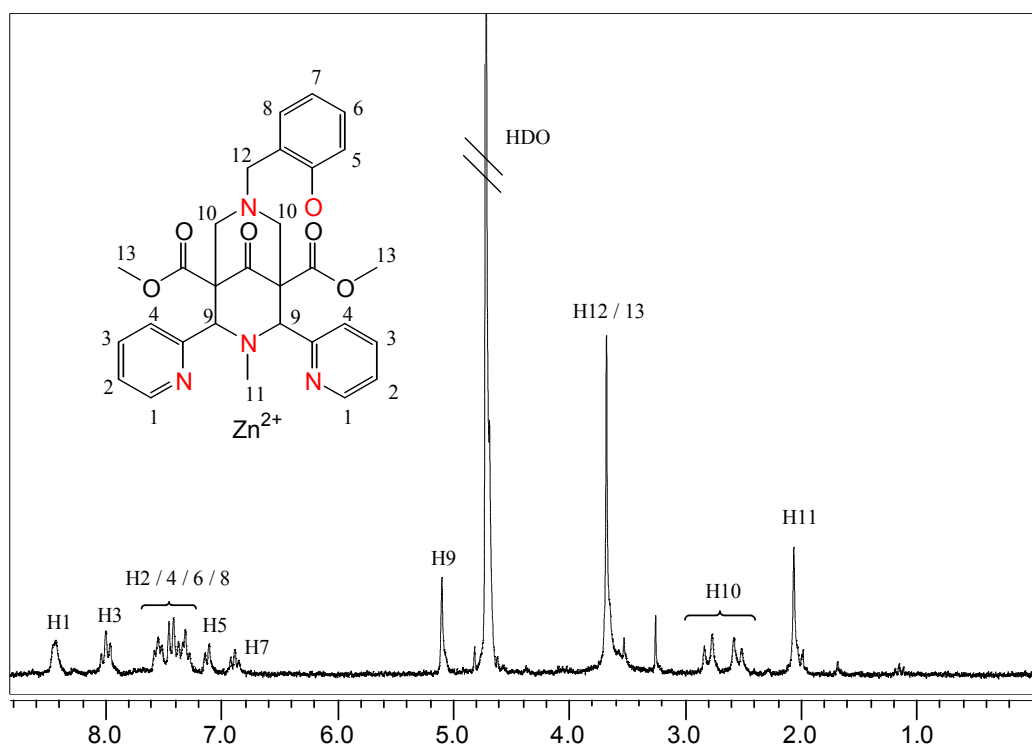


Figure 8.1. <sup>1</sup>H-NMR spectrum of [Zn<sup>II</sup>(N2py2PhO)]ClO<sub>4</sub> in D<sub>2</sub>O

Zinc(II) and cadmium(II) also form stable complexes with N2py2PhOH. Similarly to the above described case, the phenol group in [Zn<sup>II</sup>(N2py2PhO)(OH<sub>2</sub>)]ClO<sub>4</sub> and [Cd<sup>II</sup>(N2py2PhO)(OH<sub>2</sub>)]NO<sub>3</sub> is deprotonated and coordinates to the metal center (ESI-MS: 593.3 [Zn<sup>II</sup>(N2py2PhO)]<sup>+</sup>; 643.3 [Cd<sup>II</sup>(N2py2PhO)]<sup>+</sup>).

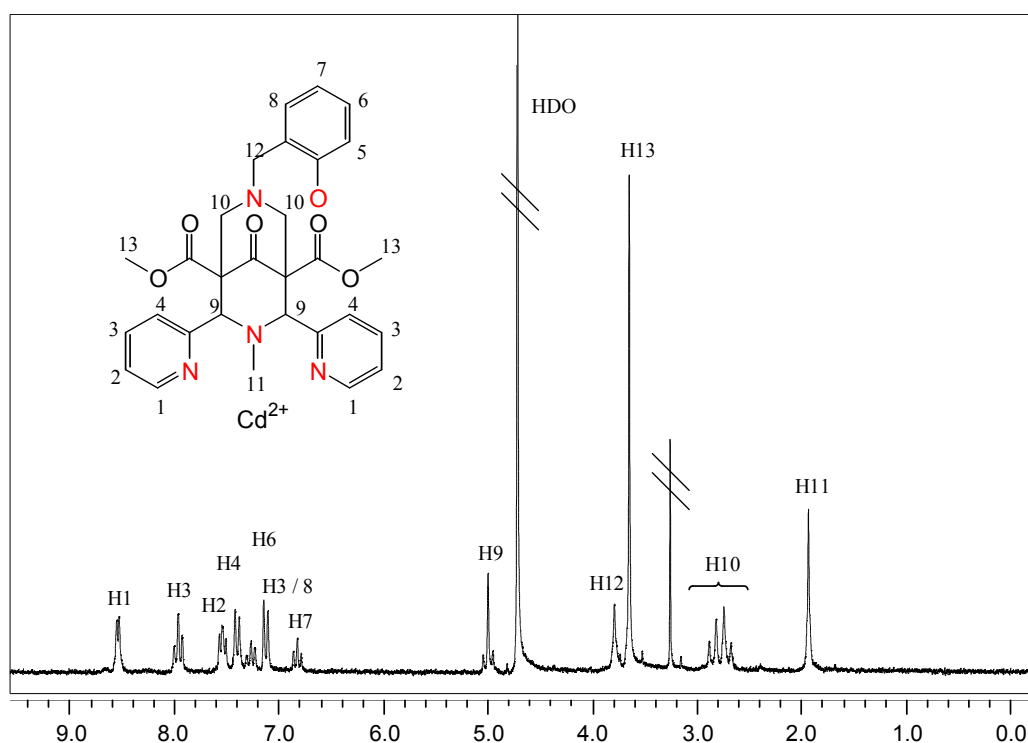


Figure 8.2.  $^1H$ -NMR spectrum of  $[Cd^{II}(N_2py_2PhO)]NO_3$  in  $D_2O$

In both cases the NMR spectra are well resolved, and the fact that only one set of peaks appears, indicates that the protons on each side of the metal center are chemically indistinguishable from each other. This is due to the high level of symmetry of the complex, with both pyridines coordinate to the metal center.

Complexation of lead(II)-acetate with  $N_2py_2PhOH$  leads to the formation of  $[Pb^{II}(N_2py_2PhOH)](OAc)_2$ , and deprotonation of the phenol unit does not take place. The removal of the phenolic proton would form acetic acid from the acetate counter anion, which is volatile enough to be eliminated from the solid by drying in vacuo, similarly to  $[Mn^{III}(N_2py_2PhO)(OAc)]OAc$  (see in this Chapter). The presence of two acetates in  $[Pb^{II}(N_2py_2PhOH)](OAc)_2$  was confirmed by elemental analysis, and  $^1H$ -NMR, where the acetate singlet was assigned to 6 protons, i.e. two acetate ions per complex (Figure 8.3). The coordination mode in this complex is different from the other complexes with this ligand: the appearance of the Bohlmann band in the IR spectrum indicates that the unpaired electrons of the amine nitrogens are not coordinated to lead(II). For steric reasons the lead(II)-ion does not match the hole size of the rigid bispidone ligand. Since the aromatic peaks in the  $^1H$ -NMR spectrum are shifted downfield when compared to the free ligand, the involvement of pyridines and the phenol group in coordination to lead(II) can be postulated.

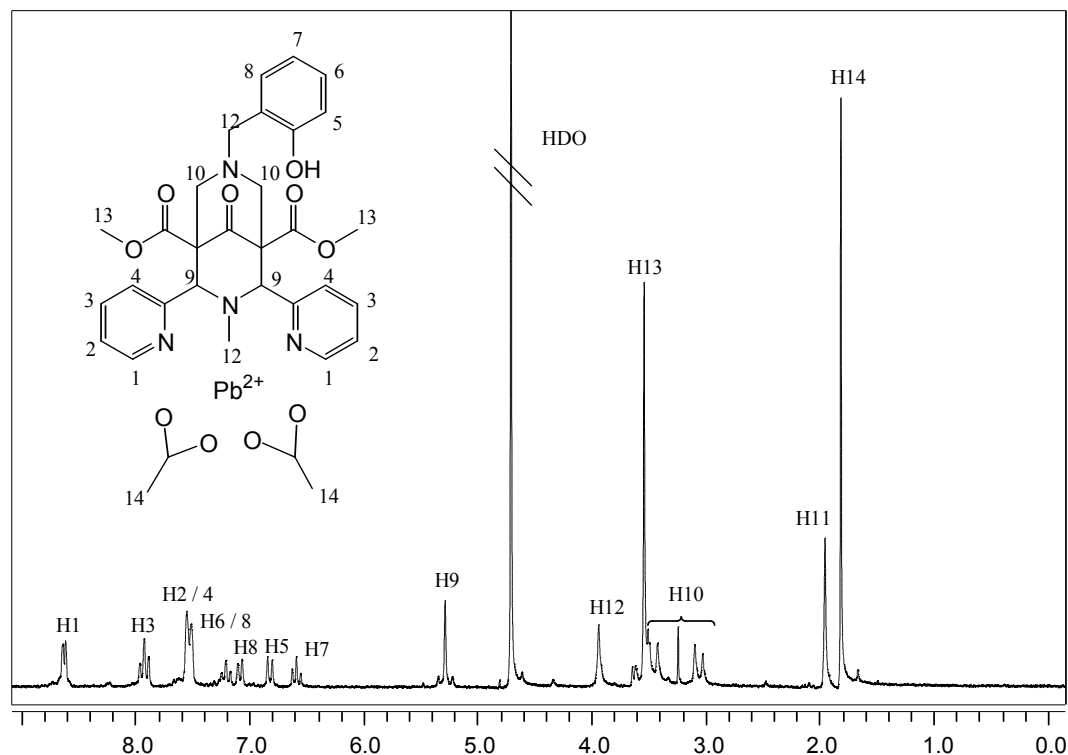
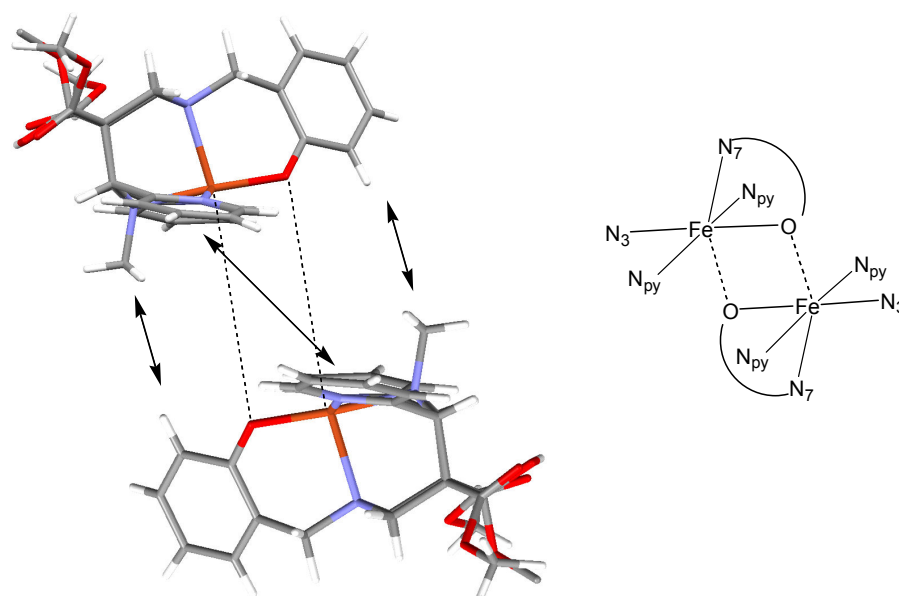


Figure 8.3.  $^1\text{H}$ -NMR spectrum of  $[\text{Pb}^{\text{II}}(\text{N}2\text{py}2\text{PhOH})](\text{OAc})_2$  in  $\text{D}_2\text{O}$

Iron(II) complexes of  $\text{N}2\text{py}2\text{PhOH}$  were synthesized in the presence and in the absence of organic base. The properties of the resulting complexes show a large variation:  $[\text{Fe}^{\text{II}}(\text{N}2\text{py}2\text{PhO})(\text{OH}_2)]\text{ClO}_4$ , which was synthesized by the addition of 1 equivalent of triethylamine, is a brown solid, and has an intense charge transfer band at 455 nm. The complex cation is +1 charged, as confirmed by ESI-MS, which indicates deprotonation and coordination of the phenolate to the iron(II) center.

The other complex, which was obtained without addition of base, is deep blue, and shows two intense bands in the UV-vis spectrum at 347 and 525 nm. The mass spectrum shows a mixture of +1 and +2 peaks, which can be explained by an incomplete deprotonation of the phenol unit (no external base was added), but may also imply a partial oxidation of the iron center to  $\text{Fe}^{\text{III}}$ . The latter interpretation is supported by the deep blue color of the compound, which is typical for mixed valent  $\text{Fe}^{\text{II}}/\text{Fe}^{\text{III}}$ -complexes with strong electronic/magnetic interaction between the metal centers of different oxidation state.<sup>135</sup> The question of how such an interaction is possible in our case, arises. Several examples for Fe-phenolate complexes are reported, which dimerize to form a diiron bis- $\mu$ -phenolato core.<sup>166-169</sup> Such a binding mode is also seen in Fe complexes with dinucleating bis-phenol macrocycles.<sup>170,171</sup> Through-bond communication between the iron centers in our complex, requires the presence of a charged bridging unit, the phenolate oxygen. Formation of this hypothetical dinuclear structure is a

serious drawback due to steric repulsion between the two bispidone ligands. In the case of sufficiently short Fe-O separations (to form a double bridged complex) the N3-methyl group in one molecule and the phenolic unit in the other one would be fairly close, which induces strong repulsion (Figure 8.4). Similarly, the pyridines in the two molecules can seriously hinder the formation of the diiron bis- $\mu$ -phenolato species. Considering only a single bridged binding mode (which still allows for interaction between the metal centers), the steric hindrance is again quite pronounced, so formation of such species is improbable.



**Figure 8.4.** Steric repulsions in the hypothetical double-bridged iron-bispidone dimer

The manganese(II) complex of N2py2PhOH was synthesized using  $\text{MnCl}_2$  as manganese source. Microanalytical data unambiguously prove that the phenolic oxygen in  $[\text{Mn}^{\text{II}}(\text{N}2\text{py}2\text{PhO})\text{Cl}]$  is deprotonated, which is the consequence of the addition of an equimolar amount of triethylamine to the reaction mixture. Interestingly, there are no charge transfer bands observed in the visible region of the UV spectrum. Probably these appear at higher energies, overlapped with other intense bands. The complex is soluble in solvents of varying polarity (from dichloromethane to ethanol), most probably because of the neutrality of  $[\text{Mn}^{\text{II}}(\text{N}2\text{py}2\text{PhO})\text{Cl}]$  species in which one chloride ion occupies the sixth coordination site the trans N7 position.

Manganese(III) complexes of N2py2PhOH and vanilbis were obtained directly from a trivalent manganese source, since attempts for the quantitative oxidation of manganese(II)

complexes, or to oxidize manganese(II) *in situ* (in presence of ligands), were unsuccessful. It has been described in this Chapter that manganese(II) complexes of bispidone ligands with an N<sub>4</sub> or N<sub>5</sub> donor set could not be oxidized by the addition of hydrogen peroxide. To obtain manganese(III) complexes with the above ligands, solid Mn(OAc)<sub>3</sub> was used as manganese source, the unreacted insoluble excess salt was removed, and complexes were isolated from the filtrate. This procedure is common in the synthesis of manganese(III)-complexes.<sup>172-174</sup> Mn<sup>III</sup>-N2py2PhOH and -vanilbis complexes were completely characterized. Microanalytical data showed that the phenol unit in both complexes is deprotonated. The elemental composition values correspond to a structure containing only two acetate anions, with the third negative charge coming from the phenolate. The UV-vis spectrum of [Mn<sup>III</sup>(N2py2PhO)(OAc)]OAc showed an intense charge transfer band appearing as shoulder around 440 nm. In manganese(III) complexes of bispidone ligands, containing N<sub>4</sub> or N<sub>5</sub> donor set, this intense shoulder in the UV-vis spectrum is missing. Since in these cases the manganese(III) source was the manganese(III) acetate salt, the intense shoulder in [Mn<sup>III</sup>(N2py2PhO)(OAc)]OAc cannot be related to the effect of coordinating acetate. If the phenolate unit was not involved in metal binding, the N2pyPhOH ligand would coordinate only with 4 nitrogen donors, and formally very similar UV-vis spectrum to manganese(III)-complexes with N<sub>4</sub> or N<sub>5</sub> donor sets, would be expected. Since this is not the case, the charge-transfer band is most probably a consequence of the phenolate moiety coordinated to the central manganese(III)-ion.

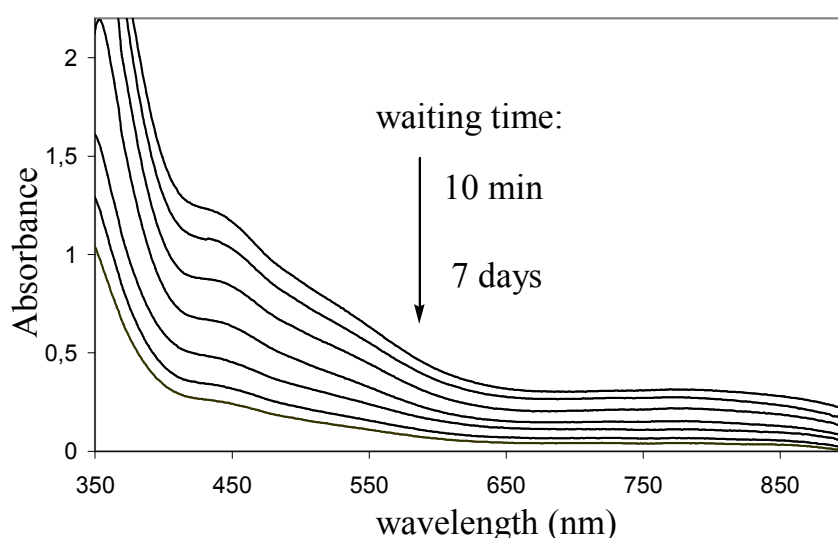


**Figure 8.6.** Time-dependent UV-vis spectra of 1.35 mM [Mn<sup>III</sup>(N2py2PhO)(OAc)]ClO<sub>4</sub> in methanol

[Mn<sup>III</sup>(N2py2PhO)(OAc)]ClO<sub>4</sub> is decomposed in methanol, as it was indicated by the time dependent UV measurements (Figure 8.6). The freshly prepared sample (of 1.0 mg/mL (1.35

mM) concentration) showed a shoulder charge-transfer peak around 440 nm, and a broad d-d band centered around 770 nm, but within a 1 week time-interval the intensity of both falls drastically and the d-d band practically disappears. For the manganese(III) complex of an analogous ligand (with pyridine, phenolate and aliphatic amine donor groups) similar decomposition was observed, and their isolated product was the manganese(II) complex of the oxidized ligand,<sup>175</sup> so that formally, an intramolecular redox process took place. In this example the central manganese(III) oxidized a secondary amine of the ligand to an imine (Figure 8.7). In case of bispidones such a scenario is not possible, since all the aliphatic nitrogen donors are tertiary amines, where hydrogen abstraction cannot occur.

Another possibility is that the changes in the UV-vis spectra are due to the removal of the phenolate from the coordination sphere of manganese(III). This would correspond to structural isomerism during the redox reaction. However, a Mn(III)-O bond with pronounced charge-transfer character is thermodynamically highly favored and represents a typical example of a hard-hard interaction (using the categories of Pearson's HSAB concept). To break a bond with a such strong ionic character would require a high activation. Without the addition of an external oxidant, this seems highly unlikely to be the case.

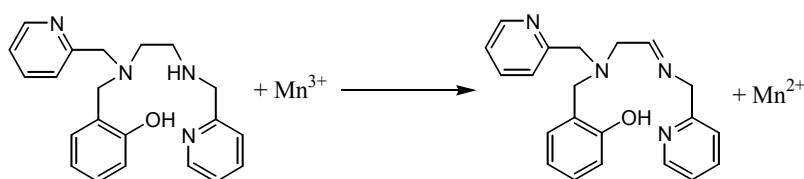


**Figure 8.7. Intramolecular redox reaction in a reported Mn(III)-complex<sup>175</sup>**

The addition of 2,4-dinitrophenylhydrazine to the methanolic solution of  $[\text{Mn}^{\text{III}}(\text{N}2\text{py}2\text{PhO})(\text{OAc})]\text{ClO}_4$  did not lead to the formation of any precipitate. This hydrazine reagent is used as qualitative test for compounds containing keto group (see Chapter 7 for details). This strongly indicates that the methanol solvent was not oxidized to formaldehyde and is therefore not involved in the reduction of manganese(III). Interestingly, a similar decay of the absorbance values was observed when  $[\text{Mn}^{\text{III}}(\text{N}2\text{py}2\text{PhO})(\text{OAc})]\text{ClO}_4$  was dissolved in water or acetonitrile.

Solution mass spectroscopic analysis was carried out *in situ*, to investigate if the N2py2PhOH ligand is involved in an intramolecular redox process. ESI-MS spectra recorded after a reaction time of 1 week, (when UV-vis spectra indicated an almost complete conversion), showed only peaks assignable to species containing the original deprotonated ligand (584.7  $[\text{Mn}^{\text{II}}(\text{N}2\text{py}2\text{PhO})]^+$ ; 602.6  $[\text{Mn}^{\text{II}}(\text{N}2\text{py}2\text{PhO})(\text{OH}_2)]^+$ ). This result indicates that the time-

dependent color change of  $\text{Mn}^{\text{III}}\text{-N2py2PhOH}$  complex is not related to any transformation in the ligand structure.

### 8.1.2. Oxidation of $\text{Fe}^{\text{II}}$ - and $\text{Mn}^{\text{II}}$ - $\text{N2py2PhOH}$ complexes with $\text{H}_2\text{O}_2$

$[\text{Fe}^{\text{II}}(\text{N2py2PhO})(\text{OH}_2)]\text{ClO}_4$  reacts immediately with the added peroxide at room temperature, the band at 525 nm is shifted to lower energy ( $\lambda_{\text{max}} = 595$  nm) and the shoulder centered at 347 nm disappears (Figure 8.8). The formed species decays within 30 minutes. Interestingly the reaction is completely quenched at  $-40^\circ\text{C}$ , no change in the UV-spectra is observed. This may be due to kinetic reasons: the activation barrier is high enough to freeze the reaction at  $-40^\circ\text{C}$ . ESI-MS spectra show the same type of signals, before and after the addition of hydrogen peroxide. The originally 1 : 1 ratio between species containing  $\text{Fe}^{2+}$  and  $\text{Fe}^{3+}$  (main peaks: 617.1  $[\text{Fe}^{\text{II}}(\text{N2py2PhO})(\text{MeOH})]^+$ , 648.4  $[\text{Fe}^{\text{III}}(\text{N2py2PhO})(\text{OMe})(\text{MeOH})]^+$ ) is changed. A decrease in intensities from signals of iron(II) and an increase for peaks with trivalent iron was observed, indicating oxidation of the metal center. The ESI-MS spectrum recorded directly after the addition of hydrogen peroxide, did not show any new peaks (in comparison with the one recorded before the addition of the oxidant), although the time-dependent UV-vis spectra undoubtedly indicated formation of an intermediate species.

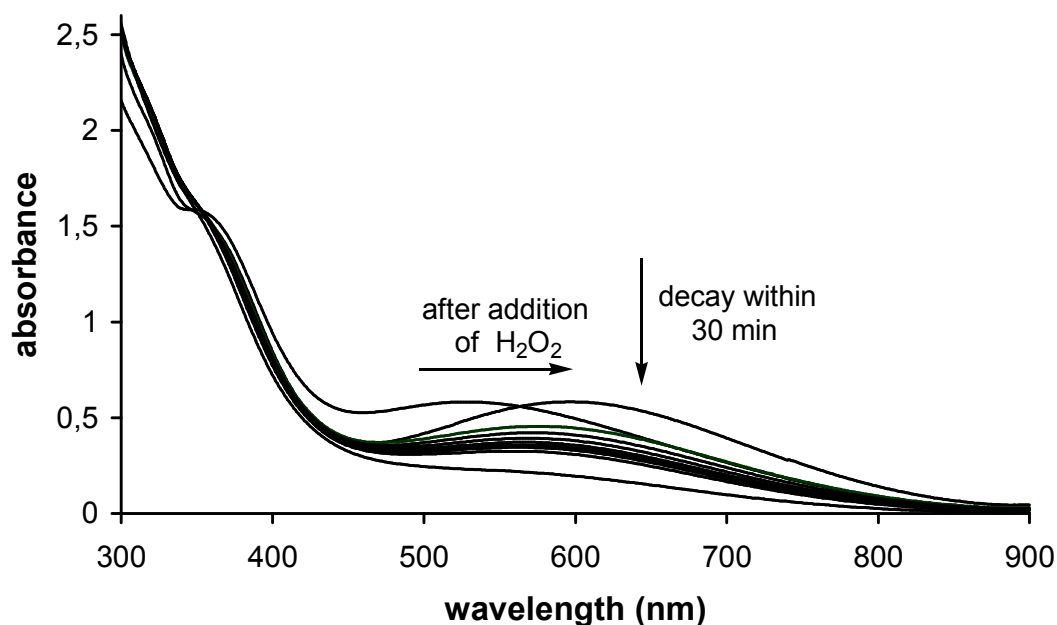
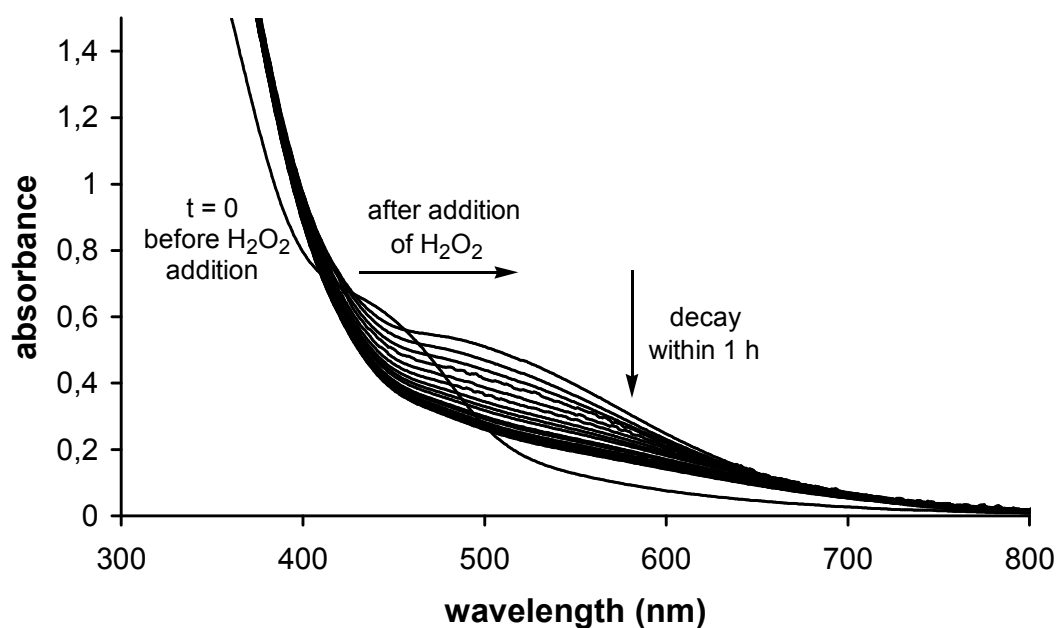


Figure 8.8. Time dependent UV-vis spectra of 0.58 mM  $[\text{Fe}^{\text{II}}(\text{N2py2PhO})(\text{OH}_2)]\text{ClO}_4$  (prepared in the absence of base), with 40 eq of  $\text{H}_2\text{O}_2$  in methanol. Spectra were in 3 minutes intervals

A very similar phenomenon was observed when hydrogen peroxide was added to the other iron(II)-phenolate complex (which was prepared in the presence of equimolar triethylamine

base). The shoulder at 455 nm is shifted to lower energies (shoulder centered at 485 nm), immediately after the addition of  $\text{H}_2\text{O}_2$ , and the intensity of this new shoulder decreased with time. Moreover, after a 1 h reaction time the shoulder almost completely disappeared (Figure 8.9). In analogy to the iron(II) complex described above, there was no intermediate formation observed at  $-40^\circ\text{C}$  in methanol. ESI-MS spectra could not provide any evidence for the intermediate species: spectra recorded before and after the addition of hydrogen peroxide were practically identical.



**Figure 8.9.** Time dependent UV-vis spectra of 1.16 mM  $[\text{Fe}^{\text{II}}(\text{N}_2\text{py}_2\text{PhO})(\text{OH}_2)]\text{ClO}_4$  (prepared in the presence of equimolar of base) in presence of 40 eq  $\text{H}_2\text{O}_2$  in methanol. Spectra were recorded in 3 minutes intervals

In methanol, the colorless  $[\text{Mn}^{\text{II}}(\text{N}_2\text{py}_2\text{PhO})\text{Cl}]$  turns brown after addition of  $\text{H}_2\text{O}_2$ , which indicates oxidation of the divalent manganese center. As will be discussed in this Chapter, manganese(II) complexes with bispidone ligands with only N-donors are completely inactive and show no reaction with hydrogen peroxide. Therefore, this is the first example of a successful chemical oxidation of a manganese(II) center in a bispidone complex. Interestingly the oxidized species is rather unstable. The methanolic solution of the brown manganese(III) complex becomes colorless within 2 days at room temperature, indicating that the originally oxidized manganese center is reduced back to the divalent state (Figure 8.5).



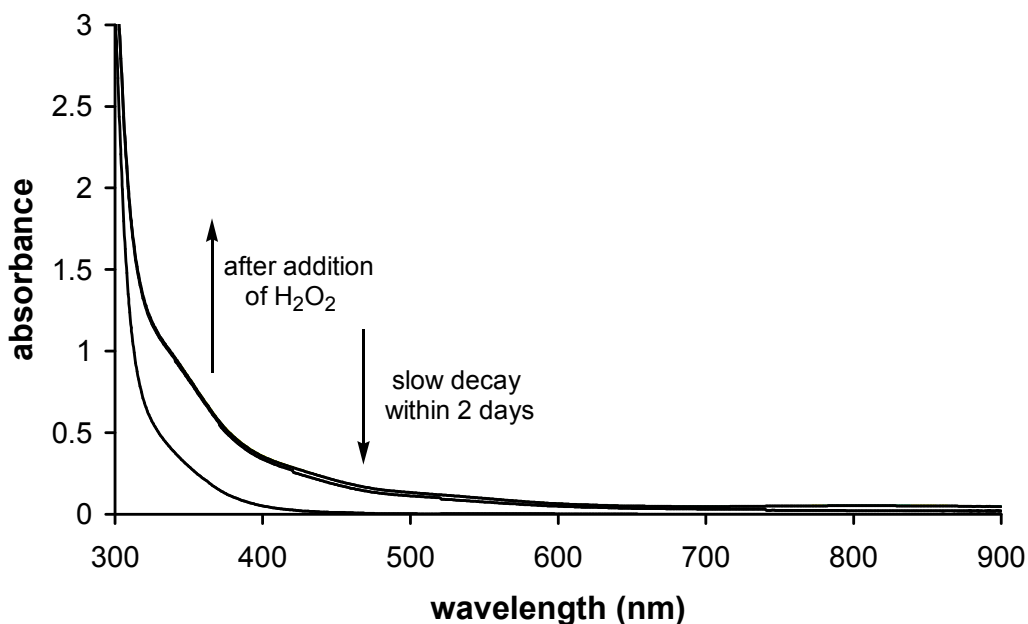


Figure 8.5. Effect of the addition of 40 eq of  $\text{H}_2\text{O}_2$  to the methanolic solution of 2.85 mM  $[\text{Mn}^{\text{II}}(\text{N}2\text{py}2\text{PhO})\text{Cl}]$

This behavior is analogous to that of the *in situ* prepared manganese(III) complex of  $\text{N}2\text{py}2\text{PhOH}$  (see below for details). The ESI-MS spectrum of the methanolic solution of  $[\text{Mn}^{\text{II}}(\text{N}2\text{py}2\text{PhO})\text{Cl}]$ , recorded 2 hours after the addition of hydrogen peroxide, showed two new peaks at 636.3 and 650.3, which were not present in the spectrum measured before the addition of the oxidant. Judging from the isotopic patterns, both complexes contain one chloride and could be assigned as  $[\text{Mn}^{\text{III}}(\text{N}2\text{py}2\text{PhO})(\text{Cl})(\text{OH}_2)]^+$  and  $[\text{Mn}^{\text{III}}(\text{N}2\text{py}2\text{PhO})(\text{Cl})(\text{MeOH})]^+$ , respectively.

## 8.2. Manganese complexes of other bispidone ligands

### 8.2.1. Synthesis and oxidation of manganese(II) complexes with $N_4$ and $N_5$ bispidone ligands

*Introduction:* It has been known for more than 100 years that a system containing  $\text{Fe}(\text{II})$  and  $\text{H}_2\text{O}_2$  is able to oxidize organic substrates.<sup>176</sup> This observation opened up a new strategy in developing efficient oxidation catalysts. The so called Fenton-chemistry has become of great interest and has been extensively investigated, both from a catalytic and a mechanistic point of view.<sup>177</sup> Iron(II) complexes of various ligand systems have been tested in this reaction, and the importance of a free-coordination site around the metal has been underlined.

Recently some highly active oxidation catalysts, using in situ prepared manganese(III)<sup>178</sup> or Mn(IV) complexes<sup>117</sup> in presence of H<sub>2</sub>O<sub>2</sub>, have been reported. These complexes have the ability to catalyze the epoxidation of olefins,<sup>40</sup> and oxidation of alcohols to aldehyde,<sup>179</sup> with high efficiency.

Iron(II) complexes of some rigid bispidine ligands have been demonstrated to be highly active catalysts in the oxidation of olefins.<sup>34</sup> From this the question arises, whether active oxidative catalysts can be obtained by forming bispidone complexes with metals other than iron. Inspired by the above mentioned results of Feringa's group, manganese-bispidine / H<sub>2</sub>O<sub>2</sub> systems were investigated in order to clarify whether there is an analogy to Fenton-chemistry with manganese.

*Synthesis of the complexes:* The synthesis of the manganese(II) complexes of N2py2, N2py3o, 6MeN2py2 and N2Im2 was carried out in two steps. First, the dichloro complex was obtained by treatment of the ligands with an equivalent of MnCl<sub>2</sub>. Since the free coordination site around the metal is supposed to play an important role in the oxidation catalysis, the strongly coordinating chloride anion was removed by the addition of silver-triflate in dry acetonitrile.

*Cyclic voltammetry:* By the replacement of chlorides with non-coordinating anions, half-wave potentials with more positive values were expected due to the lack of a charge transfer effect. A more positive value implies the stabilization of the reduced form, in this case manganese(II). Oxidation of a manganese(II) complex with a weakly coordinating neutral co-ligand was therefore expected to be rather challenging. However, the presence of a free coordination site around the central manganese ion is imperative for the oxidation with H<sub>2</sub>O<sub>2</sub>, as the oxidant has to be in contact with the central metal. Half-wave potentials were difficult to determine, since no real signals appeared. Another reason for the synthesis of manganese(III)-complexes was therefore to obtain reliable voltammograms, from which the redox potentials can be determined. In contrast to our expectations, however, this was not the case.

*Experiments with H<sub>2</sub>O<sub>2</sub>:* It has been reported that the reaction between iron(II) bispidone complexes and hydrogen peroxide leads to the formation of iron(III)-hydroperoxo species, which could be trapped at -40°C and analyzed spectroscopically.<sup>141</sup> Analogous reactions with manganese(II) complexes were carried out at -40°C, but no color change was observed. Moreover, increasing the temperature did not lead to any colored products, although the expected higher-valent manganese complexes were thought to be brown. From this, it can be

concluded that oxidation of manganese(II) bispidone complexes with  $\text{H}_2\text{O}_2$  was not occurring. Oxidants other than  $\text{H}_2\text{O}_2$  have also been tried ( $^t\text{BuOOH}$ ,  $\text{KMnO}_4$  among others), but all attempts failed.<sup>180</sup>

*Discussion:* Structural investigation of first row transition metal complexes with a rigid tetradentate bispidine ligand have shown that these metals fit well into the ligand cavity.<sup>6</sup> This was further confirmed by hole size calculations, which indicated that the coordination sphere of complexes of such ligands is elastic, and allows for their complexation with a wide range of divalent first-row transition metal ions of different size.<sup>51</sup> From the point of view of the ligands (taking only steric effects into consideration) coordination of the metal ions leads only to very small energy changes.<sup>51</sup> Oxidation of coordinated manganese to its trivalent form results in a significant compression of the central metal ion. This compression has to be reflected in the metal-donor distances, which are expectedly shorter than in the complex with manganese(II). Such shortening induces a serious strain in the ligand, as can be seen from the hole-size curves. It has been shown that, if the oxidized form is not only thermodynamically but also kinetically highly stable (e.g. oxidation of cobalt(II) to cobalt(III)), then the induced strain can be overcompensated by the high stability and inertness.<sup>51</sup> In the case of manganese, the paramagnetic  $d^5$  manganese(II) ion is oxidized to a similarly paramagnetic, kinetically labile and thermodynamically less stable manganese(III)  $d^4$  system. Here there is no extra support for the overcompensation of the strain in the ligand structure. Moreover, manganese(III) has more a hard character in terms of the HSAB theory, which means that coordination to a ligand containing only N-donors (which are relatively soft) is more disfavoured, from the view of electronics, when compared to cobalt(III). Considering the other effect, namely the induced strain in the ligand cavity, one can conclude that not only electronically, but also sterically, there is no stabilization of a complex with the oxidized central manganese.

A further point is that manganese(III) complexes are known to be strong oxidants, even the simple manganese(III) acetate salt is widely used as oxidative catalyst in the organic synthetic work.<sup>181</sup> It may be considered that, if any manganese(III) bispidone-complex is produced due to the oxidation of manganese(II) complexes with  $\text{H}_2\text{O}_2$ , the small amount of formed manganese(III) can simply decompose  $\text{H}_2\text{O}_2$ , so that there is no more oxidant available. Therefore, a possible catalase activity of manganese(III) complexes may be expected.

To ascertain whether the oxidized manganese(III) complexes are stable enough, these were prepared separately *in situ*. Manganese(III) acetate was used as metal source and was added

directly in an equimolar amount as a solid to the methanolic solution of the ligands. The formed complexes were stable, due to the acetate co-ligand, which electronically stabilizes the trivalent form of manganese by means of the electrostatic interaction induced by the negatively charged acetate. Characterization of the freshly prepared solids unambiguously showed the presence of manganese(III) (such a species is EPR silent, the typical pattern of manganese(II) was not seen in any of the cases). Storage of the solid samples for months results in faded colors and the UV-spectra confirmed that the manganese(III) content of the complexes became significantly smaller, most probably due to the reduction of the metal center to manganese(II).

It seems that the stabilization of the higher oxidation state of manganese in a bispidone complex, requires careful selection of donors. Indeed, when using a ligand containing a phenolate arm (N2py2PhOH), the lifetime of the oxidized manganese(III) species is much longer and its decomposition can be easily followed by UV-vis spectroscopy. As will be shown later in this Chapter, this phenomenon is observed not only for the oxidized manganese(II) complex but also for the in situ prepared manganese(III) complex.

*Crystal structures of [Mn<sup>II</sup>(N2py3o)Cl]Cl and [Mn<sup>II</sup>(6MeN2py2)Cl<sub>2</sub>]*

Selected bond distances, angles and torsions in the structures of [Mn<sup>II</sup>(N2py3o)Cl]Cl and [Mn<sup>II</sup>(6MeN2py2)Cl<sub>2</sub>] are tabulated in Table 8.1, along with the corresponding parameters of the known [Mn<sup>II</sup>(N2py2)Cl<sub>2</sub>] complex.

**Table 8.1 Selected bond distances and angles of [Mn<sup>II</sup>(N2py3o)Cl]Cl and [Mn<sup>II</sup>(6MeN2py2)Cl<sub>2</sub>]**

	[Mn <sup>II</sup> (N2py3o)Cl]Cl	[Mn <sup>II</sup> (6MeN2py2)Cl <sub>2</sub> ]	[Mn <sup>II</sup> (N2py2)Cl <sub>2</sub> ] <sup>182</sup>
Mn-Cl(eq)	-	2.4135(5) Å	2.404(2) Å
Mn-Cl(ax)	2.3914(6) Å	2.4864(5) Å	2.462(2) Å
Mn-N3	2.2829(17) Å	2.3337(15) Å	2.388(4) Å
Mn-N7	2.4154(18) Å	2.4491(15) Å	2.531(4) Å
Mn-Npy1	2.2714(18) Å	2.3555(15) Å	2.231(4) Å
Mn-Npy2	2.2622(17) Å	2.3652(15) Å	2.255(4) Å
Mn-Npy3	2.1910(17) Å	-	-
Npy1-Npy2	4.350 Å	4.490 Å	4.271 Å
N3-N7	2.943 Å	2.955 Å	2.961 Å
Npy1-Mn-Npy2	147.25(6) <sup>o</sup>	144.00(5) <sup>o</sup>	144.4(1) <sup>o</sup>
N3-Mn-N7	77.51(6) <sup>o</sup>	76.29(5) <sup>o</sup>	74.0(1) <sup>o</sup>
C1-C2-C <sub>ar</sub> -Npy1	-85.41 <sup>o</sup>	-85.25 <sup>o</sup>	-84.68 <sup>o</sup>
C4-C5-C <sub>ar</sub> -Npy2	86.86 <sup>o</sup>	86.76 <sup>o</sup>	90.48 <sup>o</sup>

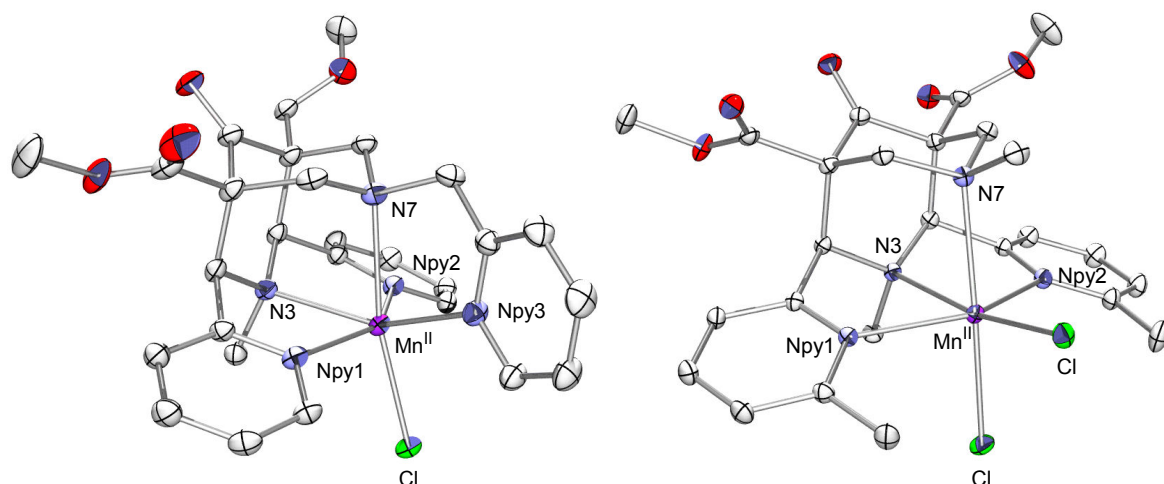


**Figure 8.10.** Crystal structures of  $[\text{Mn}^{\text{II}}(\text{N}2\text{py}3\text{o})\text{Cl}]\text{Cl}$  and  $[\text{Mn}^{\text{II}}(6\text{MeN}2\text{py}2)\text{Cl}_2]$

Due to the steric hindrance of the  $\alpha$ -methyl group on the pyridine donor in  $[\text{Mn}^{\text{II}}(6\text{MeN}2\text{py}2)\text{Cl}_2]$ , the distance between the pyridine nitrogens and the central manganese is more than 0.1 Å larger than in an analogous complex with the  $\text{N}2\text{py}2$  ligand, in which no methyl group is substituted to the pyridines.

This hindrance does not seem to have an effect on the coordination of chlorides. The Mn-Cl bond lengths are very similar to the values measured for the  $\text{N}2\text{py}2$  complex. As a counterbalance of the bond elongation of the Mn-pyridine bonds in the equatorial plane, the distance between Mn and the aliphatic amino nitrogens is smaller by 0.09 Å for the axial Mn-N7 bond and by 0.05 Å for equatorial Mn-N3.

The Mn-Cl bond length in  $[\text{Mn}^{\text{II}}(\text{N}2\text{py}3\text{o})\text{Cl}]\text{Cl}$  is significantly smaller than the corresponding bond length in the other two structures, which is probably due to the difference in the number of the coordinating chloride ions. The two chlorides in the Mn(II) complexes with the tetradentate bispidone ligands can transfer more electron density to the central Mn(II).

The Mn-N3 bond in  $[\text{Mn}^{\text{II}}(\text{N}2\text{py}3\text{o})\text{Cl}]\text{Cl}$  is also shorter, due to the lack of a trans effect, since not a chloride, but a picolyl group is ligated in trans to N3 position.

Again due to the less pronounced trans effect, the cavity size here is smaller ( $d(\text{N}3\cdots\text{N}7) = 2.943$  Å) than for manganese(II) complexes with tetradentate ligands ( $d(\text{N}3\cdots\text{N}7) = 2.955$  Å for  $[\text{Mn}^{\text{II}}(6\text{MeN}2\text{py}2)\text{Cl}_2]$ ), but this size is still larger than in the free ligand. It has been demonstrated from hole size calculations that the coordination sphere around the central metal in bispidone complexes is very elastic, binding metal ions within a large range of sizes causes only minimal strain in the cavity, when considering only the steric effects of the ligands.<sup>7</sup> Interestingly, in both structures the keto form appears, and no acetal or half-acetal is formed. It has been reported that the keto groups in the “cap” leads to a reduction in the basicity of the

amines (especially that of N7), as a result of inductive effects.<sup>6</sup> It was also highlighted that a less basic amine donor forms longer Mn-N<sub>amine</sub> bonds. However, both in [Mn<sup>II</sup>(N2py3o)Cl]Cl and [Mn<sup>II</sup>(6MeN2py2)Cl<sub>2</sub>], where the keto group in the cap is not hydrolyzed, significantly shorter Mn-N7 bonds were found than in [Mn<sup>II</sup>(N2py2)Cl<sub>2</sub>]. In case of the complex with the pentadentate ligand N2py3o, the shorter Mn-N7 distance can be explained by the geometric constraint of the attached picolyl group which coordinates in trans to N3 position.

### 8.2.2. Manganese(III) complexes of *crebis* and *tBuBis*

The dimanganese(III) complexes were prepared in a similar manner to the corresponding N2pyPhOH complex.

For *crebis*, elemental analysis confirmed the expected dinuclear structure, and the IR spectrum showed a strong resemblance to that of the [Mn<sup>III</sup>(N2py2PhO)(OAc)]OAc complex. The typical mononuclear manganese(II) pattern observed in the EPR spectrum indicates that similarly to the [Mn<sup>III</sup>(N2py2PhO)(OAc)]OAc complex, the central metal(s) are partially reduced to the divalent form, and the reduced manganese(II) centers are practically independent and do not interact with each other.

For *tBuBis*, problems with the assignment of the mass spectra and with the interpretation of the microanalytical data occurred (similarly to the copper(II)-complex of *tBuBis*, see Chapter 5 for details). Peaks assignable to Fragment<sub>1</sub> containing species appeared in the ESI-MS spectrum, both as +1 and as +2 positively charged peaks. Fragment<sub>1</sub> can be formally derived by the cleavage of the bond between N7 and the bridging methylene carbon (Figure 4.9).

In contrast to the case of the copper(II) complex, species with the cyclic dimer (Figure 4.10) were not observed, but others which can be best described as dimanganese complexes with the original *tBuBis* ligand, were seen.

Elemental analysis data can be fitted to both a dimanganese–([2+2] cyclic dimer) complex or as a mononuclear Fragment<sub>1</sub>-type complex. Similarly to the copper(II) complex of this ligand, treatment with Sephadex ion-exchange column proved the homogeneity of the substance. In this case it is difficult to provide further unambiguous proof for a mono- or dinuclear structure. Manganese(III) is expected to be EPR silent and, as it was seen for the Mn<sub>2</sub>*crebis* complex, the partially reduced manganese(II) appears in a mononuclear fashion, showing no interaction between the metal centers. EPR spectra recorded for a dinuclear manganese complex with non-interacting metal centers and for a mononuclear complex are therefore practically indistinguishable.

## 9. Experimental section

### 9.1. General

Commercially available chemicals were used without further purification. Solvents of technical quality were distilled before use.  $\text{H}_2^{18}\text{O}_2$  (90%  $^{18}\text{O}$  enriched, 2% solution in  $\text{H}_2^{16}\text{O}$ ) was obtained from ICON Services (19 Ox Bow Lane; Summit, NJ 07901 USA).

$\text{Npy}_2$ ,<sup>45</sup>  $\text{N}_2\text{py}_2$ ,<sup>52</sup>  $\text{N}_2\text{py}_3\text{o}$ ,<sup>183</sup>  $\text{N}_2\text{Im}_2$ ,<sup>59</sup>  $6\text{MeN}_2\text{py}_2$ ,<sup>50</sup>  $\text{N}_2\text{py}_2\text{PhOH}$ <sup>183</sup> were synthesized according to literature procedures.

Ligand precursors O-benzyl salicylaldehyde,<sup>61</sup> 6-formyl-2,4-di-tert-butylphenol,<sup>62</sup> O-benzyl-6-formyl-2,4-di-tert-butylphenol,<sup>63</sup> o-vanillin-aldoxime,<sup>53</sup> 2,6-bis(aminomethyl)-4-methylphenol monohydrochloride,<sup>64</sup> N-hydroxymethyl chloroacetamide<sup>58</sup> were prepared using known procedures.

All successfully obtained intermediates of *N2PhO2r* were synthesized according to the literature.<sup>59</sup>

The complexes  $[\text{Mn}^{\text{II}}(\text{N}_2\text{py}_2)(\text{Cl})_2] \cdot 2 \text{H}_2\text{O}$ ,<sup>180</sup>  $[\text{Mn}^{\text{II}}(\text{N}_2\text{py}_2)(\text{OH}_2)_2](\text{O}_3\text{SCF}_3)_2 \cdot 2 \text{H}_2\text{O}$ ,<sup>180</sup>  $[\text{V}^{\text{IV}}=\text{O}(\text{N}_2\text{py}_3\text{o})](\text{ClO}_4)_2 \cdot 3 \text{H}_2\text{O}$ ,<sup>7</sup>  $[\text{V}^{\text{V}}=\text{O}(\text{O}_2)(\text{N}_2\text{py}_3\text{o})]\text{ClO}_4 \cdot 2 \text{H}_2\text{O}$ ,<sup>7</sup>  $[\text{Co}^{\text{II}}(\text{N}_2\text{py}_2)(\text{OH}_2)_2](\text{ClO}_4)_2$ ,<sup>6</sup>  $[\text{Co}^{\text{III}}(\text{N}_2\text{py}_2\text{a})(\text{Cl})_2]\text{ClO}_4$ ,<sup>7</sup>  $[\text{Co}^{\text{III}}(\text{N}_2\text{py}_2\text{b})(\text{CO}_3)]\text{PF}_6$ <sup>7</sup> were prepared according to known procedures.

*Cyclic voltammetry* was measured with a BAS100B electrochemical apparatus with BAS100W software. The working electrode was a glassy carbon electrode, and a platinum wire was used as indicator electrode. The ionic strength was set to 0.1 M with  $\text{Bu}_4\text{NPF}_6$ . Potentials were measured against a Ag/0.01 M  $\text{AgNO}_3$  electrode. All measurements were carried out at room temperature.

*IR spectra* were recorded from KBr pellets with a 16PC FT-IR instrument of Perkin Elmer at room temperature.

*UV-vis spectra* were recorded on a double-beam Cary 1E instrument, or on a V-570 UV/Vis/NIR spectrophotometer (Jasco). When otherwise not mentioned, the measurements were carried out at room temperature.

$^1\text{H}$ - and  $^{13}\text{C}$ -NMR spectra at 200.13 and 50.54 MHz were recorded on a Bruker ARX 200 spectrometer using TMS as internal standard.

*Elemental analyses* were obtained from the microanalytical laboratory of the chemical institutes of the University of Heidelberg. For the measurements a Vario EL microanalysis apparatus from Elementar was used. The code number of each measurement is reported together with the experimentally determined values.

*Mass spectra* were obtained from the laboratories of the Institute of Organic or Inorganic Chemistry of the University of Heidelberg. Measurements were carried out on a Finnigan 8400 mass spectrometer. For FAB spectra nitrobenzyl alcohol (nibeol) was used as matrix.

*EPR spectra* were recorded from frozen solutions (DMF/water or DMF/MeCN 2:1) at 110 K using a Bruker Elexsys E 500 instrument. Electronic parameters were determined by simulation with the program XSophe.<sup>82,83</sup>

*Crystal structure determination*: Intensity data were collected on a Bruker AXS Smart1000 diffractometer at 100 K with graphite-monochromated  $\text{MoK}_\alpha$  radiation [ $\lambda = 0.71073 \text{ \AA}$ ]. Absorption corrections were made with the program SHELXTL 5.10.<sup>184</sup>

*Magnetometric measurements* were carried out on a SQUID MPMS-XL (Quantum Design), in the temperature range 2-300 K.

*Gas chromatographic analysis* was performed on a Varian 3900 gas chromatograph equipped with a flame ionization detector, using a capillary column of Phenomenex Zebron ZB-1701 (length: 30 m, internal diameter 0.25 mm). Temperature program: after 1 min with a rate of 15 °C/min from 40°C to 130°C; after 11 min with a rate of 49°C/min till 250°C.

*Molecular mechanics* calculations were performed with the MOMECC program<sup>89</sup> and force field.<sup>90</sup>

*DFT calculations* were performed with Gaussian03,<sup>185</sup> using the three-parameter hybrid exchange and correlation functional B3LYP.<sup>157,158</sup> For the geometry optimizations the 6-31G(d) basis set was used in almost all cases. In the bispidone structures the ester side chains



were removed and were replaced by hydrogen atoms. Frequency calculations were performed on all optimized structures to verify their status as true minima on the potential energy surface. The obtained frequencies were scaled with a factor of 0.9804, which is the usual method used for this basis set.<sup>186</sup> Single point energy calculations were performed on the optimized geometries using a TZVPP (cobalt) / TZV (other atoms) basis set combination. Transition state calculations were performed by QST3 or the normal TS mode. Initial guesses were generated by using the high ligand field theory option of the Jaguar 5.0 program.<sup>163</sup> (Schrodinger, LLC, Portland, Oregon, 2002)

*Haloperoxidase test:* Bromination of the organic dye Phenol Red was carried out under conditions reported by Pecoraro and coworkers.<sup>112</sup>

*Cyclohexene oxidation:* To the mixture of 2.1  $\mu\text{mol}$  vanadium complex and 2.1 mmol cyclohexene in 2.7 mL dry acetonitrile was injected 0.3 mL  $\text{H}_2\text{O}_2$  solution (prepared by mixing 60  $\mu\text{L}$  35%  $\text{H}_2\text{O}_2$  and 10 mL dry acetonitrile) with a syringe pump under 30 min. After a given “reaction time” 1 mL 6.8 mM naphthalene in acetonitrile (as internal standard) was added. Finally, the mixture was passed through a silica column, washed with ethyl acetate, and the eluate was directly analyzed by GC.<sup>59</sup>

*Oxidation of cyclooctene* was carried out according to a reported procedure<sup>34</sup>

*Hydrazine test:* 0.27 mmol cobalt(II) complex in 3 mL MeOH was mixed with 0.5 g 30%  $\text{H}_2\text{O}_2$  and after 20 h at RT, the reaction mixture was added to 10 mL hydrazine reagent solution (preparation of hydrazine reagent solution: 1 g 2,4-dinitrophenylhydrazine in 5 mL cc  $\text{H}_2\text{SO}_4$  was added slowly to a mixture of 10 mL  $\text{H}_2\text{O}$  and 35 mL 95% EtOH). The resulting orange precipitate was extracted with 5 mL toluene and dried up.

*Kinetic measurements:* Oxidation kinetics were followed by UV-vis spectroscopy. To the samples containing cobalt(II) complexes, the appropriate amount of  $\text{H}_2\text{O}_2$  was added, mixed vigorously, and the change in the UV-vis spectra recorded in a time sequence. Absorbance values at absorption maxima were collected and the pseudo-first order rate constants were determined from the slope of the semilogarithmic plots ( $\ln(A_{\text{inf}} - A_t)$  vs  $t$ )

## 9.2. Syntheses

### 9.2.1. Synthesis of ligands and precursors

#### 9.2.1.1. *Bzl-Pip*

4.10 g (23.6 mmol) dimethyl acetonedicarboxylate was dissolved in 16 mL methanol and cooled to 0°C with ice. To this solution was given dropwise 10.0 g (47.2 mmol) O-benzyl salicylaldehyde and 1.83 g (23.6 mmol) 40% (w/w) aqueous methylamine solution. The resulting yellow solution was stirred for 5 h at 0°C, and then kept at 4°C for 3 days. The formed white precipitate was collected and washed with cold methanol. Yield: 10.88 g (18.4 mmol, 78%).

*ESI(+)*: 594.2 [M+H]<sup>+</sup>

*Elemental analysis*: measured C 72.84, H 5.94, N 2.36 (15084)

calculated for C<sub>36</sub>H<sub>35</sub>NO<sub>7</sub>, MW 593.61:

C 72.65, H 5.91, N 2.37

<sup>1</sup>H-NMR(CDCl<sub>3</sub>): 12.23 (1H, s, enol-H), 7.58 (1H, d, <sup>3</sup>J = 7.4 Hz, Ar-H), 7.25 (13H, m, Ar-H), 6.87 (3H, m, Ar-H), 6.70 (1H, d, <sup>3</sup>J = 8.2 Hz, Ar-H), 5.53 (1H, s, enol=CH), 5.03 (2H, s, bz-CH<sub>2</sub>), 4.75 (2H, s, bz-CH<sub>2</sub>), 4.50 (1H, d, <sup>3</sup>J = 11.6 Hz, N-CH), 4.14 (1H, d, <sup>3</sup>J = 10.8 Hz, N-CH), 3.93 (2H, d, <sup>3</sup>J = 9.8 Hz, MeOOC-CH-C=O), 3.50 (3H, s, OCH<sub>3</sub>), 3.47 (3H, s, OCH<sub>3</sub>), 2.00 (3H, s, NCH<sub>3</sub>)

<sup>13</sup>C-NMR(CDCl<sub>3</sub>): 199.7 (1C, C=O), 171.5, 170.6 (2C, ester), 167.5 (1C, HO-C=CH), 166.6, 157.1, 156.5, 137.5, 137.1, 130.0, 129.1, 128.7, 128.6, 128.5, 128.4, 128.3, 128.2, 128.0, 127.7, 127.5, 127.4, 127.0, 126.8, 121.2, 120.8, 120.3, 112.5, 111.8 (all aromatic carbons), 100.7 (1C, HO-C=CH), 70.1, 69.6 (2C, bz-CH<sub>2</sub>O), 54.5, 52.6, 52.2, 51.8, 51.7, 50.1 (6C, OCH<sub>3</sub> + CH), 37.0 (1C, N-CH<sub>3</sub>)

#### 9.2.1.2. *6-sulfonato-2-(aminomethyl)-4-ethylphenol*

12.22 g (0.1 mol) 4-ethylphenol and 24.72 g (0.2 mol) N-hydroxymethyl-chloracetamide was added to 100 mL cc.H<sub>2</sub>SO<sub>4</sub>, and the solution was stirred for 22 h at RT. The darkened mixture was poured slowly onto ice, which lead to formation of a mixture of white precipitate and a black tar. The precipitate was collected (2,6-diamide), and the tar was purified by decantation. Addition of ethanol gave more precipitate, which was removed by filtration. To the remaining solution a mixture of 100 mL ethanol and 30 mL cc HCl was given. After 90 min reflux the solvent was partially removed to give a pale white solid. Yield: 3.22 g (14.0 mmol, 14%).

*MS(CI)*: 252.1, 415.2

*Elemental analysis:* measured C 46.22, H 5.72, N 6.24 (16979)

calculated for C<sub>9</sub>H<sub>13</sub>NO<sub>4</sub>S, MW 231.25:

C 46.74, H 5.66, N 6.06

*IR(KBr):* 3426 br, 3157 br, 2969 m, 2733 br, 2626 w, 1616 s, 1602 s, 1478 vs, 1209 vs (SO<sub>3</sub>), 1144 vs (SO<sub>3</sub>), 1026 s, 888 m, 753 m, 650 s

*<sup>1</sup>H NMR(D<sub>2</sub>O):* 7.40 (1H, d, <sup>4</sup>J = 1.9 Hz, Ar-**H**), 7.19 (1H, d, <sup>4</sup>J = 1.9 Hz, Ar-**H**), 4.03 (2H, s, CH<sub>2</sub>NH<sub>2</sub>), 2.44 (2H, q, <sup>3</sup>J = 7.6 Hz, CH<sub>2</sub>CH<sub>3</sub>), 1.01 (3H, t, <sup>3</sup>J = 7.6 Hz, CH<sub>3</sub>)

#### 9.2.1.3. *sulfobis*

To the suspension of 0.74 g (1.94 mmol) Npy2 piperidone in 15 mL ethanol was added dropwise 0.38 g (4.66 mmol) 37 w/w% aqueous formaldehyde, followed by 0.54 g (2.33 mmol) 6-sulfonato-2-(aminomethyl)-4-ethylphenol. The reaction mixture was stirred under reflux for 3 hours. After complete solvent evaporation the crude product was redissolved in small amount of ethanol. A white precipitate was formed after 2 weeks, which was filtered off, and carefully washed with small portions of ethanol. Yield: 51 mg (78 μmol, 4%).

*ESI-MS(+):* 639.4 [M+H]<sup>+</sup>, 661.3 [M+Na]<sup>+</sup>, 677.3 [M+K]<sup>+</sup>

*ESI-MS(-):* 637.3 [M-H]<sup>-</sup>

*Elemental analysis:* measured C 56.67, H 5.52, N 8.39 (17513)

calculated for C<sub>31</sub>H<sub>34</sub>N<sub>4</sub>O<sub>9</sub>S · H<sub>2</sub>O, MW 656.66:

C 56.70, H 5.52, N 8.53

*IR(KBr):* 3448 br, s, 3013 m, 2961 m, 2873 w, 2812 w, 1741 vs (C=O), 1614 m, 1591 s, 1473 s, 1439 s, 1240 vs, 1163 vs, 1024 s, 966 m, 776 m, 756 m, 641 s

#### 9.2.1.4. *o*-hydroxy benzylamine

This procedure is an improvement of a published work.<sup>48</sup> In a 500 mL three-necked flask 7 g (184.5 mmol) LiAlH<sub>4</sub> was suspended in 75 mL dry THF under argon atmosphere. The flask was then cooled down to -10°C by ice-salt mixture. To this suspension was added dropwise carefully a solution of 15 g (109.4 mmol) salicylamide in 75 mL dry THF, under Ar. The reaction mixture was stirred overnight at room temperature, followed by a reflux for 1 day. After cooling the flask, the reaction mixture was quenched by dropwise addition of 300 mL half-concentrated aqueous tartrate solution. The precipitated metal-tartrate complexes were filtered off and washed with THF. The pH of the filtrate was set to 9 by 1 M HCl and then extracted with 3 × 70 mL CH<sub>2</sub>Cl<sub>2</sub>, and the organic layers collected, which were dried on

Na<sub>2</sub>SO<sub>4</sub>. After solvent evaporation the obtained white solid was dried on vacuum line. Yield: 5.38 g (44 mmol, 40%)

*Elemental analysis:* measured C 67.88, H 7.34, N 10.98 (13736)

calculated for C<sub>7</sub>H<sub>9</sub>NO, MW 123.14:

C 68.27, H 7.36, N 11.38

<sup>1</sup>H-NMR(CDCl<sub>3</sub>): 7.14 (1H, td, <sup>3</sup>J = 7.7 Hz, <sup>4</sup>J = 1.6 Hz, H4), 6.98 (1H, dd, <sup>3</sup>J = 6.1 Hz, <sup>4</sup>J = 1.6 Hz, H6), 6.85 (1H, dd, <sup>3</sup>J = 7.3 Hz, <sup>4</sup>J = 1.1 Hz, H3), 6.78 (1H, td, <sup>3</sup>J = 7.4 Hz, <sup>4</sup>J = 1.1 Hz, H5), 4.13 (2H, s, PhCH<sub>2</sub>N) [H3 is *ortho* to OH, H6 is *ortho* to CH<sub>2</sub>NH<sub>2</sub>]

#### 9.2.1.5. N2py2PhOH

To the suspension of 1.3 g (3.38 mmol) Npy2 piperidone in 15 mL ethanol was added dropwise 0.66 g (8.12 mmol) 37 w/w% aqueous formaldehyde, followed by 0.5 g (4.06 mmol) o-hydroxy benzylamine. The reaction mixture was stirred under reflux for 3 hours, after which the solvent was completely removed. After drying the sample in vacuo overnight, it was redissolved in 3 mL ethanol and left at 4°C. After several days a white precipitate was formed which was filtered off, washed with cold ethanol and dried. Yield: 0.73 g (1.39 mmol, 41%).

*Elemental analysis:* measured C 64.96, H 5.72, N 10.52 (13084)

calculated for C<sub>29</sub>H<sub>30</sub>N<sub>4</sub>O<sub>6</sub> · 0.25 H<sub>2</sub>O, MW 535.10:

C 65.08, H 5.74, N, 10.47

*IR(KBr):* 3436 s, br, 3052 w, 3008 w, 2954 w, 2820 m, 1736 vs, 1590 s, 1434 s, 1278 vs, 1158 s, 1096 m, 954 m, 754 s

<sup>1</sup>H-NMR(CDCl<sub>3</sub>): 8.48 (2H, d, <sup>3</sup>J = 4.6 Hz, H<sub>py-α</sub>), 7.44 (6H, m, py-H), 7.08 (2H, t, <sup>3</sup>J = 7.0 Hz, phenol-H), 6.93 (1H, d, <sup>3</sup>J = 7.6 Hz, phenol-H), 6.76 (1H, d, <sup>3</sup>J = 7.2 Hz, phenol-H), 4.53 (2H, s, N-CH), 3.69 (6H, s, OCH<sub>3</sub>), 3.54 (2H, s, CH<sub>2</sub>-C<sub>6</sub>H<sub>4</sub>OH), 3.43 (2H, d, <sup>2</sup>J = 10.4 Hz, NCH<sub>2</sub>), 2.67 (2H, d, <sup>2</sup>J = 10.8 Hz, NCH<sub>2</sub>), 1.88 (3H, s, NCH<sub>3</sub>)

*Crystal structure:* co\_mt1

#### 9.2.1.6. Npy2PhOH piperidone

To an ice-cooled ethanolic solution (5 mL) of 848 mg (4.87 mmol) dimethyl (acetondicarboxylate) was added dropwise 1.043 g (9.47 mmol) picolylaldehyde, followed by 600 mg o-aminomethyl phenol (as a solid). The color of the solution turns rapidly deep red. After stirring for 30 min at 0°C, the reaction mixture was kept at 4°C. After 2 days, 2 mL of

water was added. Within some days a white precipitate was formed, which was filtered off, washed with cold ethanol, and dried in vacuo. Yield: 1.77 g (3.71 mmol, 76%)

*FAB-MS*: 476.5 [M+H]<sup>+</sup>

*Elemental analysis*: measured C 65.38, H 5.53, N 8.55 (13907)

calculated for C<sub>26</sub>H<sub>25</sub>N<sub>3</sub>O<sub>6</sub>, MW 475.47:

C 65.67, H 5.29, N 8.84

*IR(KBr)*: 3444 br, s (OH), 3282 br, s, 3076 w, 3043 w, 3009 w, 2954 w (CH<sub>2</sub>), 2925 m, 2854 m (Bohlmann), 1747 vs (C=O), 1665 s, 1588 s, 1490 m, 1437 s, 1344 m, 1259 s, 1168 m, 1102 m, 992 w, 770 m, 760 s, 749 m

<sup>1</sup>H-NMR(CDCl<sub>3</sub>): 12.62 (1H, s, enol-H), 12.49 (1H, s, enol-H), 8.58 (1H, td, <sup>3</sup>J = 4.7 Hz, <sup>4</sup>J = 1.8 Hz, H<sub>py-α</sub>), 8.47 (1H, td, <sup>3</sup>J = 4.4 Hz, <sup>4</sup>J = 1.8 Hz, H<sub>py-α</sub>), 7.62 (2H, dt, <sup>3</sup>J = 8.0 Hz, <sup>4</sup>J = 1.8 Hz, py-H), 7.54 (1H, td, <sup>3</sup>J = 7.8 Hz, <sup>4</sup>J = 1.8 Hz, py-H), 7.37 (1H, d, <sup>3</sup>J = 7.8 Hz, py-H), 7.15 (2H, m, py-H), 6.80 (4H, m, phenol-H), 4.79 (2H, s, N-CH), 4.31 (2H, d, <sup>3</sup>J = 6.8 Hz, MeOOC-CH<sub>2</sub>-C=O), 3.77 (2H, s, NCH<sub>2</sub>), 3.64 (3H, s, OCH<sub>3</sub>), 3.47 (3H, s, OCH<sub>3</sub>)

<sup>13</sup>C-NMR(CDCl<sub>3</sub>): 195.5 (1C, C=O), 171.3, 170.4 (2C, MeOOC), 167.1 (1C, HO-C=CH), 156.1, 156.0, 155.3 (3C, C<sub>q</sub>-ar), 148.0, 146.1, 135.9, 134.4, 129.2, 128.6, 122.4, 122.1, 120.7, 116.3, 115.7 (13C, C-ar), 96.6 (HO-C=CH), 61.6 (NCH<sub>2</sub>C<sub>6</sub>H<sub>4</sub>OH), 59.2, 58.2 (2C, MeOOC-CH), 51.7 (2C, OCH<sub>3</sub>), 41.3 (N-CH).

#### 9.2.1.7. 2-methoxy, 6-aminomethylphenol

The method using LiAlH<sub>4</sub> with a NaOH workup, developed by Schaefer's group was used.<sup>44</sup>

To an ice-cooled dry tetrahydrofuran suspension (15 mL) of 2 g (53.0 mmol) LiAlH<sub>4</sub> was added 3.34 g (20 mmol) o-vanillin-aldoxime in 15 mL dry THF under Ar. The reaction mixture was stirred for 4 h at RT, and then refluxed for 4 h. After cooling down the flask, 3 mL water was added dropwise, followed by 4 mL 50% NaOH solution. The formed inorganic precipitate was removed by filtration, the filtrate was concentrated to dryness. The remaining sticky solid was redissolved in minimum amount of water, and neutralized with diluted HCl. The precipitated pale yellow solid was filtered, washed with water, and dried in vacuo. Yield 1.25 g (6.0 mmol, 30%)

*ESI-MS*: 154.08 [M+H]<sup>+</sup>

*Elemental analysis*: measured C 46.27, H 5.88, N 6.25 (14456)

calculated for C<sub>8</sub>H<sub>11</sub>NO<sub>2</sub> · 0.5 H<sub>2</sub>O · 0.78 NaCl, MW 207.6:

C 46.28, H 5.82, N 6.75

<sup>1</sup>H-NMR(MeOH-d<sub>4</sub>): 6.55 (3H, m, Ar-H), 3.74 (2H, s, CH<sub>2</sub>NH<sub>2</sub>), 3.71 (3H, s, OCH<sub>3</sub>)

*9.2.1.8. vanilbis*

To a suspension of Npy2 piperidone (906 mg, 2.36 mmol) in 15 mL ethanol was added dropwise 460 mg (5.67 mmol) 37%(w/w) formaldehyde solution, followed by 600 mg (2.83 mmol) 2-methoxy, 6-aminomethylphenol. The reaction mixture was refluxed for 3 hours, then the solvent was completely evaporated. Treatment with minimum amount of water under ultrasonic bath leads to precipitate formation. The white solid was filtered off, washed with water and dried in vacuo. Yield: 0.39 g (0.71 mmol, 30%)

*FAB-MS*: 561.6 [M+H]<sup>+</sup>, 579.6 [M+H<sub>2</sub>O+H]<sup>+</sup>

*Elemental analysis*: measured C 62.61, H 5.80, N 8.95 (14548)

calculated for C<sub>30</sub>H<sub>32</sub>N<sub>4</sub>O<sub>7</sub> · EtOH, MW 606.65:

C 62.32, H 6.21, N 9.09

*IR(KBr)*: 3428 s, br (OH), 3056 w, 3000 w, 2952 w (CH<sub>2</sub>), 2903 w, 2838 w, 1740 s (C=O), 1589 m, 1465 s, 1434 s, 1350 m, 1278 s, br, 1161 m, 1080 m, 983 w, 954 w, 785 w, 751 w

*9.2.1.9. N,N-bis(2-hydroxy-3-methoxybenzyl)amine (N(PhOH)<sub>2</sub>)*

1.96 g (11.7 mmol) o-vanillinaldoxime was dissolved in 25 mL ethanol and was placed in an autoclave. 100 mg Pd (5% on charcoal) was added, and the system was hydrogenated for 3 h under intense stirring. After the reaction the solid catalyst was then filtered off on celite, which was treated with dichloromethane to redissolve the product. The collected clear solution was concentrated and the remaining solid was dried in vacuo. Yield: 1.62 g (10.6 mmol, 90%)

*MS(EI)*: 289.2 M<sup>+</sup>

*Elemental analysis*: measured C 65.62, H 6.57, N 4.82 (14148)

calculated for C<sub>16</sub>H<sub>19</sub>NO<sub>4</sub> · 0.2 H<sub>2</sub>O, MW 292.80:

C 65.63, H 6.67, N 4.78

*IR(KBr)*: 3432 br, s (OH), 3195 br, s, 3057 w, 3016 w, 2944 m, 2832 m, 1593 m, 1484 vs, 1446 s, 1370 m, 1266 vs, 1242 s, 1076 vs, 1008 m, 985 m, 941 m, 732 vs

<sup>1</sup>H-NMR(CDCl<sub>3</sub>): 6.73 (6H, m, Ar-H), 6.25 (1H, s, br, NH), 3.92 (4H, s, CH<sub>2</sub>NH), 3.87 (6H, s, OCH<sub>3</sub>)

<sup>13</sup>C-NMR(CDCl<sub>3</sub>): 147.7 (2C, C<sub>ar</sub>OMe), 146.3 (2C, C<sub>ar</sub>-OH), 123.5 (2C, C<sub>ar</sub>CH<sub>2</sub>), 122.1, 119.4, 111.0 (6C, C<sub>ar</sub>-H), 56.4 (2C, OCH<sub>3</sub>), 49.6 (2C, CH<sub>2</sub>NH)

*9.2.1.10. cresbis*

To a suspension of 4.73 g (12.33 mmol) Npy2 piperidone in 45 mL methanol was added dropwise 2.4 g (29.6 mmol) 37%(w/w) aqueous formaldehyde solution, followed by 1.5 g (7.4 mmol) 2,6-bis(aminomethyl)-4-methylcresol monohydrochloride as a solid. After this 1.026 mL (7.4 mmol) triethylamine was added to deprotonate the amino group, and the solution was refluxed for 1 h. The reaction mixture was then cooled down and the solvent completely removed by rotary evaporator. The remaining solid was redissolved in 4 mL ethanol, and the dropwise addition of water led to formation of a greenish-white precipitate, which was filtered off, washed with small amount of water, and dried in vacuo. Yield: 1.66 g (3.2 mmol, 26%)

*FAB-MS*: 982.2 [M+H]<sup>+</sup>, 557.6 [Fragment<sub>1</sub>+H]<sup>+</sup>, 425.3 [Fragment<sub>2</sub>+H]<sup>+</sup>

*Elemental analysis*: measured C 62.04, H 5.82, N 10.85 (14574)

calculated for C<sub>53</sub>H<sub>56</sub>N<sub>8</sub>O<sub>11</sub> · 2.5 H<sub>2</sub>O, MW 1026.04:

C 62.04, H 5.98, N 10.92

*IR(KBr)*: 3429 br, 3052 w, 3002 w, 2951 m (CH<sub>2</sub>), 2918 w, 2846 w, 2803 w, 1740 vs (C=O), 1632 m, 1589 m, 1468 m, 1434 s, 1349 s, 1278 br, s, 1161 w, 1096 w, 996 w, 975 w, 865 w, br, 786 m, 752 m

<sup>1</sup>H NMR: all tried solvents (CDCl<sub>3</sub>, CD<sub>3</sub>CN, CD<sub>3</sub>OD) gave broad peaks and poor baseline

*UV-vis (MeOH)*: 420 nm (sh)

*EPR* (0.1 M in DMF/H<sub>2</sub>O 2:1): 3323 G (sharp negative peak)

*9.2.1.11. 2,6-bis(aminomethyl)-4-tert-butylphenol*

A solution of 37 g HCl gas (1.015 mol) in 90 mL methanol was added at RT to 15.0 g (70 mmol) solid 2,6-bis(hydroxymethyl)-4-tert-butylphenol. The reaction mixture was stirred for 2 h (the solid dissolved within 10 minutes), after which the solvent and the excess HCl gas was removed using rotary evaporator, yielding the crude dichloride. To this sticky solid was added rapidly, under vigorous stirring, 21.76 g (157.5 mmol) hexamethylenetetramine in 450 mL methanol, whereby the dichloride intermediate dissolved within seconds. After stirring for 15 min a white precipitate formed, which was isolated via decantation (direct filtration was not possible due to the highly hygroscopic behaviour of the bis-urotropinium salt). The sticky solid was washed several times with small portions of cold methanol and finally dried in vacuo (yield: 11.1 g, 30%). The whole amount of bis-urotropinium salt (11.1 g, 21.0 mmol) was suspended in a mixture of 13 mL cc. HCl and 5 mL ethanol, and heated in an open beaker. When the solution started to boil, the solid was completely dissolved. The solvents were

continuously evaporated during boiling at atmospheric pressure. Heating was continued for 2 h, and the solvent volume was maintained constant by adding ethanol occasionally, in order to avoid heating till dryness. After 2 h a further 10 mL of cCHCl was added to the solution, which was boiled for another 2 h. Evolution of formaldehyde indicated the breakdown of the urotropinium units. The mixture was then evaporated to complete dryness to remove the excess of acid. A solution containing 4 mL concentrated ammonia and 35 mL water was added then to the mixture, which was kept under ice-bath. After 1 h, the precipitated yellow solid was collected, and dried in vacuo. Yield: 0.94 g (3.5 mmol, 5%)

*Elemental analysis:* measured C 54.05, H 8.24, N 10.55 (14939)  
 calculated for  $C_{12}H_{20}N_2O \cdot 1.6 HCl$ , MW 265.01:  
 C 54.01, H 8.16, N 10.51

*ESI-MS:* 209.4 [M+H]<sup>+</sup>

<sup>1</sup>H-NMR: not clearly resolved

#### 9.2.1.12. *tBuBis*

To a 25 mL methanolic suspension of 1.20 g (3.125 mmol) Npy2 piperidone was added 0.51 g (6.25 mmol) 37%(w/w) aqueous formaldehyde solution, followed by 0.5 g (1.875 mmol) 2,6-bis(aminomethyl)-4-tert-butylphenol × 1.6 HCl, and 411 μL (3.00 mmol) triethylamine. The mixture was refluxed for 2 h, the unreacted part of the amine was then filtered off and the filtrate completely evaporated and redissolved in 20 mL methanol. To this solution water was added dropwise, which led to a formation of a pale green precipitate which was collected by filtration, washed with water and dried in vacuo. Yield: 410 mg (0.81 mmol, 26%)

*FAB-MS:* 1025.5 [M+H]<sup>+</sup>, 599.8 [Fragment<sub>1</sub>+H]<sup>+</sup>, 425.5 [Fragment<sub>2</sub>+H]<sup>+</sup>

*ESI-MS:* 512.22 M/2 [M+2H]<sup>2+</sup>

*MALDI:* 599.4 [Fragment<sub>1</sub>+H]<sup>+</sup>, 425.3 [Fragment<sub>2</sub>+H]<sup>+</sup>

*Elemental analysis:* measured C 66.26, H 6.59, N 9.36 (15046)  
 calculated for  $C_{56}H_{62}N_8O_{11} + tBuC_6H_4OH + H_2O$ , MW 1209.30:  
 C 66.53, H 6.59, N 9.41  
 calculated for "Fragment<sub>1</sub>" · H<sub>2</sub>O,  $C_{34}H_{42}N_4O_7$ , MW 618.67:  
 C 66.00, H 6.83, N 9.06  
 calculated for "2+2 cyclic dimer"  $C_{66}H_{72}N_8O_{12} \cdot 1.5 H_2O$ , MW 1196.26:  
 C 66.26, H 6.31, N 9.37

(for the explanation of Fragment<sub>1</sub>, Fragment<sub>2</sub> and 2+2 cyclic dimer, see Section 4.4.2)



*IR(KBr)*: 3427 br, 3052 w (CH), 2953 m (CH<sub>2</sub>), 2904 w, 2865 w, 2804 w, 1740 vs (C=O), 1635 m, 1589 m, 1484 m, 1465 m, 1363 w, 1278 s, 1223 w, 1197 w, 1161 m, 1097 w, 984 m, 881 w, 787 w, 752 m

*UV-vis (MeOH)*: 416 nm ( $\epsilon=1300$ )

<sup>1</sup>H-NMR: no suitable solvent found

*EPR*: (40 mM in DMF/H<sub>2</sub>O 2:1): sharp peak at 3326 G

### 9.2.1.13. N<sub>2</sub>py<sub>2</sub>Bz

To the suspension of 10.0 g (26.08 mmol) Npy<sub>2</sub> piperidone in 110 mL ethanol was added dropwise 5.08 g (62.6 mmol) 37 w/w% aqueous formaldehyde, followed by 3.35 g (31.3 mmol) benzylamine. The reaction mixture was stirred under reflux for 3 hours. Partial solvent removal led to precipitation of the product. Yield: 7.44 g (14.3 mmol, 55%).

*FAB(+)-MS*: 515.5 [M+H]<sup>+</sup>, 537.5 [M+Na]<sup>+</sup>

*Elemental analysis*: measured C 67.54, H 5.83, N 10.97 (17915)

calculated for C<sub>29</sub>H<sub>30</sub>N<sub>4</sub>O<sub>5</sub>, MW 514.54:

C 67.69, H 5.87, N 10.89

*IR(KBr)*: 3425 br, s, 3085 w, 3057 w, 3008 m, 2987 m, 2953 m, 2855 w, 2844 m, 1739 vs, 1589 s, 1571 m, 1465 m, 1435 vs, 1349 s, 1279 vs, 1159 s, 1097 s, 982 m, 751 s, 704 m, 619 m

<sup>1</sup>H-NMR(CDCl<sub>3</sub>): 8.56 (2H, d, <sup>3</sup>J = 4.2 Hz, H<sub>py- $\alpha$</sub> ), 7.87 (2H, d, <sup>3</sup>J = 7.9 Hz, Py-H), 7.46 (2H, td, <sup>3</sup>J = 7.7 Hz, <sup>4</sup>J = 1.7 Hz, Py-H), 7.38 (5H, s, C<sub>6</sub>H<sub>5</sub>), 7.11 (2H, td, <sup>3</sup>J = 6.1 Hz, <sup>4</sup>J = 1.6 Hz, Py-H), 4.68 (2H, s, N-CH), 3.81 (6H, s, OCH<sub>3</sub>), 3.35 (2H, s, CH<sub>2</sub>Ph), 3.05 (2H, d, <sup>2</sup>J = 12.8 Hz, NCH<sub>2</sub>), 2.53 (2H, d, <sup>2</sup>J = 12.8 Hz, NCH<sub>2</sub>), 1.96 (3H, s, NCH<sub>3</sub>)

<sup>13</sup>C-NMR(CDCl<sub>3</sub>): 203.7 (1C, C=O), 168.5 (2C, COOMe), 158.4 (2C, C<sub>py-quat</sub>), 149.0 (2C, C<sub>py- $\alpha$</sub> ), 136.9 (1C, C<sub>ph-quat</sub>), 136.1 (2C, C<sub>py- $\gamma$</sub> ), 130.4 (2C, C<sub>ph-ortho</sub>), 128.4 (2C, C<sub>ph-meta</sub>), 127.6 (1C, C<sub>ph-para</sub>), 123.4 (2C, C<sub>py- $\delta$</sub> ), 122.9 (2C, C<sub>py- $\beta$</sub> ), 73.8 (2C, MeOOC-C<sub>quat</sub>-C=O), 62.1 (2C, N-CH), 59.0 (2C, OCH<sub>3</sub>), 52.5 (2C, NCH<sub>2</sub>)

## 9.2.2. Synthesis of the copper(II) complexes

### 9.2.2.1. General procedure

To a dry methanolic solution (25 mL) of 0.28 mmol ligand, was added 96.8 mg (0.28 mmol) Cu(BF<sub>4</sub>)<sub>2</sub> · 6 H<sub>2</sub>O in 5 mL methanol. The reaction mixture turns immediately intensive brown. After stirring for 2 h at RT, the solvent was evaporated and the obtained solid was washed with ethyl acetate and dried in vacuo.



Deep green solid. Yield: 217 mg (0.27 mmol, 96%)

*FAB-MS*: 592.4  $[\text{Cu}^{\text{II}}(\text{N}2\text{py}2\text{PhO})]^+$ , 610.4  $[\text{Cu}^{\text{II}}(\text{N}2\text{py}2\text{PhO})(\text{OH}_2)]^+$ ,  
624.5  $[\text{Cu}^{\text{II}}(\text{N}2\text{py}2\text{PhO})(\text{MeOH})]^+$ , 764.6  $[\text{Cu}^{\text{II}}(\text{N}2\text{py}2\text{PhO})(\text{BF}_4)_2]^+$

*Elemental analysis*: measured C 43.15, H 4.59, N 6.93 (13839)  
calculated for  $\text{C}_{29}\text{H}_{36.66}\text{N}_4\text{O}_{10}\text{B}_{1.66}\text{F}_{6.64}\text{Cu}$ , MW 808.12:  
C 43.16, H 4.56, N 6.93

*IR(KBr)*: 3448 br (OH), 3106 w, 2958 w ( $\text{CH}_2$ ), 2850 w (CH), 1734 s (C=O), 1610 m, 1478 s,  
1452 s, 1268 s, 1084 s ( $\text{BF}_4$ ), 1030 s, 766 s (py)

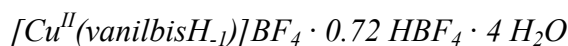
*UV-vis (MeOH)*: 450 nm ( $\epsilon = 1220$ ), 728 nm ( $\epsilon = 200$ )

(*MeCN*): 459 nm ( $\epsilon = 1290$ ), 741 nm ( $\epsilon = 240$ )

*CV(MeCN)*: -1.025 V vs. Ag/0.01 M  $\text{AgNO}_3$

*EPR* (in DMF/ $\text{H}_2\text{O}$  2:1):  $g_{zz} = 2.242$ ,  $g_{xx} = g_{yy} = 2.061$ ,  $A_{zz} = 167$ ,  $A_{xx} = A_{yy} = 18$

*Crystal structure* (co243)



Deep green solid. Yield: 222 mg (0.26 mmol, 94%)

*FAB-MS*: 622.5  $[\text{Cu}^{\text{II}}(\text{vanilbisH}_{-1})]^+$ , 640.5  $[\text{Cu}^{\text{II}}(\text{vanilbisH}_{-1})(\text{OH}_2)]^+$ ,  
654.6  $[\text{Cu}^{\text{II}}(\text{vanilbisH}_{-1})(\text{MeOH})]^+$

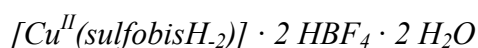
*Elemental analysis*: measured C 42.60, H 4.68, N 6.13 (14582)  
calculated for  $\text{C}_{30}\text{H}_{38.72}\text{N}_4\text{O}_{11}\text{B}_{1.72}\text{F}_{6.88}\text{Cu}$ , MW 845.2:  
C 42.63, H 4.73, N 6.63

*IR(KBr)*: 3442 br, s (OH), 2958 m ( $\text{CH}_2$ ), 2848 m (CH), 1732 vs (C=O), 1610 s, 1478 s, 1282  
s, 1258 s, 1084 vs ( $\text{BF}_4$ ), 778 m

*UV-vis(MeOH)*: 473 nm ( $\epsilon = 1040$ ), 718 nm ( $\epsilon = 220$ )

*CV(MeCN)*:  $E_a = -1018$  mV vs. Ag/0.01 M  $\text{AgNO}_3$

*EPR*(DMF/ $\text{H}_2\text{O} = 2:1$ ):  $g_{zz} = 2.242$ ,  $g_{yy} = g_{xx} = 2.061$ ,  $A_{zz} = 165$ ,  $A_{xx} = A_{yy} = 31$



Red solid. Yield: 225 mg (0.25 mmol, 88%)

*ESI(+)-MS*: 700.4  $[\text{Cu}^{\text{II}}(\text{sulfobisH}_{-1})]^+$ , 722.3  $[\text{Cu}^{\text{II}}(\text{sulfobisH}_{-2}) + \text{Na}]^+$

*Elemental analysis*: measured C 41.17, H 4.39, N 6.15 (17594)  
calculated for  $\text{C}_{31}\text{H}_{40}\text{N}_4\text{O}_{11}\text{SB}_2\text{F}_8\text{Cu}$ , MW 911.84:  
C 40.83, H 4.20, N 6.15

*IR(KBr)*: 3440 br, s, 3132 w, 3086 w, 2964 m, 2876 w, 1740 s, 1626 m, 1608 m, 1456 s, 1258 s, 1084 vs, 962 m, 784 m, 770 m, 644 m

*UV-vis (MeOH)*: 433 nm ( $\epsilon = 750$ ), 702 nm ( $\epsilon = 135$ )

*EPR*(DMF/H<sub>2</sub>O = 2:1): indicates a mixture,  $A_{zz} = 137$ ,  $g_{zz} = 2.280$  for the main component

#### *Cu<sub>2</sub>cresbis* “A”

Deep brown solid. Yield: 210 mg (0.25 mmol, 90%).

*FAB-MS*: no relevant peaks

*Elemental analysis*: measured C 41.02, H 4.54, N 6.92 (14575)

calculated for C<sub>53</sub>H<sub>56</sub>N<sub>8</sub>O<sub>11</sub>Cu<sub>2</sub>B<sub>3</sub>F<sub>12</sub> · 7 H<sub>2</sub>O · 0.66 HBF<sub>4</sub>, MW 1551.5

C 41.03, H 4.52, N 7.22

*IR(KBr)*: 3436 br, 2955 m (CH<sub>2</sub>), 1734 s (C=O), 1628 m, 1608 w, 1474 m, 1450 m, 1264 s, 1084 vs (BF<sub>4</sub>), 869 w, 772 m

*UV-vis (MeOH)*: a broad shoulder at 470 nm

*CV(MeCN)*:  $E_a = -1024$  mV,  $E_c = -592$  mV (both irrev.) vs. Ag/0.01 M AgNO<sub>3</sub>

#### 9.2.2.2. Other copper(II)-complexes

##### 9.2.2.2.1. Cu<sub>2</sub>cresbis “B”

100 mg (97.5  $\mu$ mol) cresbis in 4 mL acetonitrile was mixed with 67.3 mg (97.5  $\mu$ mol) Cu(BF<sub>4</sub>)<sub>2</sub> · 6 H<sub>2</sub>O in 4 mL acetonitrile and the mixture stirred for 10 min at RT. Thereafter 27.8  $\mu$ L (195  $\mu$ mol) triethylamine was injected and the solution stirred at RT for 30 min. The solvent was completely evaporated and the remaining solid redissolved in 1 mL acetonitrile, and kept at 4°C overnight. The formed deep brown precipitate was filtered and was dried in vacuo. Yield: 148 mg (93.7  $\mu$ mol, 96%).

*ESI-MS*: 606.03 M/2 [Cu<sub>2</sub>(cresbisH<sub>1</sub>)(BF<sub>4</sub>)(H<sub>2</sub>O)]<sup>2+</sup>

*Elemental analysis*: measured C 44.74, H 5.18, N 8.08 (14679)

calculated for C<sub>53</sub>H<sub>56</sub>N<sub>8</sub>O<sub>11</sub>Cu<sub>2</sub>B<sub>3</sub>F<sub>12</sub> · 0.5TEAHBF<sub>4</sub> · 3H<sub>2</sub>O, MW 1516.05

C 44.76, H 4.58, N 7.86

*IR(KBr)*: 3438 br, 2972 w, 2952 m (CH<sub>2</sub>), 2678 w, 2492 w, 1736 vs (C=O), 1626 s, 1608 m, 1474 s, 1450 m, 1278 s, 1266 s, 1084 vs (BF<sub>4</sub>), 1062 vs, 776 m

*UV-vis (MeOH)*: no characteristic bands

9.2.2.2.2. Cu<sub>2</sub>cresbis “C”

60 mg (38.7 μmol) Cu<sub>2</sub>cresbis “A” was redissolved in acetonitrile and passed through a small size Pasteur-pipette filled with neutral alumina. The impurities flow through the column, while the complex is stacked on the top, which is then mobilized by addition of methanol. The strong brown band was collected, the solvent was evaporated and the remaining deep brown solid was dried in vacuo. Yield: 30.8 mg (24.0 μmol, 62%)

*ESI-MS*: 605.935 M/2 [Cu<sub>2</sub>(cresbisH<sub>1</sub>)(BF<sub>4</sub>)(OH<sub>2</sub>)]<sup>2+</sup>

*Elemental analysis*: measured C 49.72, H 5.02, N 9.04 (14754)

calculated for C<sub>53</sub>H<sub>56</sub>N<sub>8</sub>O<sub>11</sub>Cu<sub>2</sub>(BF<sub>4</sub>)(OH)<sub>2</sub> · 3 H<sub>2</sub>O, MW 1281.47:

C 49.65, H 4.95, N 8.74

*IR(KBr)*: 3422 br, 2952 w (CH<sub>2</sub>), 1734 vs (C=O), 1624 s, 1607 s, 1472 s, 1437s, 1257 br, 1084 m (BF<sub>4</sub>), 963 w, 868 w, 774 m

*UV-vis (MeOH)*: shoulder at 470 nm

9.2.2.2.3. Cu<sub>2</sub>cresbis “D”

60 mg (39.6 μmol) Cu<sub>2</sub>cresbis “B” was redissolved in acetonitrile and passed through a small size Pasteur-pipette filled with neutral alumina. The impurities flow through the column, while the complex is stacked on the top, which is then mobilized by addition of methanol. The strong brown band was collected, the solvent was evaporated and the remaining deep brown solid was dried in vacuo. Yield: 35.7 mg (22.2 μmol, 56%)

*ESI-MS*: 605.935 M/2 [Cu<sub>2</sub>(cresbisH<sub>1</sub>)(BF<sub>4</sub>)(OH<sub>2</sub>)]<sup>2+</sup>

*Elemental analysis*: measured C 48.59, H 5.75, N 8.90 (14753)

calculated for C<sub>53</sub>H<sub>56</sub>N<sub>8</sub>O<sub>11</sub>Cu<sub>2</sub>(BF<sub>4</sub>)<sub>3</sub> · 2 TEA · 2 H<sub>2</sub>O, MW 1609.16

C 48.51, H 6.19, N 8.71

*IR(KBr)*: 3433 br, 2948 m (CH<sub>2</sub>), 2738 w, 2678 m, 2491 m, 1734 vs (C=O), 1624 s, 1607 s, 1473 s, 1437 s, 1261 br, 1084 s, 1036 s, 869 w, 772 m

*UV-vis (MeOH)*: shoulder at 385 nm

*CV(MeCN)*: E<sub>a</sub> = -650 mV vs. Ag/0.01 M AgNO<sub>3</sub>

9.2.2.2.4. Cu<sub>2</sub>cresbis “E”

60 mg (38.7 μmol) Cu<sub>2</sub>cresbis “A” was redissolved in acetonitrile and passed through a basic alumina column, first eluted with acetonitrile to remove impurities, and then with methanol to collect the brown band. The solvent was evaporated and the remaining deep brown solid was dried in vacuo. Yield: 31.4 mg (25.6 μmol, 66%)

*ESI-MS / FAB-MS*: not informative

*Elemental analysis*: measured C 50.37, H 5.17, N 9.11 (14932)

calculated for  $C_{53}H_{56}N_8O_{11}Cu_2(OH)_3 \cdot 6 H_2O$ , MW 1230.15:

C 50.27, H 5.57, N 8.85

*IR(KBr)*: 3417 br, s, 3006 w, 2951 m, 2846 sh, 1733 vs (C=O), 1626 s, 1607 s, 1471 s, 1436 s, 1259 br, s, 1161 w, 1084 w, 964 w, 867 m, 774 m

*UV-vis (MeOH)*: no characteristic bands

*EPR(DMF/H<sub>2</sub>O = 2:1)*: completely silent

#### 9.2.2.2.5. *Cu(II)- bis(2-hydroxy-3-methoxybenzyl)amine complex*[ $Cu_2(N(PhO)_2)_2$ ]

To 100 mg (0.346 mmol) bis(2-hydroxy-3-methoxybenzyl)amine dissolved in 15 mL dry methanol was added 119.4 mg (0.346 mmol)  $Cu(BF_4)_2 \cdot 6 H_2O$  in 4 mL methanol. After 10 min stirring at RT, 98.7  $\mu$ L (0.692 mmol) triethylamine was injected to the reaction mixture, which resulted in the formation of a dark precipitate. After a further 1 h stirring, the dark brown solid was filtered off, washed with methanol, and dried in vacuo. Yield: 116 mg (0.331 mmol, 96%)

*FAB-MS*: 703.8 [ $Cu_2(LH_2)_2+H$ ]<sup>+</sup>

*Elemental analysis*: measured C 54.46, H 4.94, N 4.04 (15790)

calculated for  $C_{16}H_{17}NO_4Cu$ , MW 350.83:

C 54.77, H 4.88, N 3.99

*IR(KBr)*: 3432 br, s (OH), 3236 sh, 3104 br, 3060 sh, 3022 w, 2998 w, 2912 w, 2862 w, 2836 m, 1594 m, 1568 s, 1484 vs, 1464 sh, 1440 m, 1350 m, 1278 vs, 1240 vs, 1194 w, 1142 w, 1088 s, 1036 m, 1002 m, 946 m, 890 m, 842 m, 736 s

### 9.2.3. Synthesis of the vanadium complexes

#### 9.2.3.1. [ $V^{IV}=O(N_2py_2)ClO_4$ ]<sub>2</sub>

0.6080 g (3.3429 mmol)  $V_2O_5$  was given to 150 ml methanol to obtain a deep yellow suspension, which was refluxed overnight. The formed green suspension was filtered off, and from the amount of the solid unreacted  $V_2O_5$  the yield of the formed  $VO(OEt)_3$  was calculated to be 0,5157 g (5.67 mmol, 84.8%). To this hot solution a solution of 2.485 g (5.67 mmol)  $N_2py_2$  in 100 mL hot ethanol was added. The yellowish/greenish mixture was refluxed for 20 h, then 1.593 g (11.34 mmol)  $NaClO_4$  was added and the solution was kept at 4°C overnight. The formed precipitate was filtered off, washed with small portions of cold ethanol and dried in vacuo. Yield: 260 mg (0.37 mmol, 7%)

*ESI-MS(MeOH)*: 521.3  $[\text{V}^{\text{IV}}=\text{O}(\text{N}2\text{py}2)(\text{OH})]^+$ , 539.3  $[\text{V}^{\text{IV}}=\text{O}(\text{N}2\text{py}2)(\text{OH})(\text{OH}_2)]^+$ , 553.3  $[\text{V}^{\text{IV}}=\text{O}(\text{N}2\text{py}2)(\text{OH})(\text{MeOH})]^+$

*Elemental analysis*: measured C 39.30, H 4.07, N 8.30 (17297)

calculated for  $\text{C}_{23}\text{H}_{26}\text{N}_4\text{O}_{14}\text{Cl}_2\text{V}$ , MW 704.34:

C 39.22, H 3.72, N 7.96

*IR(KBr)*: 3436 s, br, 3078 w (CH), 2974 ( $\text{CH}_2$ ), 1734 (C=O), 1604 m, 1474 m, 1444 m, 1270 m, 1090 ( $\text{ClO}_4$ ), 964 m, 780 m, 624 m

*UV-vis (MeOH)*: 370 nm ( $\epsilon = 910$ ), 470 nm ( $\epsilon = 350$ , sh), 590 nm ( $\epsilon = 190$ ), 680 nm ( $\epsilon = 190$ )

*EPR* (in DMF/ $\text{H}_2\text{O}$  2:1):  $g_{zz} = 1.943$ ,  $g_{yy} = g_{xx} = 1.977$ ,  $A_{zz} = -166$ ,  $A_{yy} = A_{xx} = -60$

### 9.2.3.2. $[\text{V}^{\text{IV}}=\text{O}(\text{N}2\text{py}2\text{PhO})]\text{Cl} \cdot \text{TEAHCl} \cdot 2.5 \text{H}_2\text{O}$

To 50 mL acetonitrile solution of 500 mg (0.942 mmol) N2py2PhOH was added 239 mg (0.942 mmol)  $\text{VO}_2\text{SO}_4$  in 40 mL acetonitrile, followed by 131.1  $\mu\text{L}$  (0.942 mmol) triethylamine. The reaction mixture was refluxed for 1 h, and the color of the solution turns deep green. When the solution cooled down, 200 mL water was added and the mixture was transferred to a CM Sephadex C-25 ion-exchange column. The blue band eluted by using 0.1 M NaCl was collected. Yield: 513 mg (0.630 mmol, 67%)

*ESI-MS(MeOH)*: 596.4  $[\text{V}^{\text{IV}}=\text{O}(\text{N}2\text{py}2\text{PhO})]^+$ , 614.4  $[\text{V}^{\text{IV}}=\text{O}(\text{N}2\text{py}2\text{PhO})(\text{H}_2\text{O})]^+$ , 628.4  $[\text{V}^{\text{IV}}=\text{O}(\text{N}2\text{py}2\text{PhO})(\text{MeOH})]^+$

*Elemental analysis*: measured C 51.47, H 5.97, N 8.79, Cl 8.83 (17422)

calculated for  $\text{C}_{35}\text{H}_{50}\text{N}_5\text{O}_{9.5}\text{Cl}_2\text{V}$ , MW 814.65:

C 51.60, H 6.18, N 8.60, Cl 8.71

*IR(KBr)*: 3422 br, s, 3070 w, 2980 w, 2950 w, 2676 m, 2624 m, 2498 w, 1734 vs (C=O), 1606 s, 1482 s, 1458 s, 1274 vs, 1100 vs, 974 s, 770 m, 622 m

*UV-vis (MeOH)*: 386 nm ( $\epsilon = 305$ ), 571 nm ( $\epsilon = 65$ ), 766 nm ( $\epsilon = 15$ , sh)

*EPR* (in DMF/ $\text{H}_2\text{O}$  2:1):  $g_{zz} = 1.947$ ,  $g_{yy} = 1.972$ ,  $g_{xx} = 1.979$ ,  $A_{zz} = -158$ ,  $A_{yy} = -55$ ,  $A_{xx} = -54$

### 9.2.3.3. $[\text{V}^{\text{V}}=\text{O}(\text{O}_2)(\text{N}2\text{py}2\text{PhO})]\text{Cl} \cdot 4 \text{TEAHCl} \cdot 4.5 \text{H}_2\text{O}$

To 211 mg (0.259 mmol)  $[\text{V}^{\text{IV}}=\text{O}(\text{N}2\text{py}2\text{PhO})]\text{Cl} \cdot \text{TEAHCl} \cdot 2.5 \text{H}_2\text{O}$  dissolved in 40 mL MeOH was added 3.4 g 30%(w/w)  $\text{H}_2\text{O}_2$  solution. The reaction mixture was stirred for 1 week at RT, and a color change to orange was observed. After dilution with water the mixture was transferred to a CM Sephadex C-25 ion-exchange column, and the main orange band was collected by using 0.1 M NaCl as eluent. Yield: 114 mg (88  $\mu\text{mol}$ , 34%)

*ESI-MS*: 629.3  $[\text{V}^{\text{V}}=\text{O}(\text{O}_2)(\text{N}2\text{py}2\text{PhO})]^+$ , 647.4  $[\text{V}^{\text{V}}=\text{O}(\text{O}_2)(\text{N}2\text{py}2\text{PhO})(\text{H}_2\text{O})]^+$



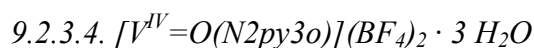
*Elemental analysis:* measured C 49.09, H 7.35, N 8.66, Cl 13.67 (17701)

calculated for  $\text{C}_{53}\text{H}_{103}\text{N}_8\text{Cl}_5\text{O}_{13.5}\text{V}$ , MW 1296.65:

C 49.09, H 8.00, N 8.64, Cl 13.67

*IR(KBr):* 3430 br, s, 2977 w, 2942 w, 2678 m, 2623 w, 2604 w, 2495 m, 1734 m, 1607 m, 1473 m, 1442 m, 1279 m, br, 1261 m, br, 1106 w, 1036 w, 959 w

*UV-vis (MeOH):* 431 nm ( $\epsilon = 240$ )



The reaction was performed in a similar fashion to that of  $[\text{V}^{\text{IV}}=\text{O}(\text{N}_2\text{py}_3\text{o})](\text{ClO}_4)_2 \cdot 3 \text{ H}_2\text{O}$  but using 0.1 M  $\text{NaBF}_4$  as eluent. Yield: 34%

*ESI-MS:* 291.5 M/2  $[\text{V}^{\text{IV}}=\text{O}(\text{N}_2\text{py}_3\text{o})]^{2+}$ , 300.4 M/2  $[\text{V}^{\text{IV}}=\text{O}(\text{N}_2\text{py}_3\text{o})(\text{H}_2\text{O})]^{2+}$ , 599.4 M  $[\text{V}^{\text{IV}}=\text{O}(\text{N}_2\text{py}_3\text{o})(\text{OH})]^+$

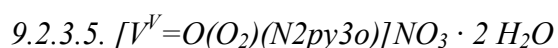
*Elemental analysis:* measured C 41.37, H 4.44, N 8.57 (17561)

calculated for  $\text{C}_{28}\text{H}_{35}\text{N}_5\text{O}_9\text{B}_2\text{F}_8\text{V}$ , MW 810.13:

C 41.50, H 4.35, N 8.65

*IR(KBr):* 3432, br, s, 3112 w, 2962 w, 1732 s, 1608 m, 1482 m, 1438 s, 1284 s, 1258 s, 1060 vs, 776 m, 658 m

*UV-vis (MeOH):* 363 nm ( $\epsilon = 290$ ), 514 nm ( $\epsilon = 30$ ), 695 nm ( $\epsilon = 29$ )



The reaction was performed in a similar fashion to that of  $[\text{V}^{\text{V}}=\text{O}(\text{O}_2)(\text{N}_2\text{py}_3\text{o})]\text{ClO}_4 \cdot 2 \text{ H}_2\text{O}$  but using 0.1 M  $\text{NaNO}_3$  as eluent. Yield: 28%

*ESI-MS(+):* 614.3  $[\text{V}^{\text{V}}=\text{O}(\text{O}_2)(\text{N}_2\text{py}_3\text{o})]^+$ , 632.4  $[\text{V}^{\text{V}}=\text{O}(\text{O}_2)(\text{N}_2\text{py}_3\text{o})(\text{H}_2\text{O})]^+$ , 646.4  $[\text{V}^{\text{V}}=\text{O}(\text{O}_2)(\text{N}_2\text{py}_3\text{o})(\text{MeOH})]^+$

*ESI-MS(-):* 738.2  $[\text{V}^{\text{V}}=\text{O}(\text{O}_2)(\text{N}_2\text{py}_3\text{o})(\text{NO}_3)_2]^-$ , 756.2  $[\text{V}^{\text{V}}=\text{O}(\text{O}_2)(\text{N}_2\text{py}_3\text{o})(\text{NO}_3)_2(\text{H}_2\text{O})]^-$ , 770.2  $[\text{V}^{\text{V}}=\text{O}(\text{O}_2)(\text{N}_2\text{py}_3\text{o})(\text{NO}_3)_2(\text{MeOH})]^-$

*Elemental analysis:* measured C 47.02, H 4.56, N 12.62 (17593)

calculated for  $\text{C}_{28}\text{H}_{33}\text{N}_6\text{O}_{13}\text{V}$ , MW 712.51:

C 47.20, H 4.67, N 11.80

*IR(KBr):* 3430 br, s, 3070 w, 2956 m, 1730 vs, 1606 s, 1480 m, 1436 m, 1384 s, 1278 m, 1250 m, 1204 w, 1158 m, 1106 m, 1060 s, 1032 m, 1006 w, 961 s, 937 m, 923 w, 830 w, 788 m, 674 m, 657 m, 585 m, 527 w

*UV-vis (MeOH):* 450 nm ( $\epsilon = 350$ , sh)

9.2.3.6.  $[V^{V}=O(^{18}O_2)(N_2py_3o)]ClO_4 \cdot 2 H_2O$ 

The reaction was performed in a similar fashion to that of  $[V^V=O(O_2)(N_2py_3o)]ClO_4 \cdot 2 H_2O$ , but using 2%  $H_2^{18}O_2$  as oxidant. Yield: 13%

*IR(KBr)*: 3422 s, br, 3120 w, 2958 w, 2852 w, 1734 vs, 1608 m, 1482 m, 1436 m, 1282 s, 1252 s, 1098 vs, 1036 sh, 1012 m, 964 m, 936 w, 914 w, 886 m, 786 m, 772 m, 624 s.

9.2.3.7.  $[V^{V}=O(^{18}O_2)(N_2py_3o)]NO_3 \cdot 2 H_2O$ 

The reaction was performed in a similar fashion to that of  $[V^V=O(O_2)(N_2py_3o)]NO_3 \cdot 2 H_2O$ , but using 2%  $H_2^{18}O_2$  as oxidant. Yield: 16%

*IR(KBr)*: 3420 br, s, 3080 br, m, 2952 m, 2852w, 1732 s, 1608 m, 1480 w, 1436 m, 1384 vs, 1278 s, 1250 s, 1162 m, 1106 m, 1060 s, 1034 m, 1012 w, 962 m, 938 m, 886 s, 786 m, sh, 776 sh, 758 m, 674 m, 658 m, 584 m, 517 m

**9.2.4. Synthesis of the cobalt complexes**9.2.4.1.  $[Co^{II}(N_2py_2PhO)(OH_2)]ClO_4 \cdot 2 H_2O$ 

To a dry methanolic solution (20 mL) of 130 mg (0.243 mmol)  $N_2py_2PhOH$  was added 88.9 mg (0.243 mmol)  $Co(ClO_4)_2 \cdot 6 H_2O$  in 5 mL MeOH. Finally 34.6  $\mu L$  (0.243 mmol) triethylamine was added, and the color of the solution turned a more intense pink. After stirring at RT for 20 min, the solvent was completely removed and treated with small amount of water, which resulted in formation of a dark brown precipitate, which was filtered off and washed with water. Drying in vacuo gives a fine pink powder. Yield: 144 mg (0.197 mmol, 81%).

*FAB-MS*: 588.6  $[Co^{II}(N_2py_2PhO)]^+$ , 606.6  $[Co^{II}(N_2py_2PhO)(OH_2)]^+$ , 620.6  $[Co^{II}(N_2py_2PhO)(MeOH)]^+$

*Elemental analysis*: measured C 47.31, H 4.83, N 7.46 (16184)

calculated for  $C_{29}H_{35}N_4O_{13}ClCo$ , MW 741.96:

C 46.94, H 4.75, N 7.55

*IR(KBr)*: 3474 br, s (OH), 2950 w ( $CH_2$ ), 2834 w (CH), 1720 vs (C=O), 1606 s, 1478 s, 1450 s, 1272 vs, 1084 vs ( $ClO_4$ ), 1020 s, 974 m, 790 s, 764 s, 622 m

*UV-vis (MeOH)*: 480 nm ( $\epsilon = 147$ ), 519 nm ( $\epsilon = 118$ ), 553 ( $\epsilon = 121$ )

*CV(MeCN)*:  $E_{1/2} = 75$  mV vs.  $Ag/0.01$  M  $AgNO_3$  ( $\Delta E$  increases from 215 mV to 500 mV with time)



9.2.4.2.  $[Co^{III}(N2py2PhOH)(Cl)]Cl_2 \cdot 5.5 H_2O$ 

169 mg (0.228 mmol)  $[Co^{II}(N2py2PhO)(OH_2)]ClO_4 \cdot 2 H_2O$  was dissolved in 25 mL MeOH and to this solution was added 800 mL 30%  $H_2O_2$  (7.76 mmol, 34 eq), and was stirred for 1 h at RT. After this, the reaction mixture was diluted with water (200 mL) and transferred to Dowex 50 column. The product was separated by washing the column with 1 M HCl. The main dark brown band was collected and completely evaporated. Yield: 137 mg (0.160 mmol, 70%).

*ESI-MS*: 623.3  $[Co^{III}(N2py2PhO)(Cl)]^+$ , 641.3  $[Co^{III}(N2py2PhO)(Cl)(OH_2)]^+$

*Elemental analysis*: measured C 43.85, H 4.99, N 7.27 (16812)

calculated for  $C_{29}H_{40}N_4O_{11.5}Cl_3Co$ , MW 793.92:

C 43.87, H 5.07, N 7.06

*IR(KBr)*: 3384 br, s (OH), 2954 w (CH<sub>2</sub>), 1734 s (C=O), 1608 m, 1478 m, 1452 m, 1274 s, 1062 m, 954 m, 774 m

*UV-vis (MeOH)*: 394 nm ( $\epsilon = 1400$ ), 557 nm ( $\epsilon = 860$ )

<sup>1</sup>H-NMR(D<sub>2</sub>O): 8.54 (2H, br, H<sub>py- $\alpha$</sub> ), 8.03 (2H, br, py-H), 7.64 (1H, d, <sup>3</sup>J = 7.95 Hz, phenol-H), 7.58 (4H, br, py-H), 7.30 (1H, t, <sup>3</sup>J = 7.7 Hz, phenol-H), 7.00 (1H, d, <sup>3</sup>J = 7.4 Hz, phenol-H), 6.82 (1H, t, <sup>3</sup>J = 7.4 Hz, phenol-H), 5.37 (2H, s, br, N-CH), 3.63 (8H, s, br, NCH<sub>2</sub>C<sub>6</sub>H<sub>4</sub>OH + OCH<sub>3</sub>), 2.52 (4H, s, br, NCH<sub>2</sub>), 2.24 (3H, s, br, NCH<sub>3</sub>)

9.2.4.3.  $[Co^{II}(N2py2Bz)(OH_2)_2](ClO_4)_2 \cdot 1.5 H_2O$ 

1.00 g (1.94 mmol) of N2py2Bz in 30 mL methanol was mixed with 0.71 g (1.94 mmol)  $Co(ClO_4) \cdot 6 H_2O$  in 10 mL methanol, and was stirred for 1 h at room temperature. After partial solvent removal a pink precipitate was formed, which was filtered off and dried. Yield: 1.58 g (1.88 mmol, 97%)

*FAB(+)-MS*: 672.4  $[Co^{II}(N2py2Bz)(ClO_4)]^+$ , 690.4  $[Co^{II}(N2py2Bz)(OH_2)(ClO_4)]^+$

*Elemental analysis*: measured C 41.61, H 4.55, N 6.58 (18015)

calculated for  $C_{29}H_{37}N_4O_{16.5}Cl_2Co$ , MW 835.44:

C 41.69, H 4.46, N 6.71

*IR(KBr)*: 3431 (br,s), 3030 (w), 2954 (m), 2852 (w), 1734 (s), 1636 (s), 1606 (m), 1471 (m, sh), 1448 (s), 1090 (vs), 963 (sh, m), 767 (m), 758 (m), 626 (s)

9.2.4.4.  $[Co^{II}(N2py2a)(OH_2)_2](ClO_4)_2 \cdot 4 H_2O$

The title complex was prepared by addition 10 eq  $\text{H}_2\text{O}_2$  into a solution containing 15 mg  $[\text{Co}^{\text{II}}(\text{N}2\text{py}2)(\text{OH}_2)_2](\text{ClO}_4)_2$  in 0.8 mL methanol. Pink crystals suitable for X-ray studies were formed after 5 days from ether diffusion.

*ESI-MS*: 546.3  $[\text{Co}^{\text{II}}(\text{N}2\text{py}2\text{aH}_1)(\text{MeOH})_2]^+$ , 614.3  $[\text{Co}^{\text{II}}(\text{N}2\text{py}2\text{a})(\text{MeOH})(\text{ClO}_4)]^+$ , 273.9,  $[\text{Co}^{\text{II}}(\text{N}2\text{py}2\text{a})(\text{MeOH})_2]^{2+}$ , 289.9  $[\text{Co}^{\text{II}}(\text{N}2\text{py}2\text{a})(\text{MeOH})_3]^{2+}$

*Elemental analysis*: measured C 34.99, H 4.30, N 7.11 (17997)

calculated for  $\text{C}_{22}\text{H}_{34}\text{N}_4\text{O}_{17}\text{Cl}_2\text{Co}$ , MW 754.36:

C 35.03, H 4.27, N 7.43

*UV-vis (MeOH)*: ( $\lambda_{\text{max}}/\text{nm}$ ) 456, 496, 534

*Crystal structure*: co\_mt3

#### 9.2.4.5. Preparation and crystallization of $[\text{Co}^{\text{III}}(\text{N}2\text{py}2\text{a})(\text{Cl})(\text{OH}_2)](\text{ClO}_4)_2$

14.7 mg (21.61  $\mu\text{mol}$ )  $[\text{Co}^{\text{III}}(\text{N}2\text{py}2\text{a})(\text{Cl})_2]\text{ClO}_4 \cdot 1.5 \text{H}_2\text{O}$  was dissolved in 3 mL water. To this solution was added 8.9 mg  $\text{AgClO}_4$  (43.2  $\mu\text{mol}$ ) in 1 mL water, which was then left under stirring in the dark overnight. The  $\text{AgCl}$  was removed by filtration and the clear solution fully evaporated. 0.75 mL methanol was then added to the solid, after which it was treated with 30 eq (61.6  $\mu\text{L}$ ) 30%  $\text{H}_2\text{O}_2$ . Crystals were grown by ether diffusion (violet needles, obtained after 2 days).

*Crystal structure*: co\_mt4

### 9.2.5. Synthesis of the manganese complexes

#### 9.2.5.1. General method for the preparation of manganese(II)-chloro complexes

To a heated methanolic solution (80 mL) of 3.88 mmol ligand was added 0.76 g (3.88 mmol)  $\text{MnCl}_2 \cdot 4 \text{H}_2\text{O}$  in 160 mL MeOH, and refluxed for 20 min. The solvent was completely removed by rotary evaporation, and a small amount of abs. ethanol was added to the sticky solid. If no precipitate was formed, the solvent was evaporated, and ethanol was added again. Addition and removal of ethanol was repeated until a white solid could be separated. The precipitate was filtered off, washed with cold ethanol, and dried under vacuum.

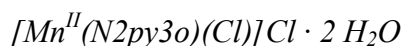
$[\text{Mn}^{\text{II}}(\text{N}2\text{py}2)(\text{Cl})_2] \cdot 2 \text{H}_2\text{O}$  <sup>180</sup>

Yield: 1.44 g (2.41 mmol, 62%).

*Elemental analysis*: measured C 46.71, H 5.35, N 8.98 (12540)

calculated for  $\text{C}_{23}\text{H}_{30}\text{N}_4\text{O}_7\text{Mn}$ , MW 600.37:

C 46.00, H 5.03, N 9.33



Yield: 2.00 g (2.95 mmol, 76%)

FAB-MS: 307.1 M/2  $[\text{Mn}^{\text{II}}(\text{N}2\text{py}3\text{o})(\text{H}_2\text{O})_2]^{2+}$ , 623.3 M  $[\text{Mn}^{\text{II}}(\text{N}2\text{py}3\text{o})(\text{Cl})(\text{H}_2\text{O})]^+$

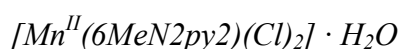
Elemental analysis: measured C 49.45, H 4.98, N 10.25 (12592)

calculated for  $\text{C}_{28}\text{H}_{33}\text{N}_5\text{O}_7\text{Cl}_2$ , MW 677.41:

C 49.64, H 4.91, N 10.34

IR(KBr): >3000 (Py, CH), 2938 w ( $\text{CH}_2$ ), 2832 m (CH), 1736 s (C=O), 1602 s (v-8a-py), 1446 s ( $\text{CH}_2$ ), 1044 s (C-OH), 772 ( $\text{C}_{\text{ar}}\text{-H}$ , 4H neighbouring)

Crystal structure (co220)



Yield: 1.56 g (2.56 mmol, 66%)

FAB-MS: 556.4  $[\text{Mn}^{\text{II}}(6\text{MeN}2\text{py}2)(\text{Cl})]^+$ , 588.4  $[\text{Mn}^{\text{II}}(6\text{MeN}2\text{py}2)(\text{Cl})(\text{MeOH})]^+$

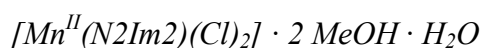
Elemental analysis: measured C 49.34, H 5.29, N 9.17 (12900)

calculated for  $\text{C}_{25}\text{H}_{32}\text{N}_4\text{O}_6\text{Cl}_2\text{Mn}$ , MW 608.37:

C 49.35, H 5.30, N 9.21

IR(KBr): 3068 w, 3010 w (Py-H), 2924 w ( $\text{CH}_2$ ), 2830 w (CH), 1734 s (C=O), 1603 s (n-8a-py), 1462 s ( $\text{CH}_2$ ), 1262 (C-OMe), 796 s ( $\text{C}_{\text{ar}}\text{-H}$ , 4H neighbouring)

Crystal structure (co223)



Yield: 1.87 g (2.87 mmol, 74%)

FAB-MS: 534.3  $[\text{Mn}^{\text{II}}(\text{N}2\text{Im}2)(\text{Cl})]^+$ , 552.4  $[\text{Mn}^{\text{II}}(\text{N}2\text{Im}2)(\text{Cl})(\text{OH}_2)]^+$ , 566.6  $[\text{Mn}^{\text{II}}(\text{N}2\text{Im}2)(\text{Cl})(\text{MeOH})]^+$

Elemental analysis: measured C 42.65, H 5.62, N 12.96 (12899)

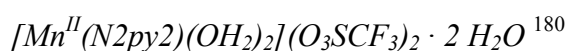
calculated for  $\text{C}_{23}\text{H}_{38}\text{N}_6\text{O}_8\text{Cl}_2\text{Mn}$ , MW 652.41:

C 42.34, H 5.86, N 12.88

IR(KBr): 3116 w, 2994 w, 2954 w ( $\text{CH}_2$ ), 2891 w, 2828 w (CH), 1730 s (C=O), 1635 s (imidazole), 1497 m, 1443 s, 1262 s (C-OMe), 1068 m, 770 w ( $\text{C}_{\text{ar}}\text{-H}$ )

9.2.5.2. *General procedure for the preparation of the triflate salts of manganese(II) aqua complexes*

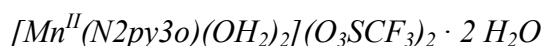
To a solution of 1.33 mmol dichloro Mn(II) complex in dry acetonitrile (250 mL) was added 2.66 mmol silver-triflate dissolved in 8 mL dry acetonitrile, the mixture was stirred for 90 min in darkness at room temperature. The formed AgCl precipitate was filtered off by glass filter and the eluate was concentrated in vacuo. If more precipitate appeared, it was removed by repeated filtration. The filtrate was concentrated and the remaining solid was dried in vacuo.



Yield: 1.09 g (1.26 mmol, 95%)

FAB-MS: 642.3  $[\text{Mn}^{\text{II}}(\text{N}2\text{py}2)(\text{O}_3\text{SCF}_3)]^+$ , 660.3  $[\text{Mn}^{\text{II}}(\text{N}2\text{py}2)(\text{O}_3\text{SCF}_3)(\text{OH}_2)]^+$ , 688.4  $[\text{Mn}^{\text{II}}(\text{N}2\text{py}2)(\text{O}_3\text{SCF}_3)(\text{EtOH})]^+$

Elemental analysis: measured C 34.48, H 3.84, N 6.49 (12620)  
calculated for  $\text{C}_{25}\text{H}_{34}\text{N}_4\text{O}_{15}\text{S}_2\text{F}_6\text{Mn}$ , MW 863.63:  
C 34.77, H 3.96, N 6.49

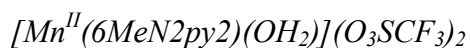


Yield: 1.20 g (1.28 mmol, 96%)

FAB-MS: 719.2  $[\text{Mn}^{\text{II}}(\text{N}2\text{py}3\text{o})(\text{O}_3\text{SCF}_3)]^+$ , 737.2  $[\text{Mn}^{\text{II}}(\text{N}2\text{py}3\text{o})(\text{O}_3\text{SCF}_3)(\text{OH}_2)]^+$

Elemental analysis: measured C 38.54, H 3.60, N 7.72 (12683)  
calculated for  $\text{C}_{30}\text{H}_{37}\text{N}_5\text{O}_{11}\text{S}_2\text{F}_6\text{Mn}$ , MW 940.66:  
C 38.30, H 3.96, N 7.45

IR(KBr): >3000 (Cpy-H), 2958 w (CH<sub>2</sub>), 2910 w (CH), 1738 s (C=O), 1604 s (ν-8a, py), 1448 s (CH<sub>2</sub>), 1276, 1030 (SO<sub>3</sub>); 1254, 1156 (CF<sub>3</sub>), 762 (C<sub>ar</sub>-H, 4H neighbouring)

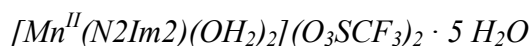


Yield: 1.01 g (1.21 mmol, 91%)

FAB-MS: 670.4  $[\text{Mn}^{\text{II}}(6\text{MeN}2\text{py}2)(\text{O}_3\text{SCF}_3)]^+$ , 688.4  $[\text{Mn}^{\text{II}}(6\text{MeN}2\text{py}2)(\text{O}_3\text{SCF}_3)(\text{OH}_2)]^+$ , 702.4  $[\text{Mn}^{\text{II}}(6\text{MeN}2\text{py}2)(\text{O}_3\text{SCF}_3)(\text{MeOH})]^+$

Elemental analysis: measured C 38.66, H 4.00, N 7.09 (12918)  
calculated for  $\text{C}_{27}\text{H}_{32}\text{N}_4\text{O}_{12}\text{S}_2\text{F}_6\text{Mn}$ , MW 835.70:  
C 38.80, H 3.86, N 6.71

IR(KBr): >3000 (Cpy-H), 2957 (CH<sub>2</sub>), 1734 s (C=O), 1606 s (ν-8a, py), 1465 s (CH<sub>2</sub>), 1272, 1027 (SO<sub>3</sub>); 1252, 1161 (CF<sub>3</sub>); 758 (C<sub>ar</sub>-H, neighbouring)



Yield: 1.00 g (1.13 mmol, 85%)

*FAB-MS*: 648.7  $[\text{Mn}^{\text{II}}(\text{N2Im2})(\text{O}_3\text{SCF}_3)]^+$ , 666.7  $[\text{Mn}^{\text{II}}(\text{N2Im2})(\text{O}_3\text{SCF}_3)(\text{OH}_2)]^+$

*Elemental analysis*: measured C 31.50, H 3.86, N 9.22 (12942)

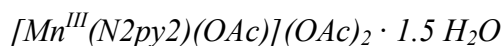
calculated for  $\text{C}_{23}\text{H}_{38}\text{N}_6\text{O}_{16}\text{S}_2\text{F}_6\text{Mn}$ , MW 887.73:

C 31.12, H 4.31, N 9.47

*IR(KBr)*: >3000 (Cpy-H), 2960 (CH<sub>2</sub>), 2902 w (CH), 1733 s (C=O), 1635 (imidazole), 1501 (imidazole), 1465 s (CH<sub>2</sub>), 1268, 1030 (SO<sub>3</sub>); 1255, 1161 (CF<sub>3</sub>); 76 (C<sub>ar</sub>-H, neighbouring)

### 9.2.5.3. General procedure for the synthesis of the Mn(III)-acetate complexes

4.56 mmol ligand in 80 mL dry methanol was warmed almost to boiling point, whereafter the ligand is completely dissolved. 1.22 g (4.56 mmol)  $\text{Mn}(\text{OAc})_3 \cdot 2 \text{H}_2\text{O}$  was added in small portions to the hot solution. After 20 min reflux the unreacted Mn-salts were removed by filtration, and the filtrate was dried in vacuo.



Yield: 2.64 g (3.78 mmol, 83%)

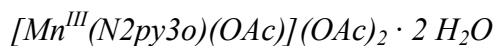
*FAB-MS*: 552.3  $[\text{Mn}^{\text{III}}(\text{N2py2})(\text{OAc})]^+$ , 570.3  $[\text{Mn}^{\text{III}}(\text{N2py2})(\text{OAc})(\text{OH}_2)]^+$ , 1061.6  $[(\text{Mn}^{\text{III}}(\text{N2py2}))_2(\text{OAc})(\text{OH})]^+$ , 1079.6  $[(\text{Mn}^{\text{III}}(\text{N2py2}))_2(\text{OAc})(\text{OH})(\text{OH}_2)]^+$

*Elemental analysis*: measured C 50.09, H 5.62, N 8.14 (13010)

calculated for  $\text{C}_{29}\text{H}_{38}\text{N}_4\text{O}_{12.5}\text{Mn}$ , MW 697.57:

C 49.92, H 5.49, N 8.03

*IR(KBr)*: 2997 w, 2950 w, 2871 w, 2826 w, 1728 vs (C=O), 1600 s (Py), 1565 s, 1559 s (OAc), 1434 s, 1429 s (CH<sub>2</sub>), 1270, 1252 s (OAc); 781 s (C<sub>ar</sub>-H)



Yield: 3.06 g (3.92 mmol, 86%)

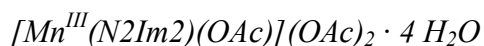
*FAB-MS*: 629.4  $[\text{Mn}^{\text{III}}(\text{N2py3o})(\text{OAc})]^+$

*Elemental analysis*: measured C 51.57, H 5.55, N 8.86 (13022)

calculated for  $\text{C}_{34}\text{H}_{42}\text{N}_5\text{O}_{13}\text{Mn}$ , MW 783.63:

C 51.77, H 5.40, N 8.94

*IR(KBr)*: 3093 w, 3064 w, 2951 w, 2916 w (CH), 1728 s (C=O), 1602 s (py), 1576 s, 1433 s (CH<sub>2</sub>), 1408 s, 1282 s, 1252 s, 1076 m, 1044 m, 1016 m, 785 m, 770 s (C<sub>ar</sub>-H)

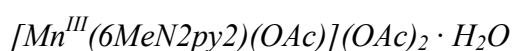


Yield: 2.45 g (3.28 mmol, 72%)

*FAB-MS*: 558.3  $[\text{Mn}^{\text{III}}(\text{N2Im2})(\text{OAc})]^+$ , 576.3  $[\text{Mn}^{\text{III}}(\text{N2Im2})(\text{OAc})(\text{OH}_2)]^+$ , 1073.7  $[(\text{Mn}^{\text{III}}(\text{N2Im2}))_2(\text{OAc})(\text{OH})]^+$

*Elemental analysis*: measured C 43.65, H 5.91, N 11.09 (13035)  
 calculated for  $\text{C}_{27}\text{H}_{45}\text{N}_6\text{O}_{15}\text{Mn}$ , MW 748.00:  
 C 43.32, H 6.05, N 11.23

*IR(KBr)*: 2990 w, 2954 w ( $\text{CH}_2$ ), 1730 s ( $\text{C}=\text{O}$ ), 1569 s, 1559 s, 1496 s, 1435 s, 1419 s, 1280 s, 1254 s (OAc), 1077 m, 1044 m, 1017 w, 957 w, 772 m ( $\text{C}_{\text{ar}}\text{-H}$ )

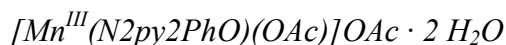


Yield: 2.44 g (3.42 mmol, 75%)

*FAB-MS*: 580.3  $[\text{Mn}^{\text{III}}(6\text{MeN2py2})(\text{OAc})]^+$ , 598.3  $[\text{Mn}^{\text{III}}(6\text{MeN2py2})(\text{OAc})(\text{OH}_2)]^+$

*Elemental analysis*: measured C 52.29, H 6.28, N 8.12 (13044)  
 calculated for  $\text{C}_{31}\text{H}_{41}\text{N}_4\text{O}_{12}\text{Mn}$ , MW 714.59:  
 C 52.10, H 5.77, N 7.84

*IR(KBr)*: 3058 w, 2990 w, 2953 w, 2927 w ( $\text{CH}$ ), 1730 s ( $\text{C}=\text{O}$ ), 1576 s, 1542 m, 1456 s, 1433 s, 1404 m, 1280 s, 1253 s (OAc), 1163 m, 1049 m, 795 m ( $\text{C}_{\text{ar}}\text{-H}$ ), 652 m



Yield: 2.64 g (3.57 mmol, 92%)

*FAB-MS*: 584.4  $[\text{Mn}^{\text{III}}(\text{N2py2PhO})]^+$ , 602.5  $[\text{Mn}^{\text{III}}(\text{N2py2PhO})(\text{OH}_2)]^+$

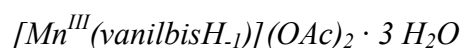
*Elemental analysis*: measured C 53.60, H 5.59, N 7.59 (13838)  
 calculated for  $\text{C}_{33}\text{H}_{39}\text{N}_4\text{O}_{12}\text{Mn}$ , MW 738.58:  
 C 53.66, H 5.32, N 7.59

*IR(KBr)*: 3422 br, 3066 w, 2954 w ( $\text{CH}_2$ ), 2844 w ( $\text{CH}$ ), 1732 s ( $\text{C}=\text{O}$ ), 1602 m, 1434 m, 1278 s, 1258 m, 1158 m, 1018 m, 766 s

*UV-vis (MeOH)*: only shoulder, no characteristic bands

*CV(MeCN)*: +37 mV vs. Ag/0.01 M  $\text{AgNO}_3$

*EPR* (in DMF/ $\text{H}_2\text{O}$  2:1):  $g = 2.006$ , A: 89, D: 75



In this reaction 0.178 mmol vanilbis and manganese(III) acetate was used. Yield: 100 mg (0.126 mmol, 71%)

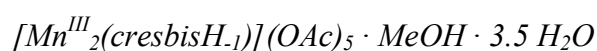
*FAB-MS*: 614.5  $[\text{Mn}^{\text{III}}(\text{vanilbisH}_1)]^+$

*Elemental analysis*: measured C 51.73, H 5.53, N 6.54 (14581)

calculated for  $\text{C}_{34}\text{H}_{43}\text{N}_4\text{O}_{14}\text{Mn}$ , MW 786.62:

C 51.91, H 5.50, N 7.09

*IR(KBr)*: 3422 br, s (OH), 3072 w, 3002 w, 2952 m ( $\text{CH}_2$ ), 2842 m, 1730 vs ( $\text{C}=\text{O}$ ), 1602 s, 1566 s, 1480 s, 1434 s, 1252 vs, 1080 s, 1018 s, 778 m, 652 w



In this reaction 150 mg (0.150 mmol) cresbis and 80.5 mg (0.300 mmol) manganese(III) acetate was used. Yield: 180 mg (0.123 mmol, 82%)

*FAB-MS*: no peaks found

*Elemental analysis*: measured C 51.92, H 5.47, N 7.57 (14576)

calculated for  $\text{C}_{64}\text{H}_{81}\text{N}_8\text{O}_{24.5}\text{Mn}$ , MW 1480.1:

C 51.93, H 5.51, N 7.57

*IR(KBr)*: 3422 br, 3002 w, 2952 m ( $\text{CH}_2$ ), 1732 vs ( $\text{C}=\text{O}$ ), 1601 a, 1568 s, 1435 s, 1257 s, 1157 m, 1102 w, 1078 w, 1051 w, 1016 m, 968 w, 870 w, 772 m, 653 m

*UV-vis (MeOH)*: no characteristic transitions

*CV(MeCN)*:  $E_{1/2} = 695 \text{ mV}$

### *Mn<sub>2</sub>-tBuBis*

In this reaction 100 mg (97.7  $\mu\text{mol}$ ) tBuBis and 52.4 mg (195.4  $\mu\text{mol}$ ) manganese(III) acetate was used. Yield: 122 mg.

*ESI-MS*: 326.60 M/2  $[(\text{Fragment}_1\text{H}_1)+\text{Mn}]^{2+}$ , 335.62 M/2  $[(\text{Fragment}_1\text{H}_1)+\text{H}_2\text{O}+\text{Mn}]^{2+}$ , 653.17 M  $[(\text{Fragment}_1\text{H}_1)+\text{Mn}]^+$ , 588.16 M/2  $[\text{Mn}_2(\text{tBuBisH}_1)(\text{MeCN})]^{2+}$ , 597.16 M/2  $[\text{Mn}_2(\text{tBuBisH}_1)(\text{MeCN})(\text{H}_2\text{O})]^{2+}$ , 606.17 M/2  $[\text{Mn}_2(\text{tBuBisH}_1)(\text{MeCN})(\text{H}_2\text{O})_2]^{2+}$

*Elemental analysis*: measured C 55.44, H 5.89, N 6.84 (15099)

calculated for  $[\text{Mn}^{\text{III}}_2(\text{CyclicDimerH}_2)(\text{OAc})_4] \cdot 5 \text{H}_2\text{O}$ , MW 1603.33:

C 55.43, H 5.90, N 6.99

calculated for  $[\text{Mn}^{\text{III}}(\text{Fragment}_1\text{H}_1)(\text{OAc})_2] \cdot 2.5 \text{H}_2\text{O}$ , MW 818.71:

C 55.74, H 6.15, N 6.84

(for the explanation of  $\text{Fragment}_1$ ,  $\text{Fragment}_2$  and 2+2 cyclic dimer, see Section 4.4.2)

*IR(KBr)*: 3406 br, 2954 m (tBu), 2866 w, 1734 s (C=O), 1570 vs (OAc), 1406 vs, 1206 s, 1154 m, 1016 m, 766 m, 650 m

*UV-vis (MeOH)*: no characteristic transitions

#### 9.2.5.4. Other manganese complexes:

##### 9.2.5.4.1. $[Mn^{II}(N2py2PhO)(Cl)] \cdot 4.5 H_2O$

150 mg (0.283 mmol) N2Py2PhOH dissolved in 10 mL dry MeOH was mixed with 55.9 mg (0.283 mmol) MnCl<sub>2</sub> · 4 H<sub>2</sub>O in 5 mL MeOH. Finally 40.35 μL (0.283 mmol) triethylamine was added, the solution was refluxed for 20 min and the solvent partially removed. By the addition of hexane a pale white precipitate was formed, which was filtered off, washed with hexane, and dried in vacuo. Yield: 198 mg (0.283 mmol, 100%)

*ESI-MS*: 584.3  $[Mn^{II}(N2py2PhO)]^+$ , 602.3  $[Mn^{II}(N2py2PhO)(OH_2)]^+$

*Elemental analysis*: measured C 49.64, H 6.09, N 8.11 (16547)

calculated for C<sub>29</sub>H<sub>38</sub>N<sub>4</sub>O<sub>10.5</sub>ClMn, MW 701.02:

C 49.68, H 5.46, N 7.99

*IR(KBr)*: 3420 br (OH), 3066 w, 2952 w (CH<sub>2</sub>), 2680 w, 1732 vs (C=O), 1602 s, 1480 s, 1446 s, 1280 br, s, 1158 m, 1072 m, 1018 s, 960 m, 768 s

*UV-vis (MeOH)*: no characteristic bands

*CV(MeCN)*: +1112 mV (rev.), +822 mV (only anodic wave, irrev.) vs. Ag/0.01 M AgNO<sub>3</sub>

##### 9.2.5.4.2. $[Mn^{III}(N2py2PhO)(OAc)]ClO_4 \cdot 4.8 H_2O$

To a dry methanolic solution (5 mL) of 88.9 mg (0.135 mmol)  $[Mn^{III}(N2py2PhO)(OAc)] OAc \cdot 2 H_2O$  was added 19.0 mg (0.135 mmol) NaClO<sub>4</sub> · H<sub>2</sub>O as a solid, the solution was stirred for 20 min at RT, after which 5 mL of Et<sub>2</sub>O was carefully added, and kept at 4°C overnight. The formed brown precipitate was collected, and washed with ether. Yield: 82 mg (98.8 μmol, 73%)

*FAB-MS*: 584.6  $[Mn^{III}(N2py2PhO)]^+$ , 602.6  $[Mn^{III}(N2py2PhO)(OH_2)]^+$

*Elemental analysis*: measured C 44.86, H 5.04, N 6.75 (16190)

calculated for C<sub>31</sub>H<sub>41.6</sub>N<sub>4</sub>O<sub>16.8</sub>ClMn, MW 829.44:

C 44.85, H 5.05, N 6.78

*IR(KBr)*: 3438 br, s, 2954 w (CH<sub>2</sub>), 1736 vs (C=O), 1478 s, 1446 m, 1270 vs, 1150 m, 1120 vs, 1080 vs (ClO<sub>4</sub>), 1018 s, 760 m, 626 m



#### 9.2.5.4.3. Mn(III) - bis(2-hydroxy-3-methoxybenzyl)amine complex $[Mn_2(N(PhO)_2)_3]$

To 100 mg (0.346 mmol) bis(2-hydroxy-3-methoxybenzyl)amine dissolved in 15 mL dry methanol was added 92.7 mg (0.346 mmol)  $Mn(OAc)_3 \cdot 2 H_2O$  as a solid. After stirring for 5 min at RT, the unreacted Mn(III) salt was removed by filtration. To the remaining clear solution 98.7  $\mu$ L (0.692 mmol) triethylamine was injected. After 10 min stirring the solvent was evaporated, and the obtained solid was dried in vacuo. Yield: 90 mg (79.5  $\mu$ mol, 69%)

*ESI-MS*: 971.6  $[Mn_2(LH_2)_3+H]^+$ , 630.5  $[Mn(LH_2)_2+H]^+$

*Elemental analysis*: measured C 50.81, H 6.50, N 3.89 (15815)

calculated for  $C_{48}H_{69}N_3O_{21}Mn_2$ , MW 1133.87:

C 50.84, H 6.13, N 3.71

*IR(KBr)*: 3424 br, 3236 w, 3058 w, 2976 w, 2936 m, 2834 m, 2676 m, 2488 w, 1570 vs, 1480 vs, 1456 s, 1438 s, 1270 s, 1236 vs, 1080 s, 1022 m, 932 m, 854 s, 738 s, 656 m, 598 m

*UV-vis (MeOH)*: a continuous shoulder.

#### 9.2.6. Other complexes of N2py2PhOH

##### 9.2.6.1. $[Ni^{II}(N2py2PhO)(OH_2)]ClO_4 \cdot 4 H_2O$

To a dry methanolic solution (20 mL) of 150 mg (0.283 mmol) N2py2PhOH was added 103.4 mg (0.283 mmol)  $Ni(ClO_4)_2 \cdot 6 H_2O$  in 5 mL MeOH. Finally 40.3  $\mu$ L (0.283 mmol) triethylamine was added and the solution was stirred for 20 min at RT. The solvent was partially removed and  $Et_2O$  was given to the solution, which was then kept at 4°C overnight. The formed precipitate was filtered off, washed with ether and dried in vacuo. Yield: 169 mg (0.218 mmol, 77%)

*ESI-MS*: 587.3  $[Ni^{II}(N2py2PhO)]^+$ , 605.4  $[Ni^{II}(N2py2PhO)(OH_2)]^+$

*Elemental analysis*: measured C 44.78, H 5.51, N 7.45 (16556)

calculated for  $C_{29}H_{39}N_4O_{15}ClNi$ , MW 777.79:

C 44.78, H 5.05, N 7.21

*IR(KBr)*: 3422 br, s (OH), 2980 w, 2952 w ( $CH_2$ ), 1734 vs (C=O), 1636 s, 1606 s, 1480 s, 1450 s, 1260 s, 1090 vs ( $ClO_4$ ), 768 m, 626 s

*UV-vis (MeOH)*: 365 nm (sh,  $\epsilon = 120$ ), 568 nm ( $\epsilon = 9$ )

*CV(MeCN)*:  $E_a = +576$  mV (irrev.) vs. Ag/0.01 M  $AgNO_3$

9.2.6.2.  $[Fe^{II}(N2py2PhO)(OH_2)](ClO_4) \cdot HClO_4 \cdot 3.3 H_2O$

To a dry methanolic solution (20 mL) of 150 mg (0.283 mmol) N2py2PhOH was added 102.6 mg (0.283 mmol)  $Fe(ClO_4)_2 \cdot 6 H_2O$  in 5 mL MeOH. During mixing the color turns deep orange. After stirring for 20 min at RT, the solvent was removed. Interestingly during the solvent evaporation the color changes to deep green/blue. The obtained solid was dried in vacuo. Yield: 225 mg (0.260 mmol, 92%)

*ESI-MS*: 585.3  $[Fe^{II}(N2py2PhO)]^+$ , 603.4  $[Fe^{II}(N2py2PhO)(OH_2)]^+$ , 617.4  $[Fe^{II}(N2py2PhO)(MeOH)]^+$ , 292.8  $[Fe^{III}(N2py2PhO)]^{2+}$ , 301.8  $[Fe^{III}(N2py2PhO)(OH_2)]^{2+}$ , 308.8  $[Fe^{III}(N2py2PhO)(MeOH)]^{2+}$

*Elemental analysis*: measured C 40.36, H 4.43, N 6.49 (16635)  
 calculated for  $C_{29}H_{38.6}N_4O_{17.3}Cl_2Fe$ , MW 862.89:  
 C 40.36, H 4.50, N 6.49

*IR(KBr)*: 3448 br, s (OH), 2958 w (CH<sub>2</sub>), 1734 s (C=O), 1608 s, 1480 m, 1450 m, 1268 s, 1094 vs (ClO<sub>4</sub>), 956 w, 766 m, 624 s

*UV-vis (MeOH)*: 347 nm (sh,  $\epsilon = 2360$ ), 525 (sh,  $\epsilon = 910$ )

*CV(MeCN)*:  $E_{1/2} = 264$  mV ( $\Delta E = 245$  mV, irreversible) vs. Ag/0.01 M AgNO<sub>3</sub>

9.2.6.3.  $[Fe^{II}(N2py2PhO)(OH_2)]ClO_4 \cdot [Et_3NH]ClO_4 \cdot 2 H_2O$

The reaction was performed analogously to that of  $[Fe^{II}(N2py2PhO)(OH_2)](ClO_4) \cdot HClO_4 \cdot 3.3 H_2O$ , but 1 eq of triethylamine was also added to the reaction mixture. Yield: 251 mg (0.266 mmol, 94%)

*ESI-MS*: 585.4  $[Fe^{II}(N2py2PhO)]^+$ , 603.4  $[Fe^{II}(N2py2PhO)(OH_2)]^+$ , 617.4  $[Fe^{II}(N2py2PhO)(MeOH)]^+$

*Elemental analysis*: measured C 44.59, H 5.56, N 7.30 (16706)  
 calculated for  $C_{35}H_{51}N_5O_{17}Cl_2Fe$ , MW 940.56:  
 C 44.69, H 5.46, N 7.45

*IR(KBr)*: 3422 br, s (OH), 3060 w, 2982 w, 2954 w (CH<sub>2</sub>), 2678 m, 1736 vs (C=O), 1592 m, 1458 s, 1282 vs, 1144 vs, 1088 vs (ClO<sub>4</sub>), 960 m, 766 m, 622 s

*UV-vis (MeOH)*: 455 nm (sh,  $\epsilon = 520$ )

9.2.6.4.  $[\text{Zn}^{\text{II}}(\text{N}2\text{py}2\text{PhO})(\text{OH}_2)](\text{ClO}_4) \cdot 4 \text{H}_2\text{O} \cdot 0.73 \text{HClO}_4$ 

The reaction was performed in a similar fashion to that of  $[\text{Fe}^{\text{II}}(\text{N}2\text{py}2\text{PhO})(\text{OH}_2)](\text{ClO}_4) \cdot \text{HClO}_4 \cdot 3.3 \text{H}_2\text{O}$ . The zinc source was  $\text{Zn}(\text{ClO}_4)_2 \cdot 6 \text{H}_2\text{O}$ . Yield: 220.9 mg (0.257 mmol, 91%)

*ESI-MS*: 593.3  $[\text{Zn}^{\text{II}}(\text{N}2\text{py}2\text{PhO})]^+$ , 611.3  $[\text{Zn}^{\text{II}}(\text{N}2\text{py}2\text{PhO})(\text{OH}_2)]^+$ , 625.3  $[\text{Zn}^{\text{II}}(\text{N}2\text{py}2\text{PhO})(\text{MeOH})]^+$

*Elemental analysis*: measured C 40.64, H 4.59, N 6.48 (16566)

calculated for  $\text{C}_{29}\text{H}_{39.73}\text{N}_4\text{O}_{17.92}\text{Cl}_{1.73}\text{Zn}$ , MW 857.81:

C 40.60, H 4.66, N 6.53

*IR(KBr)*: 3418 br, s (OH), 2956 w (CH<sub>2</sub>), 2850 w, 1736 s (C=O), 1606 m, 1480 m, 1448 s, 1288 s, 1266 s, 1108 (ClO<sub>4</sub>), 962 m, 760 m, 626 s

<sup>1</sup>H-NMR(D<sub>2</sub>O): 8.63 (2H, d, <sup>3</sup>J = 6.8 Hz, **H**<sub>py-α</sub>), 8.00 (2H, t, <sup>3</sup>J = 6.7 Hz, **H**<sub>py-γ</sub>), 7.55 (2H, t, <sup>3</sup>J = 6.8 Hz, **H**<sub>py-β</sub>), 7.28-7.58 (4H, m, **H**<sub>py-δ</sub> + meta phenol-**H**), 7.12 (1H, d, <sup>3</sup>J = 7.2 Hz, ortho phenol-**H**), 6.89 (1H, t, <sup>3</sup>J = 7.0 Hz, para phenol-**H**), 5.10 (2H, s, N-**CH**), 3.68 (8H, s, OCH<sub>3</sub> + NCH<sub>2</sub>C<sub>6</sub>H<sub>4</sub>OH), 2.80 (2H, d, <sup>2</sup>J = 13.7 Hz, N-**CH**<sub>2</sub>), 2.54 (2H, d, <sup>2</sup>J = 12.8 Hz, N-**CH**<sub>2</sub>), 2.06 (3H, s, N-**CH**<sub>3</sub>)

9.2.6.5.  $[\text{Cd}^{\text{II}}(\text{N}2\text{py}2\text{PhO})(\text{NO}_3)] \cdot \text{HNO}_3 \cdot 3.5 \text{H}_2\text{O}$ 

The reaction was performed in a similar fashion to that of  $[\text{Fe}^{\text{II}}(\text{N}2\text{py}2\text{PhO})(\text{OH}_2)](\text{ClO}_4) \cdot \text{HClO}_4 \cdot 3.3 \text{H}_2\text{O}$ . The cadmium source was  $\text{Cd}(\text{NO}_3)_2 \cdot 4 \text{H}_2\text{O}$ . Yield: 209 mg (0.252 mmol, 89%)

*ESI-MS*: 643.3  $[\text{Cd}^{\text{II}}(\text{N}2\text{py}2\text{PhO})]^+$ , 661.3  $[\text{Cd}^{\text{II}}(\text{N}2\text{py}2\text{PhO})(\text{OH}_2)]^+$ , 675.3  $[\text{Cd}^{\text{II}}(\text{N}2\text{py}2\text{PhO})(\text{MeOH})]^+$

*Elemental analysis*: measured C 42.09, H 4.56, N 10.17 (16656)

calculated for  $\text{C}_{29}\text{H}_{37}\text{N}_6\text{O}_{15.5}\text{Cd}$ , MW 830.02:

C 41.96, H 4.49, N 10.13

*IR(KBr)*: 3422 br, s (OH), 2954 w (CH<sub>2</sub>), 1736 s (C=O), 1602 s, 1458 vs, 1382 vs (NO<sub>3</sub>), 1280 s, 1018 m, 960 m, 762 m, 640 w

<sup>1</sup>H-NMR(D<sub>2</sub>O): 8.54 (2H, d, <sup>3</sup>J = 4.3 Hz, **H**<sub>py-α</sub>), 7.97 (2H, t, <sup>3</sup>J = 7.6 Hz, **H**<sub>py-γ</sub>), 7.55 (2H, t, <sup>3</sup>J = 7.5 Hz, **H**<sub>py-β</sub>), 7.40 (2H, d, <sup>3</sup>J = 7.8 Hz, **H**<sub>py-δ</sub>), 7.27 (1H, t, <sup>3</sup>J = 7.7 Hz, phenol-**H**), 7.12 (2H, d, 2H, <sup>3</sup>J = 7.9 Hz, phenol-**H**), 6.82 (1H, t, <sup>3</sup>J = 7.6 Hz, para phenol-**H**), 5.00 (2H, s, N-**CH**), 3.79 (2H, s, NCH<sub>2</sub>C<sub>6</sub>H<sub>4</sub>OH), 3.65 (6H, s, OCH<sub>3</sub>), 2.85 (2H, d, <sup>2</sup>J = 13.2 Hz, N-**CH**<sub>2</sub>), 2.71 (2H, d, <sup>2</sup>J = 13.4 Hz, N-**CH**<sub>2</sub>), 1.93 (3H, s, N-**CH**<sub>3</sub>)

9.2.6.6.  $[\text{Pb}^{\text{II}}(\text{N}2\text{py}2\text{PhOH})(\text{OAc})_2] \cdot 2 \text{H}_2\text{O}$ 

The reaction was performed in a similar fashion to that of  $[\text{Fe}^{\text{II}}(\text{N}2\text{py}2\text{PhO})(\text{OH}_2)](\text{ClO}_4) \cdot \text{HClO}_4 \cdot 3.3 \text{H}_2\text{O}$ . The lead source was  $\text{Pb}(\text{OAc})_2 \cdot 3 \text{H}_2\text{O}$ . Yield: 222 mg (0.249 mmol, 88%)

*ESI-MS*: 737.3  $[\text{Pb}^{\text{II}}(\text{N}2\text{py}2\text{PhO})]^+$ , 755.3  $[\text{Pb}^{\text{II}}(\text{N}2\text{py}2\text{PhO})(\text{OH}_2)]^+$ , 769.3  $[\text{Pb}^{\text{II}}(\text{N}2\text{py}2\text{PhO})(\text{MeOH})]^+$

*Elemental analysis*: measured C 44.04, H 4.57, N 6.37 (16657)

calculated for  $\text{C}_{33}\text{H}_{40}\text{N}_4\text{O}_{12}\text{Pb}$ , MW 891.87:

C 44.44, H 4.52, N 6.28

*IR(KBr)*: 3422 br, s (OH), 3058 w, 2952 w ( $\text{CH}_2$ ), 2844 br, m (Bohlmann), 1736 vs ( $\text{C}=\text{O}$ ), 1592 s, 1560 s, 1478 s, 1432 s, 1406 s, 1280 vs, 1156 m, 1096 m, 1010 m, 972 m, 878 w, 758 m, 660 m

$^1\text{H-NMR}(\text{D}_2\text{O})$ : 8.63 (2H, d,  $^3\text{J} = 4.4 \text{ Hz}$ ,  $\text{H}_{\text{py-}\alpha}$ ), 7.93 (2H, t,  $^3\text{J} = 7.4 \text{ Hz}$ ,  $\text{H}_{\text{py-}\gamma}$ ), 7.53 (4H, m,  $\text{H}_{\text{py-}\beta} + \text{H}_{\text{py-}\delta}$ ), 7.21 (1H, t,  $^3\text{J} = 7.3 \text{ Hz}$ , phenol-**H**), 7.14 (1H, d,  $^3\text{J} = 7.6 \text{ Hz}$ , phenol-**H**), 6.82 (1H, d,  $^3\text{J} = 8.0 \text{ Hz}$ , ortho phenol-**H**), 6.59 (1H, t,  $^3\text{J} = 7.1 \text{ Hz}$ , para phenol-**H**), 5.29 (2H, s, N-**CH**), 3.94 (2H, s,  $\text{NCH}_2\text{C}_6\text{H}_4\text{OH}$ ), 3.54 (6H, s,  $\text{OCH}_3$ ), 3.45 (2H, d,  $^2\text{J} = 13.7 \text{ Hz}$ , N-**CH}\_2**), 3.06 (2H, d,  $^2\text{J} = 13.7 \text{ Hz}$ , N-**CH}\_2**), 1.95 (3H, s, N-**CH}\_3**), 1.81 (6H, s,  $\text{OOCCH}_3$ )

## 10. References

- [1] B. Figgis, M. Hitchman, *Ligand field theory and its application*, Wiley-VCH, Weinheim, 2000
- [2] S. P. Artz, D. J. Cram, *J. Am. Chem. Soc.*, **1984**, *106*, 2160
- [3] P. Comba, *Coord. Chem. Rev.*, **1999**, *182*, 343
- [4] P. Comba, M. Kerscher, *Cryst. Eng.*, **2003**, *6*, 197
- [5] P. Comba, W. Schiek, *Coord. Chem. Rev.*, **2003**, *238-239*, 21
- [6] P. Comba, M. Kerscher, M. Merz, V. Müller, H. Pritzkow, R. Remenyi, W. Schiek, Y. Xiong, *Chem. Eur. J.*, **2002**, *8*, 5750
- [7] S. Kuwata, *Dissertation*, Universität Heidelberg, **2005**
- [8] R. G. Pearson, *J. Am. Chem. Soc.*, **1963**, *85*, 3533
- [9] G. Schwarzenbach, *Helv. Chim. Acta*, **1952**, *35*, 2344
- [10] R. D. Hancock, *J. Chem. Educ.*, **1992**, *69*, 615
- [11] P. Comba, *Coord. Chem. Rev.*, **2000**, *200-202*, 217
- [12] N. Ito, S. E. V. Phillips, K. D. S. Ladav, P. F. Knowles, *J. Mol. Biol.*, **1994**, *238*, 794
- [13] F. Himo, L. A. Eriksson, F. Maseras, P. E. M. Siegbahn, *J. Am. Chem. Soc.*, **2000**, *122*, 8031
- [14] A. Philibert, F. Thomas, C. Philouze, S. Hamman, E. Saint-Aman, J.-L. Pierre, *Chem. Eur. J.*, **2003**, *9*, 3803
- [15] J. B. Trémolières, J. B. Bieth, *Phytochemistry*, **1984**, *23*, 501
- [16] T. Klabunde, C. Eicken, J. C. Sacchettini, B. Krebs, *Nat. Struct. Biol.*, **1998**, *5*, 1084
- [17] R. Than, A. A. Feldmann, B. Krebs, *Coord. Chem. Rev.*, **1999**, *182*, 211
- [18] J. Reim, B. Krebs, *J. Chem. Soc., Dalton Trans.*, **1997**, 3793
- [19] J. Ackermann, F. Meyer, E. Kaifer, H. Pritzkow, *Chem. Eur. J.*, **2002**, *8*, 247
- [20] C. Belle, C. Beguin, I. Gautier-Luneau, S. Hamman, C. Philouze, J. L. Pierre, F. Thomas, S. Torelli, *Inorg. Chem.*, **2002**, *41*, 479
- [21] S. Torelli, C. Belle, S. Hamman, J. L. Pierre, E. Saint-Aman, *Inorg. Chem.*, **2002**, *41*, 3983
- [22] H. Börzel, P. Comba, H. Pritzkow, *J. Chem. Soc., Chem. Commun.*, **2001**, 97
- [23] K. Born, P. Comba, A. Daubinet, A. Fuchs, H. Wadepohl, in preparation
- [24] S. Torelli, C. Belle, I. Gautier-Luneau, J. L. Pierre, E. Saint-Aman, J. M. Latour, L. Le Page, D. Luneau, *Inorg. Chem.*, **2000**, *39*, 3526
- [25] A. Messerschmidt, L. Prade, R. Wever, *Biol. Chem.*, **1997**, *378*, 309

- [26] J. R. Gillette, J. V. Dingell, B. B. Brodie, *Nature*, **1958**, *181*, 898
- [27] C. Gunaratna, *Curr. Sep.*, **2000**, *19*, 17
- [28] M. Sono, M. P. Roach, E. D. Coulter, J. H. Dawson, *Chem. Rev.*, **1996**, *96*, 2841
- [29] J. Klinman, *Chem. Rev.*, **1996**, *96*, 2541
- [30] W. B. Tolman, *Acc. Chem. Res.*, **1997**, *30*, 227
- [31] D. Lee and S. J. Lippard, *Inorg. Chem.*, **2002**, *41*, 827
- [32] A. M. Calafat, L. G. Marzilli, *Inorg. Chem.*, **1993**, *32*, 2906
- [33] R. M. Hartshorn, *Dalton Trans.*, **2002**, 3214
- [34] M. R. Bukowski, P. Comba, A. Lienke, C. Limberg, C. López de Laorden, R. Mas-Ballesté, M. Merz, L. Que, Jr., *Angew. Chem.*, **2006**, accepted
- [35] J. Bautz, M. R. Bukowski, M. Kerscher, A. Stubna, P. Comba, A. Lienke, E. Münck, L. Que Jr., *Angew. Chem.*, **2006**, accepted
- [36] M. Costas, A. K. Tipton, K. Chen, D. H. Jo, L. Que Jr., *J. Am. Chem. Soc.*, **2001**, *123*, 27
- [37] K. Chen, M. Costas, J. Kim, A. K. Tipton, L. Que Jr., *J. Am. Chem. Soc.*, **2002**, *124*, 12
- [38] D. T. Sawyer, A. Sobkowiak, T. Matsushita, *Acc. Chem. Res.*, **1996**, *29*, 409
- [39] A. G. L. Ligtenbarg, R. Hage, B. L. Feringa, *Coord. Chem. Rev.*, **2003**, *237*, 89
- [40] G. Yin, M. Buchalova, A. M. Danby, C. M. Perkins, D. Kitko, J. D. Carter, W. M. Scheper, D. H. Busch, *Inorg. Chem.*, **2006**, *45*, 3467
- [41] C. Mannich, P. Mohs, *Chem. Ber.*, **1930**, *63*, 608
- [42] H. Stetter, R. Merten, *Chem. Ber.*, **1957**, *90*, 868
- [43] G. Dietz, W. Fielder, G. Faust, *Chem. Ber.*, **1969**, *102*, 4147
- [44] H. Stetter, J. Schaefer, K. Dieminger, *Chem. Ber.*, **1958**, *91*, 598
- [45] K. W. Merz, R. Haller, *Pharm. Acta Helv.*, **1963**, *38*, 442
- [46] R. Haller, *Arzn. Forsch.*, **1965**, *15*, 1327
- [47] M. J. Fernandez, J. M. Casares, E. Galvez, *J. Heterocycl. Chem.*, **1992**, *29*, 1797
- [48] O. Reany, T. Gunnlaugsson, D. Parker, *Perkin Trans. 2.*, **2000**, 1819
- [49] F. Fülöp, M. Dahlquist, K. Pihlaja, *Act. Chem. Scand.*, **1991**, *45*, 273
- [50] H. Börzel, P. Comba, K. S. Hagen, C. Katsichtis, H. Pritzkow, *Chem. Eur. J.*, **2000**, *6*, 914
- [51] C. Bleiholder, H. Börzel, P. Comba, R. Ferrari, M. Heydt, M. Kerscher, S. Kuwata, G. Laurenczy, G. A. Lawrance, A. Lienke, B. Martin, M. Merz, B. Nuber, H. Pritzkow, *Inorg. Chem.*, **2005**, *44*, 8145

- [52] U. Holzgrabe, E. Erciyas, *Arch. Pharm. (Weinheim)*, **1992**, 325, 657
- [53] E. H. Charlesworth, R. Robinson, *J. Chem. Soc.*, **1934**, 1651
- [54] H. E. Zaugg, A. D. Schaefer, *J. Chem. Soc.*, **1963**, 28, 2925
- [55] K. Michelsen, *Acta Chem. Scand.*, **1974**, A28, 428
- [56] L. Kaczmarek, R. Baliczki, *J. Prakt. Chem.*, **1994**, 336, 695
- [57] G. E. Stokker, A. A. Deana, S. J. deSolms, E. M. Schultz, R. L. Smith, E. J. Cragoe Jr., J. E. Baer, C. T. Ludden, H. F. Ruso, A. Scriabine, C. S. Sweet, L. S. Watson, *J. Med. Chem.*, **1980**, 23, 1414
- [58] A. Einhorn, T. Mauermayer, *Liebigs Ann.*, **1905**, 343, 282
- [59] M. Merz, *Dissertation*, Universität Heidelberg, **2002**
- [60] P. J. Kocienski, *Protecting groups*, 3<sup>rd</sup> Edition, Thieme Verlag: Stuttgart, 2003: Chapter 4.4.1, pp. 286-295
- [61] A. Arnone, R. Bernardi, P. Bravo, M. Frigerio, C. Ticozzi, *Gazz. Chim. Ital.*, **1989**, 119, 87
- [62] L. Deng, E. N. Jacobsen, *J. Org. Chem.*, **1992**, 57, 4320
- [63] M. Karhu, *Perkin Trans. 1*, **1979**, 1661
- [64] M. Bell, A. J. Edwards, B. F. Hoskins, E. H. Kachab, R. Robson, *J. Am. Chem. Soc.*, **1989**, 111, 3603
- [65] F. Ullmann, K. Brittner, *Chem. Ber.*, **1909**, 42, 2539
- [66] D. Black, A. J. Blake, K. P. Dancey, A. Harrison, M. McPartlin, S. Parsons, P. A. Tasker, G. Whittaker, M. Schröder, *Dalton Trans.*, **1998**, 3953
- [67] F. Hanus, E. Fuchs, *J. Prakt. Chem.*, **1939**, 153, 327
- [68] J. Whittaker, in *Metal Ions in Biological Systems*, eds. H. Sigel and A. Sigel, Marcel Dekker, New York, **1994**, 30, 315
- [69] B. A. Jazdzewski, W. B. Tolman, *Coord. Chem. Rev.*, **2000**, 202, 633
- [70] K. D. Karlin, B. I. Cohen, J. C. Hayes, A. Farooq, J. Zubieta, *Inorg. Chem.*, **1987**, 26, 147
- [71] H. Adams, N. A. Bailey, I. K. Campbell, D. E. Fenton, Q.-Y. He, *J. Chem. Soc., Dalton Trans.*, **1996**, 2233
- [72] M. M. Whittaker, W. R. Duncan, J. W. Whittaker, *Inorg. Chem.*, **1996**, 35, 382
- [73] J. A. Halfen, B. A. Jazdzewski, S. Mahapatra, L. M. Berreau, E. C. Wilkinson, L. Que Jr. W. B. Tolman, *J. Am. Chem. Soc.*, **1997**, 35, 8217
- [74] E. Bill, J. Müller, T. Weyhermüller, K. Wieghardt, *Inorg. Chem.*, **1999**, 38, 5795

- [75] Y. Wang, J. L. DuBois, B. Hedman, K. O. Hodgson, T. D. P. Stack, *Science*, **1998**, *279*, 537
- [76] M. A. Halcrow, L. M. L. Chia, X. Liu, E. J. L. McInnes, L. J. Yellowlees, I. J. Scowen, M. McPartlin, F. E. Mabbs, J. E. Davies, *J. Chem. Soc. Dalton Trans.*, **1999**, 1753
- [77] J. A. Halfen, V. G. Young, W. B. Tolman, *Angew. Chem., Int. Ed. Engl.*, **1996**, *35*, 1687
- [78] C. Gerdemann, C. Eicken, B. Krebs, *Acc. Chem. Res.*, **2002**, *35*, 183
- [79] E. I. Solomon, U. M. Sundaram, T. E. Machonkin, *Chem. Rev.*, **1996**, *96*, 2563
- [80] Y. Shimazaki, S. Huth, S. Hirota, O. Yamauchi, *Inorg. Chim. Acta*, **2002**, *331*, 168
- [81] Y. Shimazaki, S. Huth, A. Odani, O. Yamauchi, *Angew. Chem.*, **2000**, *112*, 1732
- [82] D. Wang, G. R. Hanson, *J. Magn. Reson. A*, **1995**, *117*, 1
- [83] D. Wang, G. R. Hanson, *Appl. Magn. Reson.*, **1996**, *11*, 401
- [84] P. Comba, M. Merz, H. Pritzkow, *Eur. J. Inorg. Chem.*, **2003**, 3042
- [85] P. Comba, B. Martin, A. Prikhod'ko, H. Pritzkow, H. Rohwer, *C. R. Chimie*, **2005**, *8*, 1506
- [86] H. Börzel, P. Comba, K. S. Hagen, M. Kerscher, H. Pritzkow, M. Schatz, S. Schindler, O. Walter, *Inorg. Chem.*, **2002**, *41*, 5440
- [87] H. Börzel, P. Comba, C. Katsichtis, W. Kiefer, A. Lienke, V. Nagel, H. Pritzkow, *Chem. Eur. J.*, **1999**, *5*, 1716
- [88] D. J. Hodgson, *Progr. Inorg. Chem.*, **1975**, *19*, 173
- [89] P. Comba, T. W. Hambley, G. Lauer, M. Melter, N. Okon, MOMECC97, a Molecular Modeling Package for Inorganic Compounds, Lauer & Okon Chemische Verfahrens- & Softwareentwicklung, 1997. For information contact: Lauer&Okon, Heidelberg, Germany, e-mail: [CVS-HD@T-Online.de](mailto:CVS-HD@T-Online.de)
- [90] J. E. Bol, C. Buning, P. Comba, J. Reedijk, M. Ströhle, *J. Comput. Chem.*, **1998**, *19*, 512
- [91] P. Curie, *Dissertation*, School of Physics and Industrial Chemistry, Paris, **1895**
- [92] M. M. Rogic, T. R. Demmin, *J. Am. Chem. Soc.*, **1978**, *100*, 5472
- [93] T. R. Demmin, M. D. Swerdloff, M. M. Rogic, *J. Am. Chem. Soc.*, **1981**, *103*, 5795
- [94] A. Butler, J. V. Walker, *Chem. Rev.*, **1993**, *93*, 1937
- [95] D. Rehder, *Angew., Chem. Int. Ed. Engl.*, **1991**, *30*, 148
- [96] A. Butler, M. J. Clague, G. E. Meister, *Chem. Rev.*, **1994**, *94*, 625



- [97] H. Mimoun, L. Saussine, E. Daire, M. Postel, J. Fischer, R. Weiss, *J. Am. Chem. Soc.*, **1983**, *105*, 3101
- [98] A. Shaver, J. B. Ng, A. Hall, B. S. Lum, B. I. Posner, *Inorg. Chem.*, **1993**, *32*, 3109
- [99] P. Caravan, L. Gelmini, N. Glover, F. G. Herring, H. J. H. McNeill, S. J. Rettig, I. A. Setyawati, Y. E. Sun, S. Tracey, V. G. Yuen, C. Orvig, *J. Am. Chem. Soc.*, **1995**, *117*, 127
- [100] P. Comba, N. Okon, R. Remenyi, *J. Comput. Chem.*, **1999**, *20*, 781
- [101] H. Helm, H.-J. Krüger, *Inorg. Chem.*, **1996**, *35*, 3533
- [102] G. J. Colpas, B. J. Hamstra, J. W. Kampf, V. L. Pecoraro, *J. Am. Chem. Soc.*, **1996**, *118*, 3469
- [103] C. J. Ballhausen, H. B. Gray, *Inorg. Chem.*, **1962**, *1*, 111
- [104] P. Comba, A. M. Sargeson, *Aust. J. Chem.*, **1986**, *39*, 1029
- [105] P. Comba, L. M. Engelhardt, J. M. Harrowfield, G. A. Lawrance, L. L. Martin, A. M. Sargeson, A. H. White, *J. Chem. Soc., Chem. Commun.*, **1985**, 174
- [106] R. Ma, A. Bakac, J. H. Espenson, *Inorg. Chem.*, **1992**, *31*, 1925
- [107] C. J. Cramer, W.B. Tolman, K.H. Theopold, A.L. Rheingold, *Proc. Natl. Acad. Sci. USA*, **2003**, *100*, 3635
- [108] H. Kelm, H.-J. Krüger, *Angew. Chem.*, **2001**, *113*, 2406
- [109] R. C. Thompson, *Inorg. Chem.*, **1982**, *21*, 859
- [110] R. C. Thompson, *Inorg. Chem.*, **1983**, *22*, 584
- [111] A. Messerschmidt, R. Wever, *Proc. Natl. Acad. Sci. USA*, **1996**, *93*, 392
- [112] G. J. Colpas, B. J. Hamstra, J. W. Kampf, V. L. Pecoraro, *J. Am. Chem. Soc.*, **1994**, *116*, 3627
- [113] M. J. Clague, N. L. Neder, A. Butler, *Inorg. Chem.*, **1993**, *32*, 4754
- [114] M. S. Lane, K. Burgess, *Chem. Rev.*, **2003**, *103*, 2457
- [115] P. Hoffmann, B. Meunier, *New J. Chem.*, **1992**, *16*, 559
- [116] T. Katsuki, *Coord. Chem. Rev.*, **1995**, *140*, 189
- [117] R. Hage, J. E. Iburg, J. Kerschner, J. H. Koek, E. L. M. Lempers, R. J. Martens, U. S. Racheria, S. W. Russell, T. Swarthoff, M. R. P. van Vliet, J. B. Warnaar, L. v. d. Wolf, B. Krijnen, *Nature*, **1994**, *369*, 637
- [118] L. Que Jr., W. B. Tolman, *Angew. Chem., Int. Ed. Engl.*, **1999**, *38*, 2227
- [119] K. Chen, M. Costas, J. Kim, A. K. Tipton, L. Que Jr., *J. Am. Chem. Soc.*, **2002**, *124*, 3026
- [120] J. Brinksma, R. Hage, J. Kerschner, B. L. Feringa, *Chem. Commun.*, **2000**, 537

- [121] U. Schuchardt, M. C. Guerreiro, G. B. Shul'pin, *Russ. Chem. Bull.*, **1998**, *47*, 247
- [122] D. M. Boghaei, S. Mohebi, *J. Mol. Cat. A*, **2002**, *179*, 41
- [123] E. J. Eisenbraun, R. Bader, J. W. Polackeck, E. Reif, *J. Org. Chem.*, **1963**, *28*, 2057
- [124] H. Weiner, A. Trovarelli, R. G. Finke, *J. Mol. Cat. A: Chemical*, **2003**, *191*, 217
- [125] S. C. Trewick, T. F. Henshaw, R. P. Hausinger, T. Lindahl, B. Sedgwick, *Nature*, **2002**, *419*, 174
- [126] J. T. Groves, D. V. Adhyam, *J. Am. Chem. Soc.*, **1984**, *106*, 2177
- [127] S. Mahapatra, J. A. Halfen, E. C. Wilkinson, G. Pan, X. Wang, V. G. Young Jr., C. J. Cramer, L. Que Jr., W. B. Tolman, *J. Am. Chem. Soc.*, **1996**, *118*, 11555
- [128] Y. Mekmouche, S. Ménage, C. Toia-Duboc, M. Fontecave, J-B. Galey, C. Lebrun, J. Pécaut, *Angew Chem.*, **2001**, *40*, 949
- [129] S. Mahapatra, J. A. Halfen, W. B. Tolman, *J. Am. Chem. Soc.*, **1996**, *118*, 11575
- [130] V. Mahadevan, M. J. Henson, E. I. Solomon, T. D. P. Stack, *J. Am. Chem. Soc.*, **2000**, *122*, 10249
- [131] M. Taki, S. Teramae, S. Nagatomo, Y. Tachi, T. Kitagawa, S. Itoh, S. Fukuzumi, *J. Am. Chem. Soc.*, **2002**, *124*, 6367
- [132] C. X. Zhang, H-C. Liang, E. Kim, Q-F. Gan, Z. Tyeklar, K-C. Lam, A. L. Rheingold, S. Kaderli, A. D. Zuberbühler, K. D. Karlin, *Chem. Commun.*, **2001**, 631
- [133] K. Itoh, H. Hayashi, H. Furutachi, T. Matsumoto, S. Nagatomo, T. Tosha, S. Terada, S. Fujinami, M. Suzuki, T. Kitagawa, *J. Am. Chem. Soc.*, **2005**, *127*, 5212
- [134] S. Teramae, T. Osako, S. Nagatomo, T. Kitagawa, S. Fukuzumi, S. Itoh, *J. Inorg. Biochem.*, **2004**, *98*, 746
- [135] J. Kuzelka, S. Mukhopadhyay, B. Spingler, S. J. Lippard, *Inorg. Chem.*, **2003**, *42*, 6447
- [136] S. Fallab, P. R. Mitchell, *Adv. Inorg. Bioinorg. Mech.*, **1984**, *3*, 311
- [137] K. Mochizuki, K. Ikeuchi, T. Kondo, *Bull. Chem. Soc. Jpn.*, **1998**, *71*, 2629
- [138] P. Comba, S. Kuwata, G. Linti, H. Pritzkow, M. Tarnai, H. Wadepohl, *Chem. Commun.*, accepted, **2006**, DOI:10.1039/B602571D
- [139] W. Walter, W. Francke, *Lehrbuch der organischen Chemie*, 29. Edition, S. Hirzel Verlag, Stuttgart, 1998, p. 166
- [140] N. Deno, R. E. Fruit Jr., *J. Am. Chem. Soc.*, **1968**, *90*, 3502
- [141] M. R. Bukowski, P. Comba, C. Limberg, M. Merz, L. Que Jr., T. Wistuba, *Angew. Chem.*, **2004**, *116*, 1303
- [142] J. R. L. Smith, D. N. Mortimer, *J. Chem. Soc., Chem. Commun.*, **1985**, 64

- [143] E. Baciocchi, O. Lanzalunga, A. Lapi, L. Manduchi, *J. Am. Chem. Soc.*, **1998**, *120*, 5783
- [144] A. Cuppoletti, C. Dagostin, C. Florea, C. Galli, P. Gentili, P. Lanzalunga, A. Petride, H. Petride, *Chem. Eur. J.*, **1999**, *5*, 2993
- [145] M. M. T. Khan, S. A. Mirza, H. C. Bajaj, *J. Mol. Cat.* **1986**, *37*, 253
- [146] J. Shearer, C. X. Zhang, L. Q. Hatcher, K. D. Karlin, *J. Am. Chem. Soc.*, **2003**, *125*, 12670
- [147] F. Wang, L. M. Sayre, *J. Am. Chem. Soc.*, **1992**, *114*, 248
- [148] C. A. Audeh, J. R. L. Smith, *J. Chem. Soc. B.*, **1970**, 1280
- [149] J. March, *Advanced Organic Chemistry. Reactions, Mechanisms and Structure*, 3<sup>rd</sup> ed., Wiley, New York, 1985, pp. 1083
- [150] M. Sako, K. Shimada, K. Hirota, Y. Maki, *J. Am. Chem. Soc.*, **1986**, *108*, 6039
- [151] F. Benedini, G. Galliani, M. Nali, B. Rindone, S. Tollari, *J. Chem. Soc., Perkin Trans. 2*, **1985**, 1963
- [152] R. A. Sheldon, J. K. Kochi, *Metal Catalyzed Oxidation of Organic Compounds*, Academic Press, New York, 1981, p. 28
- [153] D. A. Pratt, N. A. Porter, *Org. Lett.*, **2003**, *5*, 387
- [154] S. I. Dikalov, R. P. Mason, *Free Rad. Biol. & Med.*, **1999**, *27*, 864
- [155] A. B. Ryzhkov, P. A. Ariya, *Chem. Phys. Lett.*, **2006**, *419*, 479
- [156] R. Atkinson, *Int. J. Chem. Kinet.*, **1997**, *29*, 99
- [157] C. Lee, W. Yang, R. G. Parr, *Phys. Rev. B*, **1988**, *37*, 785
- [158] A. D. J. Becke, *Phys. Rev. A*, **1988**, *38*, 3098
- [159] S. Nui, M. B. Hall, *Chem. Rev.*, **2000**, *100*, 353
- [160] R. Ahlrichs and co-workers, 2001, <ftp://chemie.uni-karlsruhe.de/pub/basen> (Universität Karlsruhe, Karlsruhe, Germany)
- [161] A. Schäfer, H. Horn, R. Ahlrichs, *J. Chem. Phys.*, **1992**, *97*, 2571
- [162] H. Rohwer, G. Rajaraman, personal communication
- [163] Jaguar 5.0: Schrodinger, LLC, Portland, Oregon, 2002
- [164] P. A. MacFaul, D. D. M. Wayner, K. U. Ingold, *Acc. Chem. Res.*, **1998**, *31*, 159
- [165] H. Rohwer, unpublished results
- [166] A. Elmali, Y. Elerman, I. Svoboda, H. Fuess, *J. Mol. Struct.*, **2000**, *516*, 43
- [167] A. Elmali, Y. Elerman, C. T. Zeyrek, I. Svoboda, *Z. Naturforsch. B.*, **2003**, *58*, 433
- [168] A. Geiss, H. Vahrenkamp, *Eur. J. Inorg. Chem.*, **1999**, 1793

- [169] B. S. Snyder, G. S. Patterson, A. J. Abrahamson, R. H. Holm, *J. Am. Chem. Soc.*, **1989**, *111*, 5214
- [170] C. L. Spiro, S. L. Lambert, T. J. Smith, E. N. Duesler, R. R. Gagne, D. N. Hendrickson, *Inorg. Chem.*, **1981**, *20*, 1229
- [171] S. K. Dutta, J. Ensling, N. Werner, U. Florke, W. Haase, P. Gutlich, K. Nag, *Angew. Chem., Int. Ed. Engl.*, **1997**, *36*, 152
- [172] L. Dubois, D.-F. Xiang, X.-S. Tan, J. Pécault, P. Jones, S. Baudron, L. Le Pape, J.-M. Latour, C. Baffert, S. Chardon-Noblat, M.-N. Collomb, A. Deronzier, *Inorg. Chem.*, **2003**, *42*, 750
- [173] O. Horner, E. Anxolabéhère-Mallart, M.-F. Charlot, L. Tchertanov, J. Guilhem, T. A. Mattioli, A. Boussac, J.-J. Girerd, *Inorg. Chem.*, **1999**, *38*, 1222
- [174] M. U. Triller, W.-Y. Hsieh, V. L. Pecoraro, A. Rompel, B. Krebs, *Inorg. Chem.*, **2002**, *41*, 5544
- [175] C. Hureau, E. A.-Mallart, M. Nierlich, F. Gonnet, E. Riviere, G. Blondin, *Eur. J. Inorg. Chem.*, **2002**, 2710
- [176] H. J. H. Fenton, *Chem. News*, **1876**, 190
- [177] P. Wardman, L. P. Candeias, *Radiat. Res.*, **1996**, *145*, 523
- [178] J. Brinksma, M. T. Rispens, R. Hage, B. L. Feringa, *Inorg. Chim. Acta*, **2002**, *337*, 75
- [179] C. Zondervan, R. Hage, B. L. Feringa, *Chem. Commun.*, **1997**, 419
- [180] V. Müller, *Diploma work*, Universität Heidelberg, **2000**
- [181] G. Bar, *Synlett*, **2002**, 835
- [182] P. Comba, B. Kanellakopulos, C. Katsichtis, A. Lienke, H. Pritzkow, F. Rominger, *J. Chem. Soc., Dalton Trans.*, **1998**, 3997
- [183] H. Börzel, P. Comba, K. S. Hagen, Y. D. Lampeka, A. Lienke, G. Linti, M. Merz, H. Pritzkow, L. V. Tsymbal, *Inorg. Chim. Acta*, **2002**, *337*, 407
- [184] G. M. Sheldrick, *SHELXTL User's Manual*, Siemens Analytical X-Ray Instruments, 1994
- [185] M. J. Frisch, G. W. Trucks, H. B. Schlegel, G. E. Scuseria, M. A. Robb, J. R. Cheeseman, J. A. Montgomery Jr., T. Vreven, K. N. Kudin, J. C. Burant, J. M. Millam, S. S. Iyengar, J. Tomasi, V. Barone, B. Mennucci, M. Cossi, G. Scalmani, N. Rega, G. A. Petersson, H. Nakatsuji, M. Hada, M. Ehara, K. Toyota, R. Fukuda, J. Hasegawa, M. Ishida, T. Nakajima, Y. Honda, O. Kitao, H. Nakai, M. Klene, X. Ki, J. E. Knox, H. P. Hratchian, J. B. Cross, V. Bakken, C. Adamo, J. Jaramillo, R. Gomperts, R. E. Stratmann, O. Yazyev, A. J. Austin, R. Cammi, C. Pomelli, J. W.

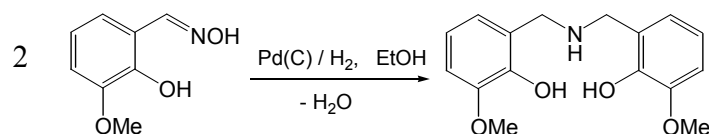
Ochterski, P. Y. Ayala, K. Morokuma, G. A. Voth, P. Salvador, J. J. Dannenberg, V. G. Zakrzewski, S. Dapprich, A. D. Daniels, M. C. Strain, O. Farkas, D. K. Malick, A. D. Rabuck, K. Raghavachari, J. B. Foresman, J. V. Ortiz, W. Cui, A. G. Baboul, S. Clifford, J. Ciolkowski, B. B. Stefanov, G. Liu, A. Liashenko, P. Piskorz, I. Komaromi, R. L. Martin, D. J. Fox, T. Keith, M. A. Al-Laham, C. Y. Peng, A. Nanayakkara, M. Challacombe, P. M. W. Gill, B. Johnson, W. Chen, M. W. Wong, C. Gonzalez, J. A. Pople, in: Gaussian 03, Revision B.03, Gaussian Inc., Wallington CT, USA, 2004

[186] A. P. Scott, L. Radom, *J. Phys. Chem.*, **1996**, *100*, 16502



## Appendix

### A. Copper(II) and manganese(III) complexes of the bisphenolamine ligand



**Scheme A1. Preparation of N,N-bis(3-methoxy-2-hydroxy-benzyl)amine**

The reaction between an equimolar mixture of copper(II) and the bisphenolamine ligand, in presence of 2 eq of triethylamine in methanol resulted in the immediate precipitate formation. Only 2:2 species could be observed in the FAB-MS spectrum, and ESI-MS confirmed that there are no charged species in solution. This means that each ligand is doubly deprotonated. Elemental analysis provided further support for this: no counter anion is present in the structure. Since it was confirmed by elemental analysis that no co-ligands coordinate to copper, saturation around the square planar copper(II) centers is only possible when considering one bridging phenolate oxygen per ligand (Figure A1). Due to the very limited solubility in any solvents, crystallization of the Cu-complex was not successful.

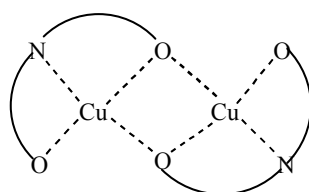
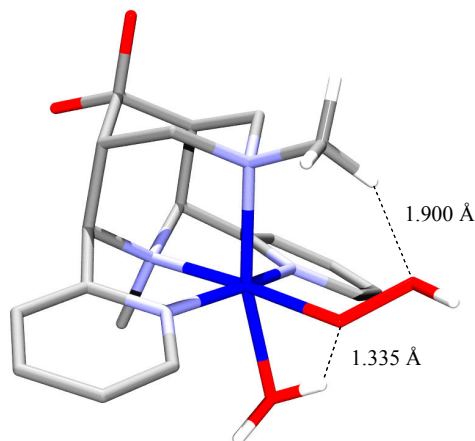


**Figure A1. Proposed coordination mode in [Cu<sub>2</sub>N(PhO)<sub>2</sub>]**

The manganese(III) complex was obtained by addition of an equimolar amount of manganese(III) acetate to the methanolic solution of the bisphenolamine ligand. In the first step the unreacted solid Mn(OAc)<sub>3</sub> was filtered off, which was followed by the addition of the 2 eq of triethylamine. To our great surprise, the stoichiometry of the precipitated complex was measured to be 2:3 (elemental analysis, ESI-MS), though the metal-to-ligand ratio was set to 1:1. Since again no counter anions are present (fit for the microanalytical data was only possible when considering only manganese(III) and ligand in 2:3 ratio), complete deprotonation of the bisphenol ligand is necessary to compensate the charge of the manganese centers. Despite our efforts, no crystals suitable for structure determination could be obtained.

## B. Additional DFT calculations for the proposed mechanistic pathway of the oxidative N-dealkylation in a cobalt-bispidone complex

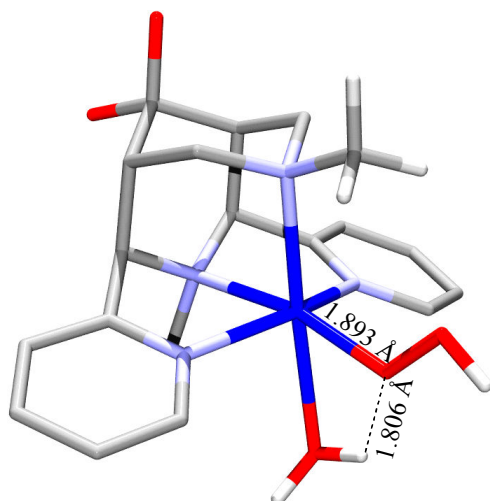
### *Optimization of the hs cobalt(II) hydroperoxo species*



**Figure B1.** Optimized structure of high-spin cobalt(II)-hydroperoxo species using STO-3G basis set

Geometry optimization for the cobalt(II)-hydroperoxo species, generated from the isomer with shorter Npy1-Npy2 separation (entry 30)<sup>6</sup> was successful using the low level STO-3G basis set (Figure B1). The optimized structure has a very short distance (1.900 Å) between the non-coordinating oxygen of the monodentate hydroperoxide and a hydrogen atom of the N7-bound methyl group. This distance is well inside the hydrogen-bond limit. The metal-bound oxygen of the hydroperoxide forms another hydrogen bond, with a hydrogen atom of the axially coordinated water ( $d(\text{O}\cdots\text{H}) = 1.335 \text{ \AA}$ ). The existence of such a chelating hydrogen bond may initiate the activation (elongation and cleavage) of the C-H bond of the N7-methyl group. An unusual feature in this structure is that the axially bound water molecule (probably as effect of the hydrogen bond) distorts the octahedral geometry, the water oxygen lies outside the axis determined by the Co-N7 bond. Unfortunately, all further calculations (including frequency calculation with STO-3G basis set, single point calculation with 6-31G(d) or TZVPP/TZV basis sets) using this optimized structure failed, due to SCF convergence problems.



*Transition state search leading to a structure with an equatorial hydroperoxide***Figure B2. Transition state with an equatorial hydroperoxide**

Attempts were made for a TS transition state search, in which only the C-H bond was elongated (to 1.3 Å) and the O-O distance left intact. The Co-O torsion was modified to bring the oxygen of peroxide close to the methyl hydrogen. Also, the geometry around the central cobalt ion was set to typical high-spin cobalt(II) distances. These TS searches lead to a structure in which the initially elongated C-H bond returns to an unstrained value and a proton from the axial water comes closer to the equatorial hydroperoxide. As product, a hydroxo / hydrogen peroxide species is probably formed through this optimized transition state. By comparison of the spin densities and Mulliken atomic charges with values obtained in other optimized structures, this transition state can be undoubtedly assigned as a cobalt(II)-hydroperoxide. Such a structure is everything but an acceptable transition state for the reaction we are studying: no oxidation of cobalt(II), break of the O-O bond of hydroperoxide or activation of the C-H bond at the N7-methyl group is indicated.

*Optimization of the ls cobalt(III) carbon-based radical species*

As first attempts for the optimization of the cobalt(III) carbon based radical species, the geometries of the ls forms of cobalt(III)-hydroxo and cobalt(III)-oxo radical species were optimized at 6-31G(d) level. The initial guess was created from the cobalt(III)-N2py2b carbonato complex, which contains the N7-bound methyl group. However, both calculations had convergence problems. This is most probably because a radical is present in these species. Considering that there are many possibilities to arrange the spins, the calculation seems to put all the free electrons on the metal and not on the carbon. For this reason, a separation of the spins and a preoptimization was necessary which gives a better guess for the required spin distribution. Structures of at the last successful iteration cycle are depicted in Figure B3.

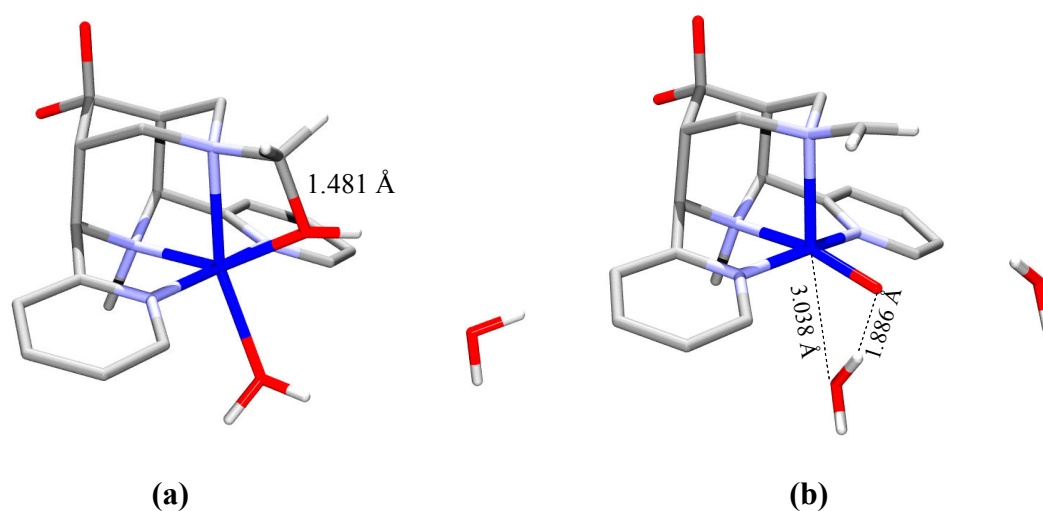


**Figure B3. Structure at the last iteration step for the (a) ls cobalt(III)-hydroxo C-radical species and (b) ls cobalt(III)-oxo C-radical species using 6-31G(d) basis set**

For the cobalt(III)-hydroxo radical case the optimization led to the removal of the spin from the carbon of the N7-methyl group by forming a hydroxymethyl unit. As discussed above, there is a tendency that the optimization moves the spins to the metal, yielding formally a “low-spin Co(II)-species”. Since it is not an optimized structure, no tabulated spin densities are available, that could prove our hypothesis.

The geometry in the last iteration step of the optimization of the low-spin cobalt(III)-oxo species shows removal of the axial water, which gets hydrogen bonded to the equatorial oxygen. The Co-N7 bond (2.376 Å) is significantly longer than the equatorial bonds ( $d(\text{Co-Npy}) = 1.946 \text{ \AA}$ ,  $d(\text{Co-N3}) = 2.013 \text{ \AA}$ ). Overestimation of the elongation along an axis is often seen in DFT calculations.

*Optimization of the cobalt(III) hydroxo carbon-based radical species with preoptimization*

Radical species for the hydrogen-peroxide route were also optimized. At the first step, initial guesses were created with Jaguar, which produced orbital coefficients corresponding to the expected spin arrangements. In contrast to our expectation, both the ls and hsbs (hs cobalt(III) with antiferromagnetically coupled C-radical) species converged to a structure where the initially radical carbon forms a further bond.

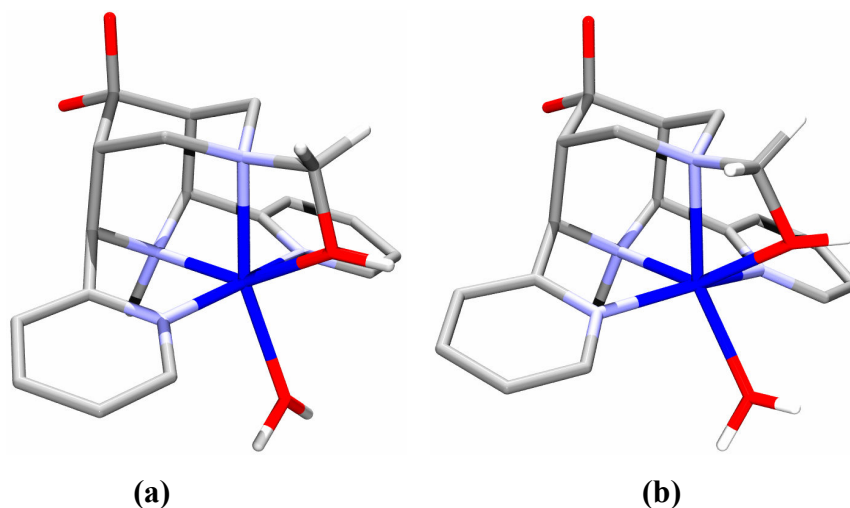


**Figure B4.** (a) Optimized structure of ls cobalt(III)-hydroxo radical species; (b) structure of hs cobalt(III)-radical species ( $S=3/2$ ) after 80 steps

In case of the ls species the N7 radical carbon binds to the equatorial hydroxide to produce an alcoholic moiety (Figure B4 a). Moreover, the cobalt - axial water bond is highly elongated. The only atom with spin density larger than 0 is the central cobalt, the spin initially “placed” on the N7-radical carbon was moved to the cobalt despite the fact that the initial guess was made with the correct spin distribution. In addition, the Mulliken atom charges for the optimized structure indicate a divalent central cobalt and a chargeless equatorial oxygen. From this the structure is best described as a cobalt(II)-N7-hydroxymethyl species.

The optimization of the hsbs species lead to a cobalt(II)-N7-hydroxymethyl species very similar to the ls analogue (Figure B4 b). The bond between the axial water and cobalt, just as in the ls species, is highly elongated. From this, it seems as though hydroxo-aqua species (similarly to cobalt(II)-hydrogen peroxide species) tend to lose their axial water, which means that the oxidation products produced from the cobalt(II)-hydrogen peroxide species do not re-establish 6-coordination around cobalt. The reason for this unusual behaviour is not clear, but may be related to the interaction between the axial water and the hydrogen directly bound to the equatorial oxygen.

## C. Selected ESI-MS spectra

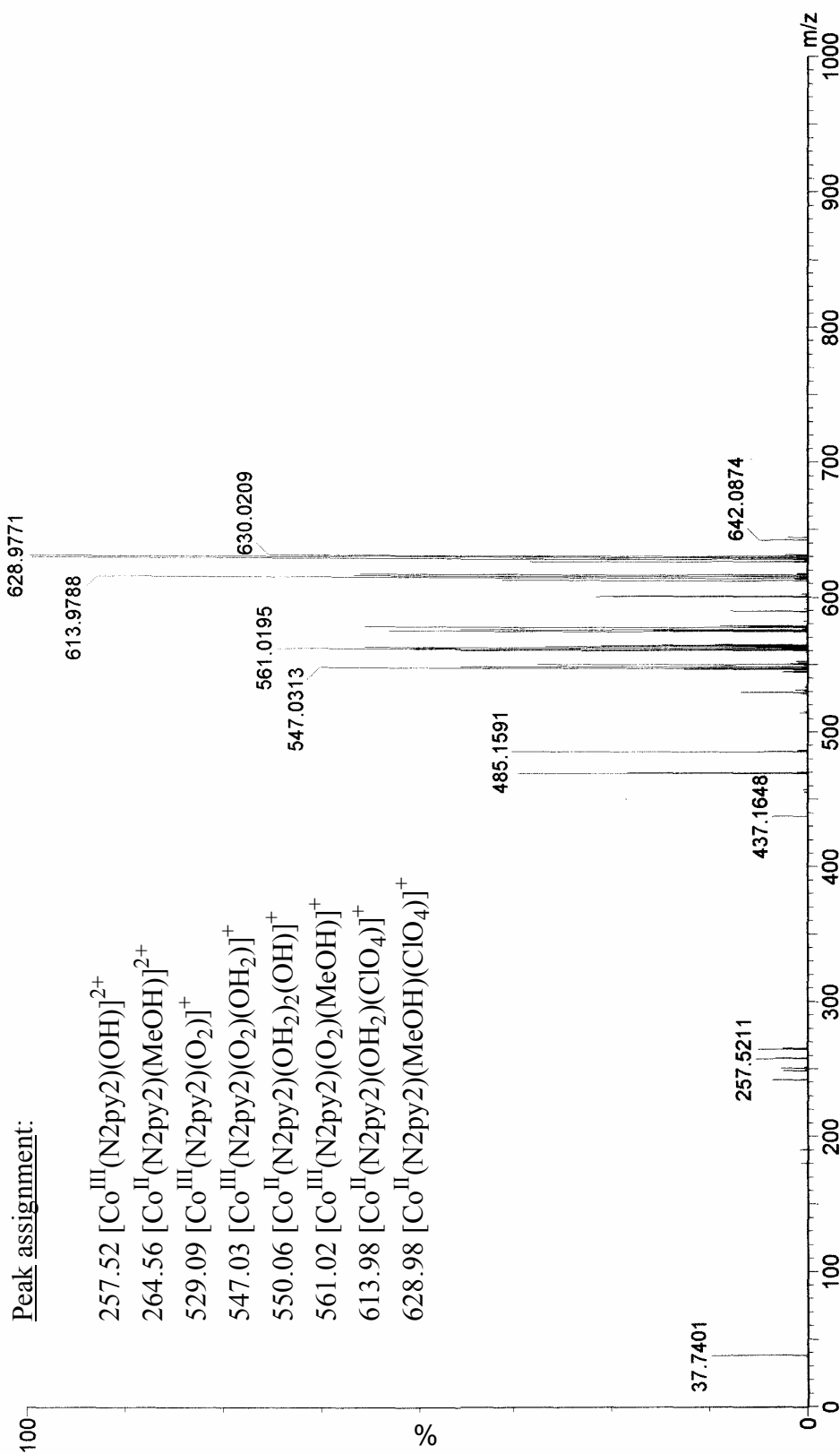


Figure C1. ESI-MS spectrum recorded for the oxidation of 11 mM  $[\text{Co}^{\text{II}}(\text{N}2\text{py}2)(\text{OH}_2)_2](\text{ClO}_4)_2$  with 170 eq  $\text{H}_2\text{O}_2$  in methanol, under anaerobic conditions

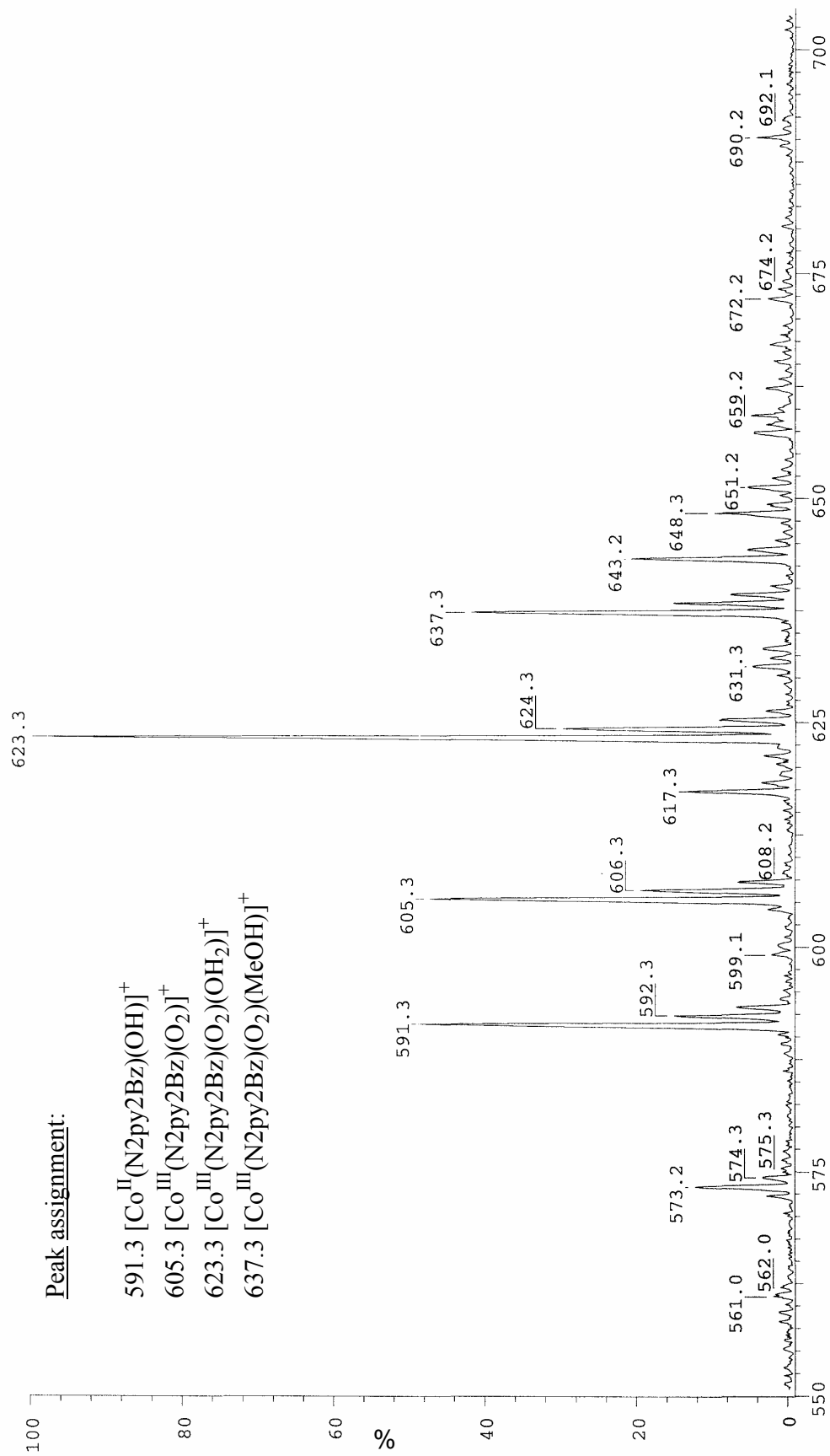


Figure C2. ESI-MS spectrum recorded for the oxidation of 6.78 mM [Co<sup>II</sup>(N2py2Bz)(OH)<sub>2</sub>](ClO<sub>4</sub>)<sub>2</sub> with 10 eq H<sub>2</sub>O<sub>2</sub> in acetonitrile

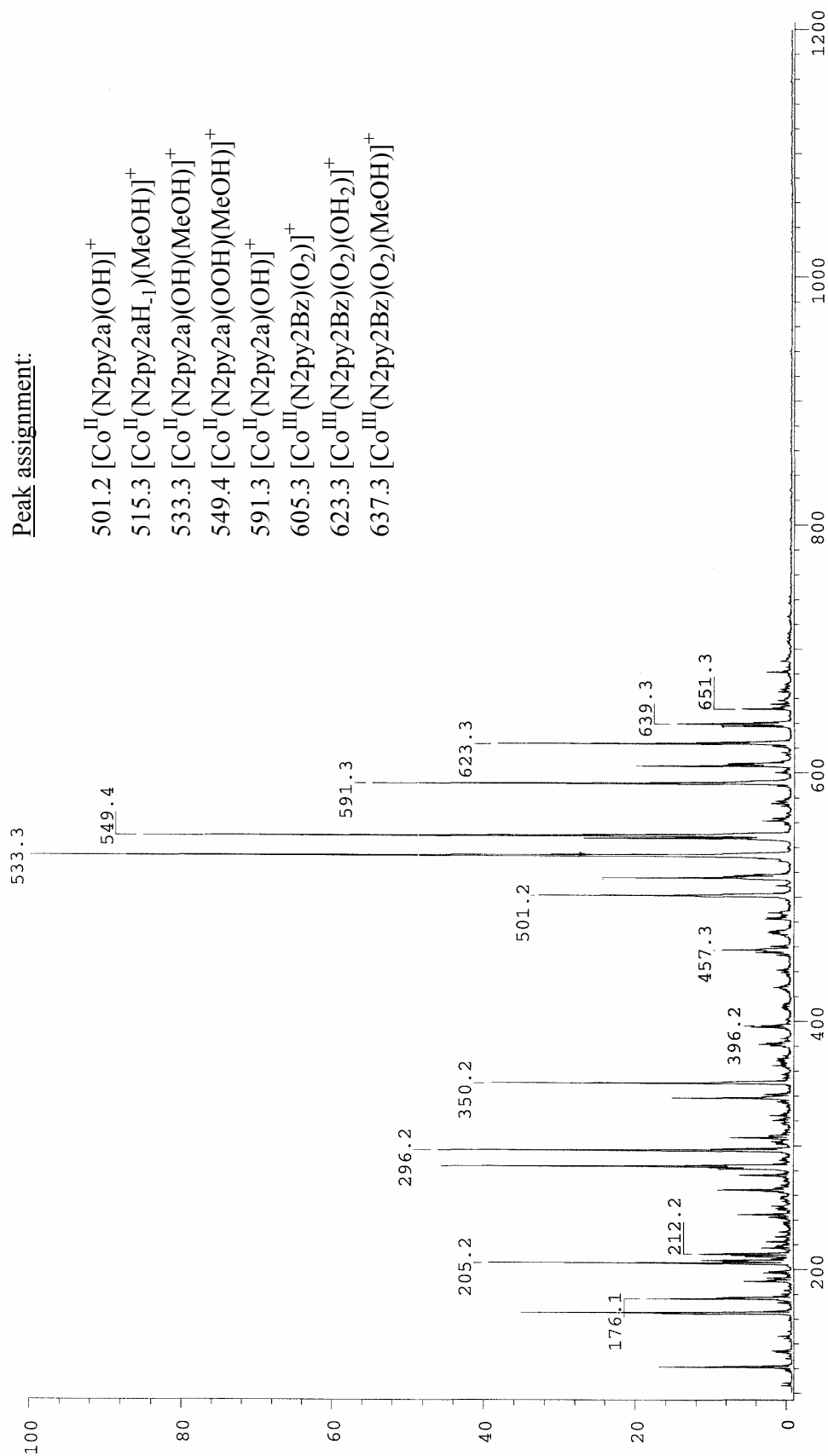


Figure C3. ESI-MS spectrum recorded for the oxidation of 11 mM  $[\text{Co}^{\text{II}}(\text{N}2\text{py}2\text{Bz})(\text{OH})_2](\text{ClO}_4)_2$  with 170 eq  $\text{H}_2\text{O}_2$  in MeOH

## D. Crystal parameters

	[Mn <sup>II</sup> (6MeN2py2)Cl <sub>2</sub> ]	[Mn <sup>II</sup> (N2py3o)Cl]Cl	N2py2PhOH	[Cu <sup>II</sup> (N2py2PhO)]BF <sub>4</sub>	[Co <sup>II</sup> N2py2a(OH <sub>2</sub> ) <sub>2</sub> ](ClO <sub>4</sub> ) <sub>2</sub>	[Co <sup>III</sup> N2py2a(OH <sub>2</sub> )Cl](ClO <sub>4</sub> ) <sub>2</sub>	
Empirical formula	C <sub>31</sub> H <sub>30</sub> Cl <sub>2</sub> N <sub>4</sub> O <sub>5</sub> Mn	C <sub>30</sub> H <sub>37</sub> Cl <sub>2</sub> N <sub>5</sub> O <sub>7</sub> Mn	C <sub>29</sub> H <sub>30</sub> N <sub>4</sub> O <sub>6</sub>	C <sub>32.5</sub> H <sub>30</sub> BF <sub>4</sub> N <sub>4</sub> O <sub>7</sub> Cu	C <sub>23</sub> H <sub>29</sub> Cl <sub>2</sub> N <sub>4</sub> O <sub>17</sub> Co	C <sub>22</sub> H <sub>26</sub> Cl <sub>3</sub> N <sub>4</sub> O <sub>16</sub> Co	
Formula weight	664.43	705.49	530.57	738.96	763.33	767.75	
Temperature	103(2) K	103(2) K	100(2) K	103(2) K	100(2) K	100(2) K	
Crystal system	monoclinic	triclinic	triclinic	triclinic	triclinic	triclinic	
Space group	P2(1)/c	P1(bar)	P1(bar)	P1(bar)	P1(bar)	P1(bar)	
Unit cell dimensions	<i>a</i> = 10.7693(5) <i>b</i> = 12.0224(6) <i>c</i> = 24.3631(11) $\alpha$ = 90° $\beta$ = 96.666(1)° $\gamma$ = 90°	<i>a</i> = 9.0362(5) <i>b</i> = 12.9725(8) <i>c</i> = 15.7660(10) $\alpha$ = 112.067(1)° $\beta$ = 90.988(1)° $\gamma$ = 103.292(1)°	<i>a</i> = 9.8304(4) <i>b</i> = 11.1525(5) <i>c</i> = 12.7347(6) $\alpha$ = 84.495(1)° $\beta$ = 70.482(1)° $\gamma$ = 78.366(1)°	<i>a</i> = 10.9150(7) <i>b</i> = 12.2034(7) <i>c</i> = 13.9905(9) $\alpha$ = 107.283(1)° $\beta$ = 108.313(1)° $\gamma$ = 102.522(1)°	<i>a</i> = 10.7753(8) <i>b</i> = 12.5214(10) <i>c</i> = 15.2590(12) $\alpha$ = 91.266(2)° $\beta$ = 109.016(2)° $\gamma$ = 111.689(10)°	<i>a</i> = 11.3500(15) <i>b</i> = 13.2623(18) <i>c</i> = 13.9803(18) $\alpha$ = 113.766(2)° $\beta$ = 91.005(3)° $\gamma$ = 109.556(2)°	<i>a</i> = 11.3500(15) <i>b</i> = 13.2623(18) <i>c</i> = 13.9803(18) $\alpha$ = 113.766(2)° $\beta$ = 91.005(3)° $\gamma$ = 109.556(2)°
Volume ; Z	3133.0(3) ; 4	1655.82(17) ; 2	1288.27(10) ; 2	1587.31(17) ; 2	1784.7(2) ; 2	1786.3(4) ; 2	
Density (calculated)	1.409	1.415	1.368	1.546	1.420	1.427	
Absorption coefficient	0.637	0.612	0.097	0.767	0.704	0.774	
F(000)	1372	734	560	758	784	784	
Crystal size	0.35 × 0.21 × 0.21	0.42 × 0.11 × 0.08	0.30 × 0.30 × 0.15	0.38 × 0.33 × 0.30	0.20 × 0.20 × 0.15	0.35 × 0.15 × 0.01	
$\theta_{\max}$	32.01	30.51	31.99	32.08	25.03	25.02	
Reflections collected	28020	27057	23079	28372	19613	19634	
Independent reflections ( <i>R</i> <sub>int</sub> )	10502 [0.0348]	10039 [0.0397]	8736 [0.0296]	10828 [0.0272]	6313 [0.0401]	6310 [0.0426]	
Parameters	509	544	509	611	401	424	
Final R1 [ <i>I</i> > 2σ( <i>I</i> )]	0.0468	0.0445	0.0459	0.0415	0.1045	0.0692	
wR2 (all data)	0.1388	0.1244	0.1292	0.1223	0.3371	0.2127	
Largest diff. peak and hole	1.579 / -0.950	0.784 / -0.668	0.549 / -0.202	1.378 / -0.562	1.843 / -1.450	1.943 / -1.247	
Sample abbreviation	CO223	CO220	co_mtl	CO243	co_mt3	co_mt4	
Structure solved by	Dr. H. Pritzkow	Dr. H. Pritzkow	Prof. H. Wadepohl	Dr. H. Pritzkow	Prof. H. Wadepohl	Prof. H. Wadepohl	





Erklärung gemäß § 7 (3) b) und c) der Promotionsordnung:

- a) ich erkläre hiermit an Eides statt, dass ich die vorgelegte Dissertation selbst verfasst und mich dabei keiner anderen als der von mir ausdrücklich bezeichneten Quellen und Hilfen bedient habe,
  
- b) ich erkläre damit, dass ich an keiner anderen Stelle ein Prüfungsverfahren beantragt bzw. die Dissertation in dieser oder anderer Form bereits anderweitig als Prüfungsarbeit verwendet oder einer anderen Fakultät als Dissertation vorgelegt habe.

Heidelberg, den 9. Mai 2006

.....  
(Máté Tarnai)



